



Research and PG Department of Chemistry

St. Thomas College (Autonomous), Thrissur, Kerala-680 001, India

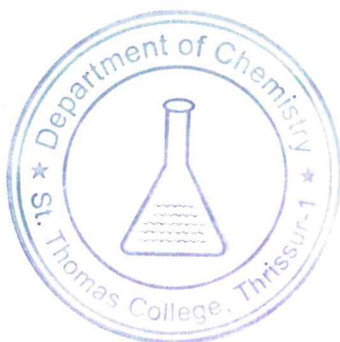
(Autonomous under University of Calicut & Nationally Reaccredited at A++ Grade by NAAC –Score 3.70 in Fourth cycle)

Dr. Jinish Antony M
Research supervisor

05/06/2023

CERTIFICATE

I hereby certify that, the CD contains the electronic copy of the revised version of the PhD thesis entitled “SYNTHETIC APPROACHES CHARACTERIZATION AND APPLICATIONS OF CONDUCTING POLYTHIOPHENE-MWCNT CARBON NANOCOMPOSITES” submitted to the University of Calicut by Ms. SWATHY T S. after incorporating the necessary corrections/suggestions made by the adjudicators. The contents in the soft copy and the thesis are the same.



Dr. JINISH ANTONY M
(Research supervisor)

Dr. JINISH ANTONY. M., Ph. D
Assistant Professor
Research & PG Department of Chemistry
St. Thomas College, Thrissur - 1

SYNTHETIC APPROACHES, CHARACTERIZATION AND APPLICATIONS OF CONDUCTING POLYTHIOPHENE-MWCNT NANOCOMPOSITES

Thesis
submitted to
University of Calicut

in partial fulfilment of the requirements
for the award of the Degree of

Doctor of Philosophy in
Chemistry

By
SWATHY T S

Under the guidance of
Dr. JINISH ANTONY M



Research & Postgraduate Department of Chemistry,
St. Thomas College (Autonomous),
Affiliated to University of Calicut
Thrissur, Kerala, 680 001

January 2023



Research and PG Department of Chemistry ST. THOMAS COLLEGE

(Autonomous)

THRISSUR - 680 001, KERALA, INDIA

(Affiliated to the University of Calicut & Nationally Re-accredited with 'A+' Grade)

Web:- <http://stthomas.ac.in>

Email:- stcthrissur@gmail.com

Phone:- +91 487 2420435

Fax:- +91 487 2421510

Date: 05/06/2023

CERTIFICATE

This is to certify that the thesis entitled "**SYNTHETIC APPROACHES, CHARACTERIZATION AND APPLICATIONS OF CONDUCTING POLYTHIOPHENE-MWCNT NANOCOMPOSITES**" is an authentic record of research work carried out by **Ms. SWATHY T S** under my supervision in partial fulfillment of the requirements for the degree of Doctor of Philosophy in Chemistry of University of Calicut and further that no part thereof has been presented before for any other degree.

Dr. JINISH ANTONY M

(Supervising Teacher)



Dr. JINISH ANTONY. M., Ph. D

Assistant Professor

Research & PG Department of Chemistry
St. Thomas College, Thrissur - 1

DECLARATION

*I hereby declare that the thesis entitled “**SYNTHETIC APPROACHES, CHARACTERIZATION AND APPLICATIONS OF CONDUCTING POLYTHIOPHENE-MWCNT NANOCOMPOSITES**”, submitted to the University of Calicut in partial fulfillment of the requirement for the award of the Degree of Doctor of Philosophy in Chemistry is a bonafied research work done by me under the supervision of **Dr.JINISH ANTONY M**, Assistant Professor, Research and Post graduate Department of Chemistry, St.Thomas College (Autonomous), Thrissur.*

I also declare that the material presented in this thesis is original and does not form the basis for the award of any other degree, diploma or other similar titles of any other university.

Date: **05/06/2023**



SWATHY T S

Acknowledgement

I am very much obliged to my research guide, **Dr. Jinish Antony M**, who made it possible to accomplish my doctoral studies successfully. I remember with grace the constant support rendered by him during the difficulties that aroused during my work period. Expressing my sincere thanks to him for the thoughtful guidance, valuable support, patience, critical comments, and warm encouragement and my gratitude remains incomplete through these limited words

I express my gratitude to our Principal **Dr. Martin K A** for his exceptional support given in my Ph. D. period. He was always approachable and contributed a lot for the development of infrastructures in our research centre. I thank the Head of our Chemistry Department, **Dr. Paulson Mathew** for his consideration and valuable support. I sincerely thank Research coordinator of St. Thomas college, **Dr. Chacko V M** for his valuable help and needed advices given during my research period.

I remember with thanks the former principals of St. Thomas' college **Dr. Joy K L**, **Dr. Ignatious Antony** and **Dr. P O Jenson** who implemented their great visions in order to develop the qualities of research. I greatly thank them for their valuable advices and support. I also extend my gratitude to the former HoDs of our Department especially **Dr. Joshy C L** and **Dr. Joby Thomas K** for their unforgettable support during my Ph. D work. I express my thanks to all other faculty members **Dr. Sunil Jose T**, **Dr. Jency Thomas K**, **Dr. Reeya Johnson**, **Dr. Joseph Joly V L**, **Prof. Aji C V**, and **Dr. Sr. Jisha Joseph** for their valuable help during my work. I sincerely thank all the non-teaching staffs of our department. They helped me a lot during my Ph. D. period. I express my gratitude to all the teaching and non-teaching staff of St. Thomas' college, Thrissur for their support in one way or the other.

I further extend my sincere thanks to **Smt. Anne Jose M**, L.F. College, Guruvayur, **Dr. Njji**, St. Josephs' College, IJK, **Dr. Xavier**, Govt. Womens' College, TVM who collaborated with us, arranged needed facilities and given valuable advices to complete different stages of my research work. I also remember and thank **Ms. Kavya**, **Ms. Athira** and **Sr. Smitha Varghese** who aided their service in various stages of my Ph D. work.

I express my sincere thanks from the bottom of my heart to my friends, senior researchers and co-researchers namely, **Dr. Aby Paul**, **Dr. Vinod P Raphael**, **Dr. Shaju K S**, **Dr. Nimmy Kuriakose**, **Ms. Rohini Das K**, **Dr. Sini Varghese**, **Dr. Drishya Sashidharan**, **Dr. Binsi M Paulson**, **Mr. Ramesh N**, **Dr. Dinoop Lal S**, **Dr. Ragi K**, **Dr. Anju Rose Puthukkara P**, **Dr. Vidhya Thomas**,

Ms.Siji T B, Ms.Memsy C K, Dr. Savitha Unnikrishnan K , Mr. Martin Francis, Ms.Raji , Ms.Nithya , Ms.Neera and Ms. Anjana I.

I always remain thankful to various institutions which provided me the facilities for conducting my work and/or analysing my samples. These institutions include, St. Josephs College, Irinjalakuda, Govt. Womens College, Trivandrum, NIIST, Trivandrum, SAIIF-STIC CUSAT, Kochi, CLIF Trivandrum, NIT, Calicut, CSIF- Calicut University, IIT-Roorkee and IUIC- MG University and various persons related to it Dr. John Naduvath and Dr. Joseph Jolly V L (WXRD), Dr. Jubey John (HR-MS), Prof. M.K, Jayaraj and Miss Anju (FT-Raman), Dr. Saju Pillai and Mr. Prasad (XPS), Dr. Viji S (MALDI-TOF), Dr. Subash (FE-SEM), Dr. Ramanathan (FT-IR), Dr. Shibuin (TGA) and Dr. Shibu (NMR), Mr. Cyril and Mr. Athul (FE-SEM).

The real strength and support I enjoyed at every instance of my research career could be credited to my family members, especially my parents and brother. Without their unmeasurable love and support, I would not have completed my thesis.

The invisible blessings that were showered on me during all the stages of my work, by God almighty gave me the courage and wisdom in apt situations through which I could complete my Ph.D. thesis work fruitfully.

I always remember with never ending gratitude, all the personalities who helped at different stages of my work physically and/or mentally. The helping hands extended by each and every one of them are well accounted for which I always debt to remain thankful.

With heartfelt gratitude

SWATHYTS



*Dedicated to
My Parents*



Preface

Conducting polymers are promising materials in different research such as medicinal, technological, and industrial fields. Conducting polymers are used alone or in combination with other attractive materials in different applications. Among the conducting polymers, polythiophenes are very attractive for their peculiar properties such as good environmental stability, optical properties, mechanical properties, and electrical conductivity. Polythiophene nanocomposites with conducting carbon nanomaterials are promising for the possibility for achieving enhancement in various properties related to it including the enhancement in electrical conductivity. One dimensional carbon nanotubes exhibiting unique mechanical, optical, thermal, and electrical properties would be a great combination for polythiophene on nanocomposites formation.

In this work, study on different synthetic approaches of polythiophene-multiwalled carbon nanotube nanocomposites, its characterization and applications were carried out. Water soluble/dispersible nature of nanocomposites is an attractive property which promises its further processability in future applications in an easy way. Unsubstituted polythiophene are water insoluble or non-dispersible in nature. Preparation of nanocomposites with suitable fillers is one of the ways to improve processability of polythiophene materials. Unsubstituted polythiophene-carbon nanotube nanocomposites were prepared by effective in-situ chemical oxidative polymerization of thiophene monomer. Achievement of attractive morphology of nanocomposites is another factor to be considered in the preparation of nanocomposites. Influence of double tail anionic surfactant AOT were identified as helping for attaining superior morphology, good processability and other properties, which is discussed in chapter 2. Another way of preparing processable and superior polythiophene carbon nanotube nanocomposites is utilizing functionalized carbon nanotubes in nanocomposites preparation. Functionalization of carbon nanotubes improves the processability by decreasing its inherent self-bundling property. Nanocomposites preparation of polythiophene with functionalized carbon nanotubes and their characterization were described in chapter 3.

Functionalized carbon nanotube-polythiophene binary nanocomposites exhibited good aqueous dispersion and further lead to preparation of higher order

ternary nanocomposites of polythiophene-functionalized multiwalled carbon nanotube with silver nanoparticles, which is discussed in chapter 4. Studies on the superior thermal and electrical properties of silver nanocomposites were also discussed in chapter 4. An elaborative study of catalytic and antibacterial properties of the prepared silver nanocomposites were presented in chapter 5. The high catalytic activity of silver nanocomposites in the model p-nitrophenol reduction reaction, its mechanism and superior antibacterial action is described in chapter 5. The study on catalytic decolourization of azo compounds were conducted with mechanistic point of view conducted in chapter 6.

Utilization of soluble polythiophene derivatives is another way of improving processable nature nanocomposites in future applications. Chapter 7 describes a simple physical mixing approach of nanocomposites preparation using substituted polythiophene, poly(3-thiophene ethanol) with functionalized multiwalled carbon nanotubes. The prepared nanocomposites exhibited stable dispersion in ethanol. The electrical and electrochemical properties of poly(3-thiophene ethanol)-functionalized multiwalled carbon nanotube nanocomposites were demonstrated as efficient electrode material in supercapacitor applications.

Abbreviations

PT	Polythiophene
CNT	Carbon nanotubes
AOT	Sodium bis(2-ethyl hexyl) sulfosuccinate
MWCNT	Multiwalled carbon nanotube
MWCNT-COOH	Functionalized multiwalled carbon nanotube
FT-IR	Fourier transform infrared
WXR D	Wide angle X-ray diffraction
EDX	Energy dispersive X-ray analysis
XPS	X-ray photoelectron spectroscopy
SEM	Scanning electron microscopy
FE-SEM	Field emission scanning electron microscopy
TEM	Transmission electron microscopy
TGA	Thermogravimetric analysis
UV-vis	Ultraviolet-visible
Ag NPs	Silver nanoparticles
P-NP	p-Nitrophenol
E. coli	Escherichia coli
AB	Azobenzene
HR-MS	High resolution mass spectroscopy
NMR	Nuclear magnetic resonance
PTE	Poly(3-thiophene ethanol)
CV	Cyclic voltammetry
GCD	Galvanostatic charge discharge

Abstract

Polythiophene-carbon nanotube nanocomposites are attractive for their peculiar properties and possibility to implement in advanced applications. In the present work, effective synthetic approaches of polythiophene-carbon nanotube nanocomposites were carried out and demonstrated them as to attain striking and improved properties.

The main objectives of our work are as follows :- (1) surfactant assisted preparation and characterization of polythiophene-carbon nanotube nanocomposites, (2) preparation of functionalized multiwalled carbon nanotube and its characterization, (3) preparation and characterization of nanocomposites of polythiophene with functionalized multiwalled carbon nanotube and their characterization, (4) preparation and characterization of nanocomposite of functionalized polythiophene with functionalized multiwalled carbon nanotube and (5) applications of polythiophene-functionalized multiwalled carbon nanotube nanocomposites .

Study on effect of double tail anionic surfactant AOT on the effective formation of polythiophene-carbon nanotube nanocomposites were carried out. Unsubstituted polythiophene carbon nanotube nanocomposites preparation was carried out with in-situ chemical oxidative polymerization of thiophene monomer using ferric chloride as oxidant in presence of surfactant AOT in chloroform medium. Functionalization of carbon nanotubes were carried out with simple acid treatment and further preparation of polythiophene-functionalized multiwalled carbon nanotube nanocomposites were conducted with in-situ chemical oxidative polymerization. General characterizations of functionalized multiwalled carbon nanotube and polythiophene-multiwalled carbon nanotube nanocomposites were carried out with FT-IR spectroscopy, Raman spectroscopy, Elemental analysis, WXRDR, EDX mapping, pH studies, and XPS analysis. Morphological characterizations were conducted with SEM and TEM analysis. Further studies such as electrical conductivity was measured using four probe conductivity meter and thermal stability analysis done with TGA. Silver nanoparticles entangled polythiophene functionalized multiwalled carbon nanotube ternary nanocomposites were subjected to various applications such as catalytic reduction of p-nitrophenol with studies on its mechanism, antibacterial applications on E. coli bacteria and catalytic decolorization of water soluble and water insoluble azo compounds including the azobenzene. Nanocomposites of functionalized conducting polymer poly(3-thiophene ethanol) with functionalized multiwalled carbon nanotube were synthesized by simple

and easily scalable physical mixing approach. Electrochemical characterization with CV and GCD analyses of nanocomposites promised the composites as efficient supercapacitor electrode materials.

സംഗ്രഹം

പോളിതയോഫീൻ - മൾട്ടിവാൾഡ് കാർബൺ നാനോട്യൂബ് നാനോകോംപോസിറ്റുകൾ ഫെറിക് ക്ലോറൈഡ് ഓക്സീകാരിയായും സോഡിയം ബിസ്(2-ഈഥൈൽ ഹെക്സൈൽ) സൾഫോസക്സിനേറ്റ് സർഫക്ടന്റും ആയി ഉപയോഗിച്ച് ക്ലോറോഫോം ലായകത്തിൽ കെമിക്കൽ ഓക്സിഡേറ്റീവ് പോളിമെറൈസേഷൻ വഴി നിർമ്മിക്കുകയും അവയുടെ വ്യത്യസ്തമായ പ്രത്യേകതകൾ പഠിക്കുകയും ചെയ്തു. പോളിതയോഫീൻ-കാർബൺ നാനോട്യൂബ് നാനോകോംപോസിറ്റും സിൽവർ നാനോപർട്ടി-ക്കിളും ചേർന്ന് ടേർണറി നാനോകോംപോസിറ്റ് നിർമ്മിക്കുകയും തുടർന്ന് ഉൽപ്രേരകം, ആന്റിബാക്ടീരിയൽ ഏജന്റ് തുടങ്ങിയ മേഖലകളിൽ ഉപയോഗപ്പെടുത്തുകയും ചെയ്തു. പോളി(3-തയോഫീൻ എഥനോൾ) മൾട്ടിവാൾഡ് കാർബൺ നാനോട്യൂബ് നാനോകോംപോസിറ്റുകൾ ലളിതമായ ഫിസിക്കൽ ബ്ലേന്റിങ് രീതിയിലൂടെ നിർമ്മിക്കുകയും അവയെ സൂപ്പർകപ്പാസിറ്റർ ഇലക്ട്രോഡ് ആയി ഉപയോഗപ്പെടുത്താൻ സാധിക്കുമെന്ന് കണ്ടെത്തുകയും ചെയ്തു.

Table of Contents

Contents	Page No.
List of Figures	vii-xiv
List of Tables	xv-xvi
Chapter 1 Introduction and Literature Review	1-20
1.1 Introduction to conducting polymer nanocomposites	3
1.2 Polythiophene and its derivatives	3
1.3 Organic/inorganic fillers in conducting polymer nanocomposites.....	5
1.4 Carbon nanotubes as fillers in conducting polymer nanocomposites....	5
1.5 Synthetic strategies and development of conducting polythiophene-carbon nanotube nanocomposites.....	6
1.6 Applications of conducting polythiophene-carbon nanotube nanocomposites.....	8
1.6.1 Sensors.....	9
1.6.2 Preparation of higher-order nanocomposites.....	10
1.6.3 Supercapacitor applications.....	10
1.6.4 EMI shielding.....	11
1.6.5 Photovoltaic cells and photodiodes.....	11
1.6.6 Transistors.....	12
1.6.7 Thermoelectric materials.....	13
References.....	14
Chapter 2 AOT Assisted Preparation of Polythiophene-MWCNT Core-shell Nanocomposites	21-50
2.1 Introduction.....	23
2.2 Experimental.....	28
2.2.1 Materials and reagents.....	28
2.2.2 Measurements and instruments.....	28
2.2.3 Synthesis of PTCNT-100.....	29
2.2.4 Synthesis of PTCNT-300 [AOT-0].....	29
2.2.5 Synthesis of PT-25.....	30
2.2.6 Synthesis of PT-25[AOT-0].....	30
2.3 Results and discussion.....	30
2.3.1 Synthesis of polythiophene and polythiophene - MWCNT nanocomposites.....	30

Table of Contents

2.3.2	Characterization of PT and PTCNT nanocomposites.....	33
2.3.3	Morphological characteristics of PT and PTCNT nanocomposites.....	37
2.3.4	Role of AOT in the formation of nanocomposite.....	38
2.3.5	Mechanism of composite formation.....	40
2.3.6	Enhancement of properties.....	41
2.4	Conclusion	45
	References	46

Chapter 3	Polythiophene-functionalized MWCNT Nanocomposite: Preparation and Properties	51-79
------------------	---	--------------

3.1	Introduction.....	53
3.2	Experimental.....	58
3.2.1	Materials and reagents	58
3.2.2	Measurements and instruments.....	58
3.2.3	Synthesis of MWCNT-COOH 5M	59
3.2.4	Synthesis of PTCNT-COOH 300	59
3.2.5	Synthesis of PT2CNT-COOH 300	59
3.3	Results and Discussion	60
3.3.1	Synthesis and characterization of functionalized MWCNT-COOHs	60
3.3.2	Synthesis and characterization of PTCNT-COOH nanocomposites	63
3.4	Conclusion	74
	References	75

Chapter 4	Silver Nanoparticles Entangled Polythiophene-Functionalized MWCNT Ternary Nanocomposites: A Green Synthetic Approach and Enhancement in Properties	81-105
------------------	---	---------------

4.1	Introduction	83
4.2	Experimental	86
4.2.1	Materials and reagents used	86
4.2.2	Measurements and instruments	86
4.2.3	Synthesis of PTCNT-COOH 300 Ag	87
4.2.4	Synthesis of MWCNT-COOH Ag	87
4.2.5	Leaching study of PTCNT-COOH 300 Ag with different pH.....	87
4.3	Results and Discussion	88
4.3.1	Synthesis and characterization of PTCNT-COOH 300 Ag and	

Table of Contents

	<i>MWCNT-COOH Ag</i>	88
4.3.2	<i>Morphological analysis of ternary and binary silver nanocomposites ..</i>	93
4.3.3	<i>Electrical conductivity and thermal stability of ternary and binary nanocomposites</i>	95
4.4	<i>Conclusion</i>	100
	<i>References</i>	101
Chapter 5 Active Solvent Hydrogen Enhanced Catalytic Reduction of p-Nitrophenol using Binary and Ternary Silver Nanocomposites and its Antibacterial Action		107-145
5.1	<i>Introduction</i>	109
5.2	<i>Experimental</i>	112
5.2.1	<i>Materials and reagents</i>	112
5.2.2	<i>Measurements and Instruments</i>	112
5.2.3	<i>Reaction kinetics using different nanocatalyst concentrations</i>	113
5.2.4	<i>Recycling studies using nanocatalysts</i>	113
5.2.5	<i>Recycling effects of nanocatalysts on morphology and composition</i>	114
5.2.6	<i>TNC catalyzed reduction in different volume percentages of glycerol-water mixtures</i>	114
5.2.7	<i>Calibration curve of 4-aminophenolate to find the relative yield of product</i>	114
5.2.8	<i>Large scale reduction of p-nitrophenol</i>	115
5.2.9	<i>Antibacterial study using ternary nanocatalyst TNC</i>	115
5.3	<i>Results and Discussion</i>	116
5.3.1	<i>Comparison of TNC and BNC nanocatalysts</i>	116
5.3.2	<i>Optimization of nanocatalyst amount</i>	122
5.3.3	<i>Recycling studies</i>	124
5.3.4	<i>Elemental composition and morphology of recycled nanocatalysts</i>	125
5.3.5	<i>Optimization of solvent-water mixture for reduction</i>	129
5.3.6	<i>Optimization of [P-NP]: [NaBH₄] molar ratio</i>	130
5.3.7	<i>The proposed mechanism for catalytic reduction</i>	132
5.3.8	<i>Relative yield and industrial-scale reduction of p-nitrophenol</i>	134
5.3.9	<i>Antibacterial activity</i>	136
5.4	<i>Conclusion</i>	139

Table of Contents

References	140
------------------	-----

Chapter 6 Ternary and Binary Silver Nanocatalysts for Reduction of Water Soluble and Insoluble Azodyes and Azobenzene	147-175
--	----------------

6.1	<i>Introduction</i>	149
6.2	<i>Experimental</i>	153
6.2.1	<i>Materials and reagents</i>	153
6.2.2	<i>Measurements and Instruments</i>	153
6.2.3	<i>Catalytic decolourisation study of methyl orange and congo red using BNC-0.04 catalyst</i>	153
6.2.4	<i>UV-vis absorption study of reductive decolourisation of methyl orange and congo red</i>	153
6.2.5	<i>Catalytic decolourisation study of methyl red and sudan III using BNC-0.04 catalyst</i>	154
6.2.6	<i>UV-vis absorption study of reductive decolourisation of methyl red and sudan III</i>	154
6.2.7	<i>Large scale reduction of azobenzene</i>	155
6.2.8	<i>Recycling studies using nanocatalysts</i>	155
6.3	<i>Results and discussion</i>	155
6.3.1	<i>Ternary and binary silver nanocomposites (TNC and BNC) as nanocatalyst for reductive decolourisation of azo dyes</i>	155
6.3.2	<i>Optimization of the amount of catalyst for reduction of water-soluble azo dyes</i>	157
6.3.3	<i>Kinetics of reductive decolourisation of water soluble organic azo dyes</i>	158
6.3.4	<i>Optimization of the amount of catalyst for reductive decolourisation of water-insoluble/partially soluble organic azo dyes</i>	160
6.3.5	<i>Kinetics of reductive decolourisation of water-insoluble/partially soluble organic azo dyes</i>	162
6.3.6	<i>Kinetics of catalytic reduction of azobenzene, recyclability studies and mechanism</i>	166

Table of Contents

6.4	<i>Conclusion</i>	171
	<i>References</i>	172
Chapter 7	CTAB Complexed Poly(3-thiophene ethanol)-- Functionalized MWCNT Nanocomposites for Supercapacitor Application	177-204
7.1	<i>Introduction</i>	179
7.2	<i>Experimental</i>	183
7.2.1	<i>Materials and reagents used</i>	183
7.2.2	<i>Measurements and instruments</i>	183
7.2.3	<i>Synthesis of PTE</i>	183
7.2.4	<i>Preparation of PTE-CTAB complex</i>	183
7.2.5	<i>Preparation of PTECNT COOH-10</i>	184
7.2.6	<i>Electrochemical characterization</i>	184
7.3	<i>Results and discussion</i>	184
7.3.1	<i>Preparation of poly(3-thiophene ethanol) (PTE) and PTECNT-COOH nanocomposites</i>	184
7.3.2	<i>Characterisation of PTE and PTECNT-COOH nanocomposites</i>	186
7.3.3	<i>Morphological and dispersion studies of polymer and PTECNT- COOH nanocomposites</i>	189
7.3.4	<i>Thermal stability and electrical conductivity of PTECNT-COOH nanocomposites</i>	192
7.3.5	<i>Electrochemical characterisation of PTECNT-COOH nanocomposites</i>	194
7.4	<i>Conclusion</i>	199
	<i>References</i>	200
Chapter 8	Summary and Conclusions.....	205-209
	Publications and Conference presentations.....	211-212

List of figures		
Chapter 1: Introduction and Literature Review		
Figure no:	Figure caption	Page No
1.1	<i>Structure of polythiophene and some of the substituted polythiophenes</i>	3
1.2	<i>Structures of positive and negative polarons and bipolarons formed in polythiophene via p-type and n-type doping respectively.....</i>	4
1.3	<i>PEDOT:PSS/CNT nanocomposites hydrogel (a), alcogel (b) and aerogel (c)</i>	6
1.4	<i>Flexible micro-supercapacitor fabricated from MnO₂/PEDOT/MWCNT nanocomposites conductive ink with polytetrafluoroethylene</i>	8
1.5	<i>Reversible ammonia sensing using polythiophene-carbon nanotube nanocomposites</i>	9
Chapter 2: AOT Assisted Preparation of Polythiophene-MWCNT Core-shell Nanocomposites		
Figure no:	Figure caption	Page No
2.1	<i>(a) Scheme for oxidative chemical polymerization of thiophene using FeCl₃ oxidant and (b) in-situ chemical oxidative polymerization of polythiophene with multiwalled carbon nanotubes (MWCNT) for nanocomposite preparation.....</i>	24
2.2	<i>(a) Schematic representation of interaction of carbon nanotubes with poly(9,9-bis (diethylaminopropyl)-2,7-fluorene-co-1,4-phenylene) and (b) illustration of the interaction of carbon nanotubes and different conducting polymers</i>	25
2.3	<i>Multiamphiphilic compatibilizer layer formations over CNT surface ...</i>	26
2.4	<i>Normal and reverse micelles formation in the bulk solution of organic solvents. Cylindrical assembly, hemispherical assembly, and a random assembly of the surfactants over CNT's surface</i>	27
2.5	<i>Schematic representation of the synthesis of polythiophene-MWCNT nanocomposite (PTCNT) in presence of AOT</i>	31
2.6	<i>Schematic representation of the synthesis of PT-25 in presence of AOT.....</i>	31
2.7	<i>FT-IR spectra of MWCNT, PT-25, PTCNT-100, PTCNT-200, PTCNT-300 and PTCNT-400</i>	33
2.8	<i>(A) Powder X-ray diffraction patterns of PT-25, PTCNT-100, PTCNT-200, PTCNT-300 and PTCNT-400. (B) A diagram exhibiting the ratio of I_{CNT} (intensity of the characteristic peak of MWCNT) to I_{PT} (intensity of characteristic X-ray diffraction peak of polythiophene) for PTCNT composites</i>	35
2.9	<i>Area under the X-ray diffraction peaks of A) amorphous region and B)</i>	36

	<i>crystalline region in PT-25 and PTCNT nanocomposites.</i>	
2.10	<i>Scanning electron microscopic (SEM) images of PT-25, MWCNT, PTCNT-100 and PTCNT-30</i>	37
2.11	<i>TEM images of MWCNT and PTCNT-100 and size calculation</i>	38
2.12	<i>Transmission electron microscopic (TEM) images of MWCNT, PTCNT-300 [AOT-0], PTCNT-100 and PTCNT-300</i>	39
2.13	<i>WXR D patterns of PTCNT-300 and PTCNT-300 [AOT-0]. Diagram exhibiting the ratio of I_{CNT} (intensity of characteristic peak of MWCNT) to I_{PT} (intensity of characteristic X-ray diffraction peak of polythiophene) for PTCNT-300 and PTCNT-300[AOT-0] (inset)</i>	40
2.14	<i>Mechanism of the formation of PT-25 and PTCNT nanocomposites</i>	41
2.15	<i>Electrical conductivity of PT-0, PT-25, PTCNT-100, PTCNT-200, PTCNT-400 and pristine MWCNT</i>	42
2.16	<i>Dispersions of MWCNT, PT-25, PTCNT-100 and PTCNT-300 in chloroform (A) and water (B). UV-vis absorption spectra of PTCNT-100, PTCNT-200, PTCNT-300 and PTCNT-400 recorded in chloroform medium (C)</i>	43
2.17	<i>Thermogravimetric analysis of PT-25, PTCNT-100 and PTCNT-300 ..</i>	44
2.18	<i>Illustration of the role of polythiophene, MWCNT and AOT in the PTCNT nanocomposite formation</i>	45

Chapter 3: Polythiophene-functionalized MWCNT Nanocomposite: Preparation and Properties

Figure no:	Figure caption	Page No
3.1	<i>Different surface functionalization strategies on carbon nanotubes</i>	54
3.2	<i>Combined covalent cum non-covalent functionalization of carbon nanotubes with molecular and polymer entities</i>	55
3.3	<i>Non-covalent functionalization (modification) of CNT with polymer and covalent functionalization (modification) of CNT with polymer</i>	58
3.4	<i>Schematic representation of the preparation of MWCNT-COOH</i>	60
3.5	<i>FTIR spectra of Pristine MWCNT, MWCNT-COOH 5M, MWCNT-COOH 10M and MWCNT-COOH-N 5M</i>	61
3.6	<i>Raman spectra of purified MWCNT and MWCNT-COOH</i>	62
3.7	<i>Schematic representation of synthesis of PTCNT-COOH nanocomposite</i>	63
3.8	<i>FT-IR spectra of pristine MWCNT, MWCNT-COOH, PTCNT-COOH 100, PTCNT-COOH 200, PTCNT-COOH 300 and PT-25</i>	65
3.9	<i>XPS spectra of pristine MWCNT, MWCNT-COOH, PTCNT-COOH 100 and PTCNT-COOH 300</i>	66
3.10	<i>Powder X-ray diffractograms of (A) MWCNT-COOH, PT-25, PTCNT-COOH 100, PTCNT-COOH 200, PTCNT-COOH 300 and pristine MWCNT (inset). (B) Comparison of X-ray diffraction diagram of</i>	

	<i>PTCNT-COOH 300, PT2CNT-COOH 300 and PT3CNT-COOH 300...</i>	67
3.11	<i>FE-SEM images of (A) MWCNT-COOH, (B) PTCNT-COOH 100, (C) PTCNT-COOH 300 and (D) HR-TEM image of PTCNT-COOH 300..</i>	68
3.12	<i>Illustration of the utilisation of defect group functionalization for the orientation of polythiophene over MWCNT surface</i>	69
3.13	<i>Dispersion of MWCNT-COOH in different solvents (A) and an aqueous dispersion of different nanocomposites (B). UV-vis spectra of PTCNT-COOH 100 in chloroform [a], PTCNT-COOH 300 in chloroform [b], PTCNT-COOH 300 in ethanol [c] and MWCNT-COOH in water [inset] (C).....</i>	70
3.14	<i>Four probe electrical conductivity of PTCNT-COOH 100, PTCNT-COOH 200, PTCNT-COOH 300, MWCNT-COOH and pristine MWCNT</i>	71
3.15	<i>TGA (A) and DTA (B) analysis of MWCNT-COOH, PTCNT-COOH 100 and PTCNT-COOH 300</i>	72
3.16	<i>Illustration of debundling effect of carbon nanotubes by carboxylic acid functionalization followed by non-covalent functionalization with polymer</i>	73
Chapter 4: Silver Nanoparticles Entangled Polythiophene - Functionalized MWCNT Ternary Nanocomposites: A Green Synthetic Approach and Enhancement in Properties		
Figure no:	Figure caption	Page No.
4.1	<i>Metal nanoparticles incorporation with different polymer-carbon nanotube nanocomposites and their scanning electron microscopic images</i>	83
4.2	<i>Different possibilities for the formation of carbon nanotube-metal nanoparticle nanocomposites</i>	84
4.3	<i>Schematic representation of the synthesis of PTCNT-COOH 300 Ag ...</i>	88
4.4	<i>FT-IR spectra of MWCNT-COOH, MWCNT-COOH Ag and PTCNT-COOH 300 Ag</i>	89
4.5	<i>FT Raman spectra of MWCNT-COOH Ag and PTCNT-COOH 300 Ag</i>	90
4.6	<i>XPS spectra of PTCNT-COOH 300 and PTCNT-COOH 300 Ag</i>	91
4.7	<i>WXR D pattern of PTCNT-COOH 300 Ag and MWCNT-COOH Ag</i>	91
4.8	<i>Dispersion of PTCNT-COOH 300 Ag (A) and MWCNT-COOH Ag (B) in different solvents. UV-vis spectra of PTCNT-COOH 300 Ag and MWCNT-COOH Ag in water and ethanol (C). UV-vis spectra of PTCNT-COOH 300 Ag in water with different concentrations (D) ...</i>	92
4.9	<i>FE-SEM images of MWCNT-COOH Ag (A), dispersed PTCNT-COOH 300 Ag (B), PTCNT-COOH 300 Ag (C (cropped image) and E) and electron diffraction pattern of PTCNT-COOH 300 Ag (D)</i>	93
4.10	<i>Transmission electron microscopic images of PTCNT-COOH 300 Ag (A) and its size calculation (by taking the average size of 10</i>	

	<i>nanoparticles) (B)</i>	94
4.11	<i>Scheme for the formation of silver nanoparticle embedded ternary nanocomposite.....</i>	95
4.12	<i>Four probe electrical conductivity measurements of PTCNT- COOH 300, PTCNT-COOH 300 Ag and MWCNT-COOH Ag and pristine MWCNT (A). The schematic illustration of polythiophene as a connecting bridge between MWCNT-COOH and silver nanoparticles (B).....</i>	96
4.13	<i>Thermograms (A) and differential thermograms (B) of PTCNT-COOH 300, MWCNT-COOH Ag and PTCNT-COOH 300 Ag</i>	97
4.14	<i>UV-vis spectra of PTCNT-COOH 300 Ag after 3 hours of stirring and washing with different media of different pH</i>	98
4.15	<i>Illustration of the formation of water-dispersible ternary nanocomposite and its advantageous outcomes</i>	100

Chapter 5: Active Solvent Hydrogen Enhanced Catalytic Reduction of p-Nitrophenol using Binary and Ternary Silver Nanocomposites and its Antibacterial Action

Figure no:	Figure caption	Page No.
5.1	<i>Illustration of formation of colloidal silver nanoparticles without having host material (A) and formation of CNT hosted silver nanoparticles (B).....</i>	109
5.2	<i>UV-Vis spectra of p-nitrophenol, p-nitrophenolate ion and reduced product p-amino phenolate ion by adding a reducing agent and a suitable catalyst.</i>	110
5.3	<i>Accounting the benefits of nanocatalysts in model nitrophenol reduction reaction</i>	111
5.4	<i>Schematic representation of reactions of (a) p-nitrophenol with NaBH₄ and (b) silver nanocatalysts (BNC/TNC) catalyzed reaction of p-nitrophenol using NaBH₄</i>	116
5.5	<i>UV-vis absorption spectra for reduction of p-nitrophenol using catalyst TNC-0.02 (A), BNC-0.02 (B), TNC-0.04 (C), BNC-0.04 (D) TNC-0.06 (E), BNC-0.06 (F), TNC-0.10 (G)and BNC-0.10 (H) in consecutive time intervals</i>	118
5.6	<i>Linear relationship plot of ln (A/A₀) against time for p-nitrophenol reduction using TNC-0.02 (A), BNC-0.02 (B), TNC-0.04 (C), BNC-0.04 (D) TNC-0.06 (E), BNC-0.06 (F), TNC-0.10 (G)and BNC-0.10 (H).....</i>	119
5.7	<i>UV-vis absorption spectra of silver nanocolloid after one day of synthesis(A) and silver nanocolloid after 7 days of synthesis(B)</i>	120
5.8	<i>UV-vis absorption spectra of reduction of p-nitrophenol using NaBH₄ using catalyst homogeneous colloidal silver nanoparticles (A) and linear relationship plot of ln(A/A₀) against time on one day after the</i>	

	<i>synthesis of silver nanocolloid (B). UV-vis absorption spectra of reduction of p-nitrophenol using NaBH₄ using catalyst homogeneous colloidal silver nanoparticles (C) and linear relationship plot of ln(A/A₀) against time on seven days after the synthesis of silver nanocolloid (D), UV-vis absorption spectra of reduction of p-nitrophenol using NaBH₄ using PTCNT-COOH 300 as catalyst (E) and reduction of p-nitrophenol using NaBH₄ using MWCNT-COOH as catalyst (F)</i>	121
5.9	<i>Plot of (A/A₀) against time for TNC catalysed reactions (A) and BNC catalysed reactions (B) for different concentrations of catalyst 0.02 mg/mL, 0.04 mg/mL, 0.06 mg/mL, and 0.10 mg/mL taken in p-nitrophenol solution</i>	122
5.10	<i>UV-vis absorption spectra of TNC 0.06 catalysed (A) and BNC-0.06 catalysed reaction (B) for successive catalytic cycles. Catalytic conversion percentage of TNC-0.06 (C) and BNC-0.06 (D) in successive catalytic cycles</i>	124
5.11	<i>X-ray diffraction patterns of TNC and recycled TNCs (A), BNC and recycled BNCs (B) after 3rd, 6th and 9th catalytic cycles. FE-SEM images of TNC (C) and BNC (D) as pristine nanocatalyst</i>	125
5.12	<i>WXR D patterns of (A) byproduct separated from the reaction residue (B) BNC-3RC and (C) BNC-3RC after repeated centrifugation and washing</i>	126
5.13	<i>XPS spectra of TNC-3RC and BNC-3RC</i>	127
5.14	<i>FE-SEM images of TNC-3RC (A) and BNC-3RC (B), EDX colour mapping of sodium in TNC-3RC (C), sodium in BNC-3RC (D), silver in TNC-3RC (E) and silver in BNC-3RC (F). Schematic representation of existence of metaborate by-product over recycled catalyst (G)</i>	129
5.15	<i>Time of decolourization plotted against different volume percentage of solvent-water mixture using P-NP: NaBH₄ molar ratio 1:1000 with TNC-0.06, BNC-0.06, TNC-0.03 and BNC-0.03 catalysts.</i>	130
5.16	<i>Time of decolourization plotted against different NaBH₄ concentrations in water and 10% glycerol-water mixture using TNC-0.06 and BNC-0.06 catalysts (A). UV-vis absorption spectra of reduction of p-nitrophenol using catalyst TNC-0.06 [PNP: NaBH₄ molar ratio 1:100](B) using BNC-0.06 [PNP: NaBH₄ molar ratio 1:100] (C) and BNC-0.03 [PNP: NaBH₄ molar ratio 1:200] [D] in 10% glycerol-water solvent mixture. UV-vis absorption spectra of reduction of p-nitrophenol using catalyst BNC-0.01 [PNP: NaBH₄ molar ratio 1:200 (E) and linear relationship plot of ln(A/A₀) against time for BNC-0.01 for PNP: NaBH₄ molar ratio 1:200 (F) in 10% glycerol-water solvent mixture</i>	131

5.17	<i>Change in pH of glycerol-water mixture (20%) by the addition of NaBH₄</i>	132
5.18	<i>Mechanism of active solvent enhanced green catalytic reduction of p-nitrophenol using NaBH₄ in 10% glycerol-water mixture</i>	134
5.19	<i>Calibration plot of p-aminophenol in different concentrations (1 × 10⁻⁷ M to 5 × 10⁻⁴ M) (A), UV-vis absorption spectra of the standard solution of p-aminophenolate ion, p-aminophenolate obtained from catalytic reduction using TNC-0.06 and BNC-0.06 (in 1 × 10⁻⁴ M) (B), reduction of p-nitrophenol in concentrated solution (10 mL, 15 g/L) using P-NP: NaBH₄ molar ratio 1:25 and BNC-0.18 (0.18 mg/mL) in 10% glycerol-water mixture (C), and UV-vis spectrum p-aminophenolate produced by bulk concentration scale reduction (D)</i>	135
5.20	<i>Photographs of mixtures of E. coli bacteria culture with different concentrations of TNC taken after overnight incubation (A). The plot of optical density versus the concentration of TNC for the antibacterial study at 660 nm (B)</i>	136
5.21	<i>Plot of optical density against concentration of TNC in lactose broth used in antibacterial study (A) and plot and photographs of comparison of antibacterial activity of MWCNT-COOH, PTCNT-COOH 300, Ag NPs, BNC and TNC (B)</i>	138
5.22	<i>Illustration of involvement of active hydrogens in catalytic hydrogenation of p-nitrophenol</i>	139

Chapter 6: Ternary and Binary Silver Nanocatalysts for Reduction of Water Soluble and Insoluble Azodyes and Azobenzene

Figure no:	Figure caption	Page No.
6.1	<i>Consecutive reduction in azo compounds to form chemo-selective product hydrazo compounds and followed by non-selective product amino aromatics by-products</i>	150
6.2	<i>Illustration of photocatalytic transfer hydrogenation of azobenzene to hydrazobenzene (A) with alcohol on cadmium sulfide (adapted from Shiraishi et al.) 2012 and (B) using NaNbO₃ catalyst (adapted from Pei et al. 2020)</i>	151
6.3	<i>Synthesis of Hydrazoarenes formation from nitroarenes and azobenzene</i>	151
6.4	<i>Chemical structure of different azo dyes</i>	155
6.5	<i>Photographs of reductive decolourisation of water-soluble azo dyes methyl orange (initial stage (A), middle stage (B) and final stage (C), and congo red (initial stage (D), middle stage (E) and final stage (F). Plots of decolourisation time against catalyst concentration used for methyl orange(G) and Congo red (H).....</i>	157
6.6	<i>UV-vis absorption spectra of catalytic reduction of methyl orange (A) and congo red (B) using BNC-0.04 catalyst in different time intervals.</i>	

	<i>Linear relationship plot of $\ln (A/A_0)$ against time for reduction of methyl orange (C) and congo red (D) using catalyst BNC-0.04.</i>	158
6.7	<i>UV-vis absorption spectra of catalytic reduction of methyl orange (A) and congo red (B) using TNC-0.04 catalyst in different time intervals. Linear relationship plot of $\ln (A/A_0)$ against time for reduction of methyl orange (C) and congo red (D) using catalyst TNC-0.04.....</i>	160
6.8	<i>Photographs of reductive decolourisation of water-insoluble or partially soluble azo dyes methyl red (initial stage (A), middle stage (B) and final stage (C), and Sudan III (initial stage (D), middle stage (E) and final stage (F). Plots of decolourisation time against the catalyst concentration used for methyl red (G) and sudan III (H).</i>	161
6.9	<i>UV-vis absorption spectra of catalytic reduction of methyl red (A) and sudan III (B) using BNC-0.04 catalyst in different time intervals. Linear relationship plot of $\ln (A/A_0)$ against time for reduction of methyl red (C) and sudan III (D) using catalyst BNC-0.04.....</i>	162
6.10	<i>UV-vis absorption spectra of catalytic reduction of methyl red (A) and sudan III (B) using TNC-0.04 catalyst in different time intervals. Linear relationship plot of $\ln (A/A_0)$ against time for reduction of methyl red (C) and sudan III (D) using catalyst TNC-0.04.</i>	163
6.11	<i>UV-vis absorption spectra of catalytic reduction of azobenzene using BNC-0.04 (A) catalyst and TNC-0.04 (C) in different time intervals. Linear relationship plot of $\ln (A/A_0)$ against time for reduction of azobenzene using catalyst BNC-0.04 (B) catalyst and TNC-0.04 (D).</i>	167
	<i>Large scale reduction of azobenzene (E)</i>	
6.12	<i>Catalytic conversion percentage of BNC-0.04 (A) and TNC-0.04 (B) in successive catalytic cycles of azobenzene reduction.</i>	168
6.13	<i>NMR spectra of azobenzene (A) and catalytic reduction product of azobenzene (B). Photographs of purchased azobenzene (C) and isolated product of azobenzene after catalytic reduction with BNC-0.18 (D)</i>	169
6.14	<i>Illustration of plausible mechanism for catalytic chemoselective hydrogenation of azobenzene</i>	170
6.15	<i>Outline of reductive treatment of azo compounds carried out in present study and their advantageous outcomes</i>	171

Chapter 7: CTAB Complexed Poly(3-thiophene ethanol) - Functionalized MWCNT Nanocomposites for Supercapacitor Application

Figure no:	Figure caption	Page No.
7.1	<i>Schematic representations of three types of capacitance based on energy storage mechanism: electrical double layer capacitance (a), reversible faradaic capacitance (b), and reversible intercalation and</i>	

	<i>exfoliation capacitance (c)</i>	179
7.2	<i>Literature reports of functionalized conducting polymer-carbon nanotube nanocomposites: (A) SWCNT-Pyrene⁺-polythiophene nanocomposite (adapted from Rahman et al. 2005), (B) polythiophene-graft-poly(methyl methacrylate) (PMMA), for poly(styreneco-acrylonitrile) (multiwalled carbon nanotube (MWCNT) composite (adapted from Kim et al. 2005) (C) Single-Stranded DNA-Single-Walled Carbon Nanotube Hybrid (adapted from Ghosh et al. 2005) and (D) conducting polyfluorene copolymer-Wrapped Carbon Nanotubes (adapted from Berger et al. 2005).</i>	180
7.3	<i>EDC-coupled 3-thiophene ethanol monomer to functionalized MWCNT and subsequent in-situ polymerization to prepare nanocomposites.....</i>	181
7.4	<i>Schematic representation of synthesis of PTE-CTAB complex</i>	185
7.5	<i>Synthesis of PTECNT-COOH nanocomposites by solution blending method</i>	186
7.6	<i>FT-IR spectra of PTE, PTE-CTAB complex, MWCNT-COOH, PTECNT-COOH 10, PTECNT-COOH 15 and PTECNT-COOH 20</i>	187
7.7	<i>Wide angle X-ray diffractograms of PTE, PTE-CTAB complex, PTECNT-COOH 10, PTECNT-COOH 15 and MWCNT-COOH (inset)</i>	188
7.8	<i>Field emission scanning electron microscopic images of (a) PTE, (b) MWCNT-COOH, (c) PTECNT-COOH 10 and (d) PTECNT-COOH 15</i>	189
7.9	<i>UV-vis absorption spectra of PTE and PTE-CTAB complex</i>	190
7.10	<i>UV-visible spectra of PTECNT-COOH 10, PTECNT-COOH 15 and PTECNT-COOH 20 in ethanol and DMSO (A) and Dispersions of PTECNT-10, PTECNT-15 and PTECNT-20 in ethanol (B).....</i>	191
7.11	<i>Formation mechanism of PTECNT-COOH nanocomposites</i>	192
7.12	<i>Thermal stability of PTE, PTECNT-COOH 10, PTECNT-COOH 15 and PTECNT-COOH 20</i>	193
7.13	<i>Four probe electrical conductivity of PTE, PTECNT-COOH 15, PTECNT-COOH 20 and MWCNT-COOH</i>	194
7.14	<i>Cyclic voltammogram of PTE (a), PTECNT-COOH 10 (b), PTECNT-COOH 15 (c) and PTECNT-COOH 20 (d) in 1M HCl electrolyte.....</i>	195
7.15	<i>Cyclic voltammogram of PTECNT-COOH 20 for different scan rates in the electrolytes 1M HCl (a), 1M H₂SO₄ (b), 1M KOH (c) and 1M Na₂SO₄ (d).....</i>	196
7.16	<i>Galvanostatic charge-discharge profile of PTECNT-COOH 20 in 1M H₂SO₄ electrolyte (a) and Cycling stability study (cyclic voltammetry) of PTECNT-COOH 20 in 1M H₂SO₄ electrolyte up to 1000 cycles (b).</i>	197
7.17	<i>Illustration of advantageous outputs of PTECNT-COOH nanocomposites preparation and supercapacitor application</i>	199

List of Tables

Chapter 2: AOT Assisted Preparation of Polythiophene-MWCNT Core-shell Nanocomposites		
Table no:	Table heading	Page No
2.1	<i>Polythiophene (PT) and PTCNT nanocomposite samples with the amount of thiophene, AOT and MWCNT, monomer to surfactant mole ratio, monomer to FeCl₃ mole ratio and yield obtained in the preparation</i>	32
2.2	<i>CHNS elemental analysis data of sulfur, carbon and hydrogen in PT-25, PT-25[AOT-0], PT-25, PTCNT-100 and PTCNT-300.....</i>	34
Chapter 3: Polythiophene-functionalized MWCNT Nanocomposite: Preparation and Properties		
Table no:	Table heading	Page No
3.1	<i>Defect group functionalisation and their relevance studied in literature</i>	56
3.2	<i>Millimoles of thiophene, AOT, and ferric chloride, amount of functionalised MWCNT-COOH, mole ratio of monomer/AOT, mole ratio of monomer/FeCl₃, elemental composition of samples and yield</i>	64
3.3	<i>Comparison of conductivity values of MWCNT, MWCNT-COOH, PTCNT and PTCNT-COOH nanocomposites</i>	72
Chapter 4: Silver Nanoparticles Entangled Polythiophene-Functionalized MWCNT Ternary Nanocomposites: A Green Synthetic Approach and Enhancement in Properties		
Table no:	Table heading	Page No.
4.1	<i>Atomic concentration of samples from XPS spectra, pH of the samples, morphology of samples, thermal stability of samples, and electrical conductivity of samples</i>	89
4.2	<i>Comparison study of our work with similar systems reported in the literature</i>	99
Chapter 5: Active Solvent Hydrogen Enhanced Catalytic Reduction of p-Nitrophenol using Binary and Ternary Silver Nanocomposites and its Antibacterial Action		
Table no:	Table heading	Page No.
5.1	<i>Name of nanocatalyst, Initial concentrations of P-NP, NaBH₄, nanocatalyst, final concentrations of P-NP, NaBH₄, nanocatalysts, solvents, rate constant (k), and the activity factor</i>	117
5.2	<i>Comparing catalysts, concentrations of reagents, rate constants, and activity factors obtained in the present study with recent other</i>	

	<i>literature reports</i>	123
5.3	<i>The atomic percentage of C, O, Na, B, Ag, and S in TNC-3RC and BNC-3RC</i>	128
Chapter 6: Ternary and Binary Silver Nanocatalysts for Reduction of Water Soluble and Insoluble Azodyes and Azobenzene		
Table no:	Table heading	Page No.
6.1	<i>Literature reports of hydrogenation of azobenzene to hydrazobenzene .</i>	152
6.2	<i>Name of azo compounds, concentration and volume of azo compounds used, amount of NaBH₄ used, name of catalyst and concentration of catalyst with respective rate constant and activity factor in the catalytic reduction/decolourisation</i>	156
6.3	<i>Comparison of present study with literature reported for catalytic decolourisation methyl orange, congo red, methyl red and Sudan III using NaBH₄ as reducing agent, in terms of the amount of azo dye used, amount of NaBH₄ used, the concentration of catalyst, type of catalyst (homogeneous or heterogeneous) and obtained rate constant ..</i>	164
Chapter 7: CTAB Complexed Poly(3-thiophene ethanol) - Functionalized MWCNT Nanocomposites for Supercapacitor Application		
Table no:	Table heading	Page No.
7.1	<i>PTECNT-COOH samples with the amount of poly(3-thiophene ethanol), CTAB surfactant and MWCNT-COOH used and yield obtained in preparation</i>	186

Chapter 1

Introduction and Literature Review

Chapter 1

1.1. Introduction to conducting polymer nanocomposites

Over the past two decades conducting polymer nanocomposites have been studied with much attention for their various synthetic approaches as well as applications.¹⁻⁴ Nanocomposites are multiphase materials which contain more than one component coexist in a nano structural confinement with other components. Conducting polymer nanocomposites are those in which one of the components is a conjugated polymer or its copolymer.⁵ Modified properties of components are achieved after combining the conjugated polymer with any other organic or inorganic substrate in composite form.^{6,7} Conducting polymers are a class of organic polymers having a continuous conjugated backbone inherently. The advantageous properties of polymeric materials on incorporation with a conducting framework could render advanced applications in appropriate fields. Various conjugated polymers are polyacetylene, polyaniline, polypyrrole, polythiophene, polyphenylenevinylene, etc.^{8,9} Conjugated polymers or their derivatives or its copolymers possess conducting or semiconducting nature, along with polymeric features like easy processability, flexibility, lightweight nature, cost effectiveness, and the other unique characteristics of each conducting polymer.⁸⁻¹¹

1.2. Polythiophene and its derivatives

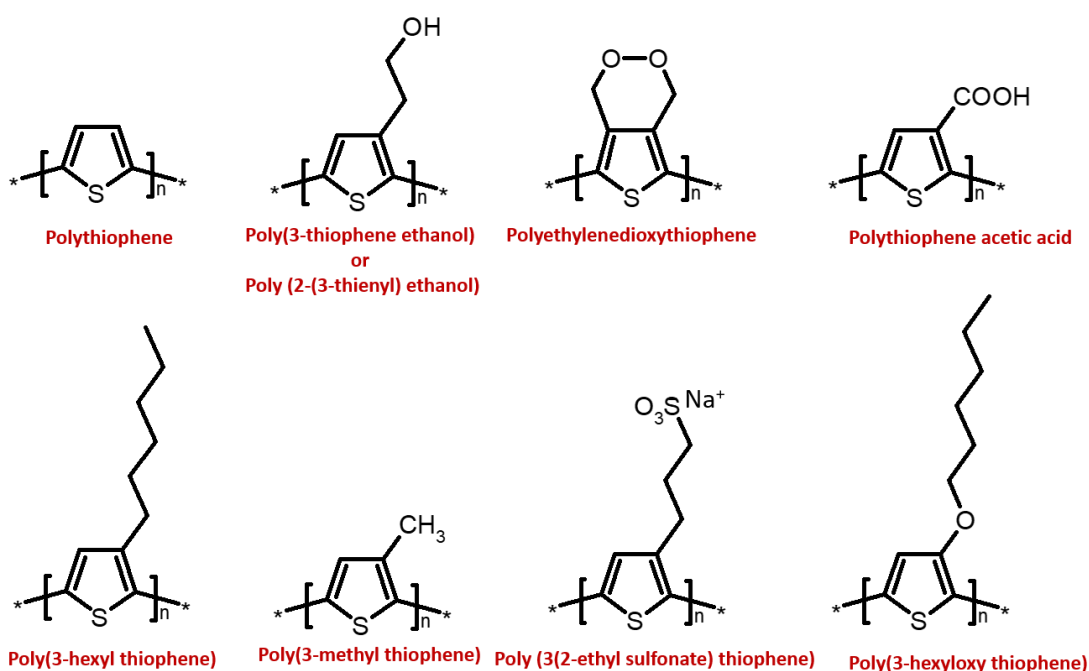


Figure 1.1. Structure of polythiophene and some of the substituted polythiophenes

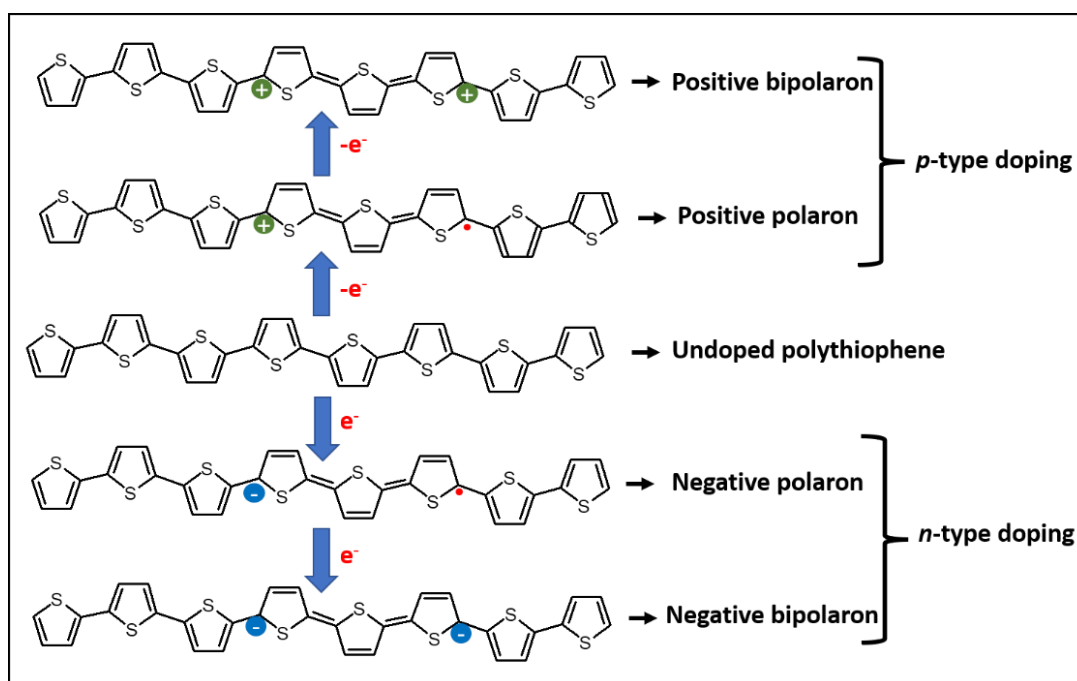


Figure 1.2. Structures of positive and negative polarons and bipolarons formed in polythiophene via *p*-type and *n*-type doping respectively.

Polythiophene and its derivatives are prominent and promising group of conducting polymer materials, holding unique characteristics such as ease of processability, good optoelectronic properties and environmental stability. Solubility or processability improvements are more prominent in polythiophene derivatives and their copolymers than in unsubstituted states. Structures of some of the substituted polythiophenes taken from literature are given in **Figure 1.1**.¹² polythiophene is distinguishable from other conducting polymers with its polymeric heterocyclic aromatic thiophene ring system existing as extended π -conjugated chains.^{13,14} Doping of conducting polymers usually improves their electrical conductivity and shifts the electrochemical potential. Many researchers have reported undoped and doped states of polythiophenes and the importance of doping to result changes in the conductivity performance of polythiophenes. Band gap tuning is usually carried out to obtain desirable electrical properties for conducting polymers. The band gap of polythiophene and its derivatives can be tuned between 1 to 3 eV. Band gap tuning could be done by inserting suitable dopants or with side chain functionalization on polymer aromatic backbone. Polythiophene usually shows conductivity through *p*-type doping. Chemical, electrochemical, or electric methods can achieve the different levels of doping.¹⁴⁻¹⁶ Insertion of a single charge on the polythiophene chain by doping creates polaron and further doping leads to the form bipolaron. Structural illustrations of *p*-type and *n*-type

polarons and bipolarons are shown in **Figure 1.2**. The *n*-type doping was also reported in polythiophenes by altering the properties of prepared polythiophene. Jayasundara and co-workers presented a theoretical study of *p* and *n*-type doping on polythiophene and polypyrrole conducting polymers.¹⁶ Polythiophenes might render their individual properties also with suitable fillers in the composite form.¹⁷

1.3. Organic/inorganic fillers in conducting polymer nanocomposites

The composites of conducting polymers in which polymers serve as matrices and the additional component(s) act as filler(s). Various inorganic or organic fillers can be chosen for nanocomposite preparation. Different fillers such as metals, metal compounds, carbon-based materials, inorganic substrates, and ceramic materials are used. The main factor determining effective nanocomposite formation and better properties is the interaction between different components in the nanocomposites.¹⁸⁻²⁶ Liu and co-workers reported the effective formation of end functional polythiophene/CdSe nanocomposite having the morphology of interpenetrated network nanorods obtained with the help of successful interaction between the components.¹⁸ Pascariu et al. reported electrochemical preparation of polythiophene-nickel nanoparticle nanocomposites with good conductivity performance.²⁴ One of the reports of carbon based nanocomposites with polythiophene by Taj et al. was the PEDOT-graphene nanocomposite formation with a narrow band gap and high dielectric properties.²⁵ Another nanocomposite of polythiophene with clay substrate was reported by Aradilla and co-workers, who suggested the material for ultracapacitor applications.^{3,26-28}

1.4. Carbon nanotubes as fillers in conducting polymer nanocomposites

Carbon nanotubes are unique one-dimensional conducting nanotubular materials exhibiting unique physical, electrical, and mechanical properties. They are generally classified as single-walled and multiwalled carbon nanotubes. Single walled nanotubes can be considered as folded graphene sheets, whereas later is multi-folded. The difficulty of using carbon nanotubes is poor processability due to the inherent bundling nature.^{29,30} Various functionalization strategies on the walls of carbon nanotubes can be adopted to decrease this self-aggregation tendency. Carbon nanotubes could act as suitable fillers in conducting polymer nanocomposites due to (i) the

Chapter 1

opportunity of polymers to wrap on the surface of carbon nanotubes utilizing weak non-covalent CH- π or π - π interaction or (ii) covalent grafting of polymers on the defective sites of carbon nanotubes walls.³¹⁻³³ Carbon nanotubes also possess a template effect for attaching polymers around it; thereby maintaining the nanotubular morphology.^{23,30} Single and multiwalled carbon nanotubes have their advantages in nanocomposites; multiwalled carbon nanotubes have the overall electronic structure less destructible on chemical treatments due to the presence of multi folds of tubular graphene layers. Multiwalled carbon nanotubes are economically more viable and could exhibit more excellent mechanical properties than single-folded carbon nanotubes.³⁴⁻³⁶

1.5. Synthetic strategies and development of conducting polythiophene-carbon nanotube nanocomposites

General strategies used to prepare polythiophene carbon nanotubes nanocomposites are

1. Carbon nanotubes or functionalised carbon nanotubes are ultrasonicated in the presence of polymer matrix.
2. In-situ polymerisation of polymer in the presence of dispersion of carbon nanotubes
3. Grafting of polymer chains from the surface of carbon nanotubes.³²

The processability of nanocomposites is a crucial factor to be considered in the preparation of nanocomposites. The processing of nanocomposites also needs significant attention to tune the composites for specific applications. Polythiophene-carbon nanotube nanocomposites could usually be made up of aerogels, thin films, pellets, conductive inks, etc. The morphological features, distribution of different components in the composites and solvent dispersibility helps to fabricate them into suitable form.^{37,38}

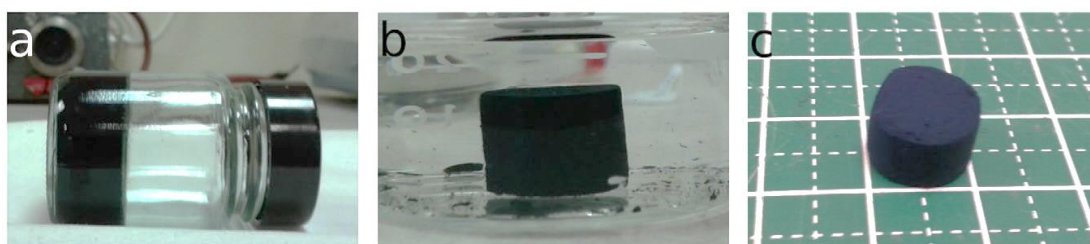


Figure 1.3. PEDOT:PSS/CNT nanocomposites hydrogel (a), alcogel (b) and aerogel (c) (adapted from Cheng et al. 2017).

Aerogel substances are distinguishable with their properties of high specific surface area, low density, and 3-dimensional porous structure. The unique nanotubular morphology of carbon nanotubes surrounded by polythiophene polymer delivers the possibility to form advantageous aerogels. Various applications of aerogels are contamination treatment, Cerenkov detector, thermal insulators, and energy storage. Besides that, biocompatible aerogels are interesting for bio implant and drug delivery. Good conductivity of the aerogels might lead to binder-free supercapacitor electrode preparation.³⁸⁻⁴¹ Cheng and co-workers reported free-standing aerogel fabrication from PEDOT: PSS/CNT nanocomposites having high specific surface area and good electrochemical performance. In this report, a hydrogel was first converted to alcogel, followed by treatment with supercritical CO₂, which resulted in the formation of free-standing aerogel (photographs of hydrogel, alcogel and aerogel adapted from the literature are given in **Figure 1.3**).³⁹ Idumath et al. conducted a detailed review of emerging trends in polymer aerogels in which they remarked carbon nanotubes-polymer nanostructures could act as promising candidates for aerogel preparation.⁴⁰ Polythiophene carbon nanotubes thin/thick films are the most demanded preparation with nanocomposites due to their distinctive properties to obtain flexibility, lightweight nature, easy fabrication, etc.^{14,29,42,43} Transparent thin films are also prepared using carbon nanotube nanocomposites.⁴³ Methods such as spin coating, solution sorting, spread casting, vacuum filtration, etc. are commonly used for nanocomposites thin film preparation. All the techniques seek the formation of stable dispersion of nanocomposites in suitable solvents.^{14,29,42,43} Wang et al. reported polythiophene-carbon nanotube nanocomposites films for chemiresistor application. They found that thicker films were needed to produce a sufficient signal-to-noise ratio.⁴² Another work done by Liyanage and co-workers addressed the fabrication of thin film transistors of poly(3-dodecylthiophene)-CNT nanocomposites, and its preparation was reported by dispersion based-sorting technique.⁴³ Pellet formation with nanocomposites is another form of fabrication of carbon nanotube-conducting polymer nanocomposites. Binder-free pellets have more significance. Carbon nanotubes alone do not give strong binder-free pellets, but composite preparation with environmentally stable polymers can render the effective formation of binder-free, firm, and non-deliquescent pellets.⁴⁴⁻⁴⁸ It is easy to study the electrical conductivity of nanocomposites samples in pellet form. Gas sensing applications are mainly reported with pelletized form of polythiophene-carbon nanotube nanocomposites.⁴⁴⁻⁴⁵ A recent report of ammonia sensing application of

Chapter 1

polythiophene carbon nanotube nanocomposites was conducted by Husain and co-workers and they conducted the study in the pelletized form of the composites.⁴⁴ Another possibility is the preparation of conducting ink with polythiophene carbon nanotube nanocomposites. The self-bundling nature of carbon nanotubes obstructs effective dispersion and thereby hinders conducting carbon ink preparation.^{34,48} Polythiophene/CNT conductive inks were not much progressed in literature today. But the possibility of using conducting polymer-wrapped carbon inks can simplify the ink printing method and thereby reduce the overall cost of application. Chen et al. fabricated conductive ink made up of MnO_2 /PEDOT/MWCNT nanocomposites with poly-tetrafluoroethylene in ethanol and demonstrated their application in flexible micro-supercapacitor (see **Figure 1.4**).⁴⁸

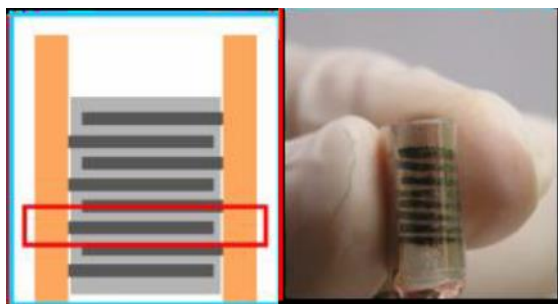


Figure 1.4. Flexible micro-supercapacitor fabricated from MnO_2 /PEDOT/MWCNT nanocomposites conductive ink with poly-tetrafluoroethylene (adapted from Chen et al. 2014).

1.6. Applications of conducting polythiophene-carbon nanotube nanocomposites

Polythiophene-carbon nanotube nanocomposites are desirable materials in different applications such as sensors, suitable nanocomposite precursors for synthesising higher order structural architectures, supercapacitor electrodes, electromagnetic interference (EMI) shielding, photovoltaic cells and photodiodes, transistors, thermoelectric films, conducting adhesives, battery electrodes, aerospace applications, etc. The properties developed are characteristics of both polythiophene and carbon nanotube fillers which depend on their ratio of mixing and on the interaction between the components to determine the appropriate field(s) of application of the nanocomposites prepared. Significant applications of polythiophene-carbon nanotubes nanocomposites are discussed briefly below.

1.6.1. Sensors

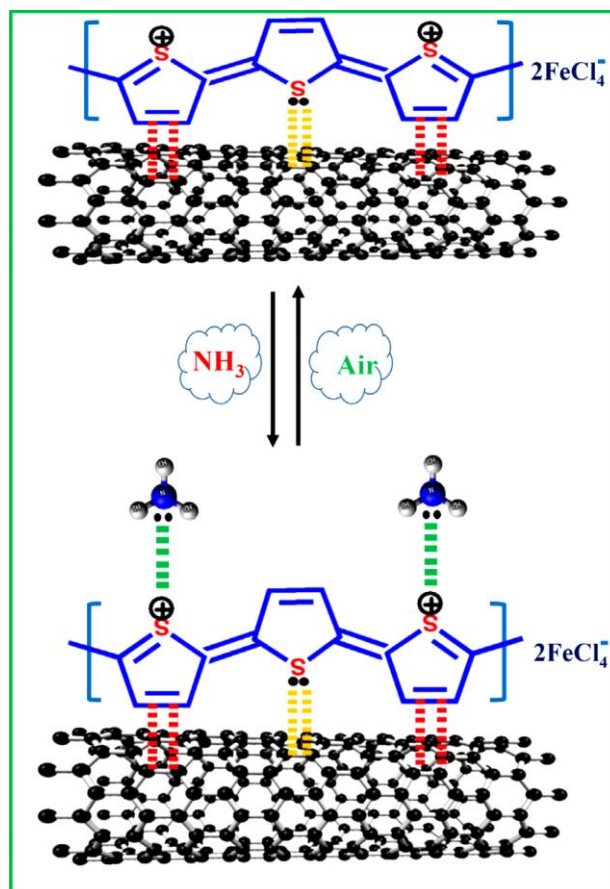


Figure 1.5. Reversible ammonia sensing using polythiophene-carbon nanotube nanocomposites (adapted from Husain et al. 2020)

Polythiophene-carbon nanotube nanocomposites are emerging as sensor materials which include electrochemical sensing, chemiresistor sensing, chemical sensing, mechanical sensing, and voltammetric sensing methods.^{42,44,45,49,50} The development of low-cost portable sensors using conducting polymer nanocomposite systems is a new field of research applying its relevant properties. Carbon nanotubes are important materials distinguishable by their property of sensitivity to environmental changes. Surface functionalization with polymers and their conducting nature can further correlate with the sensing properties of carbon nanotubes. Zhang et al. reported developing a chemiresistive sensor using polythiophene functionalized carbon nanotubes to detect n-methylphenethylamine (NMPEA) and various volatile organic compounds. This chemiresistive sensor combined on circuit boards could develop wireless communication with a cell phone accessory or computer. Combining polymer

Chapter 1

components having various recognition groups to conducting carbon nanotubes enable them to adopt suitable sensing mechanism based on the property related to the recognition of the group on the polymer.⁴⁹ Hussain et al. established a reversible chemical sensor based on electrical conductivity difference for nanocomposites interacting with the analyte ammonia (see **Figure 1.5.**)⁴⁴

1.6.2. Preparation of higher-order nanocomposites

Higher-order nanocomposites are emerging as an exciting way of preparing more efficient nanocomposites from carbon nanotubes- polythiophene binary nanocomposites.⁵¹⁻⁵⁵ The availability of an excellent structural platform helps to accommodate other materials on it. Therefore, the formation of well-oriented carbon nanotubes- conducting polymer nanocomposites is the prime factor which helps to build them up to higher-order structural architectures. Structural modification with additional fillers will lead to integrated properties of individual components.⁵¹⁻⁵³ Interaction of binary polythiophene-CNT nanocomposites with the other component would act as another important factor to form stable higher-order composites. This factor also acts as a reason for enhancement in the properties of nanocomposites.^{51,52} A report on higher-order nanocomposites by Wan and co-workers revealed incorporation of Pt nanoparticles to polythiophene-carbon nanotubes nanocomposites could effectively enrich them as an electrochemical sensor for Bisphenol A detection.⁵²

1.6.3. Supercapacitor applications

Incorporating polythiophene with carbon nanotube makes them a suitable combination for supercapacitor electrode applications by properly tuning their properties.⁵⁶⁻⁶⁰ Carbon nanotubes are promising electrode materials due to their structural and electronic properties.^{57,59} Electrical double-layer formation on the surface of carbon nanotubes is due to their capacitance performance known as electrical double layer capacitance (EDLC).⁵⁶⁻⁵⁹ Polythiophene exhibits good redox properties with less percentage EDLC characteristics and thereby exhibits pseudo capacitance.^{56,58} Many authors have reported polythiophene carbon nanotube nanocomposite based supercapacitors with high energy efficiency and good power density.⁵⁶⁻⁶⁰ One study conducted by Zhang et al. reports the supercapacitor application of polythiophene-carbon nanotube nanocomposites obtained with electropolymerization in ionic liquid microemulsion followed by composites formation.⁵⁶ Binder and additive-free

supercapacitor electrodes are more attractive. For capacitance performance, Lota et al. prepared binder-free electrodes with PEDOT and carbon nanotubes.⁵⁸ Literature studies revealed that many reports of polythiophenes nanocomposites with single and multiwalled carbon nanotubes can render good capacitor performance.⁵⁷

1.6.4. EMI shielding

Electromagnetic interference is present in devices that utilize, transfer or distribute electrical energy. Increased use of cellular towers, electronic devices, wireless networks, etc., seeks more efficiency in material related to EMI shielding.⁶¹ As nanotechnology progresses in various materials science fields, establishing efficient EMI (Electromagnetic Interference) shielding materials is considered a major area of research interest. Research related to EMI shielding materials pay attention to both synthesis and application. Continuous conducting fillers in nanocomposites for EMI shielding applications are most efficient rather than discontinuous fillers.^{62,63} Conventional EMI shielding materials are metal-based systems with many demerits such as high density, low resistance to corrosion and poor mechanical properties. Using carbon nanotubes as the filler in nanocomposites provides good mechanical strength, improved electrical conductivity and high corrosion resistance. The incorporation of polythiophene with carbon nanotubes to obtain nanocomposites having well-organized conducting networks deliver an efficient platform for high EMI shielding efficiency (EMI SE). The use of polythiophene pursues more attention related to its remarkable characteristics, such as low density, high environmental stability, good conductivity, and potential flexibility. Developments of EMI shielding materials based on polythiophene and polythiophene derivatives in the doped state as composites with carbon nanomaterials were reported.⁶³⁻⁶⁶ One of the recent reports by Preetham Bhardwaj et. al. is that polythiophene graphene grafted three-dimensional carbon fibre nanocomposites with good performance in antistatic and microwave shielding applications.⁶⁶

1.6.5. Photovoltaic cells and photodiodes

Recently conjugated polymer-based photovoltaic devices have been developed vastly for their peculiar properties, including lightweight nature, flexibility, continuous conducting framework, and good energy conversion efficiency.^{33,67-73} Along with good environmental stability, and processability, the association of efficient photoconversion

Chapter 1

groups as substituents in connection with the existing conjugated framework were reported.⁶⁹ Highest power conversion efficiency in polymer photovoltaic devices is achieved with bulk heterojunction (BHJ) materials rather than single component and bilayer solar cell materials.^{33,73} Polythiophene could act as good electron donors in combination with suitable electron acceptor materials like C₆₀ that offer maximum energy efficiency up to 7 %. Carbon nanotubes are considered good electron acceptor materials in BHJ photovoltaic devices with suitable polymeric materials like polythiophene derivatives due to ballistic conduction pathways and higher carrier movements. Planar nano-heterojunctions with conducting nanomaterials such as carbon nanotubes could define excellent energy-efficient substrates for exciton dissociation.³³ The impeding factor for obtaining good energy efficiency in such devices is (i) the aggregation tendency of carbon nanotubes on dispersing with polymeric materials and (ii) intermixed state of metallic and semiconductor carbon nanotubes. The exciton dissociation and photogeneration of photovoltaic nano-heterojunction of polythiophenes and carbon nanotubes/graphene were studied.^{33,72,73} Rahman et al. demonstrated single-walled carbon nanotubes with nanostructured ITO electrodes for a photoelectric application. Here functionalized polymers were attached with carbon nanotubes with van der Waals and electrostatic interactions.⁷⁰ Later, a work was reported by Yu et al. in which covalently grafted regioregular poly(3-hexyl thiophene) with graphene was fabricated as a heterojunction photovoltaic device using a simple solution processing approach.⁶⁷ Another work by Habisreutinger and co-workers demonstrated P3HT-wrapped carbon nanotube nanocomposites to enhance the hole extraction efficiency of perovskite solar cells.⁷⁰ Recently, Ahmed et al. reported polythiophene carbon nanotube nanocomposites as counter electrodes in dye sensitized solar cells.⁷¹

1.6.6. Transistors

The area of flexible electronics with organic thin film transistors (OTFTs) and organic semiconductors is an emerging study which could potentially replace conventional inorganic semiconductor-based electronic materials.⁷⁴ Conducting polymers or other small organic molecules having semiconductor properties are attractive for their solution processability, low-cost manufacturing, lightweight and flexible nature and low-temperature synthetic routes. However, less charge mobility and the short lifetime of such electronic materials limited its application.⁷⁴⁻⁷⁶

Conducting carbon nanotubes are promising materials for integrating with conducting polymers in organic field effect transistor systems because of their one-dimensional nanostructure with electronic charge transfer capability.⁷⁶ Application of carbon nanotubes in such electronic materials still faces challenges from their self-bundling nature and practically infusible and insoluble character. A suitable combination of conducting polythiophene with carbon nanotube having electronic interaction between components and good morphology features is attractive to electronic material devices.⁷⁴⁻⁷⁶ The switching speed of transistors is directly proportional to field effect mobilities (μ) and inversely proportional to channel length (L). Reducing the line width between the printed lines increases the transistor efficiency.⁷⁴ Park and co-workers fabricated OTFT electrodes of PEDOT: PSS/CNT having a small 7 μm channel length using an electrohydrodynamic jet printing technique. They demonstrated the composite with good dimensional stability also.⁷⁴ Soon after, another work done by Lee et al. developed PEDOT/PSS composite with single-walled carbon nanotubes that was reported as an efficient bilayer thin film transistor.⁷⁷ Recently, Kandpal and co-workers prepared poly(3-hexyl thiophene) (P3HT): MoS_2 : multiwalled carbon nanotube nanocomposites and fabricated as an electrochromic diode for rectification application by utilizing redox behavior of P3HT.⁷⁸

1.6.7. Thermoelectric materials

Thermoelectric materials directly convert heat energy into electrical energy. The use of thermoelectric materials in the field of electrical energy production might promise sustainable development by converting waste heat energies released from various sources.⁷⁹ Efficiency of thermoelectric materials can be determined with good figure of merit and power factor.⁸⁰ Carbon nanotubes are striking as thermoelectric materials because of their excellent mechanical strength, high conductivity, thermal stability, low toxicity, and lightweight nature.⁷⁹⁻⁸⁴ Incorporation of conducting polymers like polythiophene in composite form would be more better thermoelectric material as it could gain ease of processability, tunable molecular structures and mechanical flexibility.^{79,81} Polythiophenes are environmentally stable, and many of the reports based on polythiophene and its derivatives show good thermal stability and low thermal conductivity; thereby, they are suitable for fabricating thermoelectric nanocomposites.⁸⁴ Recent reports on polythiophene-carbon nanotube nanocomposites, among which Hu and co-workers reported poly(3,4-ethylenedioxy thiophene)/carbon

Chapter 1

nanotube nanocomposites, which exhibited good thermoelectric performance with power factor $19.00 \pm 1.43 \mu\text{Wm}^{-1}\text{K}^{-2}$.⁷⁹ He et al. prepared thermoelectric film made up of carbon nanotubes modified with thermally cleavable polythiophenes. The substrate-free thermoelectric film was prepared by solvent evaporation with the figure of merit of 3.1×10^{-2} and power factor of $28.8 \mu\text{Wm}^{-1}\text{K}^{-2}$ at 25°C .⁸⁰

Many other applications were also reported with polythiophene-carbon nanotube nanocomposites. Ma and co-workers reported headspace solid-phase microextraction (HS-SPME) based on gas chromatography for polycyclic aromatic hydrocarbons having low boiling points. They demonstrated the experiment in real soil samples containing naphthalene, acenaphthene, 1-methyl naphthalene and fluorene.⁸⁵ Ostrovsky et al. reported an innovative auditory neuron multielectrode array interfacing using polythiophene carbon nanotube nanocomposites for clinical cochlear implant systems.⁸⁶ Kwon and co-workers reported another application of carbon nanotubes web with carboxylated polythiophenes to assist battery electrodes for high performance.⁸⁷ Literature reports of applications of polythiophene-carbon nanotube nanocomposites revealed the importance of the combination of conducting polythiophene and the conducting filler carbon nanotubes in commercial as well as industrial applications. There are many possibilities for developing innovative nanocomposites using more efficient synthetic strategies or tuning the properties of components of nanocomposites for suitable applications.

References

1. Li, L.; Qin, Z. Y.; Liang, X.; Fan, Q. Q.; Lu, Y. Q.; Wu, W. H.; Zhu, M. F. Facile Fabrication of Uniform Core-Shell Structured Carbon Nanotube-Polyaniline Nanocomposites. *J. Phys. Chem. C* **2009**, *113* (14), 5502–5507. <https://doi.org/10.1021/jp808582f>.
2. Idumah, C. I. Novel Trends in Conductive Polymeric Nanocomposites, and Bionanocomposites. *Synth. Met.* **2021**, *273*. <https://doi.org/10.1016/j.synthmet.2020.116674>.
3. Gangopadhyay, R.; De, A. Conducting Polymer Nanocomposites: A Brief Overview. *Chem. Mater.* **2000**, *12* (3), 608–622. <https://doi.org/10.1021/cm990537f>.
4. Beitollahi, H.; Dourandish, Z.; Tajik, S.; Jahani, P. M. Application of Conductive Polymer Nanocomposites. *ACS Symp. Ser.* **2022**, *1405*, 313–344. <https://doi.org/10.1021/bk-2022-1405.ch012>.
5. Neitzel, I.; Mochalin, V.; Gogotsi, Y. Advances in Surface Chemistry of Nanodiamond and Nanodiamond-Polymer Composites. *Ultrananocrystalline Diam. Synth. Prop. Appl. Second Ed.* **2012**, 421–456. <https://doi.org/10.1016/B978-1-4377-3465-2.00013-X>.
6. Dakshayini, B. S.; Reddy, K. R.; Mishra, A.; Shetti, N. P.; Malode, S. J.; Basu, S.; Naveen, S.; Raghu, A. V. Role of Conducting Polymer and Metal Oxide-Based Hybrids for

- Applications in Amperometric Sensors and Biosensors. *Microchem. J.* **2019**, *147*, 7–24. <https://doi.org/10.1016/j.microc.2019.02.061>.
7. Kumar, G. G.; Kirubaharan, C. J.; Udhayakumar, S.; Karthikeyan, C.; Nahm, K. S. Conductive Polymer/Graphene Supported Platinum Nanoparticles as Anode Catalysts for the Extended Power Generation of Microbial Fuel Cells. *Ind. Eng. Chem. Res.* **2014**, *53* (43), 16883–16893. <https://doi.org/10.1021/ie502399y>.
 8. Pecher, J.; Mecking, S. Nanoparticles of Conjugated Polymers. *Chem. Rev.* **2010**, *110* (10), 6260–6279. <https://doi.org/10.1021/cr100132y>.
 9. Ibanez, J. G.; Rincón, M. E.; Gutierrez-Granados, S.; Chahma, M.; Jaramillo-Quintero, O. A.; Frontana-Uribe, B. A. Conducting Polymers in the Fields of Energy, Environmental Remediation, and Chemical-Chiral Sensors. *Chem. Rev.* **2018**, *118* (9), 4731–4816. <https://doi.org/10.1021/acs.chemrev.7b00482>.
 10. Salvatierra, R. V.; Oliveira, M. M.; Zarbin, A. J. G. One-Pot Synthesis and Processing of Transparent, Conducting, and Freestanding Carbon Nanotubes/Polyaniline Composite Films. *Chem. Mater.* **2010**, *22* (18), 5222–5234. <https://doi.org/10.1021/cm1012153.BHBH>
 11. Feast, W. J.; Tsibouklis, J.; Pouwer, K. L.; Groenendaal, L.; Meijer, E. W. Synthesis, Processing and Material Properties of Conjugated Polymers. *Polymer (Guildf)*. **1996**, *37* (22), 5017–5047. [https://doi.org/10.1016/0032-3861\(96\)00439-9](https://doi.org/10.1016/0032-3861(96)00439-9).
 12. Das, S.; Chatterjee, D. P.; Ghosh, R.; Nandi, A. K. Water Soluble Polythiophenes: Preparation and Applications. *RSC Adv.* **2015**, *5* (26), 20160–20177. <https://doi.org/10.1039/c4ra16496b>.
 13. Kaloni, T. P.; Giesbrecht, P. K.; Schreckenbach, G.; Freund, M. S. Polythiophene: From Fundamental Perspectives to Applications. *Chem. Mater.* **2017**, *29* (24), 10248–10283. <https://doi.org/10.1021/acs.chemmater.7b03035>.
 14. Baleg, A. A.; Masikini, M.; John, S. V.; Williams, A. R.; Jahed, N.; Baker, P.; Iwuoha, E. Conducting Polymers and Composites. **2018**, 1–54. https://doi.org/10.1007/978-3-319-92067-2_17-1.
 15. Marshall, N.; James, W.; Fulmer, J.; Crittenden, S.; Thompson, A. B.; Ward, P. A.; Rowe, G. T. Polythiophene Doping of the Cu-Based Metal-Organic Framework (MOF) HKUST-1 Using Innate MOF-Initiated Oxidative Polymerization. *Inorg. Chem.* **2019**, *58* (9), 5561–5575. <https://doi.org/10.1021/acs.inorgchem.8b03465>.
 16. Jayasundara, W. J. M. J. S. R.; Schreckenbach, G. Theoretical Study of P-and n-Doping of Polythiophene-and Polypyrrole-Based Conjugated Polymers. *J. Phys. Chem. C* **2020**, *124* (32), 17528–17537. <https://doi.org/10.1021/acs.jpcc.0c05109>.
 17. Ponomarenko, A. T.; Shevchenko, V. G.; Enikolopyan, N. S. Formation Processes and Properties of Conducting Polymer Composites. *Adv. Polym. Sci.* **1990**, *96*, 124–147. https://doi.org/10.1007/3-540-52791-5_4.
 18. Liu, J.; Tanaka, T.; Sivula, K.; Alivisatos, A. P.; Fréchet, J. M. J. Employing End-Functional Polythiophene to Control the Morphology of Nanocrystal - Polymer Composites in Hybrid Solar Cells. *J. Am. Chem. Soc.* **2004**, *126* (21), 6550–6551. <https://doi.org/10.1021/ja0489184>.
 19. Nishi, N.; Yajima, I.; Amano, K. I.; Sakka, T. Janus-Type Gold/Polythiophene Composites Formed via Redox Reaction at the Ionic Liquid|Water Interface. *Langmuir* **2018**, *34* (7), 2441–2447. <https://doi.org/10.1021/acs.langmuir.7b03792.Cfcf>
 20. Velayudham, S.; Lee, C. H.; Xie, M.; Blair, D.; Bauman, N.; Yap, Y. K.; Green, S. A.; Liu, H. Noncovalent Functionalization of Boron Nitride Nanotubes with Poly(p-Phenylene-Ethynylene)s and Polythiophene. *ACS Appl. Mater. Interfaces* **2010**, *2* (1), 104–110. <https://doi.org/10.1021/am900613j.Ggf>
 21. Zhan, C.; Yu, G.; Lu, Y.; Wang, L.; Wujcik, E.; Wei, S. Conductive Polymer Nanocomposites: A Critical Review of Modern Advanced Devices. *J. Mater. Chem. C* **2017**, *5* (7), 1569–1585. <https://doi.org/10.1039/c6tc04269d.Bvv>
 22. Husain, A.; Ahmad, S.; Mohammad, F. Synthesis, Characterisation and Ethanol Sensing Application of Polythiophene/Graphene Nanocomposite. *Mater. Chem. Phys.* **2020**, *239*, 122324. <https://doi.org/10.1016/j.matchemphys.2019.122324>.

Chapter 1

23. Kuila, B. K.; Malik, S.; Batabyal, S. K.; Nandi, A. K. In-Situ Synthesis of Soluble Poly(3-Hexylthiophene)/Multiwalled Carbon Nanotube Composite: Morphology, Structure, and Conductivity. *Macromolecules* **2007**, *40* (2), 278–287. <https://doi.org/10.1021/ma061548e>.
24. Pascariu, P.; Airinei, A.; Grigoras, M.; Vacareanu, L.; Iacomi, F. Metal-Polymer Nanocomposites Based on Ni Nanoparticles and Polythiophene Obtained by Electrochemical Method. *Appl. Surf. Sci.* **2015**, *352*, 95–102. <https://doi.org/10.1016/j.apsusc.2015.03.063>.
25. Taj, M.; Manohara, S. R.; Hanagodimath, S. M.; Gerward, L. Novel Conducting Poly(3,4-Ethylenedioxythiophene) – Graphene Nanocomposites with Gigantic Dielectric Properties and Narrow Optical Energy Band Gap. *Polym. Test.* **2020**, *90*. <https://doi.org/10.1016/j.polymertesting.2020.106650>.
26. Aradilla, D.; Azambuja, D.; Estrany, F.; Casas, M. T.; Ferreira, C. A.; Alemán, C. Hybrid Polythiophene-Clay Exfoliated Nanocomposites for Ultracapacitor Devices. *J. Mater. Chem.* **2012**, *22* (26), 13110–13122. <https://doi.org/10.1039/c2jm31372c>.
27. (1) Nezakati, T.; Seifalian, A.; Tan, A.; Seifalian, A. M. Conductive Polymers: Opportunities and Challenges in Biomedical Applications. *Chem. Rev.* **2018**, *118* (14), 6766–6843. <https://doi.org/10.1021/acs.chemrev.6b00275>.
28. Du, Y.; Shen, S. Z.; Cai, K.; Casey, P. S. Research Progress on Polymer-Inorganic Thermoelectric Nanocomposite Materials. *Prog. Polym. Sci.* **2012**, *37* (6), 820–841. <https://doi.org/10.1016/j.progpolymsci.2011.11.003>.
29. Yuan, W.; Chan-Park, M. B. Covalent Cum Noncovalent Functionalizations of Carbon Nanotubes for Effective Reinforcement of a Solution Cast Composite Film. *ACS Appl. Mater. Interfaces* **2012**, *4* (4), 2065–2073. <https://doi.org/10.1021/am300038d>.
30. Charoughchi, S.; Agbolaghi, S.; Aghapour, S.; Sarvari, R.; Abbasi, F. Polymer Wrapping: Versus Well-Oriented Crystal Growth of Polythiophenes onto Multi-Wall Carbon Nanotubes via Surface Chemical Modification and Regioregularity Deliberation. *New J. Chem.* **2018**, *42* (17), 14469–14480. <https://doi.org/10.1039/c8nj01110a>.
31. Ferguson, A. J.; Blackburn, J. L.; Holt, J. M.; Kopidakis, N.; Tenent, R. C.; Barnes, T. M.; Heben, M. J.; Rumbles, G. Photoinduced Energy and Charge Transfer in P3HT:SWNT Composites. *J. Phys. Chem. Lett.* **2010**, *1* (15), 2406–2411. <https://doi.org/10.1021/jz100768f>.
32. Philip, B.; Xie, J.; Chandrasekhar, A.; Abraham, J.; Varadan, V. K. A Novel Nanocomposite from Multiwalled Carbon Nanotubes Functionalized with a Conducting Polymer. *Smart Mater. Struct.* **2004**, *13* (2), 295–298. <https://doi.org/10.1088/0964-1726/13/2/007>.
33. Kim, H. J.; Koizhaiganova, R. B.; Karim, M. R.; Lee, G. H.; Vasudevan, T.; Lee, M. S. Synthesis and Characterization of Poly(3-Octylthiophene)/Single Wall Carbon Nanotube Composites for Photovoltaic Applications. *J. Appl. Polym. Sci.* **2010**, *118* (3), 1386–1394. <https://doi.org/10.1002/app.32436>.
34. Liang, L.; Xie, W.; Fang, S.; He, F.; Yin, B.; Tlili, C.; Wang, D.; Qiu, S.; Li, Q. High-Efficiency Dispersion and Sorting of Single-Walled Carbon Nanotubes: Via Non-Covalent Interactions. *J. Mater. Chem. C* **2017**, *5* (44), 11339–11368. <https://doi.org/10.1039/c7tc04390b>.
35. Olalde, B.; Aizpurua, J. M.; García, A.; Bustero, I.; Obieta, I.; Jurado, M. J. Single-Walled Carbon Nanotubes and Multiwalled Carbon Nanotubes Functionalized with Poly(L-Lactic Acid): A Comparative Study. *J. Phys. Chem. C* **2008**, *112* (29), 10663–10667. <https://doi.org/10.1021/jp800266j>.
36. (1) Gulotty, R.; Castellino, M.; Jagdale, P.; Tagliaferro, A.; Balandin, A. A. Effects of Functionalization on Thermal Properties of Single-Wall and Multi-Wall Carbon Nanotube-Polymer Nanocomposites. *ACS Nano* **2013**, *7* (6), 5114–5121. <https://doi.org/10.1021/nn400726g>.
37. Müller, K.; Bugnicourt, E.; Latorre, M.; Jorda, M.; Sanz, Y. E.; Lagaron, J. M.; Miesbauer, O.; Bianchin, A.; Hankin, S.; Bölz, U.; Pérez, G.; Jesdinszki, M.; Lindner, M.; Scheuerer, Z.; Castelló, S.; Schmid, M. Review on the Processing and Properties of Polymer

- Nanocomposites and Nanocoatings and Their Applications in the Packaging, Automotive and Solar Energy Fields. *Nanomaterials* **2017**, *7* (4). <https://doi.org/10.3390/nano7040074>.
38. Zhang, X.; Liu, J.; Xu, B.; Su, Y.; Luo, Y. Ultralight Conducting Polymer/Carbon Nanotube Composite Aerogels. *Carbon N. Y.* **2011**, *49* (6), 1884–1893. <https://doi.org/10.1016/j.carbon.2011.01.011>.
 39. Cheng, H.; Medina, L.; Duong, H. M. Free-Standing PEDOT:PSS/CNT Aerogels and Their Electrochemical Performance. *Mater. Technol.* **2017**, *32* (10), 622–629. <https://doi.org/10.1080/10667857.2017.1336874>.
 40. Idumah, C. I.; Ezika, A. C.; Okpechi, V. U. Emerging Trends in Polymer Aerogel Nanoarchitectures, Surfaces, Interfaces and Applications. *Surfaces and Interfaces* **2021**, *25*, 101258. <https://doi.org/10.1016/j.surfin.2021.101258>.
 41. (a) Sun, X.; Wei, Y.; Li, J.; Zhao, J.; Zhao, L.; Li, Q. Ultralight Conducting PEDOT:PSS/Carbon Nanotube Aerogels Doped with Silver for Thermoelectric Materials. *Sci. China Mater.* **2017**, *60* (2), 159–166. <https://doi.org/10.1007/s40843-016-5132-8>. (b) Hu, L.; Hecht, D. S.; Grüner, G. Carbon Nanotube Thin Films: Fabrication, Properties, and Applications. *Chem. Rev.* **2010**, *110* (10), 5790–5844. <https://doi.org/10.1021/cr9002962>.
 42. Wang, F.; Yang, Y.; Swager, T. M. Molecular Recognition for High Selectivity in Carbon Nanotube/Polythiophene Chemiresistors. *Angew. Chemie - Int. Ed.* **2008**, *47* (44), 8394–8396. <https://doi.org/10.1002/anie.200802762>.
 43. Liyanage, L. S.; Lee, H.; Patil, N.; Park, S.; Mitra, S.; Bao, Z.; Wong, H. S. P. Wafer-Scale Fabrication and Characterization of Thin-Film Transistors with Polythiophene-Sorted Semiconducting Carbon Nanotube Networks. *ACS Nano* **2012**, *6* (1), 451–458. <https://doi.org/10.1021/nn203771u>.
 44. Husain, A.; Ahmad, S.; Shariq, M. U.; Khan, M. M. A. Ultra-Sensitive, Highly Selective and Completely Reversible Ammonia Sensor Based on Polythiophene/SWCNT Nanocomposite. *Materialia* **2020**, *10*. <https://doi.org/10.1016/j.mtla.2020.100704>.
 45. Husain, A.; Ahmad, S.; Mohammad, F. Electrical Conductivity and Ammonia Sensing Studies on Polythiophene/MWCNTs Nanocomposites. *Materialia* **2020**, *14*. <https://doi.org/10.1016/j.mtla.2020.100868>. bhhb
 46. Raju, V.; Rani, J. V.; Basak, P. One-Dimensional Polythiophene/Multi-Walled Carbon Nanotube Composite Cathodes for Rechargeable Magnesium Battery: Evidence of Improved Stability and Electrochemically Induced Rearrangement in Electrode Morphology. *Electrochim. Acta* **2022**, *404*, 139707. <https://doi.org/10.1016/j.electacta.2021.139707>.
 47. Singh, R.; Shrivastava, A. K.; Bajpai, A. K. Cdse Reinforced Polythiophene Nanocomposites as Excellent Materials for Diode Applications. *Express Polym. Lett.* **2021**, *15* (1), 45–57. <https://doi.org/10.3144/expresspolymlett.2021.6>.
 48. Chen, J.; Jia, C.; Wan, Z. The Preparation and Electrochemical Properties of MnO₂/Poly(3,4-Ethylenedioxythiophene)/Multiwalled Carbon Nanotubes Hybrid Nanocomposite and Its Application in a Novel Flexible Micro-Supercapacitor. *Electrochim. Acta* **2014**, *121*, 49–56. <https://doi.org/10.1016/j.electacta.2013.12.137>.
 49. Zhang, Y.; Bunes, B. R.; Wu, N.; Ansari, A.; Rajabali, S.; Zang, L. Sensing Methamphetamine with Chemiresistive Sensors Based on Polythiophene-Blended Single-Walled Carbon Nanotubes. *Sensors Actuators, B Chem.* **2018**, *255*, 1814–1818. <https://doi.org/10.1016/j.snb.2017.08.201>.
 50. Wang, F.; Gu, H.; Swager, T. M. Carbon Nanotube/Polythiophene Chemiresistive Sensors for Chemical Warfare Agents. *J. Am. Chem. Soc.* **2008**, *130* (16), 5392–5393. <https://doi.org/10.1021/ja710795k>.
 51. Saha, S.; Singh, J. P.; Saha, U.; Goswami, T. H.; Rao, K. U. B. Structure-Property Relationship of SELF-Sustained Homogeneous Ternary Nanocomposites: Key Issues to Evaluate Properties of RrP3HT Wrapped MWNT Dispersed in TPU. *Compos. Sci. Technol.* **2011**, *71* (3), 397–405. <https://doi.org/10.1016/j.compscitech.2010.12.005>.

52. Wan, J.; Si, Y.; Li, C.; Zhang, K. Bisphenol a Electrochemical Sensor Based on Multi-Walled Carbon Nanotubes/Polythiophene/Pt Nanocomposites Modified Electrode. *Anal. Methods* **2016**, *8* (16), 3333–3338. <https://doi.org/10.1039/c6ay00850j>.
53. Inagaki, C. S.; Oliveira, M. M.; Bergamini, M. F.; Marcolino-Junior, L. H.; Zarbin, A. J. G. Facile Synthesis and Dopamine Sensing Application of Three Component Nanocomposite Thin Films Based on Polythiophene, Gold Nanoparticles and Carbon Nanotubes. *J. Electroanal. Chem.* **2019**, *840*, 208–217. <https://doi.org/10.1016/j.jelechem.2019.03.066>.
54. Dhibar, S.; Bhattacharya, P.; Ghosh, D.; Hatui, G.; Das, C. K. Graphene-Single-Walled Carbon Nanotubes-Poly(3-Methylthiophene) Ternary Nanocomposite for Supercapacitor Electrode Materials. *Ind. Eng. Chem. Res.* **2014**, *53* (33), 13030–13045. <https://doi.org/10.1021/ie501407k>.
55. Oliveira, M. M.; Zarbin, A. J. G. Carbon Nanotubes Decorated with Both Gold Nanoparticles and Polythiophene. *J. Phys. Chem. C* **2008**, *112* (48), 18783–18786. <https://doi.org/10.1021/jp8052482>.
56. Zhang, H.; Hu, Z.; Li, M.; Hu, L.; Jiao, S. A High-Performance Supercapacitor Based on a Polythiophene/Multiwalled Carbon Nanotube Composite by Electropolymerization in an Ionic Liquid Microemulsion. *J. Mater. Chem. A* **2014**, *2* (40), 17024–17030. <https://doi.org/10.1039/c4ta03369h>.
57. Wang, G.; Zhang, L.; Zhang, J. A Review of Electrode Materials for Electrochemical Supercapacitors. *Chem. Soc. Rev.* **2012**, *41* (2), 797–828. <https://doi.org/10.1039/c1cs15060j>.
58. Lota, K.; Khomenko, V.; Frackowiak, E. Capacitance Properties of Poly(3,4-Ethylenedioxythiophene)/Carbon Nanotubes Composites. *J. Phys. Chem. Solids* **2004**, *65* (2–3), 295–301. <https://doi.org/10.1016/j.jpcs.2003.10.051>.
59. Balakrishnan, K.; Kumar, M.; Subramania, A. Synthesis of Polythiophene and Its Carbonaceous Nanofibers as Electrode Materials for Asymmetric Supercapacitors. *Adv. Mater. Res.* **2014**, *938*, 151–157. <https://doi.org/10.4028/www.scientific.net/AMR.938.151>.
60. Shokry, A.; Karim, M.; Khalil, M.; Ebrahim, S.; El Nady, J. Supercapacitor Based on Polymeric Binary Composite of Polythiophene and Single-Walled Carbon Nanotubes. *Sci. Rep.* **2022**, *12* (1). <https://doi.org/10.1038/s41598-022-15477-z>.
61. Zhang, X.; Wang, X.; Lei, Z.; Wang, L.; Tian, M.; Zhu, S.; Xiao, H.; Tang, X.; Qu, L. Flexible MXene-Decorated Fabric with Interwoven Conductive Networks for Integrated Joule Heating, Electromagnetic Interference Shielding, and Strain Sensing Performances. *ACS Appl. Mater. Interfaces* **2020**, *12* (12), 14459–14467. <https://doi.org/10.1021/acsami.0c01182>.
62. Luo, X.; Chung, D. D. L. Electromagnetic Interference Shielding Using Continuous Carbon-Fiber Carbon-Matrix and Polymer-Matrix Composites. *Compos. Part B Eng.* **1999**, *30* (3), 227–231. [https://doi.org/10.1016/S1359-8368\(98\)00065-1](https://doi.org/10.1016/S1359-8368(98)00065-1).
63. Saini, P.; Aror, M. Microwave Absorption and EMI Shielding Behavior of Nanocomposites Based on Intrinsically Conducting Polymers, Graphene and Carbon Nanotubes. *New Polym. Spec. Appl.* **2012**. <https://doi.org/10.5772/48779>.
64. Kulkarni, G.; Kandesar, P.; Velhal, N.; Phadtare, V.; Jatrakar, A.; Shinde, S. K.; Kim, D. Y.; Puri, V. Exceptional Electromagnetic Interference Shielding and Microwave Absorption Properties of Room Temperature Synthesized Polythiophene Thin Films with Double Negative Characteristics (DNG) in the Ku-Band Region. *Chem. Eng. J.* **2019**, *355*, 196–207. <https://doi.org/10.1016/j.cej.2018.08.114>.
65. Wu, G.; Chen, Y.; Zhan, H.; Chen, H. T.; Lin, J. H.; Wang, J. N.; Wan, L. Q.; Huang, F. R. Ultrathin and Flexible Carbon Nanotube/Polymer Composite Films with Excellent Mechanical Strength and Electromagnetic Interference Shielding. *Carbon N. Y.* **2020**, *158*, 472–480. <https://doi.org/10.1016/j.carbon.2019.11.014>.
66. Bhardwaj, P.; Grace, A. N. Antistatic and Microwave Shielding Performance of Polythiophene-Graphene Grafted 3-Dimensional Carbon Fibre Composite. *Diam. Relat. Mater.* **2020**, *106*. <https://doi.org/10.1016/j.diamond.2020.107871>.

67. Yu, D.; Yang, Y.; Durstock, M.; Baek, J. B.; Dai, L. Soluble P3HT-Grafted Graphene for Efficient Bilayer-Heterojunction Photovoltaic Devices. *ACS Nano* **2010**, *4* (10), 5633–5640. <https://doi.org/10.1021/nn101671t>.
68. Kim, H. J.; Koizhaiganova, R. B.; Karim, M. R.; Lee, G. H.; Vasudevan, T.; Lee, M. S. Synthesis and Characterization of Poly(3-Octylthiophene)/Single Wall Carbon Nanotube Composites for Photovoltaic Applications. *J. Appl. Polym. Sci.* **2010**, *118* (3), 1386–1394. <https://doi.org/10.1002/app.32436>.
69. Rahman, G. M. A.; Guldi, D. M.; Cagnoli, R.; Mucci, A.; Schenetti, L.; Vaccari, L.; Prato, M. Combining Single Wall Carbon Nanotubes and Photoactive Polymers for Photoconversion. *J. Am. Chem. Soc.* **2005**, *127* (28), 10051–10057. <https://doi.org/10.1021/ja050396k>.
70. Habisreutinger, S. N.; Leijtens, T.; Eperon, G. E.; Stranks, S. D.; Nicholas, R. J.; Snaith, H. J. Enhanced Hole Extraction in Perovskite Solar Cells through Carbon Nanotubes. *J. Phys. Chem. Lett.* **2014**, *5* (23), 4207–4212. <https://doi.org/10.1021/jz5021795>.
71. Ahmad, Z.; Farooq, E.; Nazar, R.; Mehmood, U.; Fareed, I. Development of Multi-Walled Carbon Nanotube/Polythiophene (MWCNT/PTh) Nanocomposites for Platinum-Free Dye-Sensitized Solar Cells (DSSCs). *Sol. Energy* **2022**, *245*, 153–157. <https://doi.org/10.1016/j.solener.2022.09.010>.
72. Bindl, D. J.; Safron, N. S.; Arnold, M. S. Dissociating Excitons Photogenerated in Semiconducting Carbon Nanotubes at Polymeric Photovoltaic Heterojunction Interfaces. *ACS Nano* **2010**, *4* (10), 5657–5664. <https://doi.org/10.1021/nn1012397>.
73. Ham, M. H.; Paulus, G. L. C.; Lee, C. Y.; Song, C.; Kalantar-Zadeh, K.; Choi, W.; Han, J. H.; Strano, M. S. Evidence for High-Efficiency Exciton Dissociation at Polymer/Single-Walled Carbon Nanotube Interfaces in Planar Nano-Heterojunction Photovoltaics. *ACS Nano* **2010**, *4* (10), 6251–6259. <https://doi.org/10.1021/nn1019384>.
74. Park, S. H.; Kim, J.; Lee, S.; Lee, D. Y.; Lim, S.; Lee, J.; Kim, S. H. Organic Thin-Film Transistors with Sub-10-Micrometer Channel Length with Printed Polymer/Carbon Nanotube Electrodes. *Org. Electron.* **2018**, *52*, 165–171. <https://doi.org/10.1016/j.orgel.2017.10.023>.
75. Park, S. J.; Lee, J.; Seo, S. E.; Kim, K. H.; Park, C. S.; Lee, S. H.; Ban, H. S.; Lee, B. D.; Song, H. S.; Kim, J.; Lee, C. S.; Bae, J.; Kwon, O. S. High-Performance Conducting Polymer Nanotube-Based Liquid-Ion Gated Field-Effect Transistor Aptasensor for Dopamine Exocytosis. *Sci. Rep.* **2020**, *10* (1). <https://doi.org/10.1038/s41598-020-60715-x>.
76. Liyanage, L. S.; Lee, H.; Patil, N.; Park, S.; Mitra, S.; Bao, Z.; Wong, H. S. P. Wafer-Scale Fabrication and Characterization of Thin-Film Transistors with Polythiophene-Sorted Semiconducting Carbon Nanotube Networks. *ACS Nano* **2012**, *6* (1), 451–458. <https://doi.org/10.1021/nn203771u>.
77. Lee, T.; Kwon, W.; Park, M. Highly Conductive, Transparent and Metal-Free Electrodes with a PEDOT:PSS/SWNT Bilayer for High-Performance Organic Thin Film Transistors. *Org. Electron.* **2019**, *67*, 26–33. <https://doi.org/10.1016/j.orgel.2019.01.008>.
78. Kandpal, S.; Ghosh, T.; Rani, C.; Tanwar, M.; Sharma, M.; Rani, S.; Pathak, D. K.; Bhatia, R.; Sameera, I.; Jayabalan, J.; Kumar, R. Bifunctional Application of Viologen-MoS₂-CNT/Polythiophene Device as Electrochromic Diode and Half-Wave Rectifier. *ACS Mater. Au* **2021**, *2* (3), 293–300. <https://doi.org/10.1021/acsmaterialsau.1c00064>.
79. He, P.; Shimano, S.; Salikolimi, K.; Isoshima, T.; Kakefuda, Y.; Mori, T.; Taguchi, Y.; Ito, Y.; Kawamoto, M. Noncovalent Modification of Single-Walled Carbon Nanotubes Using Thermally Cleavable Polythiophenes for Solution-Processed Thermoelectric Films. *ACS Appl. Mater. Interfaces* **2019**, *11* (4), 4211–4218. <https://doi.org/10.1021/acsami.8b14820>.
80. Yu, C.; Choi, K.; Yin, L.; Grunlan, J. C. Light-Weight Flexible Carbon Nanotube Based Organic Composites with Large Thermoelectric Power Factors. *ACS Nano* **2011**, *5* (10), 7885–7892. <https://doi.org/10.1021/nn202868a>.
81. Tonga, M.; Wei, L.; Wilusz, E.; Korugic-Karasz, L.; Karasz, F. E.; Lahti, P. M. Solution-Fabrication Dependent Thermoelectric Behavior of Iodine-Doped Regioregular and

Chapter 1

- Regiorandom P3HT/Carbon Nanotube Composites. *Synth. Met.* **2018**, *239*, 51–58. <https://doi.org/10.1016/j.synthmet.2018.03.007>.
82. Wang, D.; Su, Y.; Chen, D.; Wang, L.; Xiang, X.; Zhu, D. Preparation and Characterization of Poly(3-Octylthiophene)/Carbon Fiber Thermoelectric Composite Materials. *Compos. Part B Eng.* **2015**, *69*, 467–471. <https://doi.org/10.1016/j.compositesb.2014.10.007>.
83. Hu, X.; Chen, G.; Wang, X. An Unusual Coral-like Morphology for Composites of Poly(3,4-Ethylenedioxythiophene)/Carbon Nanotube and the Enhanced Thermoelectric Performance. *Compos. Sci. Technol.* **2017**, *144*, 43–50. <https://doi.org/10.1016/j.compscitech.2017.03.018>.
84. Wang, L.; Jia, X.; Wang, D.; Zhu, G.; Li, J. Preparation and Thermoelectric Properties of Polythiophene/Multiwalled Carbon Nanotube Composites. *Synth. Met.* **2013**, *181*, 79–85. <https://doi.org/10.1016/j.synthmet.2013.08.011>.
85. Ma, X.; Huang, P.; Dang, X.; Ai, Y.; Zheng, D.; Chen, H. MWCNTs/MnO₂ Nanocomposite-Based Polythiophene Coating for Solid-Phase Microextraction and Determination of Polycyclic Aromatic Hydrocarbons in Soil. *Microchem. J.* **2019**, *146*, 1026–1032. <https://doi.org/10.1016/j.microc.2019.02.031>.
86. Ostrovsky, S.; Hahnwald, S.; Kiran, R.; Mistrik, P.; Hessler, R.; Tscherter, A.; Senn, P.; Kang, J.; Kim, J.; Roccio, M.; Lellouche, J. P. Conductive Hybrid Carbon Nanotube (CNT)-Polythiophene Coatings for Innovative Auditory Neuron-Multi-Electrode Array Interfacing. *RSC Adv.* **2016**, *6* (48), 41714–41723. <https://doi.org/10.1039/c5ra27642j>.
87. Kwon, Y. H.; Park, J. J.; Housel, L. M.; Minnici, K.; Zhang, G.; Lee, S. R.; Lee, S. W.; Chen, Z.; Noda, S.; Takeuchi, E. S.; Takeuchi, K. J.; Marschilok, A. C.; Reichmanis, E. Carbon Nanotube Web with Carboxylated Polythiophene “Assist” for High-Performance Battery Electrodes. *ACS Nano* **2018**, *12* (4), 3126–3139. <https://doi.org/10.1021/acsnano.7b08918>.

Chapter 2

AOT Assisted Preparation of Polythiophene- MWCNT Core-shell Nanocomposites

Chapter 2

2.1. Introduction

Conducting polymer-carbon nanotube nanocomposites are suitable materials for fabricating electrochemical sensors, supercapacitors, thermoelectric devices, solar cell devices, micro-electro-mechanical systems (MEMS), corrosion resistive coatings, temperature sensors, and electromagnetic interference shielding (EMI) devices.¹⁻¹² Conducting polymer-carbon nanotube composite materials have distinctive and superior control in many properties like enhanced electrical conductivity, efficient electromagnetic wave absorbing character, sharper electrochemical responses, thermal conductivity, optical tunability, and mechanical stability.^{11,13-16} The specific properties achieved by nanocomposite formation could determine its performance in device fabrication. The properties are very much dependent on the structure and constitution of nanocomposites.^{11,17,18} The structure-property relationships set in the nanocomposites could also result from the order of nano dimensions involved in nanomaterials. Another advantage of using nanocomposites is that they could provide modified properties than their components.¹³⁻²¹ Different conducting polymers such as polyaniline, polypyrrole, polythiophene, polyphenylenevinylene and their derivatives were reported as suitable for nanocomposite preparation.^{22,23} Amongst conducting polymers, polythiophene and its derivatives are significant due to their unique electrical, thermal and optical properties. Besides that, polythiophene exhibits good environmental stability also.²²⁻²⁷ Multiwalled carbon nanotubes (CNTs) are suitable materials for preparing nanocomposites with conducting polymers. Multiwalled carbon nanotubes possess a unique one-dimensional structure, large surface-to-volume ratio, stiffness, conductive nature and high mechanical strength. Carbon nanotubes find many applications in broad areas such as chemical sensors, field emission materials, hydrogen energy storage, nano-electronic devices, catalyst support and so on.²⁸⁻³⁴

Creating well-dispersed forms of pristine carbon nanotubes is challenging due to their high aspect ratio and self-aggregating property. Nano-dispersion of carbon nanotubes can be achieved by chemical strategies such as polymer nanocomposite formation, physical mixing with suitable stabilizing agents like block co-polymers, or surfactants as dispersants. Nanocomposite formation with suitable organic polymers is an attractive way of forming nano-dispersion, since it involves inexpensive and easy synthetic approaches.³¹⁻⁴⁰ The polymer-carbon nanotube nanocomposites formation can be accomplished viz; in-situ polymerization of monomer in the presence of dispersed

CNT or post-polymerization mixing of polymer and CNT.^{15,41,42} In-situ polymerization is the appropriate method for creating nanocomposite, if the monomer is soluble in suitable solvents and the polymer formed is insoluble. The post-polymerization mixing could not be taken as an able method if the polymer has insolubility in mixing solvent. Thiophene monomer is readily soluble in almost all organic solvents; thus, in-situ polymerization can be carried out for nanocomposite preparation. Three methods of polythiophene preparation are generally reported; electropolymerization, metal-catalyzed coupling reactions and oxidative chemical polymerization.⁴³ Chemical oxidative polymerization is advantageous for bulk polymer production in a short reaction time and with a simple reaction setup.⁴⁴ Ferric chloride (FeCl_3) is the most common oxidizing agent used for the oxidative polymerization of thiophene (see **Figure 2.1. a**).^{41,42,44} In-situ polymerization of thiophene in the presence of carbon nanotubes produces polythiophene-CNT nanocomposites (see **figure 2.1. b**). The sonication method can be used to create a dispersion of carbon nanotubes. Mild bath sonication helps to disperse carbon nanotubes without making many defects to the CNT's electronic structure.

In-situ chemical oxidative polymerization

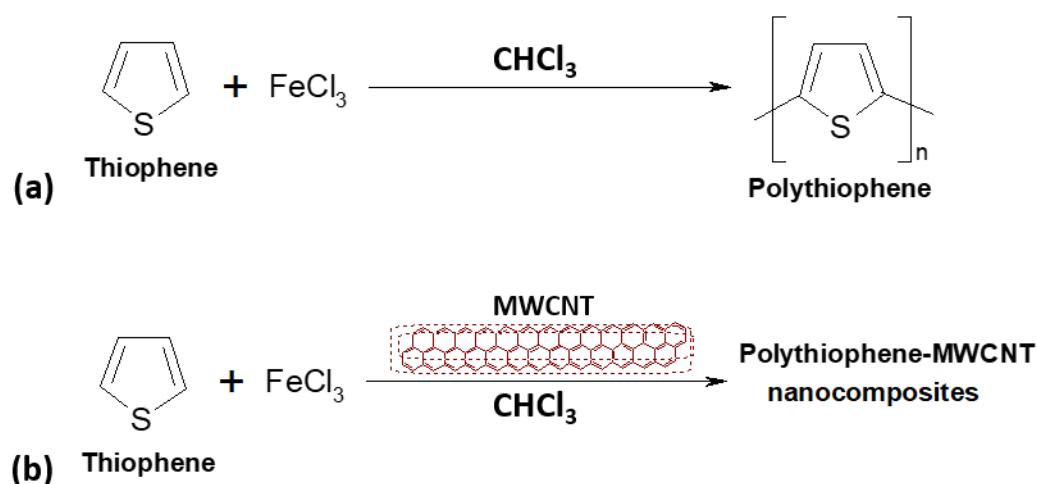


Figure 2.1. (a) Scheme for oxidative chemical polymerization of thiophene using FeCl_3 oxidant and (b) in-situ chemical oxidative polymerization of polythiophene with multiwalled carbon nanotubes (MWCNT) for nanocomposite preparation.

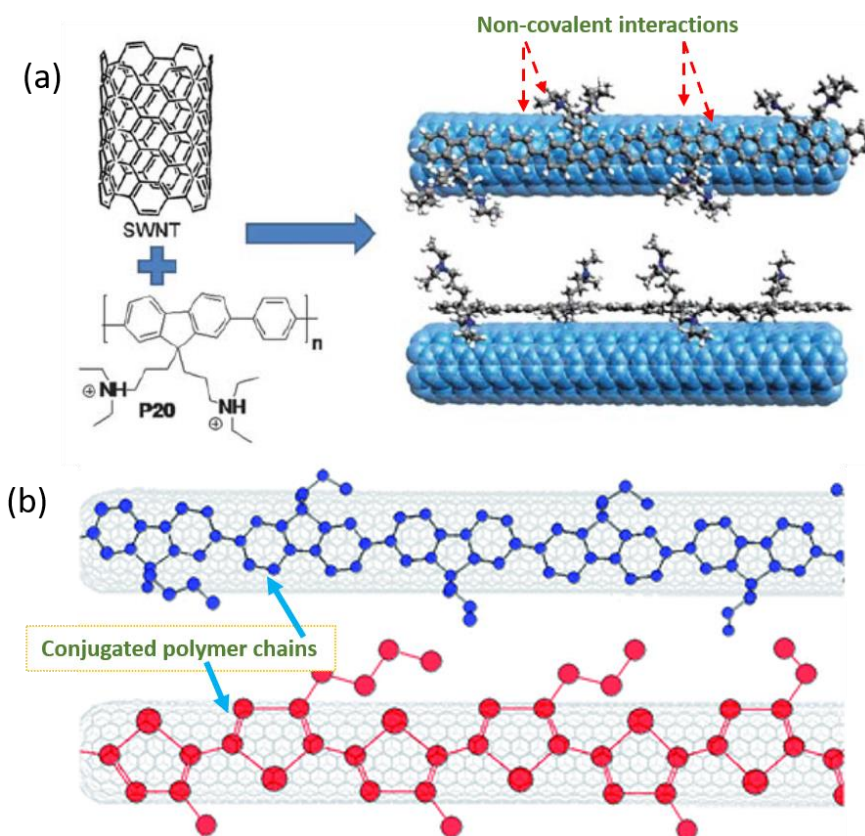


Figure 2.2. (a) Schematic representation of interaction of carbon nanotubes with poly(9,9-bis (diethylaminopropyl)-2,7-fluorene-co-1,4-phenylene). (Adapted from Casagrande et al. 2010) and (b) illustration of the interaction of carbon nanotubes and different conducting polymers (Adapted from Tuncel 2011).

Polybenzimidazole, polyaniline, polypyrrole, polyphenylenes, polyphenylenevinylenes, their substituted derivatives and co-polymers could act as suitable conjugated polymer materials for nanocomposite preparation with carbon nanotubes (see **Figure 2.2.**).³⁵ Conjugated polymers interact with carbon nanotube surfaces via π - π stacking and van der Waals interactions leading to wrapping or adsorptive non-helical interaction. Zhai et al. functionalized carbon nanotubes with conjugated block copolymers having non-conjugated blocks, which provided tunable functionality.³⁹ Lin and co-workers studied conducting polymers and reported that polymers structurally similar to CNT could act as suitable aspirants for surface functionalization.⁴⁵ Mandal et al. prepared MWCNT nanocomposite with the polymer compatibilizer containing thiophene moiety substituted with poly(dimethylamino ethyl methacrylate) (PDMAEMA) group. The authors pointed out that non-covalent functionalization on MWCNT is superior to covalent functionalization to enhance its mechanical and

Chapter 2

electrical conductivity properties with poly(vinylidene fluoride).⁴⁶ Cho et al. designed structurally tailored multi-amphiphilic compatibilizers of pyrene-functionalized block co-polymers to attach to the walls of multiwalled carbon nanotubes (see **Figure 2.3.**). Non-covalent functionalization of CNT's surface with multi-amphiphilic compatibilizer improved dispersion stability, solubility manipulation, and hybridization with silver nanoparticles.⁴⁷

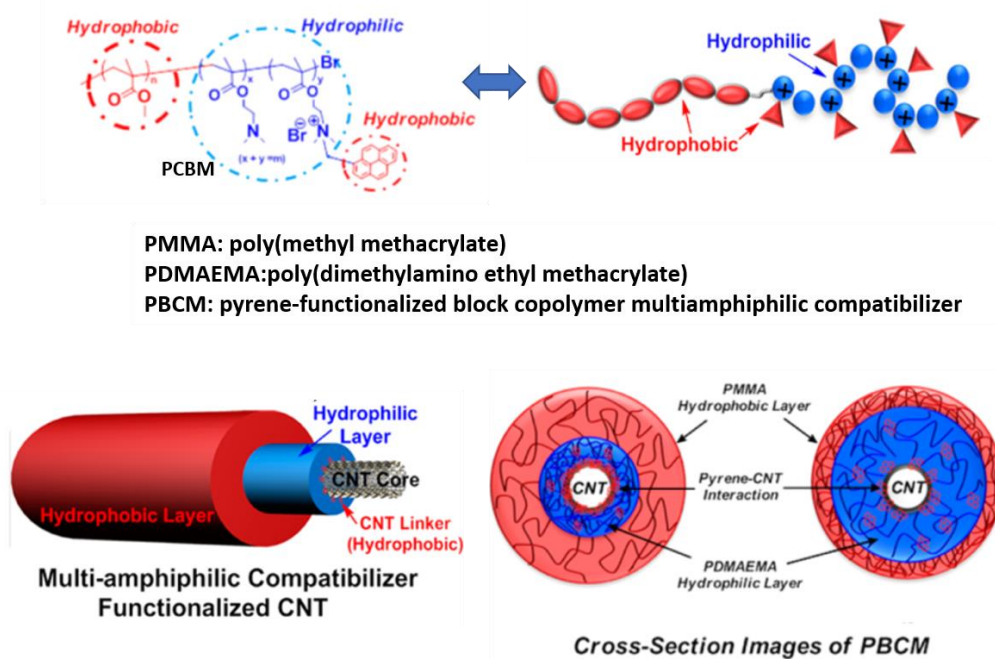


Figure 2.3. Multiamphiphilic compatibilizer layer formations over CNT surface (adapted from Cho et al. 2015)

Interfacial interaction between polymer and carbon nanotubes improved by adding surfactants resulting in stable dispersion and further material advancement of the system.⁴⁸ Literature studies shows different surfactants to improve the disentanglement process of CNT bundles.⁴⁸⁻⁵¹ Some surfactants were also reported as dopants and wetting agents for polymer-CNT structures. Surfactants have also been reported as intermediates to determine the morphological peculiarities of nanocomposites by controlling interfacial interaction between polymer and carbon nanotubes (see **Figure 2.4.**). The self-assembled nature of surfactants has the potential for constructing nanocomposites with morphology control. Surfactant assembly favourably interacts with nanocomposite constituents utilizing weak non-covalent forces like hydrogen bonding, hydrophobic effect, and van der Waals interactions. Promising polymer-surfactant complexation occurs at critical micellar concentrations

(CMC) and above; surfactant concentration should be kept at a minimum. Different types of surfactants, such as cationic, anionic, or non-ionic, exhibit distinct assembling behaviour depending on the polarity of the solvents. The intrinsic amphiphilic nature of surfactants due to polar head - non-polar tail structure facilitates two significant structural features: self-assembly formation in bulk solution and interfacial adsorption behaviour at surfaces. Micellar orientation of surfactants on the dispersed form of carbon nanotube surfaces is possible through hydrophobic interaction between the non-polar tail of surfactant molecules and hydrophobic walls of CNT (see **Figure 2.4.**)⁵¹⁻⁵³ Instead of single-tailed surfactants, the use of double-tailed surfactants can reduce interfacial tension formed due to excessive interfacial interaction in its assembled form.^{54,55}

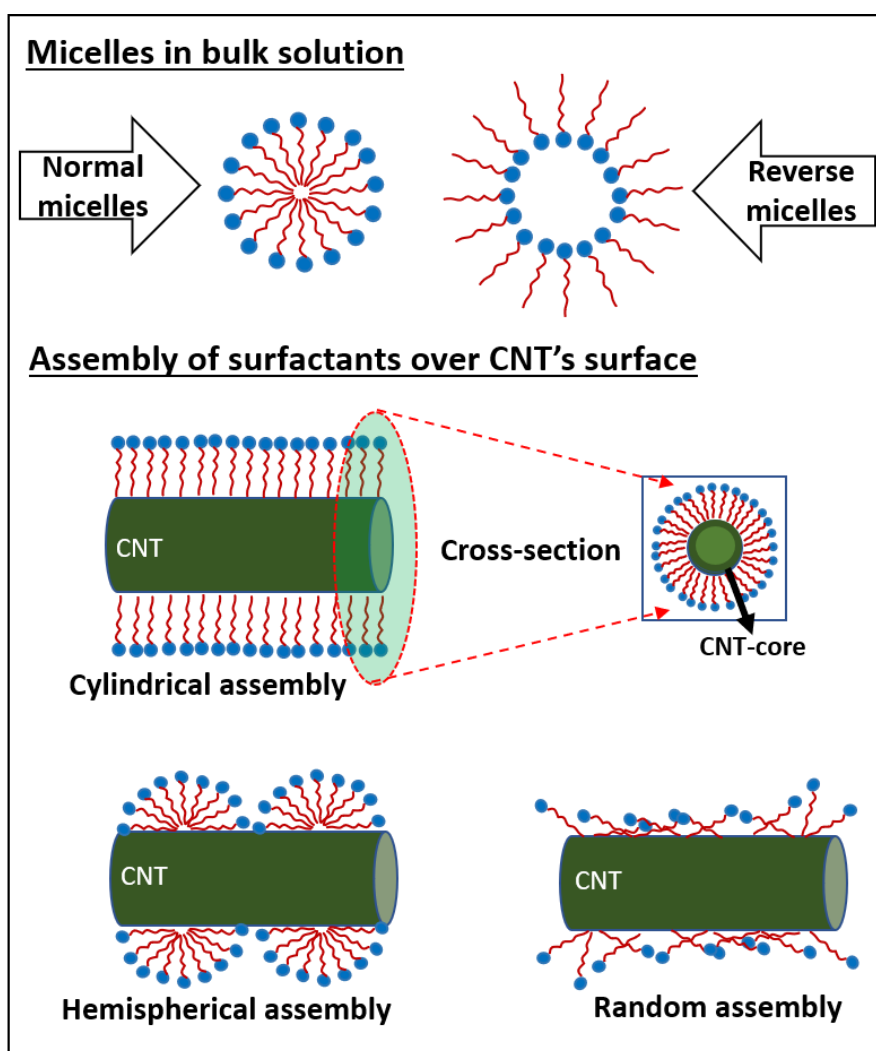


Figure 2.4. Normal and reverse micelles formation in the bulk solution of organic solvents. Cylindrical assembly, hemispherical assembly and a random assembly of the surfactants over CNT's surface.

Chapter 2

In this chapter, polythiophene-multiwalled carbon nanotube nanocomposites (PTCNT) have been prepared by in-situ chemical oxidative polymerization of thiophene monomer in the presence of anionic double-tailed AOT surfactant and dispersed form of multiwalled carbon nanotubes (MWCNT) in chloroform. Oxidative polymerization was achieved with the oxidizing agent ferric chloride (FeCl_3). The versatile double-tailed anionic surfactant AOT [sodium bis (2-ethyl hexyl) sulfosuccinate] has its advantages, such as easy microemulsion formation without supplementing co-surfactants, double-tailed nature, good interfacial activity, and surface energy benefits in its self-assembled form.^{54,55} Anionic surfactant AOT stabilizes the thiophene monomer and MWCNT via micelle interactions. MWCNT was used here as a one-dimensional tubular template for the attachment of polythiophene. Polythiophene was employed here to enhance the solubility and processability of MWCNT in a nanocomposite state. Fourier transform infrared spectroscopy (FT-IR), elemental analysis, and powder X-ray diffraction analysis (P-XRD) confirmed the nanocomposite formation. The core-shell morphology of the nanocomposite was observed by scanning electron microscopy (SEM) and high-resolution-transmission electron microscopy (HR-TEM) imaging. Stable dispersion of PTCNT nanocomposites was obtained in chloroform solvent, and UV-vis absorption spectra were recorded in their dispersed state. This chapter outlines the facile surfactant-AOT mediated in-situ polymerization strategy to develop highly ordered, conductive, dispersible, and thermally stable polythiophene-multiwalled carbon nanotube nanocomposites.

2.2. Experimental

2.2.1. Materials and reagents: Thiophene, Ferric chloride, sodium bis (2-ethyl hexyl) sulfosuccinate (AOT) and multiwalled carbon nanotubes were purchased from Sigma Aldrich. Deionized water, chloroform and acetone were purchased from Merck chemicals, India.

2.2.2. Measurements and instruments: FT-IR spectra of the samples were recorded using the KBr pellet method by Shimadzu IR Affinity 1 FT-IR spectrometer. UV-vis absorption spectra of samples were recorded using Shimadzu UV-Visible spectrometer, UV 1800 series in deionized water and HPLC-grade chloroform solvent. CHNS elemental analyses of the samples were carried out using elementar vario EL III element analyser. Powder X-ray diffraction (P-XRD) analyses of the samples were conducted

using PANALYTICAL, Aeris research with 2θ value ranging from 5° - 90° . Scanning electron microscopic (SEM) imaging was conducted using JEOL Model JSM-6390LV Scanning electron microscope. High resolution transmission electron microscopic (HR-TEM) images were recorded with JEOL/JEM 2100 instrument with 200 KV with magnification 2000x-1500000x. The electrical conductivity of the samples was measured using Keithleys four probe conductivity meter. Thermogravimetric analysis (TGA) was carried out using Perkin Elmer, Diamond TG/DTA.

2.2.3. Synthesis of PTCNT-100: Monomer thiophene (1 mL, 12.50 mmol) and surfactant AOT (0.22 g, 0.50 mmol) was dissolved in chloroform (20 mL) and sonicated for 5 min. MWCNT (0.10 g) was added to the AOT-thiophene mixture in chloroform and sonicated for 10 min. The dispersed form of FeCl_3 in 10 mL chloroform was added drop by drop to the AOT-thiophene-MWCNT mixture and then sonicated for 15 min. Subsequently, the reaction mixture was magnetically stirred for 3 h. Polymer nanocomposite thus obtained was filtered and washed using water and acetone. The resultant composite was then dried in a vacuum oven at 60°C . Yield: 0.82 g. FT-IR (KBr , cm^{-1}) 1667, 1536, 1028 (w), 779 (w), 668. Elemental analysis (anal., wt %): C, 41.14; S, 17.80; H, 3.02.

PTCNT-200, PTCNT-300 and PTCNT-400 were prepared using the same procedure as above by changing the quantity of MWCNT as 0.20, 0.30 and 0.40 g, respectively. The figures in the sample code represent the milligrams of multiwalled carbon nanotubes used in preparing the respective nanocomposites. The samples PTCNT-200, PTCNT-300 and PTCNT-400, yielded 1.12 g, 1.16 g and 1.22 g of nanocomposite products

2.2.4. Synthesis of PTCNT-300 [AOT-0]: Monomer thiophene (1 mL, 12.50 mmol) was dissolved in chloroform (20 mL) without AOT surfactant and sonicated for 5 min. MWCNT (0.30 g) was added to the thiophene dissolved in chloroform and sonicated for 10 min. The FeCl_3 dispersed in 10 mL chloroform was added drop by drop to the thiophene-MWCNT mixture and then sonicated for 15 min. Subsequently, the reaction mixture was magnetically stirred for 3 h. Polymer nanocomposite thus obtained was filtered and washed using water and acetone. The resultant composite was then dried in a vacuum oven at 60°C . Yield: 0.98 g.

Chapter 2

2.2.5. Synthesis of PT-25: Monomer thiophene (1 mL, 12.50 mmol) and surfactant AOT (0.22 g, 0.50 mmol) was dissolved in chloroform (20 mL) and sonicated for 5 min. The FeCl₃ dispersed in 10 mL chloroform was added drop by drop to the AOT-thiophene mixture and then sonicated for 15 min. Subsequently, the reaction mixture was magnetically stirred for 3 h. The brown powder formed was filtered and washed using water and acetone. The resultant polythiophene obtained was then dried in a vacuum oven at 60°C. Yield = 0.58 g. FT-IR (KBr, cm⁻¹) 1658, 1526, 1326, 1112, 1025, 787 and 688. Elemental analysis (anal., wt %): C, 53.73; S, 31.21; H, 3.74.

2.2.6. Synthesis of PT-25[AOT-0]: Monomer thiophene (1 mL, 12.50 mmol) was dissolved in chloroform (20 mL) without AOT surfactant and sonicated for 5 min. The dispersed form of FeCl₃ in 10 mL chloroform was added drop by drop to the thiophene-CHCl₃ mixture and then sonicated for 15 min. Subsequently, the reaction mixture was magnetically stirred for 3 h. A brown powder thus formed was filtered and washed using water and acetone. The resultant polythiophene obtained was then dried in a vacuum oven at 60°C. Yield = 0.62 g. Elemental analysis (anal., wt %): C, 44.97; S, 26.71; H, 2.89.

2.3. Results and discussion

2.3.1. Synthesis of polythiophene and polythiophene-MWCNT nanocomposites

Polythiophene-multiwalled carbon nanotube nanocomposites (PTCNTs) were prepared by in-situ chemical oxidative polymerization of thiophene in the presence of multiwalled carbon nanotubes (MWCNT) and surfactant sodium bis (2-ethyl hexyl) sulfosuccinate (AOT) in chloroform solvent (see **Figure 2.5.**). Polythiophene (PT) was polymerized using ferric chloride as an oxidant in chloroform with and without using surfactant AOT were represented as PT-25 and PT-25[AOT-0]. Surfactant AOT was added to the reaction medium to form micelles that stabilize the monomer and act as a dopant in the conducting polymer structure. In PT-25, thiophene was added to the solution of AOT in chloroform solvent; consequently, a thiophene-AOT complex micelles combination was obtained (see **Figure 2.6.**)⁵⁵⁻⁵⁷ Polymerization of thiophene and in-situ nanocomposite formation were carried out using FeCl₃. The addition of AOT surfactant resulted in improved dispersion of MWCNT in chloroform by reducing the bundling forces between nanotubes.⁵⁰

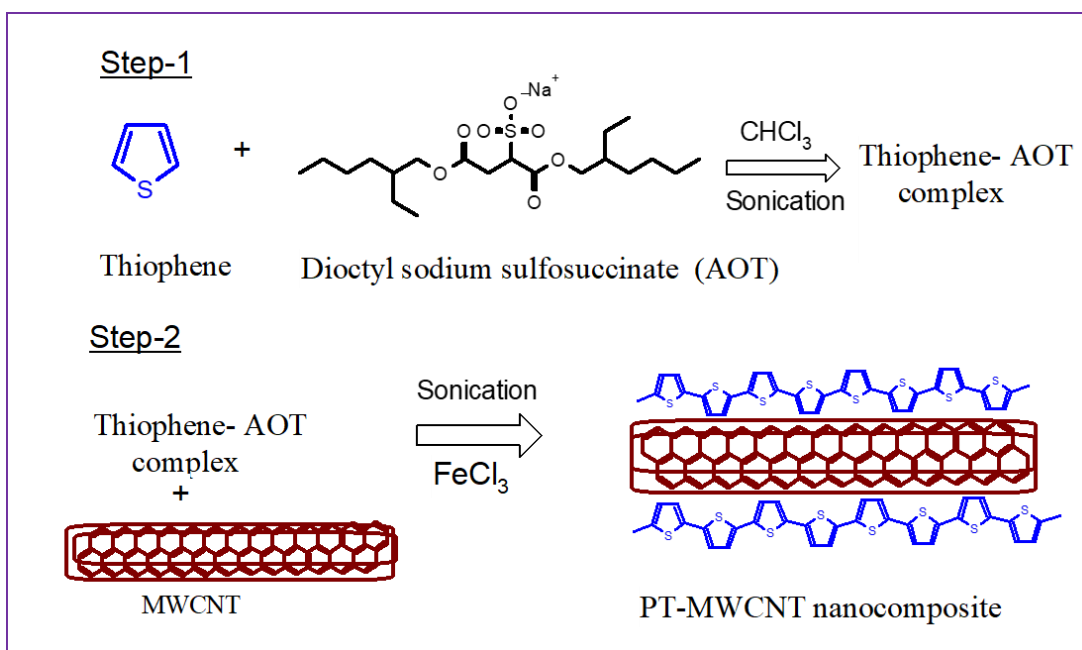


Figure 2.5. Schematic representation of the synthesis of polythiophene-MWCNT nanocomposite (PTCNT) in presence of AOT.

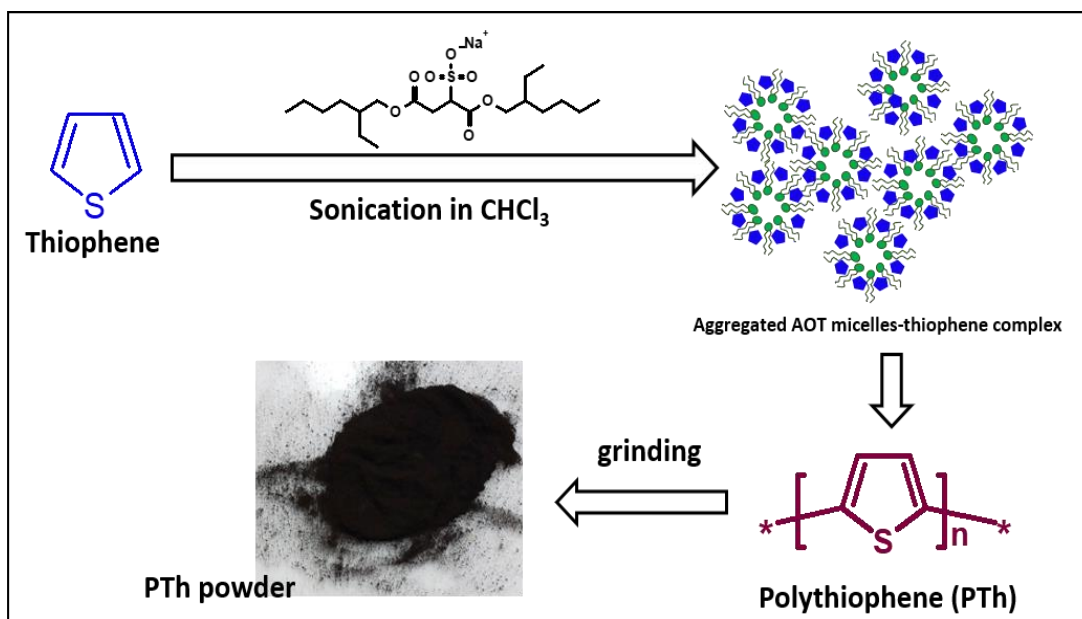


Figure 2.6. Schematic representation of the synthesis of PT-25 in presence of AOT

Chapter 2

Table 2.1. Polythiophene (PT) and PTCNT nanocomposite samples with the amount of thiophene, AOT and MWCNT, monomer to surfactant mole ratio, monomer to FeCl₃ mole ratio and yield obtained in the preparation.

Sample	Thiophene (mmol)	AOT (mmol)	MWCNT (mg)	Monomer/AOT mole ratio	Monomer/FeCl ₃ mole ratio	Yield (mg)
PT-25	12.50	0.50	0	1 :1/25	1 :1.2	584
PT-25[AOT-0]	12.50	0	0	NA	1 :1.2	620
PTCNT-100	12.50	0.50	100	1 :1/25	1 :1.2	829
PTCNT-200	12.50	0.50	200	1 :1/25	1 :1.2	1115
PTCNT-300	12.50	0.50	300	1 :1/25	1 :1.2	1166
PTCNT-400	12.50	0.50	400	1 :1/25	1 :1.2	1211
PTCNT-300[AOT-0]	12.50	0	300	NA	1 :1.2	960

In-situ chemical oxidative polymerization of thiophene was carried out in the presence of MWCNT to result in polythiophene-MWCNT nanocomposites in one step. Polythiophene (PT-25) was prepared by chemical oxidative polymerization technique using FeCl₃ as an oxidant in the presence of surfactant AOT in chloroform medium. Oxidative polymerization of thiophene without surfactant AOT forms polythiophene PT-25[AOT-0]. The monomer (thiophene) to surfactant (AOT) mole ratio was taken as 1:1/25, twenty-five times lower than monomer concentration and denoted as PT-25. The monomer (thiophene) to oxidant (FeCl₃) mole ratio was 1:1.2, a slight excess ferric chloride than monomer.^{41,42,44} Chemical oxidative polymerization of thiophene in the presence of MWCNT resulted in the simultaneous production of PTCNT nanocomposites with respective compositions. The amount of MWCNT was varied as 100 mg, 200 mg, 300 mg and 400 mg (~10 to 40 weight % of thiophene monomer) to prepare four different compositions of nanocomposites such as PTCNT-100, PTCNT-200, PTCNT-300 and PTCNT-400 respectively. PTCNT-300 [AOT-0] was also prepared using the same synthetic procedure of PTCNT-300 without supplementing the AOT surfactant. The addition of ferric chloride to the AOT-thiophene mixture in chloroform resulted in a dark brown-colored polythiophene powder as the final product. More than 80% yield (polythiophene product) was obtained from the synthesis after

washing, filtration and drying. The quantity of each reagent taken for the preparation of PT-0, PT-25 and PTCNT composites and corresponding yields obtained are given in **Table 2.1**.

2.3.2. Characterization of PT and PTCNT nanocomposites

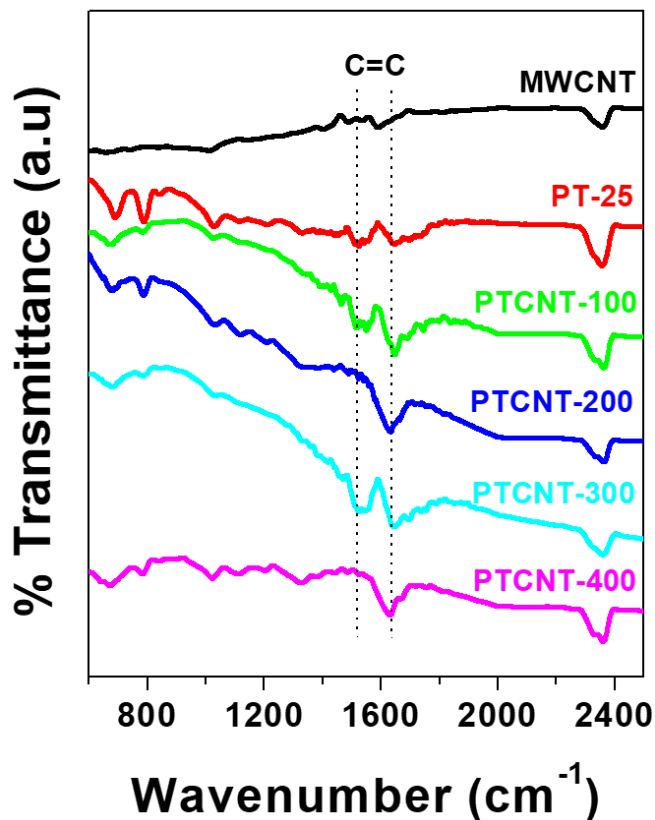


Figure 2.7. FT-IR spectra of MWCNT, PT-25, PTCNT-100, PTCNT-200, PTCNT-300 and PTCNT-400

Fourier transform infrared spectroscopy (FT-IR) analysis was carried out to characterize polythiophene-MWCNT nanocomposites by preparing thin pellets of samples with KBr. FT-IR spectra of PTCNT nanocomposites were compared with MWCNT and polythiophene (PT-25) (see **Figure 2.7.**). Characteristic peaks of MWCNT corresponding to aromatic asymmetric and symmetric stretching were very weak owing to the good symmetric nature of carbon nanotubes resulting in poor dipole moment changes. FT-IR spectrum of PT-25 exhibited peaks at 1658, 1526, 1326, 1112, 1025, 787 and 688 cm⁻¹. The strong peak appeared at 1658 and 1526 cm⁻¹ due to C=C asymmetric and symmetric stretching contribution from thiophene ring moiety. The C-S stretching and the C-S out of plane bending deformation mode vibrations arise at 688 and 787 cm⁻¹ respectively.⁵⁸⁻⁶² FT-IR spectra of PTCNT composites (PTCNT-100,

Chapter 2

PTCNT-200, PTCNT-300 and PTCNT-400) have characteristic peaks of polythiophene. The characteristic C-S vibrations of polythiophene at 688 cm^{-1} and 787 cm^{-1} appeared weak in nanocomposites as the multiwalled carbon nanotube interaction increased in the composite. At the same time, characteristic stretching vibrations of thiophene ring moiety at 1658 and 1526 cm^{-1} in the nanocomposites were more intense than PT-25 due to the appearance of sp^2 hybridized aromatic asymmetric and symmetric stretching of carbon nanotubes in the same regions.

Table 2.2. Elemental analysis data of sulfur, carbon and hydrogen in PT-25, PT-25[AOT-0], PTCNT-100 and PTCNT-300

Sample	Element present (%)			C/S ratio
	Sulfur	Carbon	Hydrogen	
PT-25	31.21	53.73	3.74	1.72
PT-25[AOT-0]	26.71	44.97	2.89	1.68
PTCNT-100	17.80	41.14	3.02	2.31
PTCNT-300	18.60	56.21	1.80	3.02

*C/S ratio is ratio of percentage of carbon and sulfur obtained from elemental analysis.

Elemental analysis (CHNS analysis) was conducted for PT-25, PT-25[AOT-0], PTCNT-100 and PTCNT-300 in order to analyse the percentage of carbon, sulfur and hydrogen present in the samples (see **Table 2.2.**). Among the samples, the overall weight percentage of sulfur was highest in polymer PT-25. The higher percentage of sulfur, carbon and hydrogen in PT-25 compared to PT-25[AOT-0] was due to the incorporation of sulfur-containing AOT surfactant in the former via doping. The sulfur amount is less for composites than polymers because grouping of PT with carbon nanotubes decreases the fraction of sulfur in nanocomposite samples. The percentage of sulfur in PTCNT-300 and PTCNT-100 are relatively in the same range. The percentage of carbon was highest in PTCNT-300, as it contained the highest proportion of carbon nanotubes. The percentage of hydrogen obtained from the analysis was highest in polymeric form, whereas in carbon nanotube composites, the hydrogen content decreases. The ratio of carbon to sulphur percentage from elemental analysis in PT-25, PT-25 [AOT-0], PTCNT-100 and PTCNT-200 was calculated as 1.72, 1.68, 2.31 and 3.02 respectively. PT-25 exhibit higher carbon to sulfur ratio than PT-25 [AOT-0], due to the incorporation of AOT surfactant containing carbon bearing long

hexyl and ethyl chains. In PTCNT-100, the carbon to sulphur ratio is greater compared to PT-25. This might be due to incorporation of carbon nanotubes in PTCNT-100. The carbon to sulfur ratio is further increases in PTCNT-200 and PTCNT-300 as we add more amount of carbon nanotubes in former one (see **Table 2.2**).

Powder X-ray diffraction analysis was carried out to study the solid-state ordering of PTCNT nanocomposites formed (see **Figure 2.8. A**). Diffraction pattern of

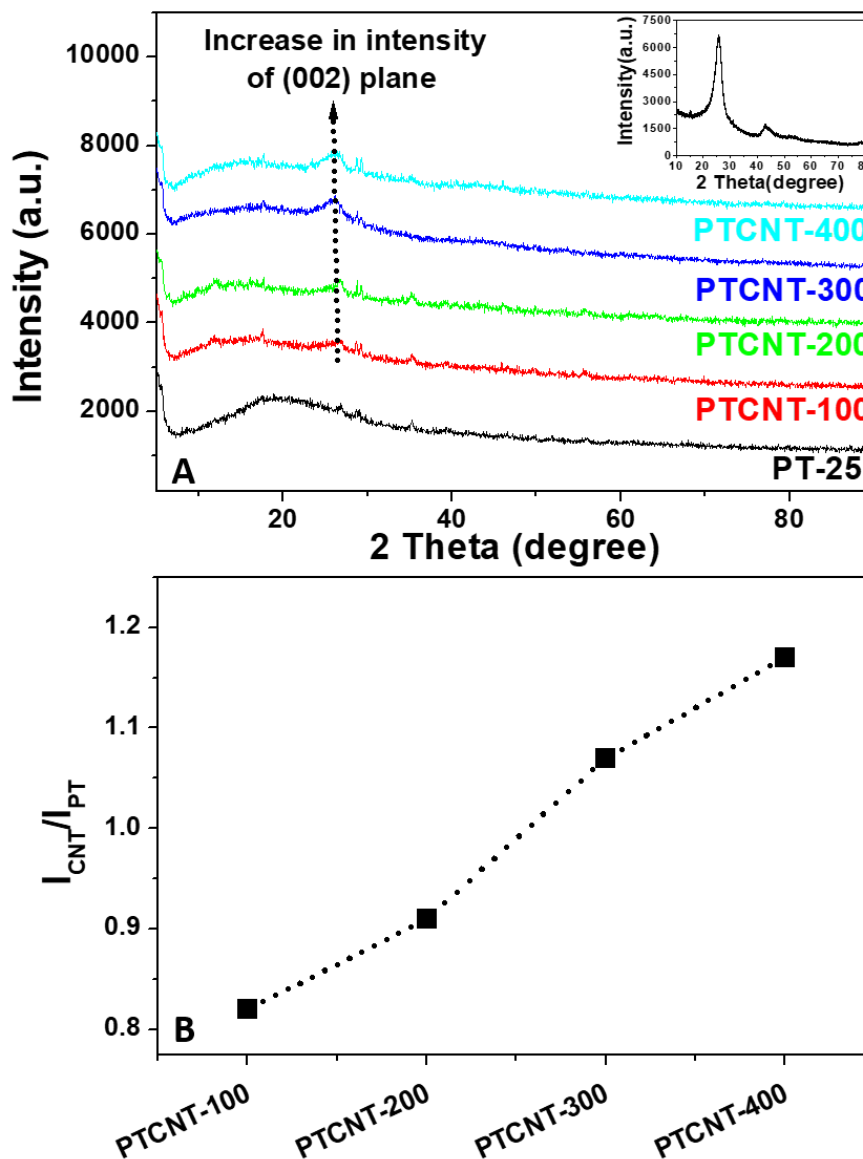


Figure 2.8. (A) Powder X-ray diffraction patterns of PT-25, PTCNT-100, PTCNT-200, PTCNT-300 and PTCNT-400. (B) A diagram exhibiting the ratio of I_{CNT} (intensity of the characteristic peak of MWCNT) to I_{PT} (intensity of characteristic X-ray diffraction peak of polythiophene) for PTCNT composites.

Chapter 2

PT-25 showed an amorphous peak between 2θ values 12° and 25° with a maximum centered at 17.7° , representing the amorphous domain of polymer. MWCNT gave a diffraction pattern at 2θ value 26.10° , attributing to (002) diffraction plane between concentric layers of multiwalled carbon nanotubes.^{63,64} Characteristic peaks due to (002) diffraction plane of carbon nanotubes is shown in the inset of **figure 2.8.A**. Among the nanocomposites, the intensity of the characteristic diffraction peak from (002) plane of carbon nanotubes increases for the increasing weight percentage of MWCNT, due to which the peak is more prominent in PTCNT-300 and PTCNT-400. The ratio of the intensity maximum of the characteristic peak of carbon nanotubes (I_{CNT}) to the intensity maximum of polythiophene diffraction peak (I_{PT}) was calculated for PTCNT-100, PTCNT-200, PTCNT-300 and PTCNT-400 as 0.82, 0.90, 1.07 and 1.17 respectively (see **Figure 2.8. B**). PTCNT-100 exhibited the lowest and PTCNT-400 had the highest $I_{\text{CNT}}/I_{\text{PT}}$ value. The intensity ratio increased with the increasing weight percentage of MWCNT in the nanocomposites. The decrease of the amorphous domain of polythiophene with MWCNT nanocomposites also denotes that the amorphous domain is considerably suppressed via wrapping polymer chains around the MWCNT walls. The area corresponding to amorphous region ($2\theta = 12$ to 25°) of PT-25 was higher than PTCNT nanocomposites (see Figure 2.9 A). The suppressed amorphous area of PTCNT nanocomposites reveals that the PTCNT composites exhibited better solid state ordering compared to PT-25. The area under crystalline peak at $2\theta = 26.10^\circ$ of PTCNT composites increased with the addition of MCNT to the PT-25 (Figure 2.9 B).

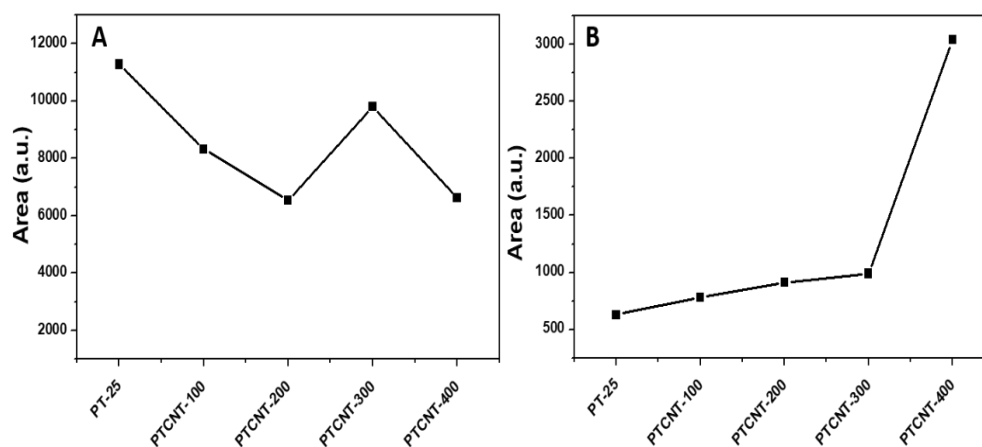


Figure 2.9. Area under the X-ray diffraction peaks of A) amorphous region and B) crystalline region in PT-25 and PTCNT nanocomposites.

2.3.3. Morphological characteristics of PT and PTCNT nanocomposites

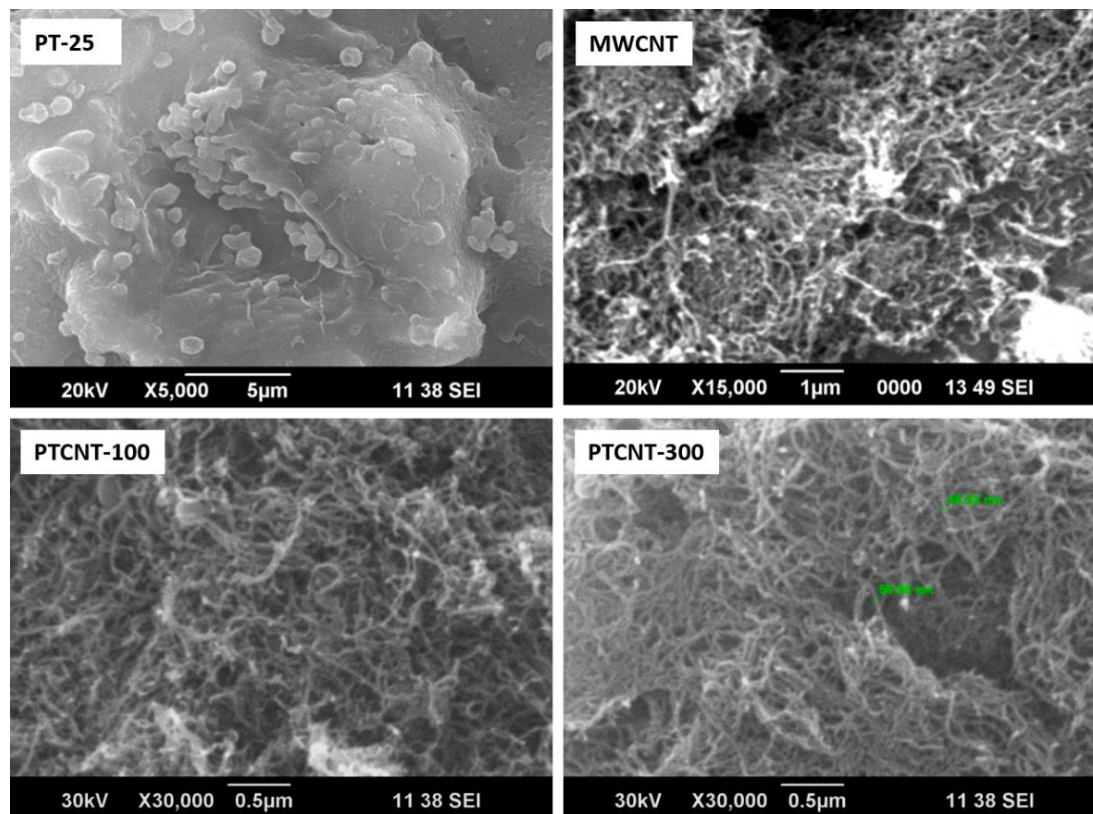


Figure 2.10. Scanning electron microscopic (SEM) images of PT-25, MWCNT, PTCNT-100 and PTCNT-300

Scanning electron microscopic analyses were carried out to examine the morphology of polythiophene and polythiophene-MWCNT nanocomposites (see **Figure 2.10**). Polythiophene appeared as sub-microspherical particles, whereas PTCNTs (PTCNT-100 and PTCNT-300) exhibited fibre-like nanostructures. Nanofibrous morphology observed in PTCNT nanocomposites was matching with the inherent nanotubular structure of MWCNT. Nanocomposites attained nanofibrous morphology since growing chain of polythiophene was attached on the surface of dispersed MWCNT during polymerization. This revealed that MWCNT performed as a template in the nanocomposite formation by regulating the morphology of PTCNTs to a nanofibrous frame.

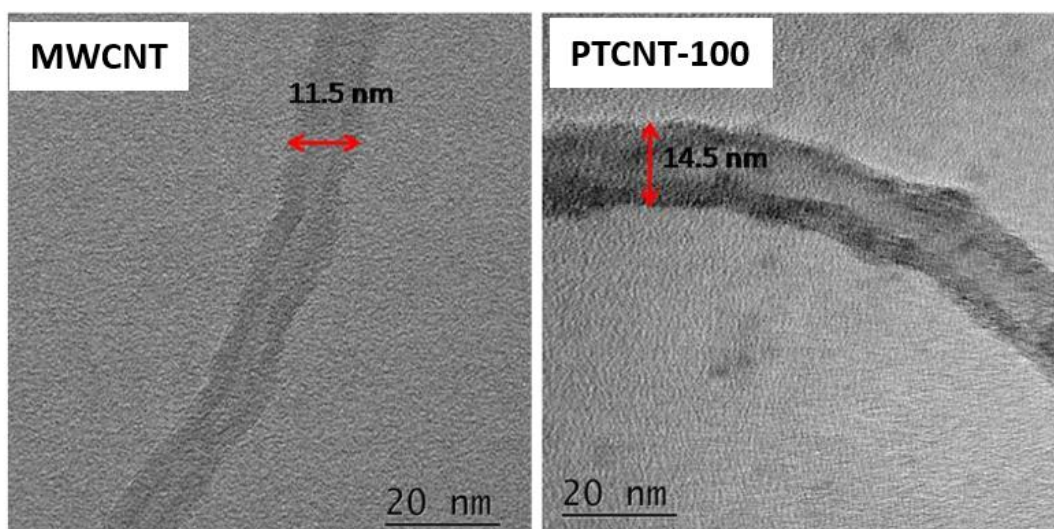


Figure 2.11. TEM images of MWCNT and PTCNT-100 and size calculation

Transmission electron microscopic (TEM) analysis was used to ascertain the nanocomposite size and other physical characteristics (see **Figure 2.11.** and **Figure 2.12.**). Multiwalled carbon nanotubes contained an inner unfilled lighter area, indicating the tubular structure in its TEM images. An outer layer of carbon nanotube was visible as a dark area covering the inner tube.^{41,42} The average inner diameter of carbon nanotube and PTCNT-100 nanocomposites was 5 nm. The outer diameter of MWCNT was observed to be 12 ± 2 nm, whereas the outer diameter in PTCNT-100 composites was observed to be increased from 3 to 15 nm compared to pristine CNT. The thick outer layer of PTCNT-100 composite was observed around the surface MWCNT. The result indicated that polythiophene was grown as an outer shell around the surface of carbon nanotubes. Therefore, the polythiophene-MWCNT nanocomposite could be understood as a core-shell nanotubular structure; a thick outer shell was growing up around the inner tubular MWCNT core.

2.3.4. Role of AOT in the formation of nanocomposite

The role of AOT in the formation of nanocomposites PTCNTs was ascertained using transmission electron microscopy. PTCNT-300-[AOT-0] appeared as phase-separated; on the other hand, PTCNT-100 and PTCNT-300 seemed to have the same nanofibrous morphology of MWCNT without having a separated polythiophene matrix. (see **Figure 2.12.**)^{41,42} This revealed the importance of surfactant AOT for the PTCNT's nanotubular structure formation. The composite prepared without adding AOT surfactant largely retained bulk polymer mass separated from the carbon nanotube

surfaces. The AOT supports the growth of polythiophene chains around the tubular MWCNT template for effective core-shell nanocomposite formation.

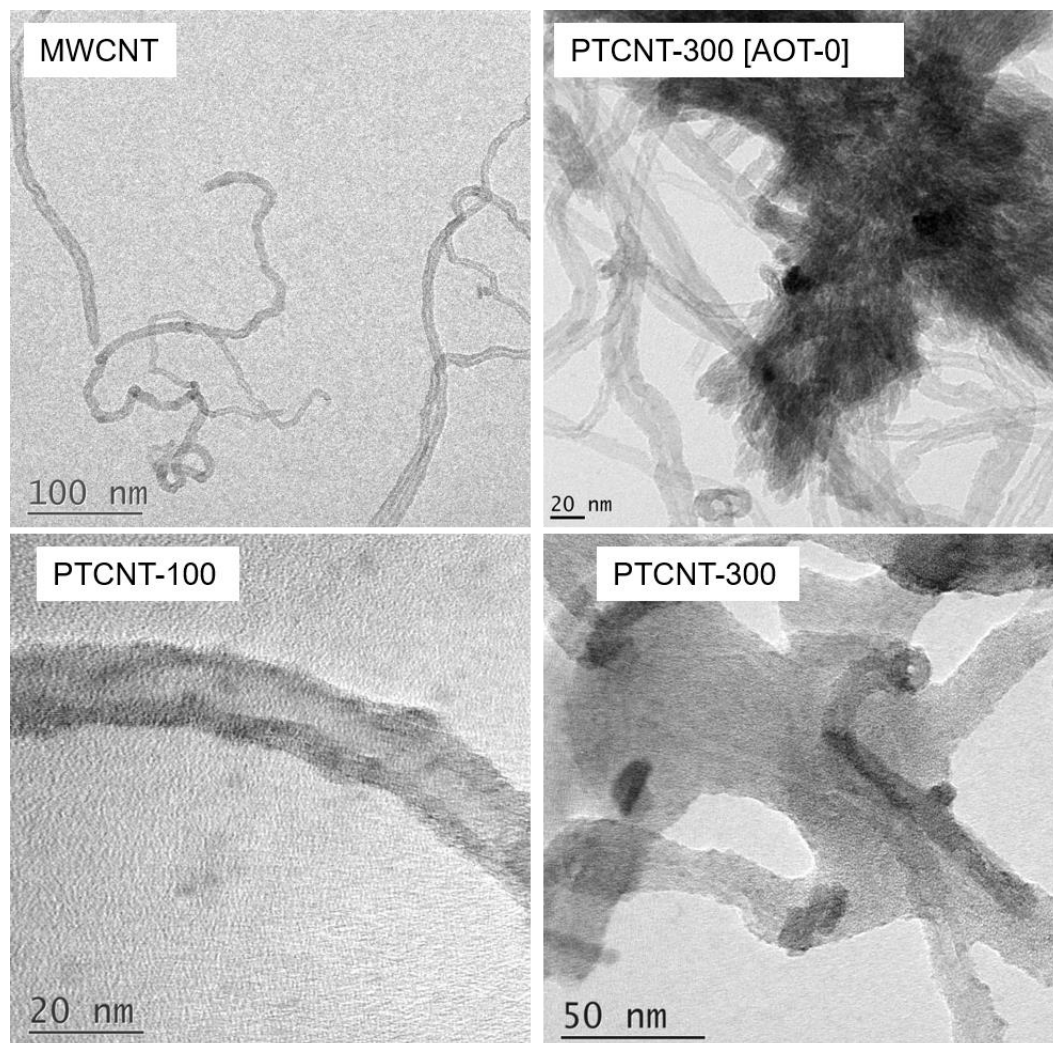


Figure 2.12. Transmission electron microscopic (TEM) images of MWCNT, PTCNT-300 [AOT-0], PTCNT-100 and PTCNT-300

The difference in the WXR patterns of PTCNT-300 and PTCNT-300 [AOT-0] confirmed the notable role of surfactant AOT in the nanocomposite formation (see **Figure 2.13.**). The broad, amorphous peak of polythiophene was observed to be more suppressed in PTCNT-300 than in PTCNT-300 [AOT-0]. The graph was plotted for the intensity ratio of (002) plane of MWCNT (I_{CNT}) to amorphous polythiophene (I_{PT}) (see **Figure 2.13. inset**). The I_{CNT}/I_{PT} value was higher for PTCNT-300 than PTCNT-300[AOT-0] due to the suppression of the amorphous peak of polythiophene by pi-pi stacking interaction with MWCNT. Due to the inappropriate orientation of both components, the phase-separated polythiophene could not interact effectively with

MWCNT by weak non-covalent forces. The double-tailed AOT upholds the stacking interaction between polythiophene and MWCNT for the generation of core-shell PTCNT nanocomposites.

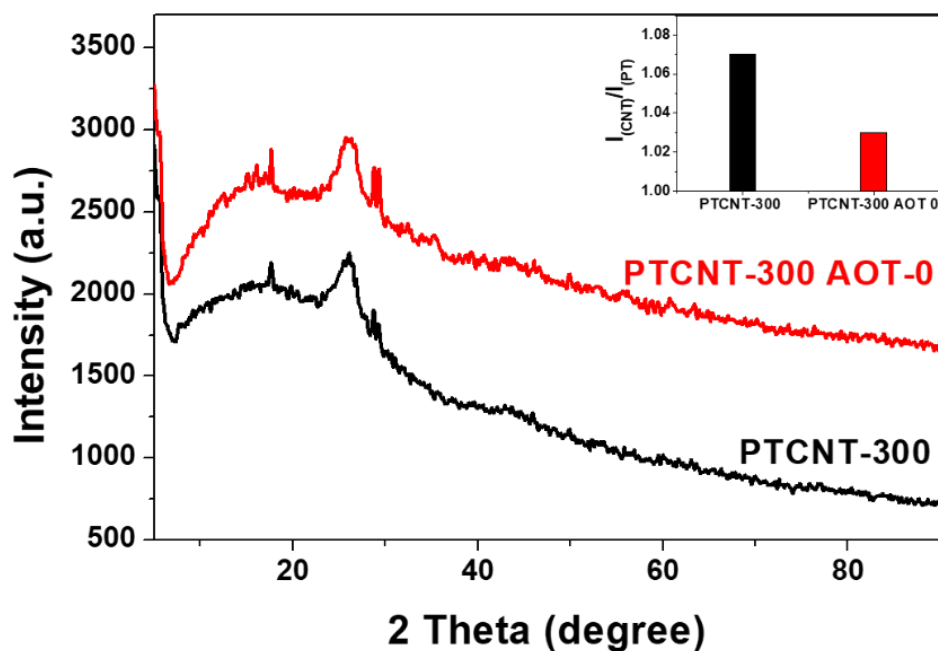


Figure 2.13. WXR D patterns of PTCNT-300 and PTCNT-300[AOT-0]. Diagram exhibiting the ratio of I_{CNT} (intensity of characteristic peak of MWCNT) to I_{PT} (intensity of characteristic X-ray diffraction peak of polythiophene) for PTCNT-300 and PTCNT-300[AOT-0] (inset)

2.3.5. Mechanism of composite formation

The formation mechanism of PTCNT nanocomposites was proposed based on the evidence obtained from FT-IR spectra, WXR D patterns and morphological analyses. Thiophene was polymerized in the presence of double tail surfactant sodium bis (2-ethyl hexyl) sulfosuccinate; the nearly spherical shaped polymer microparticles were formed. AOT and thiophene monomer in soluble form combined to form micellar aggregates complex in chloroform medium. Thiophene monomer gets oriented with the shape of micelles in chloroform, thereby stabilizing the monomer with spherical micelles. The addition of MWCNT to the AOT- thiophene micellar complex resulted in the migration of aggregates to the surface of MWCNT with the help of mild sonication. Entanglements of carbon nanotubes also get released up to a limit with the help of sonication-assisted micellar aggregate's interaction with the surface of nanotubes. Then the oxidative polymerization of thiophene with $FeCl_3$ causes the

polymer to grow up on the outer surface of MWCNT. As a result, a thick nano-layer instead of sub-microspheres formed in pure polymeric form. The mechanism of the PT and PTCNT composite formation is represented in **Figure 2.14**.

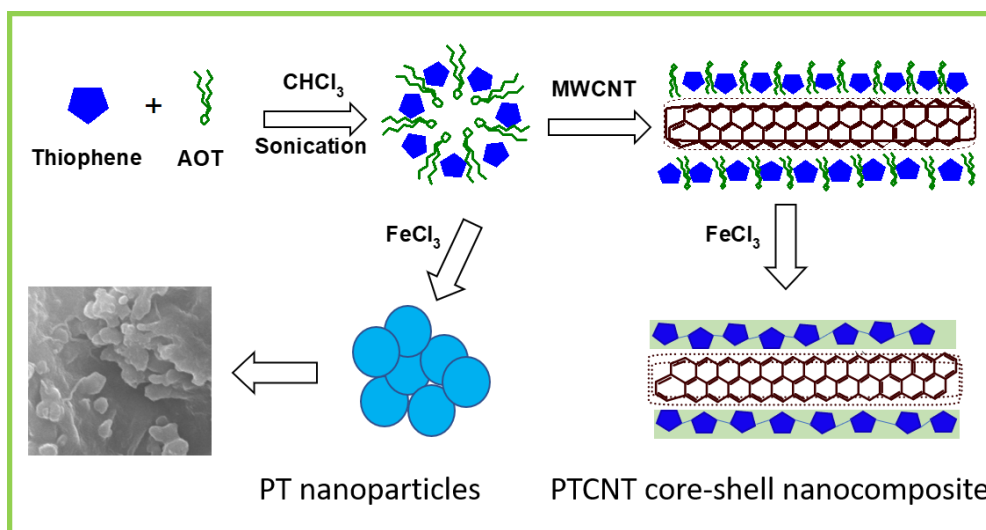


Figure 2.14. Mechanism of the formation of PT-25 and PTCNT nanocomposites

2.3.6. Enhancement of properties

The electrical conductivity of the samples was measured using Keithley four-probe electrical conductivity meter. The average conductivity measured at four points of the pelletized sample was taken as values. A graph was plotted for the average value of conductivity against the corresponding samples (see **Figure 2.15**). Conductivity of PT-25[AOT-0], PT-25, PTCNT-100, PTCNT-200, PTCNT-300 and PTCNT-400 and MWCNT were 4.7×10^{-5} , 7.3×10^{-3} , 3.58×10^{-1} , 3.98×10^{-1} , 2.2×10^{-2} , 3.40×10^{-1} and 8.66 S/cm respectively.^{40,41,65} PT-25 exhibited a higher value of conductivity relative to PT-25[AOT-0]. The enhancement in conductivity was due to the effective doping that occurred at the thiophene rings of PT-25. The AOT successfully enacted the role of dopant on the polymeric chains. The conductivity of PTCNT composites was observed as 1.5 times higher order of magnitude than PT-25. The conductivity enhancement in PTCNT nanocomposites was due to the effective charge transport between conducting polythiophene and multiwalled carbon nanotubes.

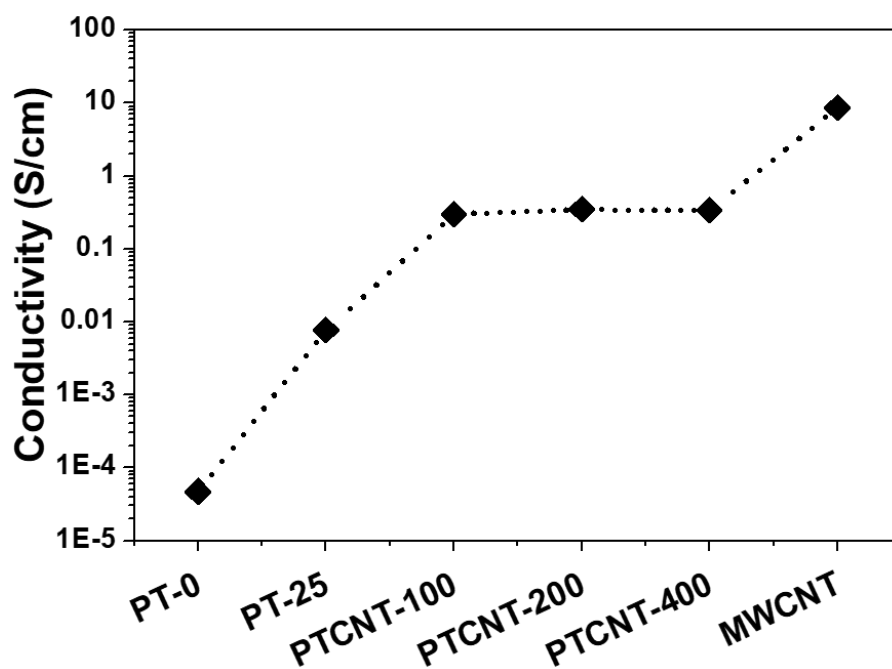


Figure 2.15. Electrical conductivity of PT-0, PT-25, PTCNT-100, PTCNT-200, PTCNT-400 and pristine MWCNT.

The inherent bundling nature of MWCNT made its dispersion uneasy. Mild sonication has power limits to separate the CNT bundles because of the lengthier CNT structure; however, strong sonication might shorten the CNT length and damage the CNT surface. MWCNT does not exhibit good dispersion in chloroform and water (see **Figure 2.16. A and B**). One of the effective ways to create the dispersible nature of carbon nanotubes was making MWCNT into nanocomposites with structurally similar polymers. Conducting polythiophene was utilized here to modify the surface of CNT to attain dispersible nature. Polythiophene-multiwalled carbon nanotube nanocomposites exhibited stable dispersion in chloroform with the assistance of mild sonication. Non-covalent forces working between polythiophene and MWCNT helped to overcome the self-aggregating nature of MWCNT. PTCNT nanocomposites have poor dispersion in an aqueous medium due to the polythiophene coating, which is hydrophobic in water (see **Figure 2.16. A and B**). The PTCNT-300[AOT-0], which was devoided AOT and poorly soluble in chloroform and water, exhibited a slight improvement in water dispersibility after adding AOT via sonicating for 15 minutes. Improvement could be attributed to the post-doping effect of AOT on polythiophene and its surfactant effect.

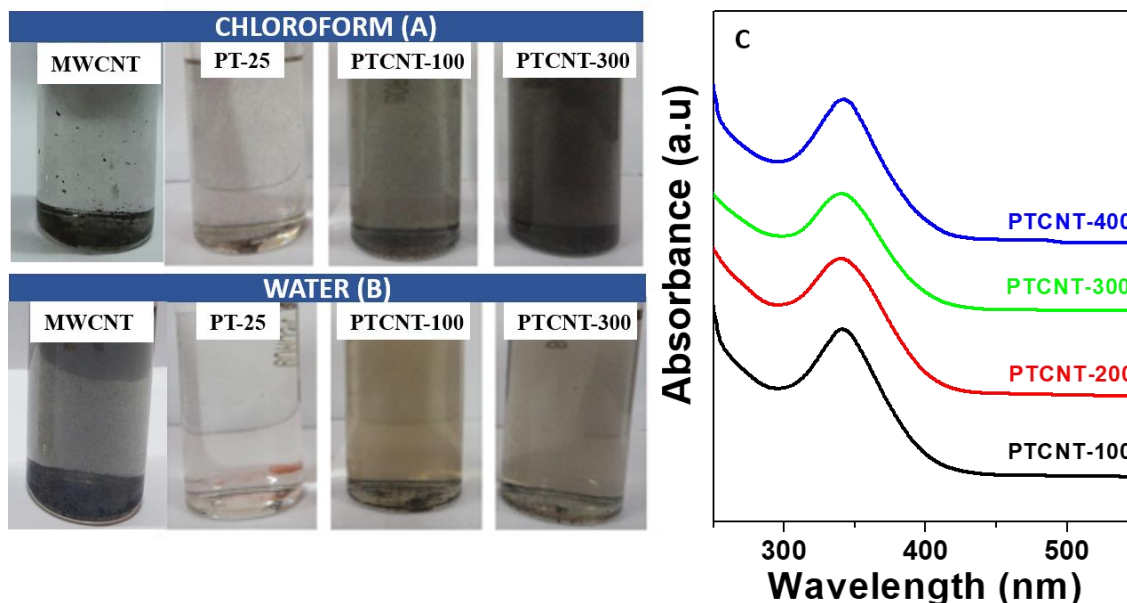


Figure 2.16. Dispersions of MWCNT, PT-25, PTCNT-100 and PTCNT-300 in chloroform (A) and water (B). UV-vis absorption spectra of PTCNT-100, PTCNT-200, PTCNT-300 and PTCNT-400 recorded in chloroform medium (C).

UV-vis absorption spectra of PTCNT-100, PTCNT-200, PTCNT-300 and PTCNT-400 in chloroform were shown in **Figure 2.16. C**. Stable dispersions of PTCNT composites in chloroform enabled to record UV-vis absorption spectra. A well-resolved characteristic peak corresponding to polythiophene was obtained at 340 nm due to the polaron- π transition in polythiophene chains.^{46,66} UV-vis peak of PTCNT composites corresponding to carbon nanotubes (<275 nm) could not be resolved since it merged with the UV-solvent cut-off peaks of CHCl_3 solvent (240 and 260 nm).^{67,68} Poor dispersibility of polythiophene and MWCNT carbon nanotubes hampered our efforts to take UV-vis absorption in chloroform. The dispersible nature of MWCNT was found to be improved by the addition of AOT surfactant.

Thermal stability of the samples PT-25, PTCNT-100 and PTCNT-300 were studied by thermogravimetric analysis (TGA). Thermograms of PT-25, PTCNT-100 and PTCNT-300 were recorded at a heating rate of 20°C/min in a nitrogen atmosphere (see **Figure 2.17.**). The polymer samples exhibited 10% weight loss when the temperature reached 250-280°C.^{58,69} The composites PTCNT -100 and PTCNT-300 showed higher thermal stability than the polymer PT-25 in higher temperatures due to

incorporating a more thermally stable carbon nanotube. The weight percentage of polymer composite decreased to 65-75% in the temperature range of 500-600°C due to carbon decomposition from the polymer chain.

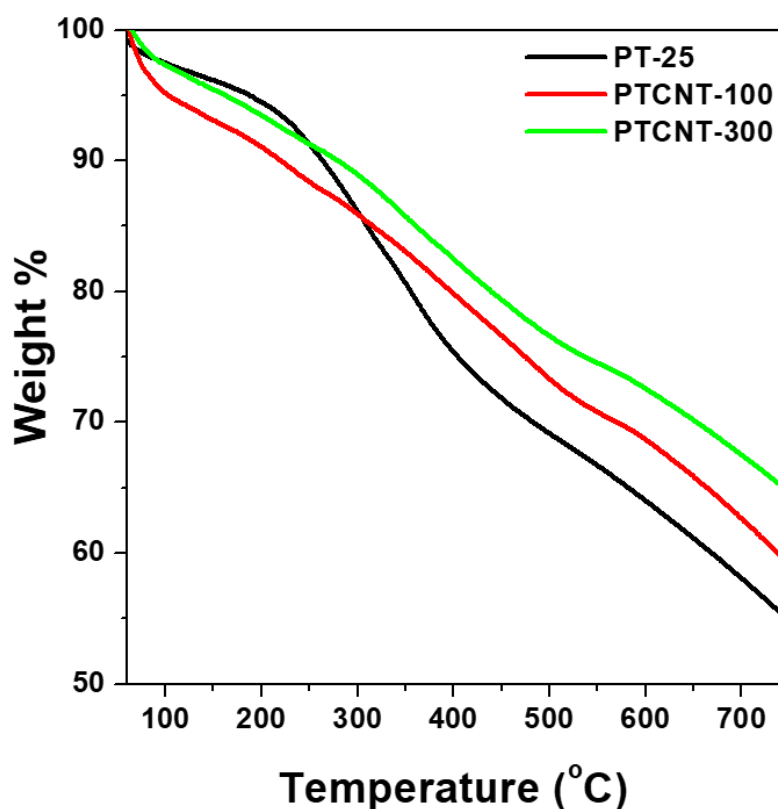


Figure 2.17. Thermogravimetric analysis of PT-25, PTCNT-100 and PTCNT-300

PTCNT binary composites have two major components; polythiophene (PT) and multiwalled carbon nanotubes (MWCNT). Thiophene was used as a monomer to obtain the polymeric component in the nanocomposite. Polythiophene thick coating prevents the self-aggregation of carbon nanotubes and produces dispersion in chloroform. The use of conducting polymer helped to maintain appreciably good conductivity value for composite by involving charge transport with carbon nanotube. Another component is MWCNT which was added as such to the reaction mixture. MWCNT was used as a permanent template for achieving morphologically distinctive nanofibrous structures. The major contribution of conductivity of nanocomposite came from carbon nanotubes' electronic structure. The presence of MWCNT is also the reason for the improved thermal stability of PTCNT nanocomposites. AOT was used in less proportion in the preparation stage to act as a surfactant supplement and dopant. The role of double tail surfactant sodium bis (2-ethyl hexyl) sulfosuccinate in nanocomposite formation and enhanced properties were notable based on different

analytical techniques such as X-ray diffraction, transmission electron microscopic imaging, UV-vis absorption spectra, monitoring dispersion stability and conductivity measurements. AOT acted as a stabilizing agent, dopant and surfactant in nanocomposite preparation stage. It also helps for stacking interaction between polymer and CNT; thereby responsible for the core-shell morphology of nanocomposite. Dispersion of nanocomposites were achieved with the help of stabilizing agent AOT. These stable dispersions enabled to record well-resolved peak in the UV-vis spectrum of nanocomposites (see **Figure 2.18.**).

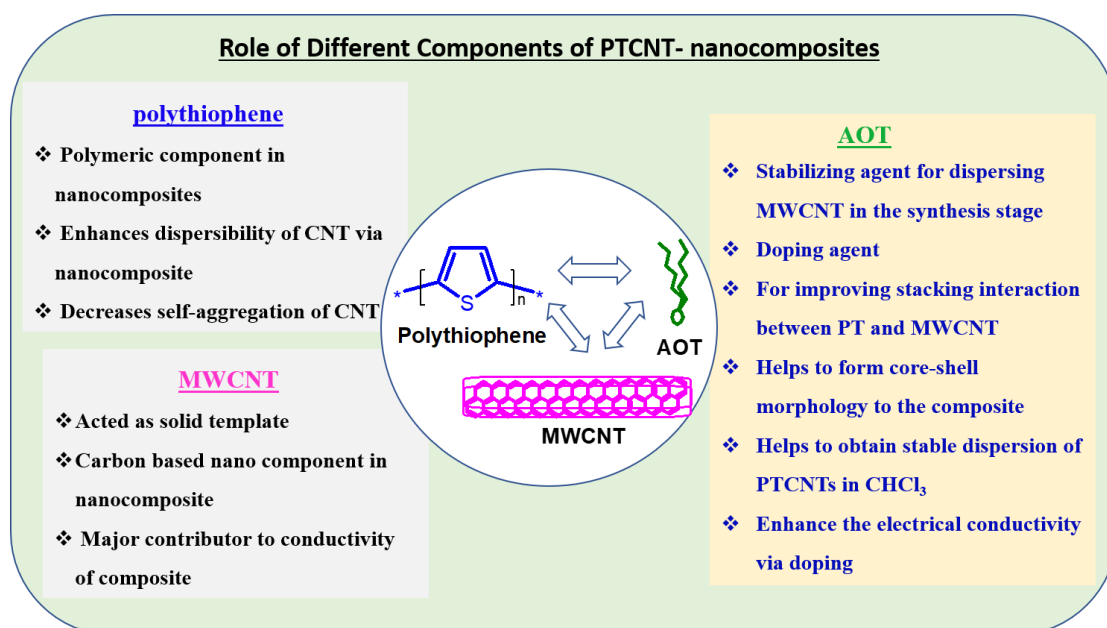


Figure 2.18. Illustration of the role of polythiophene, MWCNT and AOT in the PTCNT nanocomposite formation.

2.2. Conclusion

In conclusion, we have prepared polythiophene-multiwalled carbon nanotube nanocomposites (PTCNTs) via in-situ chemical oxidative polymerization of thiophene in the presence of AOT surfactant (monomer to surfactant mole ratio: 1:1/25). Polymerization was carried out using the oxidant FeCl_3 in chloroform medium. FT-IR spectroscopy characterizes the stretching and bending vibrations of polythiophene and MWCNT indicating the formation of the nanocomposite. The percentage of sulfur in elemental analysis validated the systematic increase of weight percentage of carbon nanotube in PTCNTs. X-ray diffraction pattern of nanocomposites exhibited a broad, amorphous peak of polythiophene with 2θ ranging from 12° - 25° and a sharp peak from (002) plane of MWCNT centered at 26° . In WXR scan, an increase in the intensity of

Chapter 2

MWCNT diffraction peak and a decrease in the intensity of the amorphous peak of polythiophene was observed by adding a higher weight percentage of carbon nanotubes in the composites. Scanning electron micrographs of PTCNT-100 and PTCNT-300 displayed characteristic nanofibrous morphology. Transmission electron microscopic (TEM) images exhibited core-shell morphology to PTCNT-100 and PTCNT-300; CNT's tubular core was covered with a thick polythiophene shell. The outer shell diameter of nanocomposites was observed to be 3 to 12 nm increase than the outer tube diameter of pristine MWCNT. AOT has an inevitable role as a surfactant and dopant in forming core-shell morphology and π - π stacking interaction of PT with MWCNT in the nanocomposites. The well-resolved peak corresponding to the polaron- π transition in the polythiophene chain was obtained in the UV-vis spectrum of nanocomposites. Electrical conductivity enhancement in AOT-doped polythiophene (PT-25) and AOT-undoped polythiophene revealed the role of anionic surfactant AOT for stabilizing charges formed on conducting polymer chains on oxidation. The nanocomposite conductivity was 1.5 times higher-order in magnitude than PT-25 because effective charge transport occurred between conductive polythiophene and CNT. The nanocomposites also showed better thermal stability up to 500°C. In summary, results obtained from various analyses and enhanced properties of nanocomposites indicate the major role of AOT in the effective formation of solid state-ordered, conducting and dispersible core-shell PTCNT nanocomposites.

References

1. Gangopadhyay, R.; De, A. Conducting Polymer Nanocomposites: A Brief Overview. *Chem. Mater.* **2000**, 12 (3), 608–622. <https://doi.org/10.1021/cm990537f>.
2. Rajesh; Ahuja, T.; Kumar, D. Recent Progress in the Development of Nano-Structured Conducting Polymers/Nanocomposites for Sensor Applications. *Sensors Actuators, B Chem.* **2009**, 136 (1), 275–286. <https://doi.org/10.1016/j.snb.2008.09.014>.
3. Al-Mashat, L.; Shin, K.; Kalantar-Zadeh, K.; Plessis, J. D.; Han, S. H.; Kojima, R. W.; Kaner, R. B.; Li, D.; Gou, X.; Ippolito, S. J.; Wlodarski, W. Graphene/Polyaniline Nanocomposite for Hydrogen Sensing. *J. Phys. Chem. C* **2010**, 114 (39), 16168–16173. <https://doi.org/10.1021/jp103134u>.
4. Chang, C. M.; Weng, C. J.; Chien, C. M.; Chuang, T. L.; Lee, T. Y.; Yeh, J. M.; Wei, Y. Polyaniline/Carbon Nanotube Nanocomposite Electrodes with Biomimetic Hierarchical Structure for Supercapacitors. *J. Mater. Chem. A* **2013**, 1 (46), 14719–14728. <https://doi.org/10.1039/c3ta13758a>.
5. Liu, X.; Zheng, Y.; Wang, X. Controllable Preparation of Polyaniline-Graphene Nanocomposites Using Functionalized Graphene for Supercapacitor Electrodes. *Chem. - A Eur. J.* **2015**, 21 (29), 10408–10415. <https://doi.org/10.1002/chem.201501245>.

- Tang, Q.; Cai, H.; Yuan, S.; Wang, X. Counter Electrodes from Double-Layered Polyaniline Nanostructures for Dye-Sensitized Solar Cell Applications. *J. Mater. Chem. A* **2013**, 1 (2), 317–323. <https://doi.org/10.1039/c2ta00026a>.
- Dawan, F.; Jin, Y.; Goettert, J.; Ibekwe, S. High Functionality of a Polymer Nanocomposite Material for MEMS Applications. *Microsyst. Technol.* **2008**, 14 (9–11), 1451–1459. <https://doi.org/10.1007/s00542-008-0577-4>.
- Ago, H.; Petritsch, K.; Shaffer, M. S. P.; Windle, A. H.; Friend, R. H. Composites of Carbon Nanotubes and Conjugated Polymers for Photovoltaic Devices. *Adv. Mater.* **1999**, 11 (15), 1281–1285. [https://doi.org/10.1002/\(SICI\)1521-4095\(199910\)11:15<1281::AID-ADMA1281>3.0.CO;2-6](https://doi.org/10.1002/(SICI)1521-4095(199910)11:15<1281::AID-ADMA1281>3.0.CO;2-6).
- Curran, S. A.; Ajayan, P. M.; Blau, W. J.; Carroll, D. L.; Coleman, J. N.; Dalton, A. B.; Davey, A. P.; Drury, A.; McCarthy, B.; Maier, S.; Strevens, A. A Composite from Poly(m-Phenylenevinylene-Co-2,5-Dioctoxy-p-Phenylenevinylene) and Carbon Nanotubes: A Novel Material for Molecular Optoelectronics. *Adv. Mater.* **1998**, 10 (14), 1091–1093. [https://doi.org/10.1002/\(sici\)1521-4095\(199810\)10:14<1091::aid-adma1091>3.0.co;2-l](https://doi.org/10.1002/(sici)1521-4095(199810)10:14<1091::aid-adma1091>3.0.co;2-l).
- Kim, J. Y.; Kim, M.; Kim, H. M.; Joo, J.; Choi, J. H. Electrical and Optical Studies of Organic Light Emitting Devices Using SWCNTs-Polymer Nanocomposites. *Opt. Mater. (Amst)*. **2003**, 21 (1–3), 147–151. [https://doi.org/10.1016/S0925-3467\(02\)00127-1](https://doi.org/10.1016/S0925-3467(02)00127-1).
- Lu, X.; Zhang, W.; Wang, C.; Wen, T. C.; Wei, Y. One-Dimensional Conducting Polymer Nanocomposites: Synthesis, Properties and Applications. *Prog. Polym. Sci.* **2011**, 36 (5), 671–712. <https://doi.org/10.1016/j.progpolymsci.2010.07.010>.
- Liu, Y.; Kumar, S. Polymer/Carbon Nanotube Nano Composite Fibers-A Review. *ACS Appl. Mater. Interfaces* **2014**, 6 (9), 6069–6087. <https://doi.org/10.1021/am405136s>.
- Wang, L.; Lu, X.; Lei, S.; Song, Y. Graphene-Based Polyaniline Nanocomposites: Preparation, Properties and Applications. *J. Mater. Chem. A* **2014**, 2 (13), 4491–4509. <https://doi.org/10.1039/c3ta13462h>.
- Kim, K. H.; Jo, W. H. A Strategy for Enhancement of Mechanical and Electrical Properties of Polycarbonate/Multi-Walled Carbon Nanotube Composites. *Carbon N. Y.* **2009**, 47 (4), 1126–1134. <https://doi.org/10.1016/j.carbon.2008.12.043>.
- Karim, M. R.; Lee, C. J.; Lee, M. S. Synthesis and Characterization of Conducting Polythiophene/Carbon Nanotubes Composites. *J. Polym. Sci. Part A Polym. Chem.* **2006**, 44 (18), 5283–5290. <https://doi.org/10.1002/pola.21640>.
- Mandal, A.; Nandi, A. K. Physical Properties of Poly(Vinylidene Fluoride) Composites with Polymer Functionalized Multiwalled Carbon Nanotubes Using Nitrene Chemistry. *J. Mater. Chem.* **2011**, 21 (39), 15752–15763. <https://doi.org/10.1039/c1jm12926k>.
- Kałuża, D.; Jaworska, E.; Mazur, M.; Maksymiuk, K.; Michalska, A. Multiwalled Carbon Nanotubes-Poly(3-Octylthiophene-2,5-Diyl) Nanocomposite Transducer for Ion-Selective Electrodes: Raman Spectroscopy Insight into the Transducer/Membrane Interface. *Anal. Chem.* **2019**, 91 (14), 9010–9017. <https://doi.org/10.1021/acs.analchem.9b01286>.
- He, P.; Shimano, S.; Salikolimi, K.; Isoshima, T.; Kakefuda, Y.; Mori, T.; Taguchi, Y.; Ito, Y.; Kawamoto, M. Noncovalent Modification of Single-Walled Carbon Nanotubes Using Thermally Cleavable Polythiophenes for Solution-Processed Thermoelectric Films. *ACS Appl. Mater. Interfaces* **2019**, 11 (4), 4211–4218. <https://doi.org/10.1021/acsami.8b14820>.
- Gao, J.; Zhao, B.; Itkis, M. E.; Bekyarova, E.; Hu, H.; Kranak, V.; Yu, A.; Haddon, R. C. Chemical Engineering of the Single-Walled Carbon Nanotube-Nylon 6 Interface. *J. Am. Chem. Soc.* **2006**, 128 (23), 7492–7496. <https://doi.org/10.1021/ja057484p>.
- Chen, J.; Ramasubramaniam, R.; Xue, C.; Liu, H. A Versatile, Molecular Engineering Approach to Simultaneously Enhanced, Multifunctional Carbon Nanotube-Polymer Composites. *Adv. Funct. Mater.* **2006**, 16 (1), 114–119. <https://doi.org/10.1002/adfm.200500590>.

Chapter 2

21. Schmidt, G.; Malwitz, M. M. Properties of Polymer-Nanoparticle Composites. *Curr. Opin. Colloid Interface Sci.* **2003**, 8 (1), 103–108. [https://doi.org/10.1016/S1359-0294\(03\)00008-6](https://doi.org/10.1016/S1359-0294(03)00008-6).
22. Heeger, A. J.; Sariciftci, N. S.; Nanddas, B. E. *Semiconducting and metallic polymers*. 2010. ISBN: 9780198528647
23. Skotheim, T. A.; Reynlod, J. R. *Handbook of Conducting Polymers, 2 Volume Set*; 2007. <https://doi.org/10.1201/b12346>.
24. Dan, L. I.; Huang, J.; Kaner, R. B. Polyaniline Nanofibers: A Unique Polymer Nanostructure for Versatile Applications. *Acc. Chem. Res.* **2009**, 42 (1), 135–145. <https://doi.org/10.1021/ar800080n>.
25. Huang, J.; Virji, S.; Weiller, B. H.; Kaner, R. B. Nanostructured Polyaniline Sensors. *Chem. - A Eur. J.* **2004**, 10 (6), 1314–1319. <https://doi.org/10.1002/chem.200305211>.
26. Tyler McQuade, D.; Pullen, A. E.; Swager, T. M. Conjugated Polymer-Based Chemical Sensors. *Chem. Rev.* **2000**, 100 (7), 2537–2574. <https://doi.org/10.1021/cr9801014>.
27. Anderson, M. R.; Mattes, B. R.; Reiss, H.; Kaner, R. B. Conjugated Polymer Films for Gas Separations. *Science* (80-.). **1991**, 252 (5011), 1412–1415. <https://doi.org/10.1126/science.252.5011.1412>.
28. Dresselhaus, M. S.; Dresselhaus, G.; Avouris, P. Carbon nanotubes: Synthesis structure, properties, and applications. Springer, Heidelberg, **2001**, 80.
29. Ajayan, P. M. Nanotubes from Carbon. *Chem. Rev.* **1999**, 99 (7), 1787–1799. <https://doi.org/10.1021/cr970102g>.
30. Baughman, R. H.; Zakhidov, A. A.; De Heer, W. A. Carbon Nanotubes - The Route toward Applications. *Science* (80-.). **2002**, 297 (5582), 787–792. <https://doi.org/10.1126/science.1060928>.
31. Haddon, R. C. Carbon Nanotubes. *Acc. Chem. Res.* **2002**, 35 (12), 997. <https://doi.org/10.1021/ar020259h>.
32. Lee, T. Y.; Alegaonkar, P. S.; Yoo, J. B. Fabrication of Dye Sensitized Solar Cell Using TiO₂ Coated Carbon Nanotubes. *Thin Solid Films* **2007**, 515 (12), 5131–5135. <https://doi.org/10.1016/j.tsf.2006.10.056>.
33. Conway, B. E. *Electrochemical Supercapacitors*; 1999. <https://doi.org/10.1007/978-1-4757-3058-6>.
34. Liu, Z.; Jiao, L.; Yao, Y.; Xian, X.; Zhang, J. Aligned, Ultralong Single-Walled Carbon Nanotubes: From Synthesis, Sorting, to Electronic Devices. *Adv. Mater.* **2010**, 22 (21), 2285–2310. <https://doi.org/10.1002/adma.200904167>.
35. Tuncel, D. Non-Covalent Interactions between Carbon Nanotubes and Conjugated Polymers. *Nanoscale* **2011**, 3 (9), 3545. <https://doi.org/10.1039/c1nr10338e>.
36. Tummala, N. R.; Morrow, B. H.; Resasco, D. E.; Striolo, A. Stabilization of Aqueous Carbon Nanotube Dispersions Using Surfactants: Insights from Molecular Dynamics Simulations. *ACS Nano* **2010**, 4 (12), 7193–7204. <https://doi.org/10.1021/nn101929f>.
37. Grossiord, N.; Loos, J.; Regev, O.; Koning, C. E. Toolbox for Dispersing Carbon Nanotubes into Polymers to Get Conductive Nanocomposites. *Chem. Mater.* **2006**, 18 (5), 1089–1099. <https://doi.org/10.1021/cm051881h>.
38. Zou, J.; Liu, L.; Chen, H.; Khondaker, S. I.; McCullough, R. D.; Huo, Q.; Zhai, L. Dispersion of Pristine Carbon Nanotubes Using Conjugated Block Copolymers. *Adv. Mater.* **2008**, 20 (11), 2055–2060. <https://doi.org/10.1002/adma.200701995>.
39. Zou, J.; Khondaker, S. I.; Huo, Q.; Zhai, L. A General Strategy to Disperse and Functionalize Carbon Nanotubes Using Conjugated Block Copolymers. *Adv. Funct. Mater.* **2009**, 19 (3), 479–483. <https://doi.org/10.1002/adfm.200800542>.
40. Dyke, C. A.; Tour, J. M. Overcoming the Insolubility of Carbon Nanotubes Through High Degrees of Sidewall Functionalization. *Chem. - A Eur. J.* **2004**, 10 (4), 812–817. <https://doi.org/10.1002/chem.200305534>.
41. Saini, V.; Li, Z.; Bourdo, S.; Dervishi, E.; Xu, Y.; Ma, X.; Kunets, V. P.; Salamo, G. J.; Viswanathan, T.; Biris, A. R.; Saini, D.; Biris, A. S. Electrical, Optical, and Morphological

- Properties of P3ht-Mwnt Nanocomposites Prepared by In Situ Polymerization. *J. Phys. Chem. C* **2009**, 113 (19), 8023–8029. <https://doi.org/10.1021/jp809479a>.
42. Kuila, B. K.; Malik, S.; Batabyal, S. K.; Nandi, A. K. In-Situ Synthesis of Soluble Poly(3-Hexylthiophene)/Multiwalled Carbon Nanotube Composite: Morphology, Structure, and Conductivity. *Macromolecules* **2007**, 40 (2), 278–287. <https://doi.org/10.1021/ma061548e>.
43. Mishra, A. K.; Agrawal, N. R.; Das, I. Synthesis of Water Dispersible Dendritic Amino Acid Modified Polythiophenes as Highly Effective Adsorbent for Removal of Methylene Blue. *J. Environ. Chem. Eng.* **2017**, 5 (5), 4923–4936. <https://doi.org/10.1016/j.jece.2017.09.017>.
44. Jiang, C.; Chen, G.; Wang, X. High-Conversion Synthesis of Poly(3,4-Ethylenedioxythiophene) by Chemical Oxidative Polymerization. *Synth. Met.* **2012**, 162 (21–22), 1968–1971. <https://doi.org/10.1016/j.synthmet.2012.09.008>.
45. Lin, Y.; Zhou, B.; Fernando, K. A. S.; Liu, P.; Allard, L. F.; Sun, Y. P. Polymeric Carbon Nanocomposites from Carbon Nanotubes Functionalized with Matrix Polymer. *Macromolecules* **2003**, 36 (19), 7199–7204. <https://doi.org/10.1021/ma0348876>.
46. Mandal, A.; Nandi, A. K. Noncovalent Functionalization of Multiwalled Carbon Nanotube by a Polythiophene-Based Compatibilizer: Reinforcement and Conductivity Improvement in Poly(Vinylidene Fluoride) Films. *J. Phys. Chem. C* **2012**, 116 (16), 9360–9371. <https://doi.org/10.1021/jp302027y>.
47. Cho, K. Y.; Yeom, Y. S.; Seo, H. Y.; Park, Y. H.; Jang, H. N.; Baek, K. Y.; Yoon, H. G. Rational Design of Multiamphiphilic Polymer Compatibilizers: Versatile Solubility and Hybridization of Noncovalently Functionalized CNT Nanocomposites. *ACS Appl. Mater. Interfaces* **2015**, 7 (18), 9841–9850. <https://doi.org/10.1021/acsami.5b01849>.
48. Clavé, G.; Delpont, G.; Roquelet, C.; Lauret, J. S.; Deleporte, E.; Vialla, F.; Langlois, B.; Parret, R.; Voisin, C.; Roussignol, P.; Jousselmé, B.; Gloter, A.; Stephan, O.; Filoramo, A.; Derycke, V.; Campidelli, S. Functionalization of Carbon Nanotubes through Polymerization in Micelles: A Bridge between the Covalent and Non-covalent Methods. *Chem. Mater.* **2013**, 25 (13), 2700–2707. <https://doi.org/10.1021/cm401312v>.
49. Kang, Y.; Taton, T. A. Micelle-Encapsulated Carbon Nanotubes: A Route to Nanotube Composites. *J. Am. Chem. Soc.* **2003**, 125 (19), 5650–5651. <https://doi.org/10.1021/ja034082d>.
50. Tkalya, E. E.; Ghislandi, M.; de With, G.; Koning, C. E. The Use of Surfactants for Dispersing Carbon Nanotubes and Graphene to Make Conductive Nanocomposites. *Curr. Opin. Colloid Interface Sci.* **2012**, 17 (4), 225–232. <https://doi.org/10.1016/j.cocis.2012.03.001>.
51. Wang, Y.; Santos, P. J.; Kubiak, J. M.; Guo, X.; Lee, M. S.; Macfarlane, R. J. Multistimuli Responsive Nanocomposite Tectons for Pathway Dependent Self-Assembly and Acceleration of Covalent Bond Formation. *J. Am. Chem. Soc.* **2019**, 141 (33), 13234–13243. <https://doi.org/10.1021/jacs.9b06695>.
52. Wang, H. Dispersing Carbon Nanotubes Using Surfactants. *Curr. Opin. Colloid Interface Sci.* **2009**, 14 (5), 364–371. <https://doi.org/10.1016/j.cocis.2009.06.004>.
53. Gong, X.; Liu, J.; Baskaran, S.; Voise, R. D.; Young, J. S. Surfactant-Assisted Processing of Carbon Nanotube/Polymer Composites. *Chem. Mater.* **2000**, 12 (4), 1049–1052. <https://doi.org/10.1021/cm9906396>.
54. Czajka, A.; Hazell, G.; Eastoe, J. Surfactants at the Design Limit. *Langmuir* **2015**, 31 (30), 8205–8217. <https://doi.org/10.1021/acs.langmuir.5b00336>.
55. Giddings, L. D.; Olesik, S. V. A Study of AOT Reverse Micelles in Liquids at Ambient and High Pressure. *Langmuir* **1994**, 10 (9), 2877–2883. <https://doi.org/10.1021/la00021a008>.
56. Jang, J.; Yoon, H. Formation Mechanism of Conducting Polypyrrole Nanotubes in Reverse Micelle Systems. *Langmuir* **2005**, 21 (24), 11484–11489. <https://doi.org/10.1021/la051447u>.

57. Sheu, E. Y.; Chen, S. H.; Huang, J. S. Structure, Interaction, and Growth of Sodium Dodecyl-o-Xylenesulfonate Micelles in Aqueous Solutions. *J. Phys. Chem.* **1987**, 91 (6), 1535–1541. <https://doi.org/10.1021/j100290a049>.
58. Gök, A.; Omastová, M.; Yavuz, A. G. Synthesis and Characterization of Polythiophenes Prepared in the Presence of Surfactants. *Synth. Met.* **2007**, 157 (1), 23–29. <https://doi.org/10.1016/j.synthmet.2006.11.012>.
59. Liu, R.; Liu, Z. Polythiophene: Synthesis in Aqueous Medium and Controllable Morphology. *Chinese Sci. Bull.* **2009**, 54 (12), 2028–2032. <https://doi.org/10.1007/s11434-009-0217-0>.
60. Qiao, X.; Wang, X.; Mo, Z. The FeCl₃-Doped Poly(3-Alkythiophenes) in Solid State. *Synth. Met.* **2001**, 122 (2), 449–454. [https://doi.org/10.1016/S0379-6779\(00\)00587-7](https://doi.org/10.1016/S0379-6779(00)00587-7).
61. Kiani, G.; Sheikhoie, H.; Rostami, A. Highly enhanced electrical conductivity and thermal stability of polythiophene/single-walled carbon nanotubes nanocomposite. *Iran. Polym. J.* 2011, 20(8), 623–632.
62. Ballav, N.; Biswas, M. Preparation and Evaluation of a Nanocomposite of Polythiophene with Al₂O₃. *Polym. Int.* **2003**, 52 (1), 179–184. <https://doi.org/10.1002/pi.1001>.
63. Tian, Z. Q.; Jiang, S. P.; Liang, Y. M.; Shen, P. K. Synthesis and Characterization of Platinum Catalysts on Multiwalled Carbon Nanotubes by Intermittent Microwave Irradiation for Fuel Cell Applications. *J. Phys. Chem. B* **2006**, 110 (11), 5343–5350. <https://doi.org/10.1021/jp056401o>.
64. Xu, D.; Lu, P.; Dai, P.; Wang, H.; Ji, S. In Situ Synthesis of Multiwalled Carbon Nanotubes over LaNiO₃ as Support of Cobalt Nanoclusters Catalyst for Catalytic Applications. *J. Phys. Chem. C* **2012**, 116 (5), 3405–3413. <https://doi.org/10.1021/jp211009g>.
65. Lee, S. J.; Lee, J. M.; Cheong, I. W.; Lee, H.; Kim, J. H. A Facile Route of Polythiophene Nanoparticles via Fe³⁺-Catalyzed Oxidative Polymerization in Aqueous Medium. *J. Polym. Sci. Part A Polym. Chem.* **2008**, 46 (6), 2097–2107. <https://doi.org/10.1002/pola.22544>.
66. Philip, B.; Xie, J.; Chandrasekhar, A.; Abraham, J.; Varadan, V. K. A Novel Nanocomposite from Multiwalled Carbon Nanotubes Functionalized with a Conducting Polymer. *Smart Mater. Struct.* **2004**, 13 (2), 295–298. <https://doi.org/10.1088/0964-1726/13/2/007>.
67. Salami-Kalajahi, M.; Haddadi-Asl, V.; Behboodi-Sadabad, F.; Rahimi-Razin, S.; Roghani-Mamaqani, H. Properties of PMMA/Carbon Nanotubes Nanocomposites Prepared by “Grafting through” Method. *Polym. Compos.* **2012**, 33 (2), 215–224. <https://doi.org/10.1002/pc.22141>.
68. Grassi, G.; Scala, A.; Piperno, A.; Iannazzo, D.; Lanza, M.; Milone, C.; Pistone, A.; Galvagno, S. A Facile and Ecofriendly Functionalization of Multiwalled Carbon Nanotubes by an Old Mesoionic Compound. *Chem. Commun.* **2012**, 48 (54), 6836–6838. <https://doi.org/10.1039/c2cc31884a>.
69. Rohini Das, K.; Jinish Antony, M. Synthesis and Characterisation of Water Dispersible Copolymer Submicron Spheres of Poly-(Phenylenediamine-Co-N-Sulfopropyl Aniline) via Random Copolymerisation. *Polymer (Guildf)*. **2016**, 87, 215–225. <https://doi.org/10.1016/j.polymer.2016.01.078>.

Chapter 3

Polythiophene-functionalized MWCNT Nanocomposites: Preparation and Properties

Chapter 3

3.1. Introduction

Comprehensive knowledge of conducting polymers and carbon nanotubes available in the literature is beneficial for developing conducting nanocomposites of conducting polymers with carbon nanotubes. The critical parameters for such nano composite preparation include compatibility of component phases and changes in optoelectrical and mechanical properties.¹⁻¹⁰ However, the creation of nanocomposites confronts some technical difficulties also. The difficulty in improving the solubility or dispersibility of individual components in the reaction medium due to the hydrophobic nature of carbon nanotubes and conducting polymer is a significant obstacle for preparing nanocomposites.^{10,11} Aggregation tendency of carbon nanotubes in bundled form is another factor that hinders the formation of dispersed CNTs for nanocomposites preparation.^{6,10}

Suitable surface functionalization techniques can minimize the aggregation tendency of carbon nanotubes. The surface functionalization of carbon nanotubes can be carried out by a covalent or non-covalent approach. Small functional groups introduced to the surface of carbon nanotube can be further derivatised to larger chemical entities^{12,13-15} or grafting of polymer on the surface of CNT through covalent bonding^{16,17} or non-covalent orientation of small molecules on the surface of CNT^{18,19} and non-covalent wrapping of polymer chains on CNT surface.^{15,20} Different functionalization practices of carbon nanotubes are shown in **Figure 3.1**. Covalent attachment of hydrophilic functional groups is better practice than relatively weak non-covalent modification for providing higher solvent compatibility and strong interfacial interaction with other matrices in its composite state.^{14,19,21} Excessive covalent functionalization or functionalization under harsh conditions could create good coverage of functional groups, however it might severely damage the intrinsic molecular structure of CNT and produce smaller carbonaceous fragments.^{14,15,20} Therefore, covalent modification of CNT furnishing moderate degree of functionalization would be more preferable.²¹⁻²³ Non-covalent functionalization is an attractive method to cover a large area of carbon nanotubes by suitably orienting the molecular or polymer moieties by weak non-covalent interactions such as hydrogen bonding, π - π stacking interactions, van der Waals force of attraction, etc. Non-covalent functionalization strategy provide less firmness to composite framework than the

covalent method because of weak non-bonded forces of attraction between the components.^{19,24} But the advantage of non-covalent method of functionalization is that it does not significantly destruct the π -conjugated network structure.^{19,25}

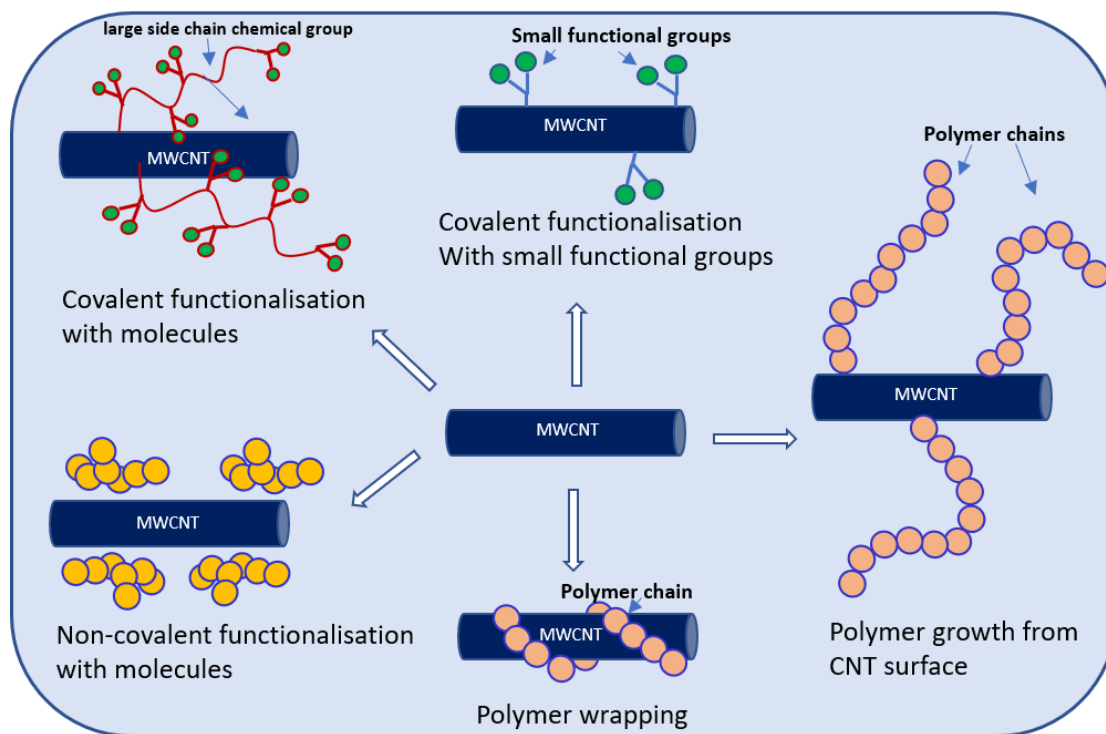


Figure 3.1. Different surface functionalization strategies on carbon nanotubes.

We could observe that covalent and non-covalent approaches to CNT functionalization impart their advantages and possess some limitations also. Hence, it would be more noteworthy to adopt the combined use of both covalent and non-covalent functionalization strategies for modifying carbon nanotubes. The strategy and protocol selected should be simple to execute and easy to be scaled up.^{19,20,23,24,26} Yuan and Chan-Park reported that covalent combined with non-covalent functionalization of single-walled carbon nanotubes synergistically improved both carbon nanotube dispersion and nanotube phase transfer /matrix interfacial strength, leading to superior mechanical reinforcement in polymer nanocomposites (see **Figure 3.2. (1)**).²⁶ Clave et al. reported immobilisation of organic molecules in the internal hydrophobic cores of micelles followed by in-situ polymerisation around the nanotube scaffold. They adopted the combined use of covalent and non-covalent approaches for the specific modification of carbon nanotubes.¹⁹ Berger and co-workers introduced a phase transfer method for polymer-wrapped single-walled carbon nanotubes to create luminescent

aryl defects. They proposed that the material as an efficient near-infrared light emitting diode as thin film (see **Figure 3.2. (2)**).¹² The combined use of covalent and non-covalent functionalization promoted solvent compatibility of the compound by minimizing the drawbacks arising from both the functionalization strategies.^{12,19,26,27} In that way, mild covalent modification of CNT prior to non-covalent attachment of bulky conjugated polymer would be a better strategy to strengthen the interfacial interaction between the less destructed state of nanotubes and the polymer.^{12,15,19}

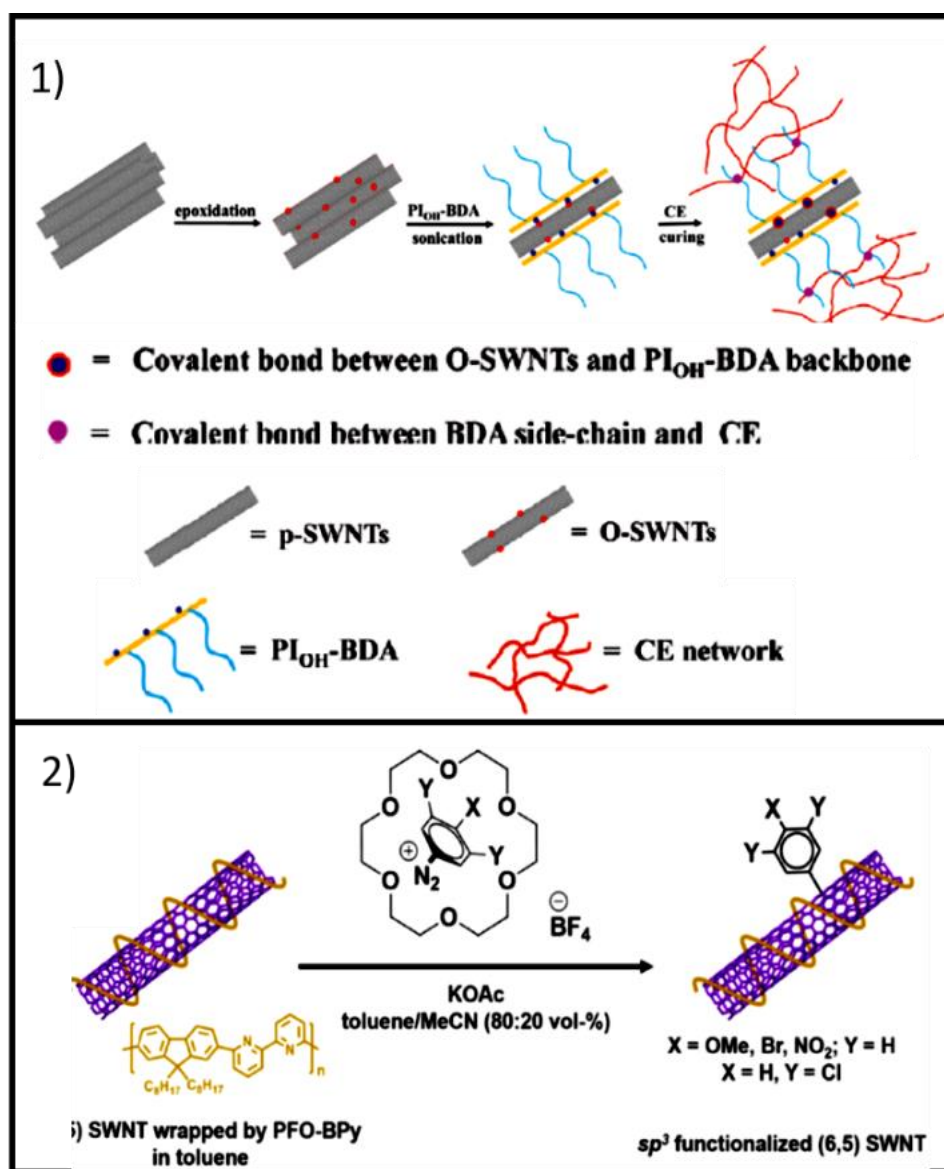


Figure 3.2. Combined covalent cum non-covalent functionalization of carbon nanotubes with molecular and polymer entities adapted from 1)Yuan and Chan-Park 2012 and 2) Berger et al. 2019.

Table 3.1. Defect group functionalization and their relevance seen in the literature.

Sl. no.	Method of functionalization	Defect group/s	Other materials incorporated	Relevance of work	Ref.
1	Electrochemical reduction	Aryl groups	-	Solubility enhancement, Switching and memory behaviour	28
2	Chemical (at 80-90°C)	Alkyl groups terminated with carboxylic acid groups and their extended amides	-	Large diamagnetic susceptibility based on theoretical study	29
3	Chemical	Carboxylic acid group	Polyvinyl alcohol	Polymer nanocomposite preparation	30
4	Free radical reaction	Alkyl groups and its derivatives	-	Improved solubility, high degree of functionalization	31
5	chemical	Carboxylic acid group	Different polymeric and oligomeric compounds	Enhanced solubility and strong luminescence emissions	32
6	Nitrogen glow discharge	C≡N group	-	Microwave generated nitrogen plasma as source of nitrogen containing functional groups	33
7	Chemical (argon ion treatment)	Free radical groups	-	Controlled functionalization using 2 ke V Ar ⁺	34
8	Chemical	Carboxylic acid groups	Derivatized polyimide	Nanocomposite formation with higher dispersibility	35
9	chemical	amine	-	Improved CO ₂ adsorption	23
10	chemical	Carboxylic acid group	Polyvinyl alcohol	Increase in mechanical strength	36
11	Microwave excited Ar/O ₂ surface wave plasma treatment	Oxygen containing functional groups	-	Good dispersion in water	37
12	Chemical	Carboxylic acid groups	polythiophene	Bilayer photovoltaics	9
13	Chemical (Hydrothermal oxidation)	Oxygen functional groups	-	Studied advantages of nitric acid oxidation	39
14	Chemical	Amide groups having phenolic linker	Single chain variable fragment protein	Detection of prostate cancer	38

Insertion of functional groups on the surface of CNT helps to improve its disentanglement and solvent compatibility in polar solvents.^{31,32,39} Some of the defect group functionalization approaches selected from the literature and their relevance are summarised in **Table 3.1**. The tabulated data showed that functionalized carbon nanotubes, independently and in a composite state, have their own relevance in terms of property enhancement or in suitable applications.^{9,23,28-39} Carboxylic acid groups and other oxygen-containing functional groups could be inserted on the CNT surface by adopting simple acid treatment methods. Here the polar nature of such defect functional groups can facilitate the formation of dispersible carbon nanotubes in polar medium.^{14,26} Acid treatment would be attractive as a simple functionalizing strategy without damaging the intrinsic chemical structure of CNT and enhancing the water dispersion by the involvement of hydrogen bonding between carboxylic acid functional groups and water molecules. Polymers or other structurally related molecules are usually being selected for further modifications in the acid-functionalized carbon nanotubes.^{13,18,26} Polymer can be combined with functionalized CNT by covalent or non-covalent modification (see **Figure 3.3**).^{12,26,27}

In this chapter, carboxylic acid functionalization of multi-walled carbon nanotubes were carried out using oxidative treatment with HNO₃ followed by a non-covalent approach of nanocomposite preparation with conducting polythiophene in the presence of AOT surfactant. In effect, covalent functionalization followed by non-covalent modification was implemented here as a preparation strategy for nanocomposites. Defect group functionalization improved the non-covalent compatibility of carbon nanotubes with polythiophene matrix via enhancing non-covalent surface interactions. FT-IR and Raman spectra were recorded to analyse the acid functionalization of MWCNT. The MWCNT-COOH and PTCNT-COOH nanocomposites were characterized using FT-IR analysis, elemental analysis, X-ray photoelectron spectroscopy, X-ray diffraction analysis and pH measurements. Morphological analyses were also conducted with FE-SEM and HR-TEM imaging. UV-vis absorption spectra were recorded in the dispersed state of the nanocomposite in chloroform medium. Thermal stability and electrical conductivity were also measured. The chapter has given immense attention for describing the formation of polythiophene-functionalised MWCNT core-shell nanocomposite with enhanced electrical conductivity and thermal stability.

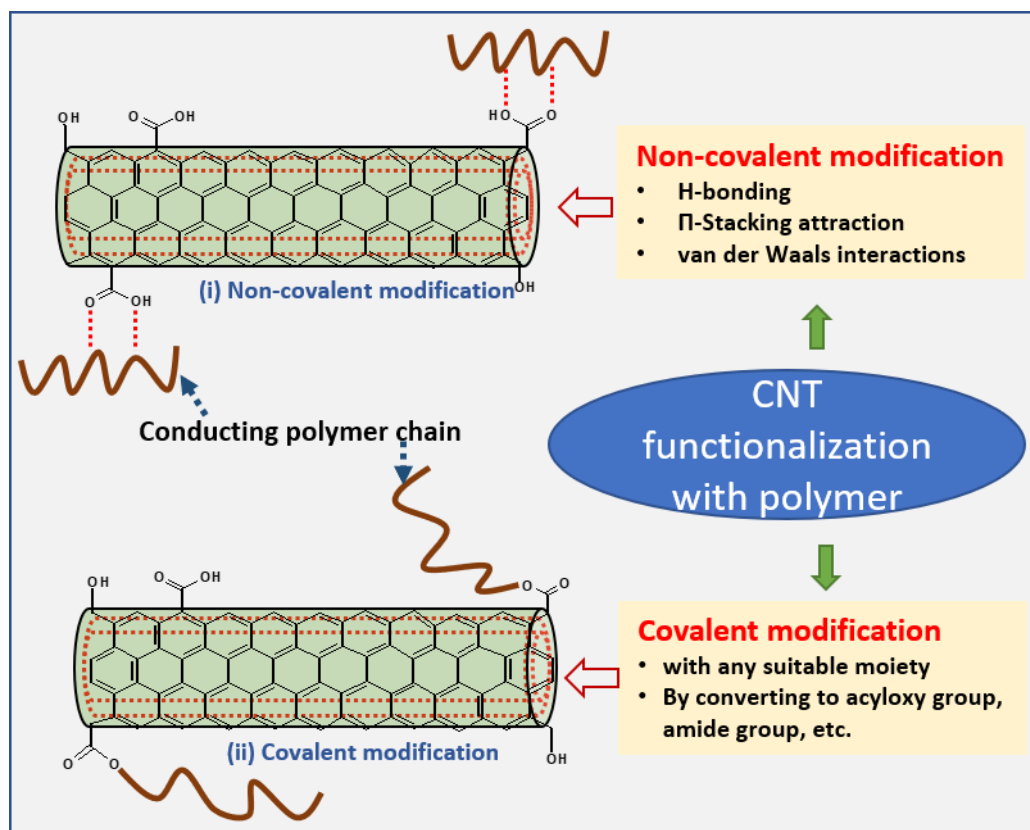


Figure 3.3. Non-covalent functionalization (modification) and covalent functionalization (modification) of CNT with polymer.

3.2. Experimental

3.2.1. Materials and reagents: Thiophene, ferric chloride, sodium bis (2-ethyl hexyl) sulfosuccinate (AOT) and multi-walled carbon nanotubes were purchased from Sigma Aldrich and used without further purification. Deionized water, conc. HNO_3 , chloroform and acetone were purchased from Merck chemicals, India.

3.2.2. Measurements and instruments: FT-IR spectra of the samples were recorded using KBr pellet method by Shimadzu IR Affinity 1 spectrometer. The elemental analyses (CHNS) of the samples were carried out using elemental vario EL III element analyser. Powder X-ray diffraction (P-XRD) analyses of the samples were conducted using PANALYTICAL, Aeris research with 2θ values ranging from 5° - 90° . pH studies were carried out with HM digital PH-80 Temp hydrotester. Scanning electron microscopic (SEM) imaging were conducted using JEOL Model JSM-6390LV scanning electron microscope. Transmission electron microscopic (TEM) images were

recorded with JEOL/JEM 2100 instrument having a capacity of 200 KV with magnification 2000x-1500000x. Electrical conductivity of the samples were measured using DFP-RM-200 with constant current source Model CCS-01 and DC microvoltmeter. UV-visible absorption spectra of the samples were recorded with HPLC grade chloroform and double deionized water as solvent using Shimadzu UV-Visible spectrophotometer 1800 series. Thermogravimetric analysis (TGA) was carried out using Perkin Elmer, Diamond TG/DTA.

3.2.3. Synthesis of MWCNT-COOH 5M: MWCNT (0.40 g) was added to nitric acid (5 M, 50 mL) taken in an RB flask and then sonicated for 15 min for making dispersion. The reaction mixture was refluxed at 100 °C for 7 h with magnetic stirring. The refluxed reaction mixture was washed with deionized water until the pH of the filtrate became neutral. This was then washed with acetone, filtered and dried in vacuum oven at 60° C for 3 h. Yield: 0.36 g. FT-IR (KBr, cm^{-1}) 1465, 1504, 1648, 1698, 1741.

3.2.4. Synthesis of PTCNT-COOH 300: Monomer thiophene (1 mL, 12.50 mmol) and surfactant AOT (0.22 g, 0.50 mmol) was dissolved in chloroform (20 mL) and sonicated for 5 min. MWCNT-COOH (0.30 g) was added to the AOT-thiophene mixture in chloroform and sonicated for 10 min. The dispersed form of FeCl_3 in 10 mL chloroform was added drop by drop to the AOT-thiophene-MWCNT-COOH mixture and then sonicated for 15 min. Subsequently, the reaction mixture was magnetically stirred for 3 h. Polymer nanocomposite thus obtained was filtered and washed using water and acetone. The resultant composite was then dried in a vacuum oven at 60°C. Yield: 0.82 g. FT-IR (KBr, cm^{-1}) 1667, 1536, 1028 (w), 779 (w), 668. Elemental analysis (anal., wt %): C, 41.14; S, 17.80; H, 3.02.

PTCNT-COOH 100 and PTCNT-COOH 200 were prepared using the same procedure as above by changing the quantity of MWCNT to 0.10 and 0.20 g, respectively. The figures mentioned in sample codes PTCNT-COOH 100, PTCNT-COOH 200 and PTCNT-COOH 300 represent the amount of multi-walled carbon nanotubes used in milligrams for the preparation of respective nanocomposites. Preparation of PTCNT-COOH 100 and PTCNT-COOH 200 yielded 1.16 g and 1.22 g of nanocomposites, respectively.

3.2.5. Synthesis of PT2CNT-COOH 300: Monomer thiophene (0.5 mL, 6.25 mmol) and AOT (0.11 g, 0.25 mmol) were dissolved in chloroform (10 mL) and sonicated for

5 min. To the monomer-AOT solution mixture, MWCNT-COOH (0.075 g) was added and sonicated for 10 min. Ferric chloride (1.22 g, 7.50 mmol) dispersed in 5 mL chloroform was added drop by drop to monomer-surfactant-MWCNT mixture and sonicated for 15 min. After that, it was stirred using a magnetic stirrer for 3 h. The resultant polymer-nano composites were washed using water and acetone and finally filtered by suction pump. The composite obtained was dried in vacuum oven at 60°C for 3 h. Yield: 0.193 g.

PT3CNT-COOH-300 was prepared using the same procedure by changing the amount of thiophene to 0.75 mL (9.36 mmol). The yield obtained for PT3CNT-COOH 300 was 0.278 g.

3.3. Results and Discussion

3.3.1. Synthesis and characterization of functionalized MWCNT-COOHs

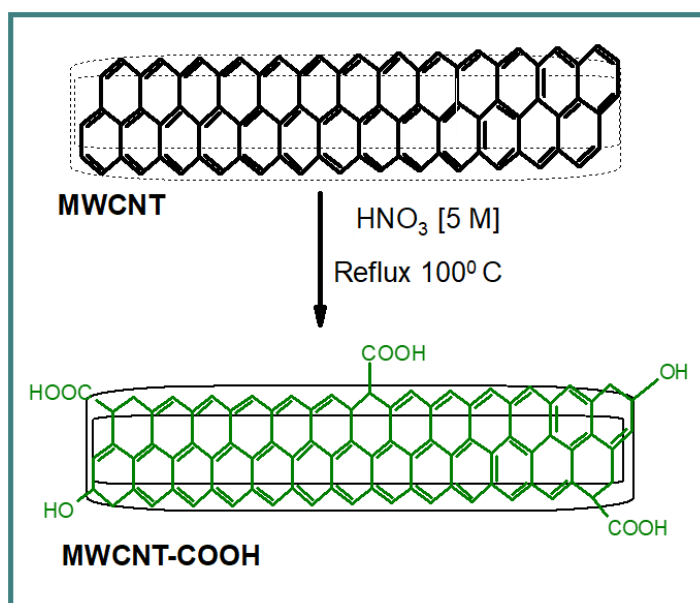


Figure 3.4. Schematic representation of the preparation of MWCNT-COOH

Carboxylic acid-functionalized multi-walled carbon nanotubes were prepared by refluxing MWCNT with nitric acid at 100°C for 7 h. Different reagent conditions adopted for acid functionalization involve treatment with 5 M HNO₃, 10 M HNO₃, and combined use of 5 M HNO₃ along with NaNO₃, producing functionalized MWCNTs named MWCNT-COOH 5M, MWCNT-COOH 10M and MWCNT-COOH-N 5M respectively. Treatment with nitric acid creates defective sites on the walls of carbon nanotubes and produce different functional groups like

carboxylic acid, hydroxyl group, aldehyde and keto group, etc.²⁵ Inherent agglomeration tendency of carbon nanotubes always hinders the processability in applications. Literature studies reveals that the acid functionalization of carbon nanotubes is an uncomplicated and cost-effective way to improve the dispersion in polar solvents.^{14,25} Schematic representation of the synthesis of MWCNT-COOH 5M is given in **Figure 3.4**.

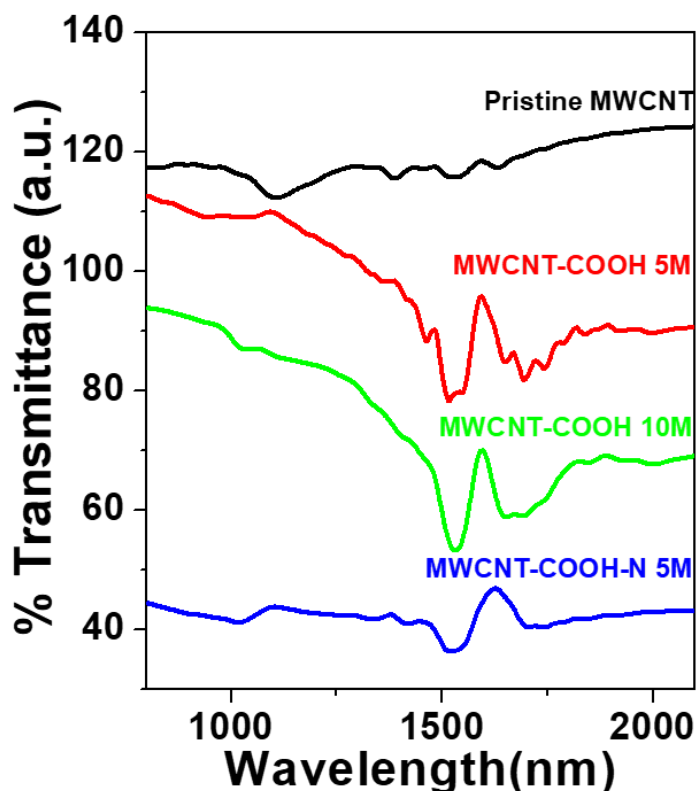


Figure 3.5. FT-IR spectra of Pristine MWCNT, MWCNT-COOH 5M, MWCNT-COOH 10M and MWCNT-COOH-N 5M

Structural changes on the walls of multi-walled carbon nanotubes were studied by fourier transform infrared spectroscopy by making thin pellets of samples with KBr powder. FT-IR spectra of pristine MWCNT, MWCNT-COOH 5M, MWCNT-COOH 10M and MWCNT-COOH-N 5M are shown in **Figure 3.5**. Pristine MWCNTs have shown characteristic peaks at 1528 and 1641 cm^{-1} due to in-plane vibrations of graphitic walls of carbon nanotubes and C=C stretching vibrations of carbon nanotubes, respectively.^{40,41} Good symmetry of the carbon nanotube produces weak dipole moment changes and hence poor signals.⁴² MWCNT-COOH 5M, MWCNT-COOH 10M and MWCNT-COOH-N 5M exhibited strong infrared signals compared with pristine

MWCNT. Functionalized MWCNT-COOH samples showed peaks at 1465, 1528, 1648, 1698 and 1741 cm^{-1} due to C-O bending of aliphatic alcohol, in-plane vibrations of graphitic walls, C=C stretching vibrations, C=O stretching vibrations of carbonyl (keto or aldehyde functional group) and carboxylic groups respectively.⁴¹⁻⁴³ The broad peaks corresponding to hydrogen-bonded -OH functional groups, including water molecules attached to CNT, were present in the range 3612 - 3744 cm^{-1} .⁴³ The above outcomes indicated that the chemical treatment with HNO_3 produces defective sites functional groups on carbon nanotubes, including carboxylic acid groups. A comparison of the FT-IR spectra of MWCNT-COOH 5M, MWCNT-COOH 10M and MWCNT-COOH-N 5M suggested that MWCNT-COOH 5M exhibits good functionalization peaks with minimum use of nitric acid. Thereby MWCNT-COOH 5M was used for further preparations of polythiophene-MWCNT composites. The name MWCNT-COOH 5M is abbreviated as MWCNT-COOH for the remaining studies.

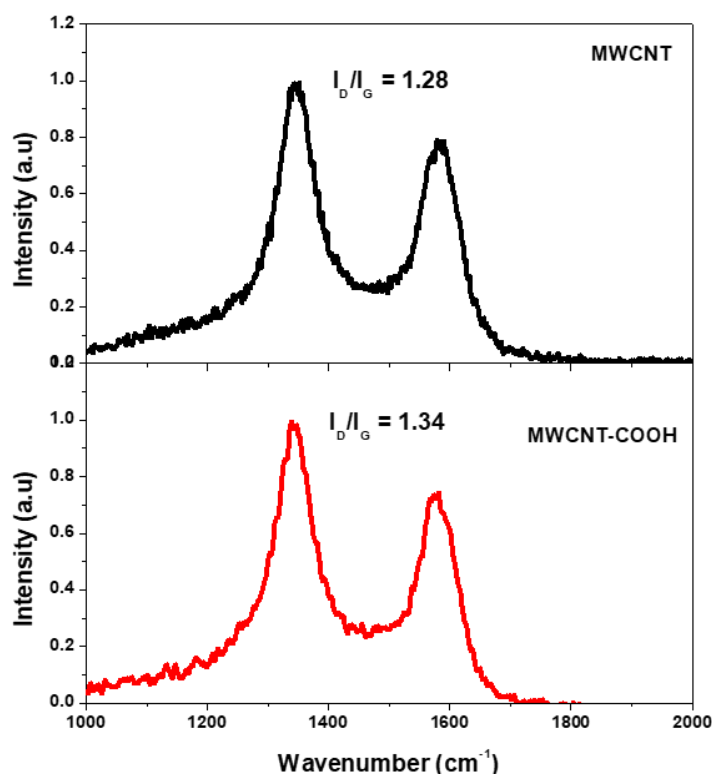


Figure 3.6. Raman spectra of purified MWCNT and MWCNT-COOH

Raman spectroscopy of purified MWCNT and functionalised MWCNT-COOH has been carried out to determine the degree of disorder in the graphitic structure of multi-walled carbon nanotube (see **Figure 3.6.**). Carbon nanotubes was purified by sonicating MWCNT with 0.5 M HNO_3 for 15 min followed by magnetic stirring for 30

min at room temperature. Pristine MWCNT may contain amorphous carbon and catalytic impurities, which could be removed with acid washing. The characteristic peaks of multi-walled carbon nanotube termed as G band and D-band were present at 1576 cm^{-1} and 1348 cm^{-1} , respectively. The G band was due to in-plane tangential stretching of the graphitic carbon-carbon bonds in graphene sheets and the D band was due to the presence of amorphous carbon and disordered structure in CNT.⁴¹⁻⁴³ The I_D/I_G ratio for purified MWCNT and functionalized MWCNT-COOH were found to be 1.28 and 1.34 respectively. The acid washing removes the impurities of pristine MWCNT, however, acid oxidation produced functionalization of carbon nanotube along with the removal of impurities, which resulted in a higher I_D/I_G ratio for functionalised MWCNT-COOH.^{41,42}

3.3.2. Synthesis and characterization of PTCNT-COOH nanocomposites

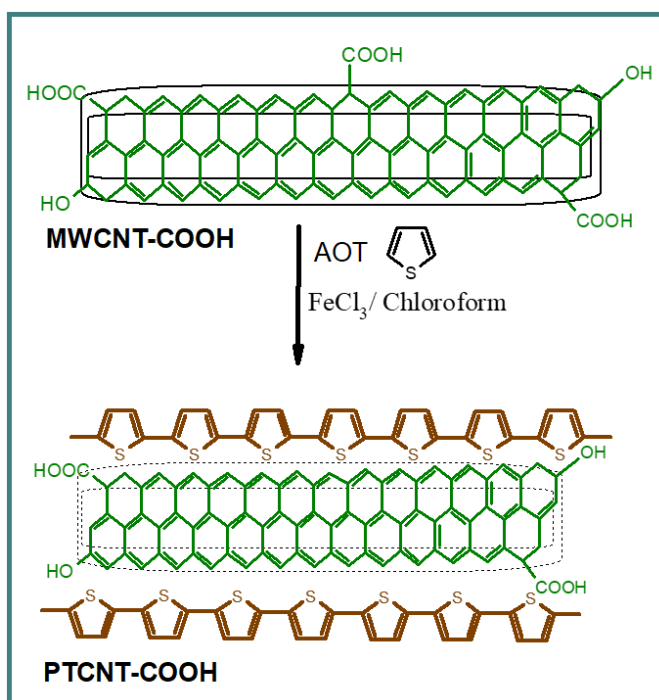


Figure 3.7. Schematic representation of the synthesis of PTCNT-COOH nanocomposites.

Polythiophene-functionalized multi-walled carbon nanotube nanocomposites (PTCNT-COOHs) were prepared by *in situ* oxidative chemical polymerization of thiophene monomer in the presence of functionalized multi-walled carbon nanotubes (MWCNT-COOH) using ferric chloride as the oxidizing agent and sodium bis(2-ethylhexyl) sulfosuccinate (AOT) as anionic surfactant. Thiophene-AOT micellar

Chapter 3

complexes get attached to the walls of multi-walled carbon nanotubes through non-covalent interaction and get polymerized by oxidizing agents to result in water-dispersible core-shell nanostructured polythiophene-functionalized MWCNT-COOH nanocomposites.⁴⁴⁻⁴⁷ The highly dispersed nature of MWCNT-COOH in CHCl_3 helps to orient thiophene-AOT micellar complexes near the locality of functionalized multi-walled carbon nanotubes, which in turn facilitates the polymerization of thiophene to take place quickly on the surface of multi-walled carbon nanotubes.⁴⁴ Scheme for the synthesis of PTCNT-COOH composite is represented in **Figure 3.7**. Details regarding the concentration of thiophene, AOT, and ferric chloride and the amount of MWCNT-COOH and the yield obtained were given in **Table 3.2**.

Table 3.2. Millimoles of thiophene, AOT, and ferric chloride, amount of functionalized MWCNT-COOH, mole ratio of monomer/AOT, mole ratio of monomer/ FeCl_3 , elemental composition of samples and yield.

Samples	Thiophene (mmol)	AOT (mmol)	FeCl_3 (mmol)	MWCNT – COOH added (mg)	Monomer /AOT mole ratio	Monomer/ FeCl_3 mole ratio	Elemental Composition (%)			Yield (mg)
							C	H	S	
PTCNT-COOH 100	12.50	0.50	15.00	100	1:1/25	1:1.2	61.52	0.41	26.72	490
PTCNT-COOH 200	12.50	0.50	15.00	200	1:1/25	1:1.2	-	-	-	600
PTCNT-COOH 300	12.50	0.50	15.00	300	1:1/25	1:1.2	66.58	0.31	17.53	700

The FT-IR spectroscopic studies of PT-25, pristine MWCNT, MWCNT-COOH and PTCNT-COOHs (100, 200 and 300) were carried out (see **Figure 3.8**). The PT-25 has two major characteristic peaks that appeared at 787 and 688 cm^{-1} due to C-H out-of-plane deformation and C-S stretching of thiophene ring moiety.⁴⁸ PTCNT-COOHs (100, 200 and 300) have shown well matched strong infrared signals with functionalized multi-walled carbon nanotubes (MWCNT-COOH). Functionalized MWCNT-COOH samples have shown peaks at 1465, 1528, 1648, 1698 and 1741 cm^{-1} due to C-O bending of aliphatic alcohol, in-plane vibrations of graphitic walls, C=C stretching vibrations, C=O stretching vibrations of carbonyl (keto or aldehyde functional group) and carboxylic acid groups respectively.⁴¹⁻⁴³ PTCNT-COOHs

nanocomposites (100, 200 and 300) have the two extra peaks of polythiophene at 785 and 675 cm^{-1} corresponding to C-H out of plane deformation and C-S stretching of polythiophene chains in addition to the peaks in MWCNT-COOH.⁴⁸

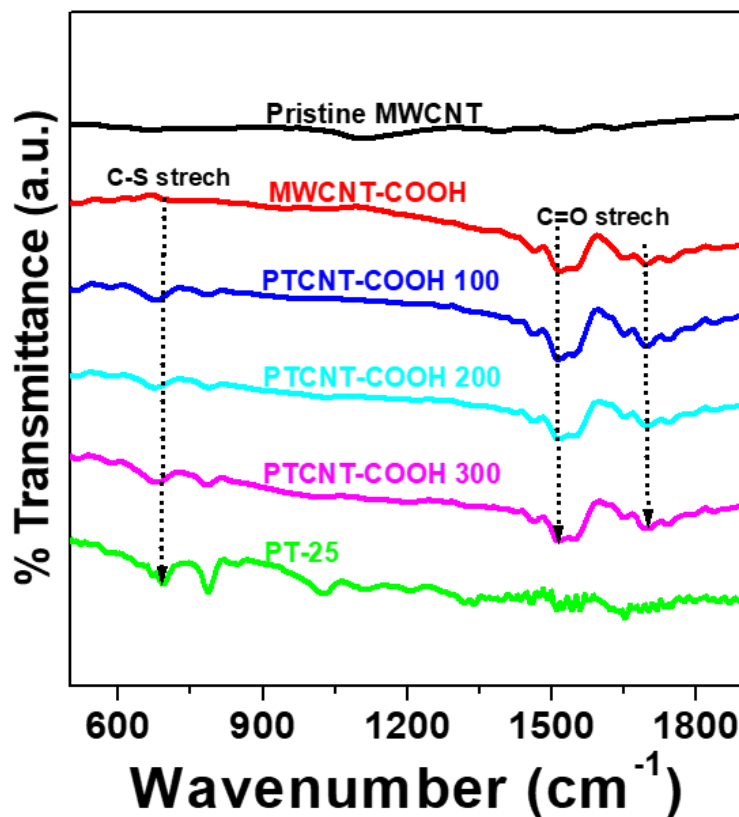


Figure 3.8. FT-IR spectra of pristine MWCNT, MWCNT-COOH, PTCNT-COOH 100, PTCNT-COOH 200, PTCNT-COOH 300 and PT-25.

The pH studies of aqueous dispersed forms of the samples such as functionalized MWCNT-COOH, PTCNT-COOH 100, PTCNT-COOH 200 and PTCNT-COOH 300 were carried out using a pH meter. The pH value of MWCNT-COOH was obtained as 4.8, which is acidic due to the dissociation of H^+ ion from carboxylic acid groups. The pH values of PTCNT-COOH 300, PTCNT-COOH 200 and PTCNT-COOH 100 gradually increased to 5.4, 6.2 and 6.7, respectively. This increase in pH (decrease in acidity) was attributed to the lesser amount of MWCNT-COOH added (300 to 100 mg) to each composite systems but not due to the suppression of dissociation of the hydrogen ions by the polythiophene layer. Therefore, free carboxylic acid groups on MWCNT-COOH make relatively more acidic, whereas in nanocomposites (PTCNT-COOHs) decrease in acidity was due to composite formation. Elemental analysis (CHNS analysis) was taken to analyze

the compositional ratio of carbon, hydrogen and sulfur present in the composites of PTCNT-COOH 100 and PTCNT-COOH 300. PTCNT-COOH 300 has a lesser compositional weight percentage of sulfur due to a higher proportion of CNT compared to that of PTCNT-COOH 100.

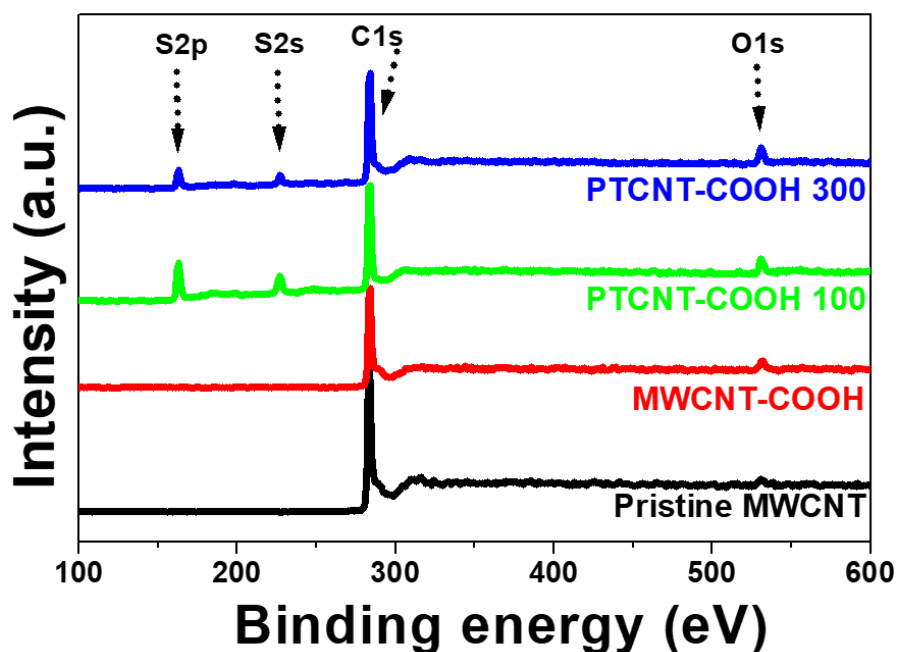


Figure 3.9. XPS spectra of pristine MWCNT, MWCNT-COOH, PTCNT-COOH 100 and PTCNT-COOH 300.

The X-ray photoelectron spectroscopy (XPS) was employed for the detailed elemental study of pristine MWCNT, functionalized MWCNT-COOH, PTCNT-COOH 100 and PTCNT-COOH 300 and to obtain an understanding of their functionalization ratio (see **Figure 3.9.**). Pristine MWCNT has shown an intense high peak at 283.25 eV and a very weak intensity peak at 531.45 eV corresponding to C 1s and O 1s, respectively. MWCNT-COOH exhibited an intense peak at 283.45 eV corresponding to C 1s and a relatively intense peak at 531.6 eV corresponding to O 1s. Furthermore, an enhancement in the XPS peak intensity was observed for the O 1s peak of functionalized MWCNT-COOH compared with pristine MWCNT, which attributes the formation of oxygen containing functional groups as defective sites.⁴³ Samples like PTCNT-COOH 100 and PTCNT-COOH 300 have their spectral profiles with characteristic peaks of sulfur at 226.95 (S 2s) and 162.75 (S 2p) eV in addition to C 1s and O 1s peaks, which confirms the presence of polythiophene in PTCNT-COOHs.^{49,50} The PTCNT-COOH 100 nanocomposite contains a high polythiophene compositional

ratio, which was evident from its dominating sulphur peak intensity compared with PTCNT-COOH 300.

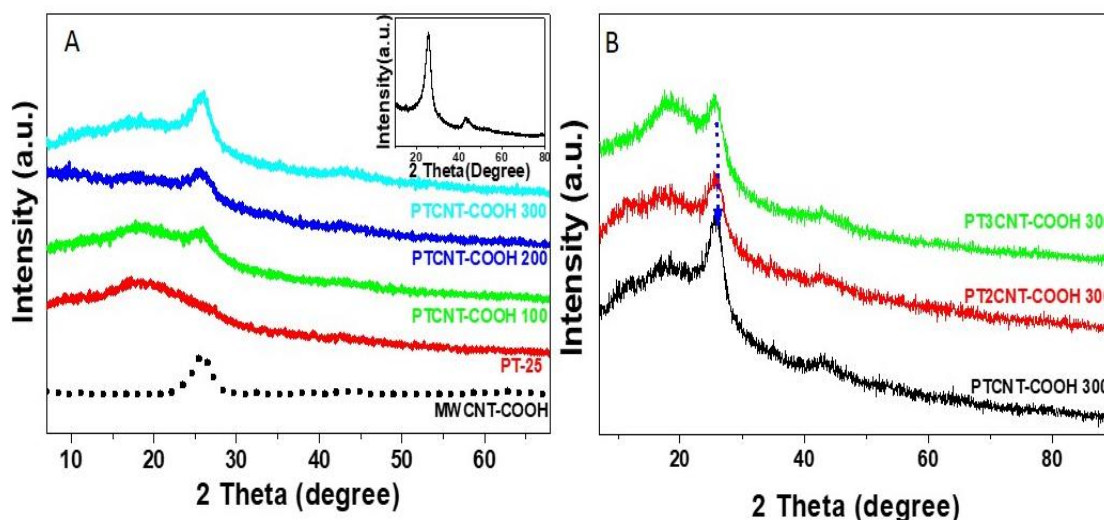


Figure 3.10. Powder X-ray diffractograms of (A) MWCNT-COOH, PT-25, PTCNT-COOH 100, PTCNT-COOH 200, PTCNT-COOH 300 and pristine MWCNT (in inset). (B) Comparison of X-ray diffraction diagram of PTCNT-COOH 300, PT2CNT-COOH 300 and PT3CNT-COOH 300.

X-ray diffractograms of functionalized MWCNT-COOH, polythiophene (PT), PTCNT-COOH 100, PTCNT-COOH 200 and PTCNT-COOH 300 have been analysed to understand the extent of solid-state packing of polymer matrix on CNT (see **Figure 3.10. A**). The functionalized MWCNT-COOH mainly exhibited an intense peak at 2θ value 25.85° attributing to the (002) diffraction plane of MWCNT having graphitic structure.^{30,50} Typical polythiophene (PT) has the broad amorphous peak centered at 18.68° .^{30,51} A Polythiophene-functionalized multi-walled carbon nanotube nanocomposites such as PTCNT-COOH 100, PTCNT-COOH 200 and PTCNT-COOH 300 exhibited a broad peak centered at 18.53° beside the (002) plane diffraction peak of carbon nanotube graphitic structure at 26.02° . On moving from PTCNT-COOH 100 to PTCNT-COOH 300, the intensity of broad amorphous peak of polythiophene goes down and the intensity of the (002) plane diffraction peak goes up. This result points out that PTCNT-COOH 300 provides more surface area on the CNT backbone compared to PTCNT-COOH 200 and PTCNT-COOH 100 for covering polythiophene nanolayer around the nanotube surface.⁵¹⁻⁵⁴ The low compositional ratio of thiophene in PTCNT-COOH 300 was reversed by increasing the thiophene monomer in feed (see

Figure 3.10. B for XRD pattern of PT2CNT-300 and PT3CNT-300). As the ratio of thiophene in feed increases on the CNT surface, the intensity of the amorphous polythiophene peak increases. X-ray diffraction patterns of polythiophene-CNT nanocomposites indicate that larger surface area of carbon nanotubes delivers more ordering in the polymer arrangement as nanolayer on CNT's surface.

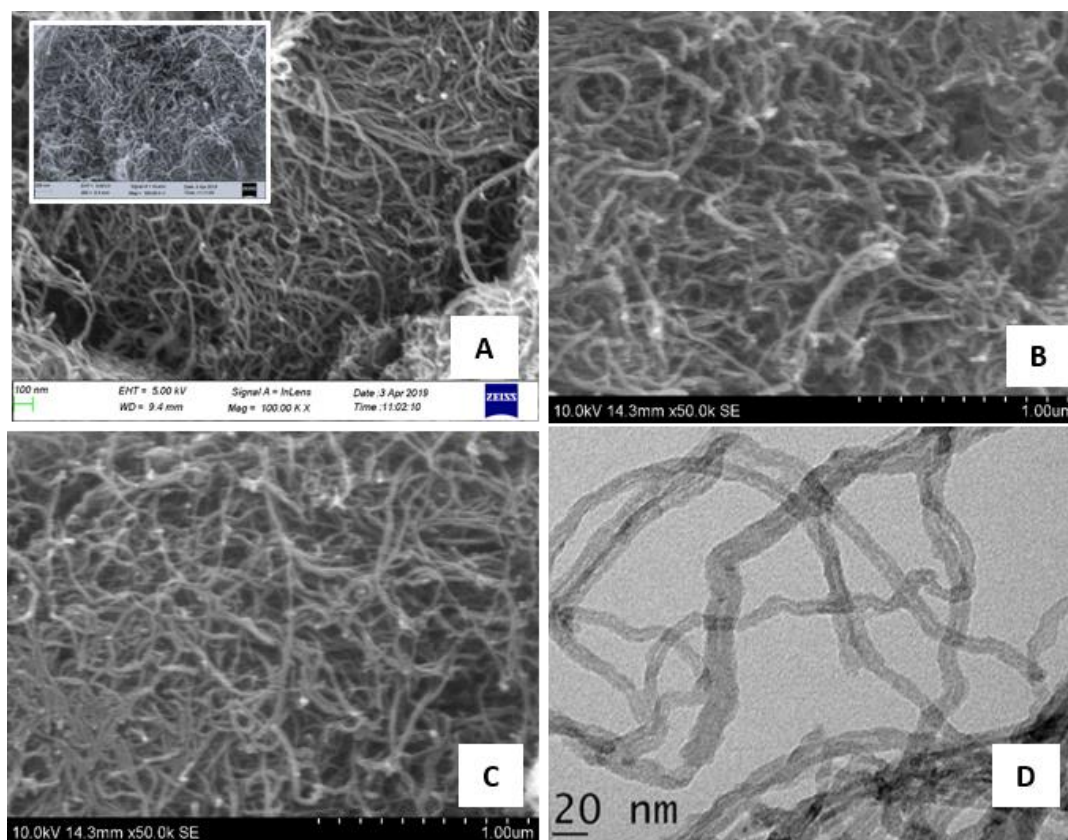


Figure 3.11. FE-SEM images of (A) MWCNT-COOH, MWCNT (in inset), (B) PTCNT-COOH 100, (C) PTCNT-COOH 300 and (D) HR-TEM image of PTCNT-COOH 300

The morphological characterisations of functionalized MWCNT-COOH and PTCNT-COOHs (100 and 300) were analysed using scanning electron microscopy (see **Figure 3.11.**). FE-SEM images of pristine MWCNT (inset of **Figure 3.11. A**) revealed its aggregated bundled nature, whereas surface oxidized MWCNT-COOH produced well separated carbon nanotubes after purification and washing (see **Figure 3.11. A**). These functionalized carbon nanotubes (MWCNT-COOH) could act as nano-tubular templates to accommodate in-situ formed polythiophene. The length of CNTs were not much cut shortened on acid treatment. In particular, binary nanocomposites such as PTCNT-COOH 300 composite have shown an increase in thickness without any phase separation (see **Figure 3.11. C**). Detailed morphological features and the inner

dimensions of the nanocomposite (PTCNT-COOH 300) have been investigated using transmission electron microscopy (TEM) (see **Figure 3.11. D**). TEM images revealed the remarkable thick outer layer having outer diameter of 14.80 ± 5 nm and inner tube diameter of 4.20 ± 2 nm. Higher outer to inner diameter ratio suggested that polythiophene was attached on the surface of the MWCNT as an outer layer through weak non-covalent interactions to form a thicker PT shell on the CNT core. An illustration of polythiophene chains orientation over MWCNT-COOH is represented in **Figure 3.12**.

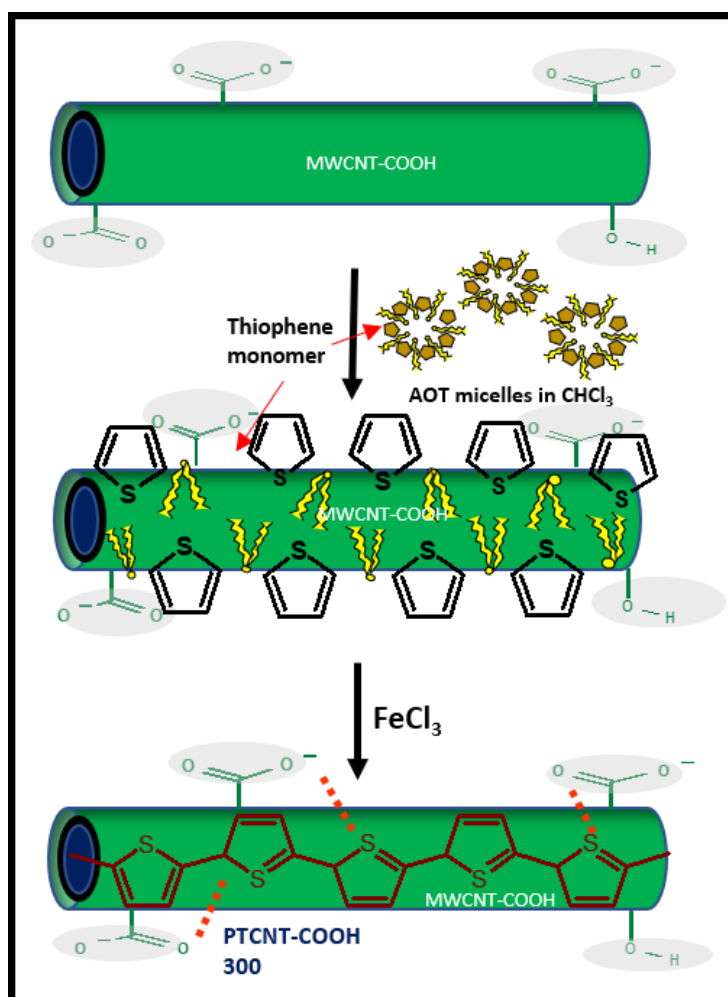


Figure 3.12. Illustration of the utilisation of defect group functionalization for the orientation of polythiophene over MWCNT surface.

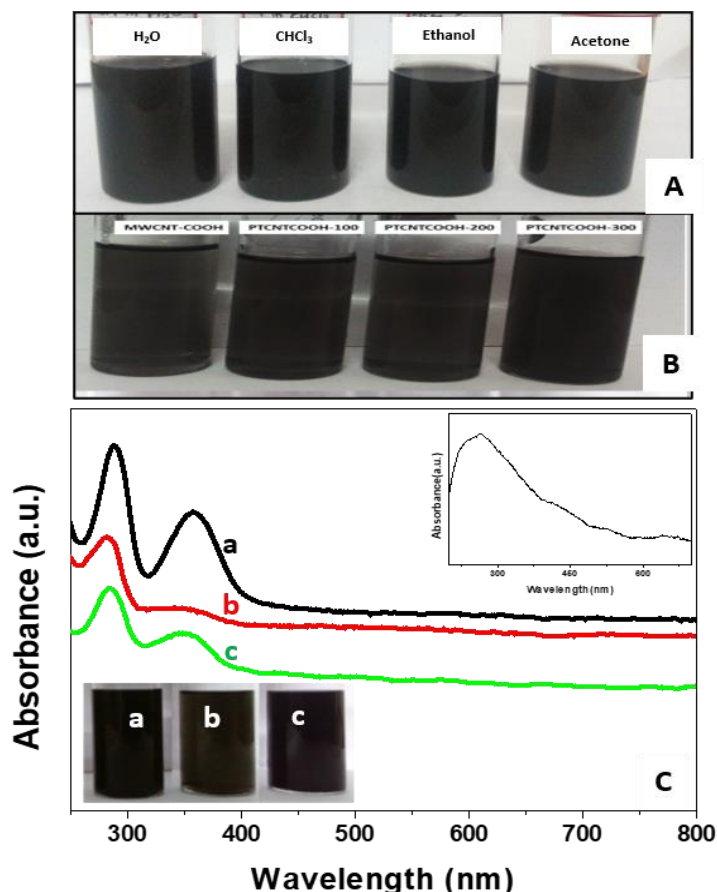


Figure 3.13. Dispersion of MWCNT-COOH in different solvents (A) and aqueous dispersions of different nanocomposites (B). UV-vis spectra of PTCNT-COOH 100 in chloroform [a], PTCNT-COOH 300 in chloroform [b], PTCNT-COOH 300 in ethanol [c] and MWCNT-COOH in water [inset](C).

The pristine multi-walled carbon nanotubes were usually insoluble in common solvents, mainly due to the bundling nature of carbon nanotubes and lack of functionalization. However, the covalent functionalization of multi-walled carbon nanotube by acid oxidation introduces polar groups such as carboxylic acid, hydroxyl and carbonyl groups which enhance the solubility, especially in polar solvents. The functionalised MWCNT-COOH covered with conducting polymers also reduces the bundling effect via repulsion between the tethered polymer chains creating an energy barrier against aggregation by controlling intertube potential.⁵² Theoretical aspects of simulation study based on the interaction of conducting polymers with carbon nanotubes also communicate that those non-covalent interactions could better enhance the dispersibility and hence the processability.^{53,54} Sonication of functionalized MWCNT-COOH and PTCNT-COOHs (100, 200 and 300) nanocomposites in water,

ethanol and chloroform have produced fairly stable dispersions (see **Figure 3.13. A and B**). The functionalized multi-walled carbon nanotubes (MWCNT-COOH) have shown absorption maximum at 260 nm due to aromatic π - π^* absorption of carbon nanotube.^{9,55} The UV-vis spectra of PTCNT-COOH 100 in chloroform and PTCNT-COOH 300 in ethanol and chloroform have shown well resolved peak at 360 nm in addition to a peak at 280 nm. The characteristic peak at 360 nm was due to polaron- π transition of polythiophene, which was intense for PTCNT-COOH 100.^{9,55} The sample PTCNT-COOH 100 possesses less amount of functionalized MWCNT-COOH (100 mg) than PTCNT-COOH 300 (300 mg), therefore thick layer present in PTCNT-COOH-100 must have resulted in strong absorption of polaron transition (see **Figure 3.13. C**).⁵⁶

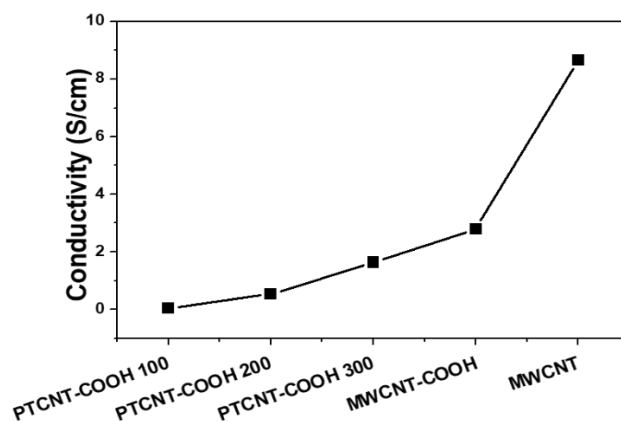


Figure 3.14. Four probe electrical conductivity of PTCNT-COOH 100, PTCNT-COOH 200, PTCNT-COOH 300, MWCNT-COOH and pristine MWCNT.

The electrical conductivities of pelletized pristine MWCNT, MWCNT-COOH, PTCNT-COOH 100, PTCNT-COOH 200 and PTCNT-COOH 300 were measured using four probe electrical conductivity meter (see **Figure 3.14**). Electrical conductivities of pristine MWCNT, MWCNT-COOH, PTCNT-COOH 100, PTCNT-COOH-200 and PTCNT-COOH 300 measured were 8.66 S/cm, 2.80 S/cm, 4.42×10^{-2} S/cm, 5.30×10^{-1} S/cm and 1.64 S/cm respectively. Multi-walled carbon nanotubes exhibited a drop in electrical conductivity on acid functionalization. The decrease in electrical conductivity was due to the development of defective sites for functional group formation on the π -conjugated backbone.⁵⁷ Association of polythiophene with MWCNT-COOH also decreased the overall conductivity in nanocomposites (PTCNT-COOH 100, PTCNT-COOH 200 and PTCNT-COOH 300) due to the presence of high weight percentage of polythiophene which is individually less conducting than MWCNT. A comparison of the electrical conductivity of PTCNT-COOH with PTCNT

nanocomposites was given in **Table 3.3**. The electrical conductivities of both PTCNT-COOH and PTCNTs undergo increment with an increase in functionalized or non-functionalized carbon nanotubes. Among the nanocomposites with lesser carbon nanotube content, PTCNT-100 has better conductivity than PTCNT-COOH 100, whereas, in nanocomposites with higher carbon nanotube, PTCNT-COOH-200 and PTCNT-COOH-300 has better conductivity than PTCNT composites. The enhanced electrical conductivity of these polythiophene-functionalized carbon nanotube nanocomposites (PTCNT-COOH 200 and PTCNT-COOH 300) might be due to the effective electron transport between conducting polythiophene and carbon nanotubes within the well-formed core-shell nanostructure.^{58,59} In addition to some of the non-covalent interactions present in PTCNT composites (discussed in Chapter 2), the formation of core shell morphology was furthermore reinforced in PTCNT-COOH composites by hydrogen bonding between functional groups formed on acid treatment and sulfur atoms in the polythiophene chains.

Table 3.3. Comparison of conductivity values of PT-25, MWCNT, MWCNT-COOH, PTCNT and PTCNT-COOH nanocomposites

Sample	Conductivity (S/cm)	Sample	Conductivity (S/cm)
PT-25	7.3×10^{-3}	-	-
PTCNT-100	3.58×10^{-1}	PTCNT-COOH 100	4.42×10^{-2}
PTCNT-200	3.98×10^{-1}	PTCNT-COOH 200	5.30×10^{-1}
PTCNT-400	3.40×10^{-1}	PTCNT-COOH 300	1.64
MWCNT	8.66	MWCNT-COOH	2.80

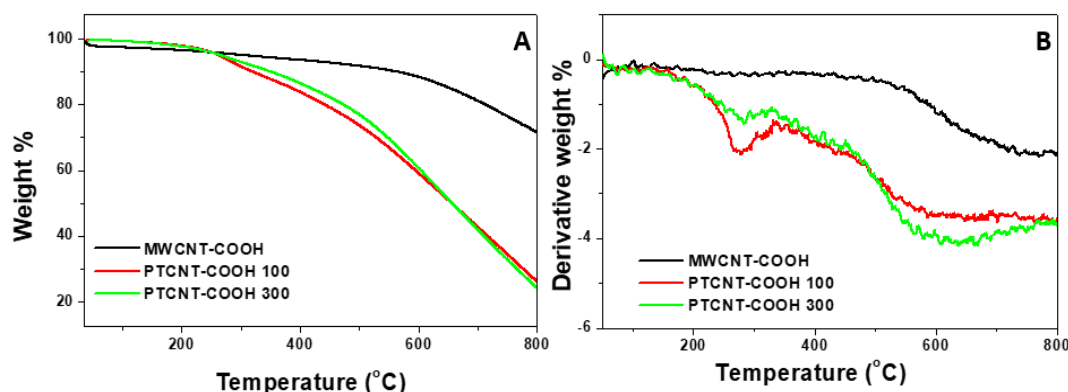


Figure 3.15. TGA (A) and DTA (B) analysis of MWCNT-COOH, PTCNT-COOH 100 and PTCNT-COOH 300

Thermal stability of MWCNT-COOH, PTCNT-COOH 100, PTCNT-COOH 300 were analysed in the scan rate of 20°C/min with nitrogen atmosphere (see **Figure 3.15.**). Functionalized MWCNT-COOH exhibited only 10% weight loss up to 620°C due to its graphitic network structure. PTCNT-COOH 100 and PTCNT-COOH 300 nanocomposites showed 10% weight loss up to 350°C. PTCNT-100 and PTCNT-300 nanocomposites (discussed in Chapter 2) exhibited approximately 15% weight loss up to 350°C. Therefore, PTCNT-COOH composites have shown comparably higher thermal stability than PTCNT composites up to 350°C. Thermal degradation up to this temperature was due to polymer degradation from the carbon chain. A better polymer interaction with a carbon nanotube via non-covalent interaction in PTCNT-COOH might have facilitated higher thermal stability than PTCNT nanocomposites. At higher temperature regions (beyond 400°C), the thermal degradation is due to the breakdown of the carbon nanotube structure. At this stage, PTCNTs have slightly better thermal stability than PTCNT-COOHs because the thermal degradation of MWCNT-COOH was faster than pristine MWCNT. Discrete stages of decomposition during the temperature scan were examined with differential thermal analysis. The decomposition of functionalized MWCNT-COOH was observed from 510°C with a one step decomposition. PTCNT-COOH 100 and PTCNT-COOH 300 were observed to decompose in two steps; starting from 260°C to 340°C due to the degradation of polythiophene and the other one starting from 470°C owes to the structural decomposition of CNT.^{58,59}

The advantages of enhanced properties of PTCNT-COOH nanocomposites compared to individual components (MWCNT-COOH and polythiophene) can pave the way for utilisation of composite in numerous applications (see **Figure 3.16.**). The preparation of easily processable materials is a major area of research these days. Achievement of stable dispersion would create debundled carbon nanotubes in its composite structure, which further enhances the processability of the material when they are used in various applications. Stable aqueous dispersions would be more attractive than other dispersion mediums because the solvent water is accepted as universal and green solvent. The prepared nanocomposites PTCNT-COOHs have given stable dispersions in water or other polar solvents and have attractive properties like good electrical conductivity and thermal stability, with striking relevance in various applications.

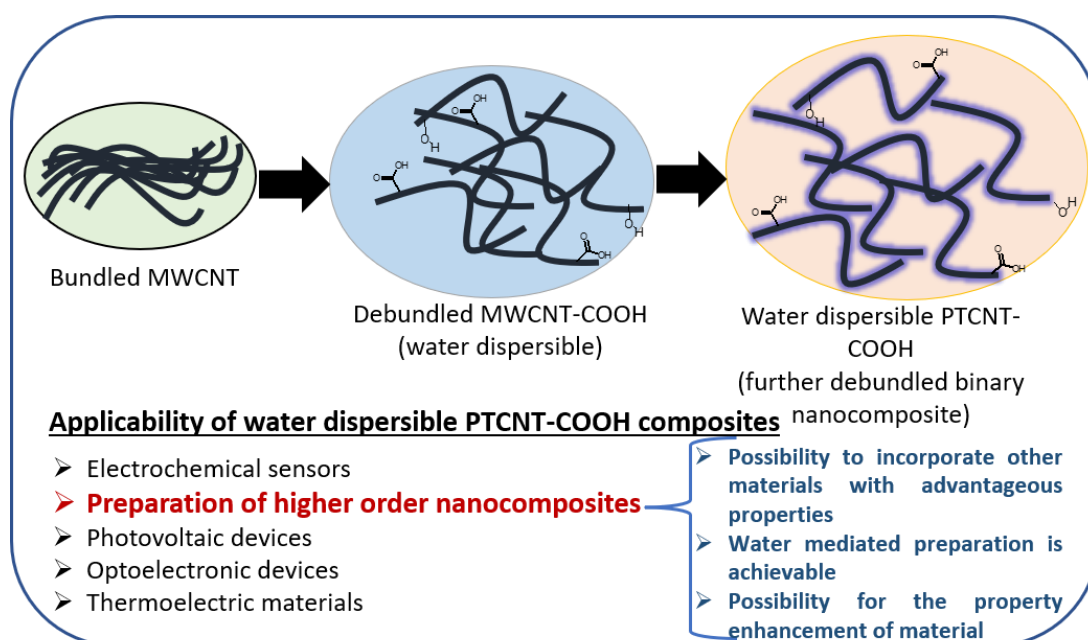


Figure 3.16. Illustration of debundling effect of carbon nanotubes by carboxylic acid functionalization followed by non-covalent functionalization with polymer

3.4. Conclusion

In a nutshell, polythiophene-functionalized carbon nanotube nanocomposites (PTCNT-COOHs) were synthesised by in-situ chemical oxidative polymerisation of thiophene monomer using ferric chloride as oxidising agent in the dispersion of functionalized MWCNT-COOH in chloroform and AOT as the surfactant. Functionalized MWCNT-COOH was prepared by refluxing with 5 M nitric acid. The formation of polythiophene-MWCNT-COOH composite was primarily ascertained with fourier transform Infrared spectra and X-ray photoelectron spectroscopy. The pH studies indicated the acidic nature of MWCNT- COOH and PTCNT-COOHs due to presence of carboxyl acid functional groups on the CNT surface. X-ray photoelectron spectroscopic peaks confirmed the functionalization of MWCNT-COOH with oxygen containing functional groups and presence of polythiophene in PTCNT-COOH nanocomposites. The variation in XPS peak intensity shows the proportional correlation between polymer and CNT components in PTCNT-COOH composites. X-ray diffractograms revealed the formation of polythiophene nanolayer on the MWCNT-

COOH surface via non-bonding interactions like π - π stacking assembling and hydrogen bonding interactions. Field emission scanning electron microscopic images revealed the nanotubular morphology of PTCNT nanocomposites as same as that of multi-walled carbon nanotubes, but with more thickened walls on nanocomposite. The thicker outer tube diameter of PTCNT-COOH 300 was measured as 14.80 ± 5 nm by TEM analysis. Polythiophene chains in ordered arrangement on MWCNT-COOH walls were established as an energy barrier against tubular aggregation. The well dispersed state of MWCNT-COOH and PTCNT-COOHs in less aggregated form has given well-resolved peaks for UV-visible absorption spectra in water and ethanol medium. PTCNT-COOH nanocomposites were also found to be exhibited good electrical conductivity up to the order of 10^{-1} S/cm and good enough thermal stability up to 480°C. PTCNT-COOH composites have high dispersibility in green solvent water and other properties suitable for various applications.

References

1. T. A. Skotheim, J. R. Reynolds, *Conjugated Polymers. Theory, Synthesis, Properties and Characterization* (2007).
2. Spitalsky, Z.; Tasis, D.; Papagelis, K.; Galiotis, C. Carbon Nanotube-Polymer Composites: Chemistry, Processing, Mechanical and Electrical Properties. *Prog. Polym. Sci.* **2010**, *35* (3), 357–401. <https://doi.org/10.1016/j.progpolymsci.2009.09.003>.
3. Shirakawa, H. The Discovery of Polyacetylene Film: The Dawning of an Era of Conducting Polymers (Nobel Lecture). *Angew. Chemie - Int. Ed.* **2001**, *40* (14), 2574–2580. [https://doi.org/10.1002/1521-3773\(20010716\)40:14<2574::aid-anie2574>3.0.co;2-n](https://doi.org/10.1002/1521-3773(20010716)40:14<2574::aid-anie2574>3.0.co;2-n).
4. Guldi, D. M.; Rahman, G. M. A.; Zerbetto, F.; Prato, M. Carbon Nanotubes in Electron Donor - Acceptor Nanocomposites. *Acc. Chem. Res.* **2005**, *38* (11), 871–878. <https://doi.org/10.1021/ar040238i>.
5. Gong, X.; Liu, J.; Baskaran, S.; Voise, R. D.; Young, J. S. Surfactant-Assisted Processing of Carbon Nanotube/Polymer Composites. *Chem. Mater.* **2000**, *12* (4), 1049–1052. <https://doi.org/10.1021/cm9906396>.
6. Chen, W. C.; Lien, H. T.; Cheng, T. W.; Su, C.; Chong, C. W.; Ganguly, A.; Chen, K. H.; Chen, L. C. Side Group of Poly(3-Alkylthiophene)s Controlled Dispersion of Single-Walled Carbon Nanotubes for Transparent Conducting Film. *ACS Appl. Mater. Interfaces* **2015**, *7* (8), 4616–4622. <https://doi.org/10.1021/am507774c>.
7. C. Zhan, G. Yu, Y. Lu, L. Wang, E. Wujcik, S. Wei, Conductive polymer nanocomposites: a critical review of modern advanced devices, *J. Mater. Chem. C* **5** (2017), 5 1569–1585. doi:10.1039/c6tc04269d.
8. Miller, A. J.; Hatton, R. A.; Silva, S. R. P. Water-Soluble Multiwall-Carbon-Nanotube-Polythiophene Composite for Bilayer Photovoltaics. *Appl. Phys. Lett.* **2006**, *89* (12). <https://doi.org/10.1063/1.2356115>.
9. Miller, A. J.; Hatton, R. A.; Silva, S. R. P. Water-Soluble Multiwall-Carbon-Nanotube-Polythiophene Composite for Bilayer Photovoltaics. *Appl. Phys. Lett.* **2006**, *89* (12). <https://doi.org/10.1063/1.2356115>.
10. Koval'chuk, A. A.; Shchegolikhin, A. N.; Shevchenko, V. G.; Nedorezova, P. M.; Klyamkina, A. N.; Aladyshev, A. M. Synthesis and Properties of Polypropylene/Multiwall

- Carbon Nanotube Composites. *Macromolecules* **2008**, *41* (9), 3149–3156. <https://doi.org/10.1021/ma800297e>.
11. Mondal, R. K.; Dubey, K. A.; Bhardwaj, Y. K. Role of the Interface on Electron Transport in Electro-Conductive Polymer-Matrix Composite: A Review. *Polym. Compos.* **2021**, *42* (6), 2614–2628. <https://doi.org/10.1002/pc.26018>.
 12. Berger, F. J.; Lüttgens, J.; Nowack, T.; Kutsch, T.; Lindenthal, S.; Kistner, L.; Müller, C. C.; Bongartz, L. M.; Lumsargis, V. A.; Zakharko, Y.; Zaumseil, J. Brightening of Long, Polymer-Wrapped Carbon Nanotubes by Sp³ Functionalization in Organic Solvents. *ACS Nano* **2019**, *13* (8), 9259–9269. <https://doi.org/10.1021/acsnano.9b03792>.
 13. Hill, D. E.; Lin, Y.; Rao, A. M.; Allard, L. F.; Sun, Y. P. Functionalization of Carbon Nanotubes with Polystyrene. *Macromolecules* **2002**, *35* (25), 9466–9471. <https://doi.org/10.1021/ma020855r>.
 14. Yu, H.; Jin, Y.; Peng, F.; Wang, H.; Yang, J. Kinetically Controlled Side-Wall Functionalization of Carbon Nanotubes by Nitric Acid Oxidation. *J. Phys. Chem. C* **2008**, *112* (17), 6758–6763. <https://doi.org/10.1021/jp711975a>.
 15. Palacin, T.; Le Khanh, H.; Joussetme, B.; Jegou, P.; Filoramo, A.; Ehli, C.; Guldi, D. M.; Campidelli, S. Efficient Functionalization of Carbon Nanotubes with Porphyrin Dendrons via Click Chemistry. *J. Am. Chem. Soc.* **2009**, *131* (42), 15394–15402. <https://doi.org/10.1021/ja906020e>.
 16. Dyke, C. A.; Tour, J. M. Covalent Functionalization of Single-Walled Carbon Nanotubes for Materials Applications. *J. Phys. Chem. A* **2004**, *108* (51), 11151–11159. <https://doi.org/10.1021/jp046274g>.
 17. Kong, H.; Gao, C.; Yan, D. Controlled Functionalization of Multiwalled Carbon Nanotubes by in Situ Atom Transfer Radical Polymerization. *J. Am. Chem. Soc.* **2004**, *126* (2), 412–413. <https://doi.org/10.1021/ja0380493>.
 18. Chen, R. J.; Zhang, Y.; Wang, D.; Dai, H. Noncovalent Sidewall Functionalization of Single-Walled Carbon Nanotubes for Protein Immobilization [11]. *J. Am. Chem. Soc.* **2001**, *123* (16), 3838–3839. <https://doi.org/10.1021/ja010172b>.
 19. Clavé, G.; Delpont, G.; Roquelet, C.; Lauret, J. S.; Deleporte, E.; Vialla, F.; Langlois, B.; Parret, R.; Voisin, C.; Roussignol, P.; Joussetme, B.; Gloter, A.; Stephan, O.; Filoramo, A.; Derycke, V.; Campidelli, S. Functionalization of Carbon Nanotubes through Polymerization in Micelles: A Bridge between the Covalent and Noncovalent Methods. *Chem. Mater.* **2013**, *25* (13), 2700–2707. <https://doi.org/10.1021/cm401312v>.
 20. Simmons, T. J.; Bult, J.; Hashim, D. P.; Linhardt, R. J.; Ajayan, P. M. Noncovalent Functionalization as an Alternative to Oxidative Acid Treatment of Single Wall Carbon Nanotubes with Applications for Polymer Composites. *ACS Nano* **2009**, *3* (4), 865–870. <https://doi.org/10.1021/nn800860m>.
 21. Wang, S. Optimum Degree of Functionalization for Carbon Nanotubes. *Curr. Appl. Phys.* **2009**, *9* (5), 1146–1150. <https://doi.org/10.1016/j.cap.2009.01.004>.
 22. Buffa, F.; Hu, H.; Resasco, D. E. Side-Wall Functionalization of Single-Walled Carbon Nanotubes with 4-Hydroxymethylaniline Followed by Polymerization of ϵ -Caprolactone. *Macromolecules* **2005**, *38* (20), 8258–8263. <https://doi.org/10.1021/ma050876w>.
 23. Lourenço, M. A. O.; Fontana, M.; Jagdale, P.; Pirri, C. F.; Bocchini, S. Improved CO₂ Adsorption Properties through Amine Functionalization of Multi-Walled Carbon Nanotubes. *Chem. Eng. J.* **2021**, *414*, 128763. <https://doi.org/10.1016/j.cej.2021.128763>.
 24. Bilalis, P.; Katsigiannopoulos, D.; Avgeropoulos, A.; Sakellariou, G. Non-Covalent Functionalization of Carbon Nanotubes with Polymers. *RSC Adv.* **2014**, *4* (6), 2911–2934. <https://doi.org/10.1039/c3ra44906h>.
 25. Bose, S.; Khare, R. A.; Moldenaers, P. Assessing the Strengths and Weaknesses of Various Types of Pre-Treatments of Carbon Nanotubes on the Properties of Polymer/Carbon Nanotubes Composites: A Critical Review. *Polymer (Guildf)*. **2010**, *51* (5), 975–993. <https://doi.org/10.1016/j.polymer.2010.01.044>.

26. Yuan, W.; Chan-Park, M. B. Covalent Cum Noncovalent Functionalizations of Carbon Nanotubes for Effective Reinforcement of a Solution Cast Composite Film. *ACS Appl. Mater. Interfaces* **2012**, *4* (4), 2065–2073. <https://doi.org/10.1021/am300038d>.
27. Kainz, Q. M.; Schätz, A.; Zöpfl, A.; Stark, W. J.; Reiser, O. Combined Covalent and Noncovalent Functionalization of Nanomagnetic Carbon Surfaces with Dendrimers and BODIPY Fluorescent Dye. *Chem. Mater.* **2011**, *23* (16), 3606–3613. <https://doi.org/10.1021/cm200705d>.
28. Bahr, J. L.; Yang, J.; Kosynkin, D. V.; Bronikowski, M. J.; Smalley, R. E.; Tour, J. M. Functionalization of Carbon Nanotubes by Electrochemical Reduction of Aryl Diazonium Salts: A Bucky Paper Electrode. *J. Am. Chem. Soc.* **2001**, *123* (27), 6536–6542. <https://doi.org/10.1021/ja010462s>.
29. Peng, H.; Alemany, L. B.; Margrave, J. L.; Khabashesku, V. N. Sidewall Carboxylic Acid Functionalization of Single-Walled Carbon Nanotubes. *J. Am. Chem. Soc.* **2003**, *125* (49), 15174–15182. <https://doi.org/10.1021/ja037746s>.
30. Lin, Y.; Zhou, B.; Fernando, K. A. S.; Liu, P.; Allard, L. F.; Sun, Y. P. Polymeric Carbon Nanocomposites from Carbon Nanotubes Functionalized with Matrix Polymer. *Macromolecules* **2003**, *36* (19), 7199–7204. <https://doi.org/10.1021/ma0348876>.
31. Ying, Y.; Saini, R. K.; Liang, F.; Sadana, A. K.; Billups, W. E. Functionalization of Carbon Nanotubes by Free Radicals. *Org. Lett.* **2003**, *5* (9), 1471–1473. <https://doi.org/10.1021/ol0342453>.
32. Lin, Y.; Zhou, B.; Martin, R. B.; Henbest, K. B.; Harruff, B. A.; Riggs, J. E.; Guo, Z. X.; Allard, L. F.; Sun, Y. P. Visible Luminescence of Carbon Nanotubes and Dependence on Functionalization. *J. Phys. Chem. B* **2005**, *109* (31), 14779–14782. <https://doi.org/10.1021/jp053073j>.
33. Khare, B.; Wilhite, P.; Tran, B.; Teixeira, E.; Fresquez, K.; Mvondo, D. N.; Bauschlicher, C.; Meyyappan, M. Functionalization of Carbon Nanotubes via Nitrogen Glow Discharge. *J. Phys. Chem. B* **2005**, *109* (49), 23466–23472. <https://doi.org/10.1021/jp0537254>.
34. Yang, D. Q.; Rochette, J. F.; Sacher, E. Controlled Chemical Functionalization of Multiwalled Carbon Nanotubes by Kilolectronvolt Argon Ion Treatment and Air Exposure. *Langmuir* **2005**, *21* (18), 8539–8545. <https://doi.org/10.1021/la0514922>.
35. Hill, D.; Lin, Y.; Qu, L.; Kitaygorodskiy, A.; Connell, J. W.; Allard, L. F.; Sun, Y. P. Functionalization of Carbon Nanotubes with Derivatized Polyimide. *Macromolecules* **2005**, *38* (18), 7670–7675. <https://doi.org/10.1021/ma0509210>.
36. Hou, Y.; Tang, J.; Zhang, H.; Qian, C.; Feng, Y.; Liu, J. Functionalized Few-Walled Carbon Nanotubes for Mechanical Reinforcement of Polymeric Composites. *ACS Nano* **2009**, *3* (5), 1057–1062. <https://doi.org/10.1021/nn9000512>.
37. Chen, C.; Liang, B.; Ogino, A.; Wang, X.; Nagatsu, M. Oxygen Functionalization of Multiwall Carbon Nanotubes by Microwave-Excited Surface-Wave Plasma Treatment. *J. Phys. Chem. C* **2009**, *113* (18), 7659–7665. <https://doi.org/10.1021/jp9012015>.
38. Lerner, M. B.; D'Souza, J.; Pazina, T.; Dailey, J.; Goldsmith, B. R.; Robinson, M. K.; Johnson, A. T. C. Hybrids of a Genetically Engineered Antibody and a Carbon Nanotube Transistor for Detection of Prostate Cancer Biomarkers. *ACS Nano* **2012**, *6* (6), 5143–5149. <https://doi.org/10.1021/nn300819s>.
39. Likodimos, V.; Steriotis, T. A.; Papageorgiou, S. K.; Romanos, G. E.; Marques, R. R. N.; Rocha, R. P.; Faria, J. L.; Pereira, M. F. R.; Figueiredo, J. L.; Silva, A. M. T.; Falaras, P. Controlled Surface Functionalization of Multiwall Carbon Nanotubes by HNO₃ Hydrothermal Oxidation. *Carbon N. Y.* **2014**, *69*, 311–326. <https://doi.org/10.1016/j.carbon.2013.12.030>.
40. Osswald, S.; Havel, M.; Gogotsi, Y. Monitoring Oxidation of Multiwalled Carbon Nanotubes by Raman Spectroscopy. *J. Raman Spectrosc.* **2007**, *38* (6), 728–736. <https://doi.org/10.1002/jrs.1686>.
41. Avilés, F.; Cauich-Rodríguez, J. V.; Moo-Tah, L.; May-Pat, A.; Vargas-Coronado, R. Evaluation of Mild Acid Oxidation Treatments for MWCNT Functionalization. *Carbon N. Y.* **2009**, *47* (13), 2970–2975. <https://doi.org/10.1016/j.carbon.2009.06.044>.

42. Osorio, A. G.; Silveira, I. C. L.; Bueno, V. L.; Bergmann, C. P. H₂SO₄/HNO₃/HCl-Functionalization and Its Effect on Dispersion of Carbon Nanotubes in Aqueous Media. *Appl. Surf. Sci.* **2008**, *255* (5 PART 1), 2485–2489. <https://doi.org/10.1016/j.apsusc.2008.07.144>.
43. Stobinski, L.; Lesiak, B.; Kövér, L.; Tóth, J.; Biniak, S.; Trykowski, G.; Judek, J. Multiwall Carbon Nanotubes Purification and Oxidation by Nitric Acid Studied by the FTIR and Electron Spectroscopy Methods. *J. Alloys Compd.* **2010**, *501* (1), 77–84. <https://doi.org/10.1016/j.jallcom.2010.04.032>.
44. Swathy, T. S.; Jose, M. A.; Antony, M. J. AOT Assisted Preparation of Ordered, Conducting and Dispersible Core-Shell Nanostructured Polythiophene – MWCNT Nanocomposites. *Polymer (Guildf)*. **2016**, *103*, 206–213. <https://doi.org/10.1016/j.polymer.2016.09.047>.
45. Jinish Antony, M.; Albin Jolly, C.; Rohini Das, K.; Swathy, T. S. Normal and Reverse AOT Micelles Assisted Interfacial Polymerization for Polyaniline Nanostructures. *Colloids Surfaces A Physicochem. Eng. Asp.* **2019**, *578*, 123627. <https://doi.org/10.1016/j.colsurfa.2019.123627>.
46. M. A. Jose, S. Varghese, Antony M. J. *In situ* chemical oxidative polymerisation for ordered conducting polythiophene nanostructures in presence of dioctyl sodium sulfosuccinate, IJC-A 55A (2016) 291-297.
47. R. Liu, Z. Liu, Polythiophene: Synthesis in aqueous medium and controllable morphology, *Sci. Bull.* **54** (2009), *54*, 2028–2032. doi:10.1007/s11434-009-0217-0.
48. Gök, A.; Omastová, M.; Yavuz, A. G. Synthesis and Characterization of Polythiophenes Prepared in the Presence of Surfactants. *Synth. Met.* **2007**, *157* (1), 23–29. <https://doi.org/10.1016/j.synthmet.2006.11.012>.
49. Dabera, G. D. M. R.; Jayawardena, K. D. G. I.; Prabhath, M. R. R.; Yahya, I.; Tan, Y. Y.; Nismy, N. A.; Shiozawa, H.; Sauer, M.; Ruiz-Soria, G.; Ayala, P.; Stolojan, V.; Adikaari, A. A. D. T.; Jarowski, P. D.; Pichler, T.; Silva, S. R. P. Hybrid Carbon Nanotube Networks as Efficient Hole Extraction Layers for Organic Photovoltaics. *ACS Nano* **2013**, *7* (1), 556–565. <https://doi.org/10.1021/nn304705t>.
50. Cao, A.; Xu, C.; Liang, J.; Wu, D.; Wei, B. X-Ray Diffraction Characterization on the Alignment Degree of Carbon Nanotubes. *Chem. Phys. Lett.* **2001**, *344* (1–2), 13–17. [https://doi.org/10.1016/S0009-2614\(01\)00671-6](https://doi.org/10.1016/S0009-2614(01)00671-6).
51. Senthilkumar, B.; Thenamirtham, P.; Kalai Selvan, R. Structural and Electrochemical Properties of Polythiophene. *Appl. Surf. Sci.* **2011**, *257* (21), 9063–9067. <https://doi.org/10.1016/j.apsusc.2011.05.100>.
52. Shvartzman-Cohen, R.; Nativ-Roth, E.; Baskaran, E.; Levi-Kalisman, Y.; Szeleifer, I.; Yerushalmi-Rozen, R. Selective Dispersion of Single-Walled Carbon Nanotubes in the Presence of Polymers: The Role of Molecular and Colloidal Length Scales. *J. Am. Chem. Soc.* **2004**, *126* (45), 14850–14857. <https://doi.org/10.1021/ja046377c>.
53. Hooper, J. B.; Schweizer, K. S. Theory of Phase Separation in Polymer Nanocomposites. *Macromolecules* **2006**, *39* (15), 5133–5142. <https://doi.org/10.1021/ma060577m>.
54. Tummala, N. R.; Morrow, B. H.; Resasco, D. E.; Striolo, A. Stabilization of Aqueous Carbon Nanotube Dispersions Using Surfactants: Insights from Molecular Dynamics Simulations. *ACS Nano* **2010**, *4* (12), 7193–7204. <https://doi.org/10.1021/nn101929f>.
55. Ago, H.; Kugler, T.; Cacialli, F.; Salaneck, W. R.; Shaffer, M. S. P.; Windle, A. H.; Friend, R. H. Work Functions and Surface Functional Groups of Multiwall Carbon Nanotubes. *J. Phys. Chem. B* **1999**, *103* (38), 8116–8121. <https://doi.org/10.1021/jp991659y>.
56. Liang, L.; Xie, W.; Fang, S.; He, F.; Yin, B.; Tlili, C.; Wang, D.; Qiu, S.; Li, Q. High-Efficiency Dispersion and Sorting of Single-Walled Carbon Nanotubes: Via Non-Covalent Interactions. *J. Mater. Chem. C* **2017**, *5* (44), 11339–11368. <https://doi.org/10.1039/c7tc04390b>.
57. Razavi, R.; Zare, Y.; Rhee, K. Y. A Two-Step Model for the Tunneling Conductivity of Polymer Carbon Nanotube Nanocomposites Assuming the Conduction of Interphase Regions. *RSC Adv.* **2017**, *7* (79), 50225–50233. <https://doi.org/10.1039/c7ra08214b>.

58. Kuila, B. K.; Malik, S.; Batabyal, S. K.; Nandi, A. K. In-Situ Synthesis of Soluble Poly(3-Hexylthiophene)/Multiwalled Carbon Nanotube Composite: Morphology, Structure, and Conductivity. *Macromolecules* 2007, 40 (2), 278–287. <https://doi.org/10.1021/ma061548e>.
59. Saini, V.; Li, Z.; Bourdo, S.; Dervishi, E.; Xu, Y.; Ma, X.; Kunets, V. P.; Salamo, G. J.; Viswanathan, T.; Biris, A. R.; Saini, D.; Biris, A. S. Electrical, Optical, and Morphological Properties of P3ht-Mwnt Nanocomposites Prepared by In Situ Polymerization. *J. Phys. Chem. C* 2009, 113 (19), 8023–8029. <https://doi.org/10.1021/jp809479a>.

Chapter 3

Chapter 4

Silver Nanoparticles Entangled Polythiophene- Functionalized MWCNT Ternary Nanocomposites: A Green Synthetic Approach and Enhancement in Properties

4.1. Introduction

The preparation of higher-order structural architectures from binary nanocomposites would be advantageous for their better performance or for exploring more areas of application.¹⁻³ Functionalized multiwalled carbon nanotube nanocomposites with conducting polymer via the formation of core-shell morphology can act as an effective synergistic host to accommodate different materials. A sizeable surface-to-volume ratio in nanostructured conducting polythiophene-CNT nanocomposites would be beneficial to incorporate additional nanofillers to the surface of its lightweight framework.^{4,5}

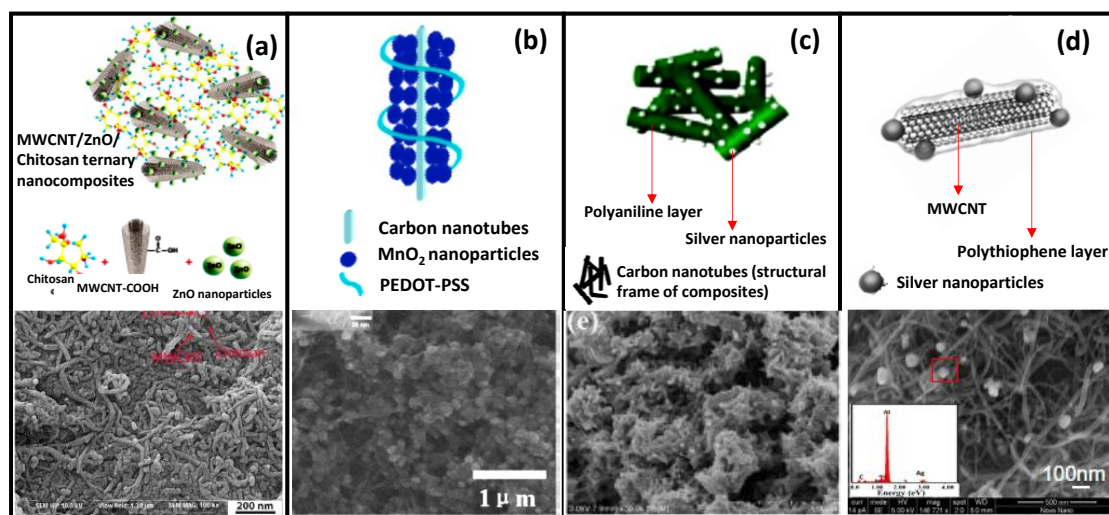


Figure 4.1. Metal nanoparticles incorporation with different polymer-carbon nanotube nanocomposites and their scanning electron microscopic images (adapted from (a) malekkiani et al. 2022 (b) Hou et al. 2010 (c) Tang et al. 2016 and (d) Patole et al. 2015.)

Incorporating metal nanoparticles as fillers into conducting polymer-carbon nanotube nanocomposites find new applications by gaining additional properties with enhanced performance. Structurally different morphologies can be obtained for such ternary nanocomposites based on synthetic routes, types of polymer, and the nature of the incorporated metal. Some of the reports of ternary systems of polymer-carbon nanotube nanocomposites with metal nanoparticles are shown in **figure 4.1.**⁶⁻⁹ Silver nanoparticles are an attractive choice among metal fillers as it exhibits high electrical and thermal conductivity.¹⁰ Distinct characteristics of silver nanoparticles rendering different applications such as catalysis, surface-plasmon resonance, antimicrobial

action, surface-enhanced Raman scattering tags, therapeutic usages, electrochemical applications, electromagnetic interference (EMI) shielding etc.¹¹⁻¹³ However, the long-term use of bare silver nanoparticles as such is not viable due to the high surface charges on nanoparticles, which create low negative fermi potential and get aggregated easily.¹⁴ Stable silver nanoparticles require suitable capping agents to avoid their tendency of aggregation.¹² Inorganic or polymeric stabilizing supports can be effectively used against aggregation and promote the silver nanoparticle's stability.^{14,15}

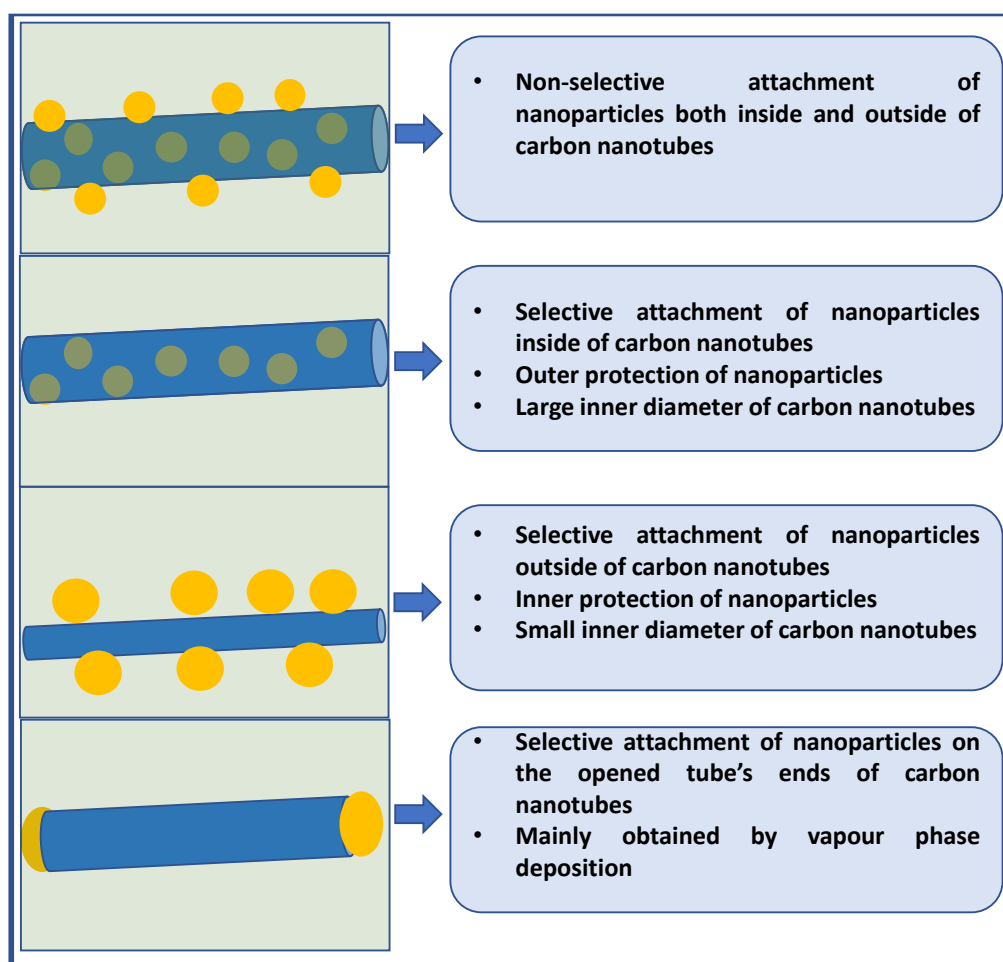


Figure 4.2. Different possibilities for the formation of carbon nanotube-metal nanoparticle nanocomposites.

The incorporation of silver nanoparticles with polymer materials can generally be carried out in two different ways. One method is the *in-situ* synthesis of silver nanoparticles in the presence of a polymer scaffold. The second method is the *ex-situ* attachment of silver nanoparticles to the desired polymer material.^{15,16} Preparation of silver nanoparticles with polymerization in a single step is also reported rarely.¹⁷ An

Preparation of Silver Nanoparticles Entangled Ternary Nanocomposites

advantage of *in-situ* preparation is the uniform attachment of soluble silver ions with the pre-structured polymer framework, producing a homogeneous distribution of nanoparticles with the solid matrix.¹⁵ Selection of suitable polymer material should also be required for excellent properties. Conducting polythiophene exhibits good environmental stability and compatibility with silver nanoparticles.¹⁸ Polymer alone or in hybrid/composite form could be used as a suitable scaffold to accommodate silver nanoparticles. The structural features of scaffolding materials are essential to control the size, shape and assembly of metal nanoparticles formed.^{19,20} Among different scaffolding materials to accommodate *in-situ* formed silver nanoparticles, core-shell structured polythiophene-carbon nanotube binary nanocomposites would be attractive for its typical characteristics such as one-dimensional nano-structural confinement, conducting host framework, good thermal stability and ability to form a stable aqueous dispersion. Methods of area specific and area non-specific attachment of metal nanoparticles in carbon nanotubes are schematically represented in **Figure 4.2**. The selective area attachment of nanoparticles on inner walls, outer walls and/or end caps are possible, and they possess unique benefits leading to specific applications.²¹⁻²⁵

Adopting green approaches for silver nanoparticles embedded polythiophene-functionalized multiwalled carbon nanotube ternary nanocomposites can render several benefits, such as cost-effectiveness, good dispersibility in the aqueous phase, high electrical conductivity, and thermal stability.^{26,27} Applications of prepared silver nanocomposites will be determined by their processability and other properties.²⁸ Studies on ternary nanocomposites incorporating stable silver nanoparticles into polythiophene-functionalized multiwalled carbon nanotubes were rarely reported. Patole et al. reported the preparation of PEDOT/PSS-ethylenediamine functionalized multiwalled carbon nanotube-silver nanoparticle nanocomposites by reduction of AgNO₃ using NaBH₄ in dichloromethane medium for improving electrical conductivity and thermal properties of polycarbonate matrix. Studies on the bicomponent systems, such as polythiophene-silver nanocomposites or carbon nanotube-silver nanocomposites, were conducted by various researchers. A recent literature review by Al-Refai et. al. based on polythiophene nanocomposites discusses the advantages and relevance of incorporating nanomaterials such as metal nanoparticles and carbon nanotubes into polythiophene matrix.²⁸ The ternary structural combination of silver

nanoparticles into a polythiophene-carbon nanotube nanocomposite framework could open up various applications with cohesive properties.

In the present chapter, we have put forward a facile and green synthetic approach for developing silver nanoparticles embedded in polythiophene-functionalized multiwalled carbon nanotube nanocomposites by reduction of silver nitrate using ascorbic acid (Vitamin-C) in an aqueous medium. Binary nanocomposite (PTCNT-COOH 300) acted as a nanofibrous template in which silver nanoparticles grew to form a ternary nanocomposite. Here, the polythiophene-functionalized multiwalled carbon nanotube nanocomposites act as a stable framework to accommodate and protect highly labile silver atoms as solid nanoparticles; otherwise, it might agglomerate in the absence of a strong capping agent. Interestingly, the tangled silver nanoparticles embedded ternary polythiophene-functionalized MWCNT nanocomposites having good dispersibility in water, high electrical conductivity, good solid-state ordering, and high thermal stability were established.

4.2. Experimental

4.2.1. Materials and reagents used: Silver nitrate and multiwalled carbon nanotubes (MWCNT) were purchased from Sigma Aldrich. Ascorbic acid, sodium hydroxide, hydrochloric acid, acetic acid, ammonium hydroxide, acetone and deionized water were purchased from Merck chemicals India.

4.2.2. Measurements and instruments: Fourier transform-infrared spectra of the samples were recorded by Shimadzu IR Affinity 1 spectrometer using the KBr pellet method. Raman spectra of samples were taken by LabRam spectrometer by HORIBA JOBIN YVON using argon ion laser of wavelength 514.5 nm. UV-vis spectra of the samples were recorded by Shimadzu UV-Visible spectrophotometer, UV 1800 series in the range 200-800 nm with HPLC grade chloroform, ethanol and deionized water. The powder wide-angle X-ray diffraction of the samples was measured using PANALYTICAL, Aeris research with 2θ values ranging from 5 to 80°. The field emission scanning electron microscope (FE-SEM) images were recorded by ZEISS SIGMATM field emission scanning electron microscope. The transmission electron microscopic analysis was carried out by JEOL/JEM 2100 instrument having a capacity of 200 KV and with magnification 2000X – 1500000X. Thermogravimetric analysis (TGA) of the samples was measured using Perkin Elmer, Diamond TG/DTA in an inert

Preparation of Silver Nanoparticles Entangled Ternary Nanocomposites

atmosphere of nitrogen at a heating rate of 20°C. The four-probe electrical conductivity of the samples was measured using DFP-RM-200 with constant current source Model CCS-01 and DC microvoltmeter. The pH measurements were carried out using HM digital PH -80 Temp hydro tester. The XPS analysis was carried out using PHI 5000 Versa Probe III instrument. Both wide scan spectra (in the range of 150-600 eV) and narrow scan spectra of individual elements were carried out with XPS spectra.

4.2.3. Synthesis of PTCNT-COOH 300 Ag: The sample PTCNT-COOH 300 (0.16 g) was dispersed in 500 mL of deionized water by sonication. Ascorbic acid (8.81 g, 5.00 mmol) was added to the above binary composite, followed by the addition of NaOH solution (10 M, 20 mL, 21.00 mmol) with magnetic stirring for 5 min and allowed to equilibrate the pH for 3 h. Fresh AgNO₃ solution (5 mL, 0.30 M, 1.50 mmol) was added to this mixture under strong stirring conditions for 30 s, followed by gentle stirring for 30 min at room temperature. The mixture was kept undisturbed for 12 h and then washed with deionized water (till the pH of the filtrate became neutral from alkaline). The ternary nanocomposite mixture was finally washed with acetone and dried in a vacuum oven at 70°C. Yield: 0.28 g. FT-IR (KBr, cm⁻¹) 693, 787, 1534, 1646, 1695, and 1747.

4.2.4. Synthesis of MWCNT-COOH Ag: MWCNT-COOH (0.16 g) was dispersed in 500 mL of deionized water by sonication. Ascorbic acid (8.81g, 5.00 mmol) was added to the above dispersion followed by the addition of NaOH solution (10 M, 20 mL, 21.00 mmol) with magnetic stirring for 5 min and allowed to equilibrate the pH for 3 h. Fresh AgNO₃ solution (5 mL, 0.30 M, 1.50 mmol) was then added to this mixture under strong stirring conditions for 30 s followed by gentle stirring for 30 min at room temperature. The mixture was kept undisturbed for 12 h and then washed with deionized water (till the pH of the filtrate became neutral from alkaline). The binary silver nanocomposite mixture was finally washed with acetone and dried in a vacuum oven at 70°C. Yield: 0.31 g. FT-IR (KBr, cm⁻¹) 1550, 1646, 1705, 1754.

4.2.5. Leaching study of PTCNT-COOH 300 Ag with different pH: PTCNT-COOH 300 Ag (0.010 g) was dispersed in HCl (15 mL, 1M, pH: 0.8) by sonication for 5 min. Then it was magnetically stirred for 3 h. It was washed with water, filtered and the residue obtained was dried in a vacuum oven at 60°C for 1 h. The above residue was subjected to record UV-Vis spectra by dispersing in water.

The above procedure was repeated by changing the medium into CH_3COOH (1M, pH:2.8), water (pH:7.0), NH_4OH (1M, pH:11.5) and NaOH (1M, pH:12.8).

4.3. Results and Discussion

4.3.1 Synthesis and characterization of PTCNT-COOH 300 Ag and MWCNT-COOH Ag

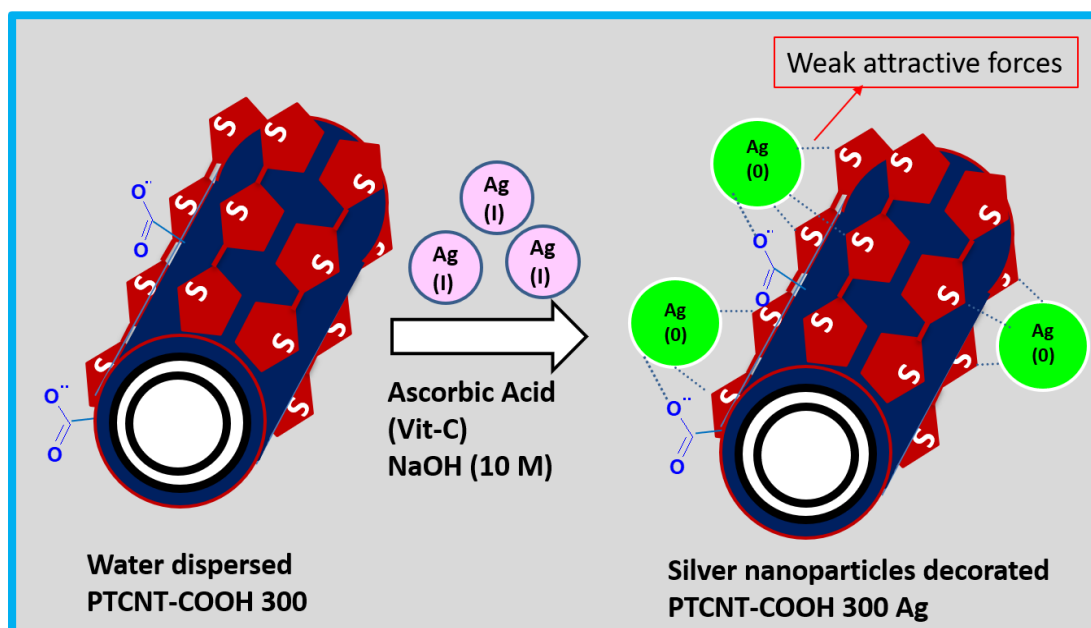


Figure 4.3. Schematic representation of the synthesis of PTCNT-COOH 300 Ag

The ternary silver nanocomposite PTCNT-COOH 300 Ag was prepared by reducing silver nitrate solution to silver nanoparticles using ascorbic acid as the reducing agent in the presence of aqueous dispersed PTCNT-COOH 300 nanocomposites. The formation of PTCNT-COOH 300 Ag is schematically represented in **Figure 4.3.** (see **Table 4.1.** also) Ascorbic acid (vitamin C) is a green and bio-friendly reducing reagent. Silver nitrate reduction was carried out in the presence of stable aqueous dispersion of PTCNT-COOH composites discussed in chapter 3. Sonication for 15 min produced stable dispersion of binary PTCNT-COOH 300 nanocomposites. Here, the PTCNT-COOH 300 functioned as a hard template to accommodate the reduced form of silver nanoparticles by providing a large enough surface area in its nanotubular assembly. The synthesis was carried out in basic pH \approx 10. Control on pH was carried out by adding NaOH solution. The same procedure was also used to synthesize binary silver nanocomposites named MWCNT-COOH Ag formed

Preparation of Silver Nanoparticles Entangled Ternary Nanocomposites

by reduction of silver nitrate in presence of functionalized MWCNT-COOH (conducting polythiophene is not present).

Table 4.1. Atomic concentration of samples from XPS spectra, pH of the samples, morphology of samples, thermal stability of samples, and electrical conductivity of samples.

Samples	Components	Type of Nano composites	Atomic Concentration from XPS (%)				pH	Shape	Thermal Stability (°C)	Conductivity (S/cm)
			C 1s	O 2s	S 2p	Ag 3d				
MWCNT-COOH	-	-	94.42	5.58	-	-	4.8	nanotubes	560	2.80
PTCNT-COOH-300	Thiophene + MWCNT-COOH	Binary	88.63	5.70	5.68	-	5.4	PT covered Nanotubes	340	1.64
MWCNT-COOH Ag	MWCNT-COOH + Ag	Binary	-	-	-	-		Nanoparticles + nanotubes	750	12.40
PTCNT-COOH 300 Ag	Thiophene + Ag + MWCNT-COOH	Ternary	86.66	7.75	4.22	2.37	7.0	Nanoparticles + PT covered Nanotubes	620	80.76

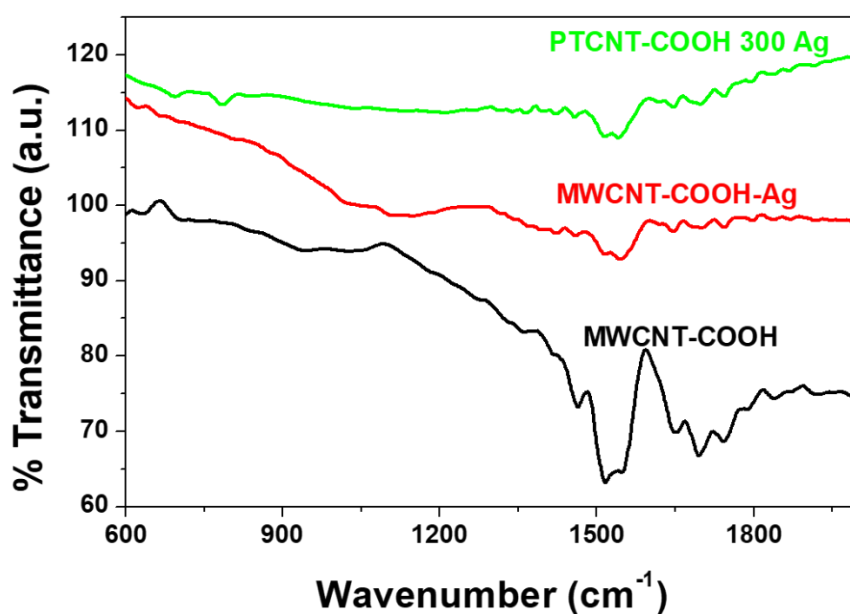


Figure 4.4. FT-IR spectra of MWCNT-COOH, MWCNT-COOH Ag and PTCNT-COOH 300 Ag.

PTCNT-COOH 300 Ag and MWCNT-COOH Ag were subjected to FT-IR studies to characterize the formation of respective nanocomposites (see **Figure 4.4.**). The functionalized MWCNT-COOH Ag have shown peaks of MWCNT-COOH at 1534 cm^{-1} , 1646 cm^{-1} , 1695 cm^{-1} and 1747 cm^{-1} corresponding to in-plane vibrations of graphitic walls, C=C stretching vibrations, carbonyl groups and C=O stretching vibration in acid groups respectively. PTCNT-COOH 300 Ag sample has shown characteristic peaks of thiophene at 787 cm^{-1} and 693 cm^{-1} due to C-H out-of-plane deformation mode and C-S stretching mode of the thiophene ring in addition to the peaks of MWCNT-COOH. MWCNT-COOH Ag and PTCNT-COOH 300 Ag samples have shown a decline in carbonyl stretching frequency at 1695 and 1747 cm^{-1} , which could be attributed to the nanocomposites formation with silver.²⁹⁻³² FT-Raman spectra of PTCNT-COOH 300 Ag and MWCNT-COOH Ag in powder form were recorded using 514.5 nm argon laser (see **Figure 4.5.**). MWCNT-COOH Ag has shown characteristic G band and D band at 1576 cm^{-1} and 1348 cm^{-1} , respectively. In the case of PTCNT-COOH 300 Ag, an additional intense peak was observed at 1450 cm^{-1} due to symmetric in-phase vibration of the polythiophene chain, which showed the presence of polythiophene in the ternary nanocomposite.^{32,33}

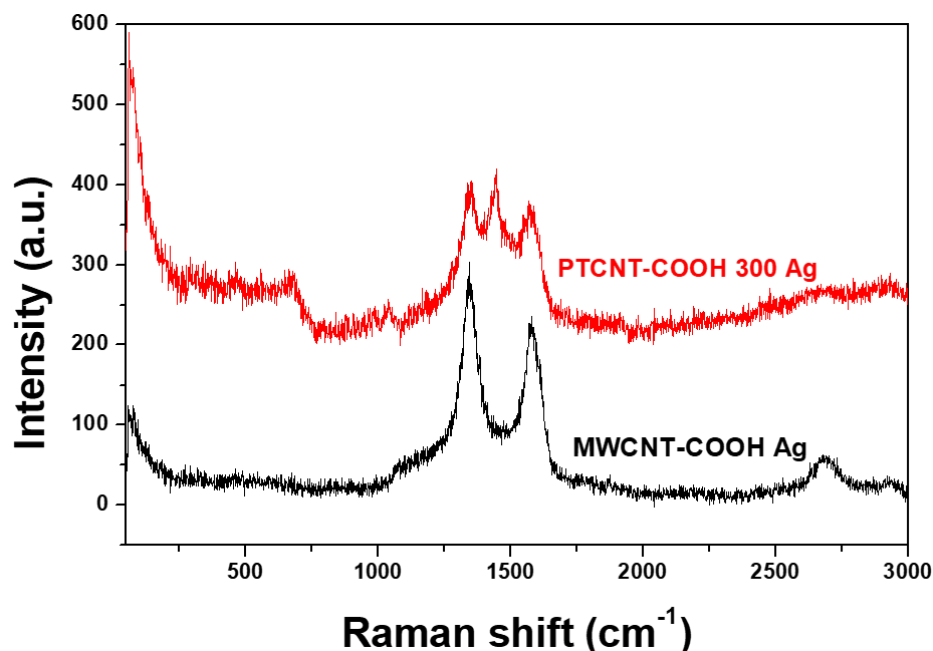


Figure 4.5. FT Raman spectra of MWCNT-COOH Ag and PTCNT-COOH 300 Ag

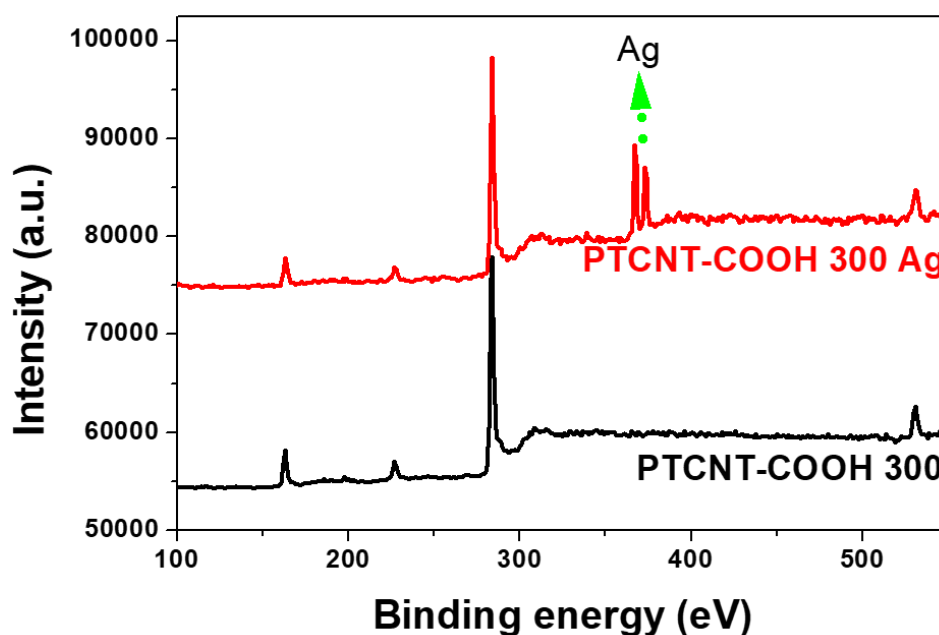


Figure 4.6. XPS spectra of PTCNT-COOH 300 and PTCNT-COOH 300 Ag

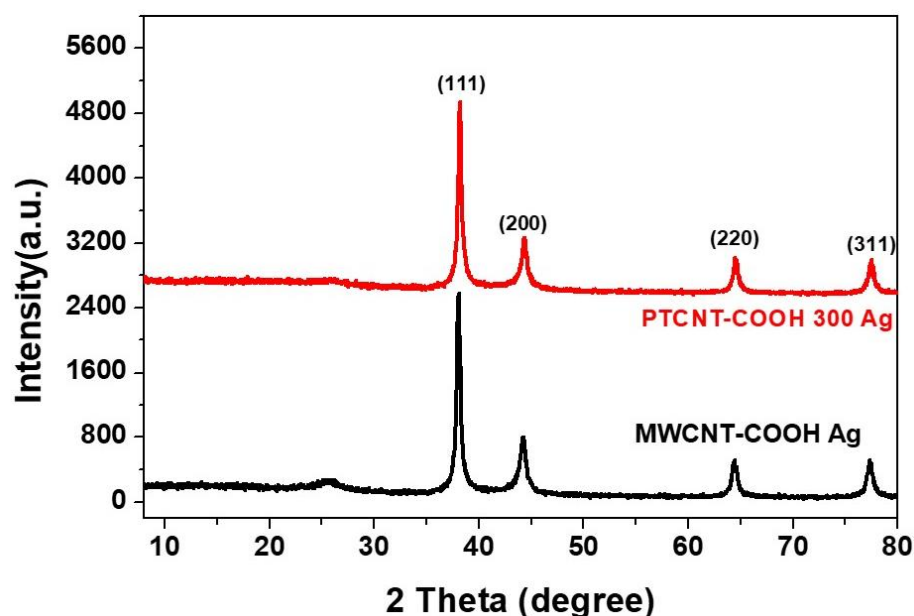


Figure 4.7. WXR D pattern of PTCNT-COOH 300 Ag and MWCNT-COOH Ag

The X-ray photoelectron spectra of PTCNT-COOH 300 and PTCNT-COOH 300 Ag have shown peaks at 162.75 eV, 226.95 eV, 283.25 eV and 531.45 eV corresponding to binding energies of S 2p, S 2s, C 1s and O 1s respectively. In addition, ternary silver nanocomposites PTCNT-COOH 300 Ag have shown peaks of silver atoms at 367.45 and 373.45 eV representing binding energies of $3d^{5/2}$ and $3d^{3/2}$ respectively, which indicates the formation of silver nanoparticles in the

nanocomposites (see **Figure 4.6**).³⁴ Wide angle X-ray diffraction studies of PTCNT-COOH 300 Ag and MWCNT-COOH Ag have also been carried out to confirm the formation of silver nanoparticles in conducting polythiophene-functionalized MWCNT nanocomposites (see **Figure 4.7**). Both the samples have shown highly crystalline peaks at 2θ values 38.15° , 44.33° , 64.52° and 77.46° , which represent Bragg's reflections from (111), (200), (220) and (311) planes of Ag nanoparticles in nanocomposites.³⁵ The weak peak at 2θ value 26.69° was due to diffraction from (002) plane of the graphitic structure of CNT.³⁶ The presence of highly crystalline silver nanoparticles increases the overall solid state ordering of the samples.

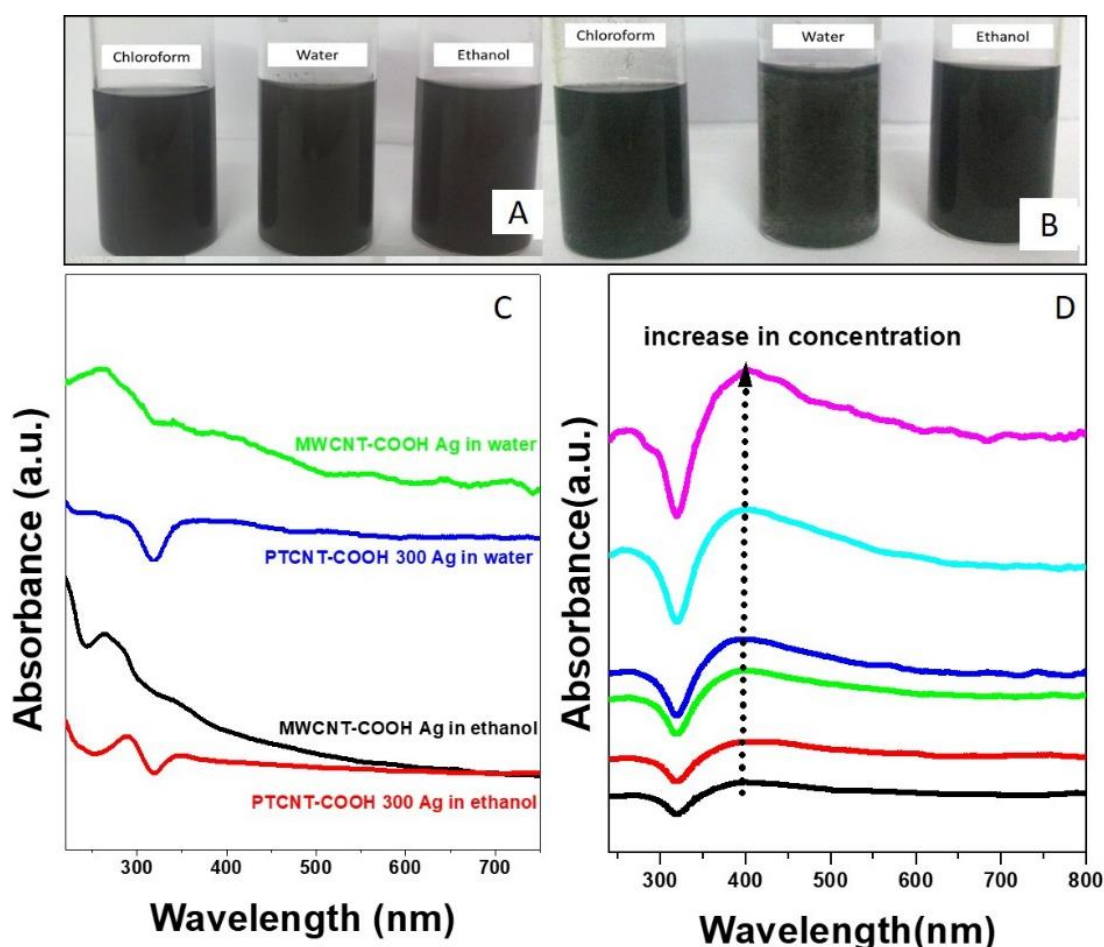


Figure 4.8. Dispersion of PTCNT-COOH 300 Ag (A) and MWCNT-COOH Ag (B) in different solvents. UV-vis spectra of PTCNT-COOH 300 Ag and MWCNT-COOH Ag in water and ethanol (C). UV-vis spectra of PTCNT-COOH 300 Ag in water with different concentrations (D).

MWCNT-COOH Ag and PTCNT-COOH 300 Ag could be easily dispersed in water and ethanol, allowing us to record the UV-vis absorption spectra (see **Figure**

4.8.). The tendency of formation of stable dispersions was retained in ternary composite by keeping an energy barrier against aggregation. Whereas, in the case of binary silver nanocomposite the dispersion get settled down after 30 min. The UV-vis absorption spectra have shown absorption maxima at 285 nm due to the π - π^* absorption from multiwalled carbon nanotube. The ternary nanocomposites PTCNT-COOH 300 Ag samples in water and ethanol have shown polaron- π peak at 360 nm. Surprisingly, the longer wavelength peak at 360 nm was extended as shoulder up to 550 nm, which could be attributed to the surface plasmon resonance of silver nanoparticles.^{37,38}

4.3.2. Morphological analysis of ternary and binary silver nanocomposites

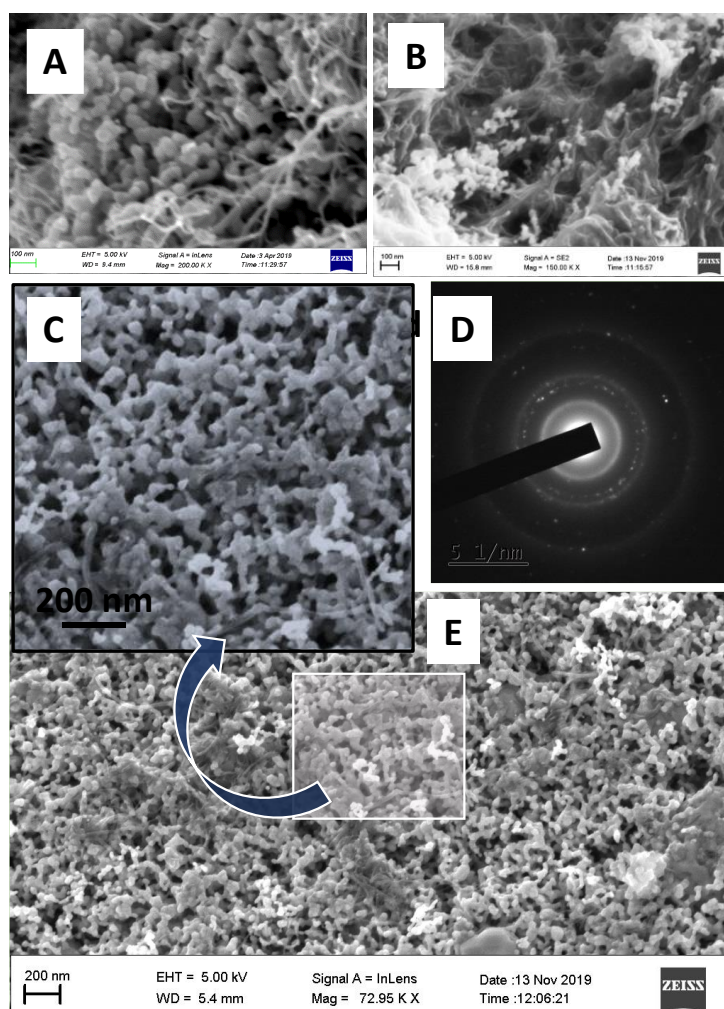


Figure 4.9. FE-SEM images of MWCNT-COOH Ag (A), dispersed PTCNT-COOH 300 Ag (B), PTCNT-COOH 300 Ag (C (cropped image) and E) and electron diffraction pattern of PTCNT-COOH 300 Ag (D)

The field emission scanning electron microscopic images of MWCNT-COOH Ag and PTCNT-COOH 300 Ag and dispersed PTCNT-COOH 300 Ag exhibited silver nanoparticles embedded the conducting polymer-carbon nanocomposites (see **Figure 4.9. (A),(B), (C) and (E)**). The striking observation made from field emission-scanning electron microscopy images of PTCNT-COOH 300 Ag was that embedded silver nanoparticles exhibited a tangled nature and spaces were observed between each nanotube of ternary nanocomposites. The predominant involvement of the non-covalent interaction of PTCNT-COOH 300 with silver nanoparticles (Ag) was evident from these images. Here nanocomposite were appeared without aggregation of silver atoms.

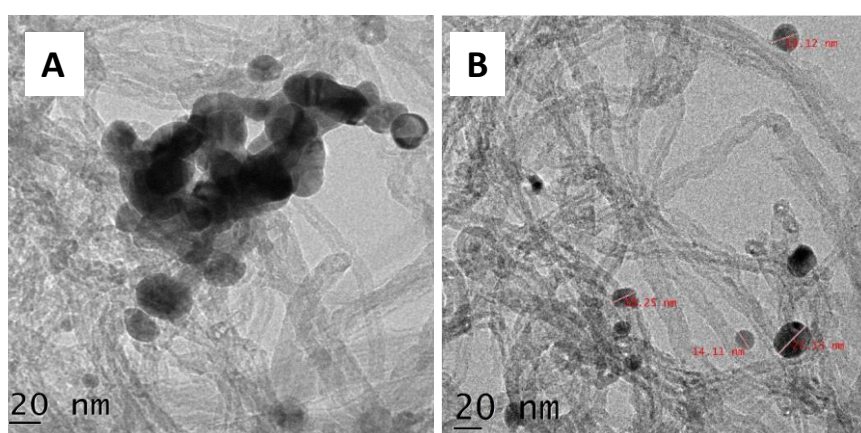


Figure 4.10. Transmission electron microscopic images of PTCNT-COOH 300 Ag (A) and its size calculation (by taking the average size of 10 nanoparticles) (B)

Transmission electron microscopic analysis of the nanoparticles has revealed the formation of tangled solid silver nanoparticles over PTCNT-COOH nanocomposites with an average size of 25 ± 5 nm obtained as an average of 10-12 nanoparticles (see **Figure 4.10.**). Entangled silver nanoparticles embedded over polythiophene-functionalized multiwalled carbon nanotube appear as aggregated silver particles. However, there were isolated nanoparticles in the PTCNT-COOH fibrous matrix and a close look at the silver nanoparticles revealed that they were embedded in the nanocomposite matrix. PTCNT-COOH 300 Ag has a ring-like electron diffraction pattern with bright spots, which indicates that Ag nanoparticles are crystalline (see **Figure 4.9. (D)**).³⁹

It is important to note that silver nanoparticles have nearly spherical shapes even though they exist in tangled fashion, as seen in **Figure 4.11**. In the case of ternary silver nanocomposites formation, the Ag^+ ions from silver nitrate were attracted to sulfur

Preparation of Silver Nanoparticles Entangled Ternary Nanocomposites

atoms in the heterocyclic polythiophene chains and get reduced to silver nanoparticles by accepting electrons from ascorbic acid present in the aqueous dispersion. Ascorbic acid itself is converted to semidehydroascorbic acid radical ion and then to dehydroascorbic acid.^{34,40} Anchoring of silver nanoparticles to the surface of the nanocomposites occurs via its complex formation with the sulfur atoms and the carboxylate group contained in PTCNT-COOH nanocomposites.^{41,42} The sulfur atoms in closely packed polythiophene chains can assist the silver nanoparticles to decorate over the PTCNT-COOH 300 in a tangling fashion along with the carboxylic group of functionalized carbon nanotubes using the non-covalent force of interactions.

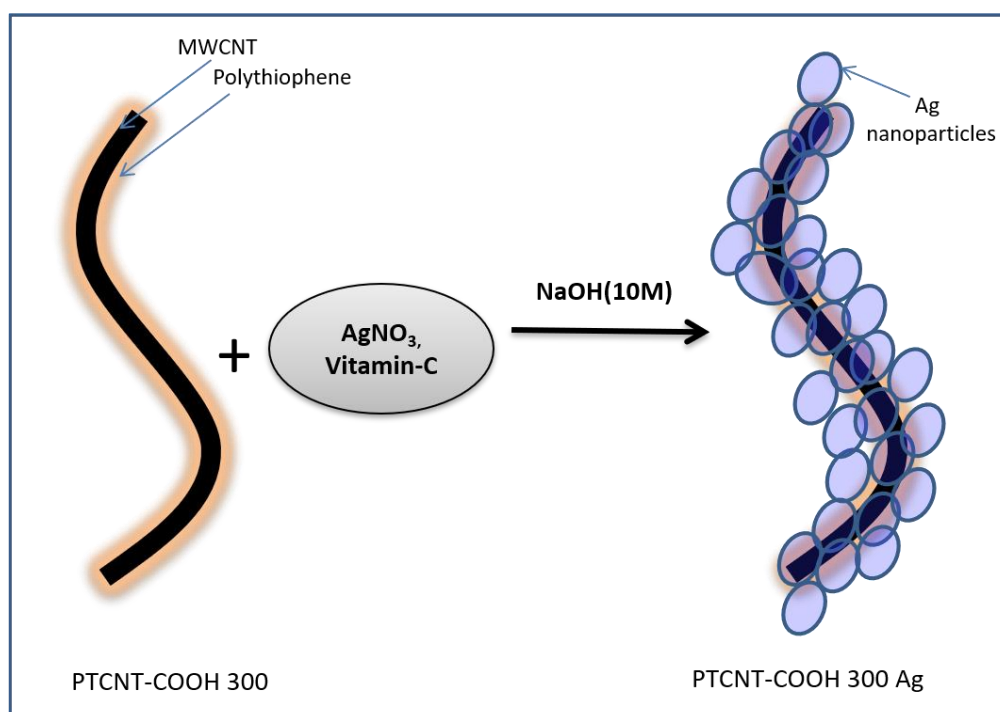


Figure 4.11. Scheme for the formation of silver nanoparticle embedded ternary nano composite.

4.3.3. Electrical conductivity and thermal stability of ternary and binary nanocomposites

The four-probe electrical conductivity of the samples was recorded by DFP-RM-200 four-probe set-up with a constant current. The electrical conductivity of the samples was measured at four different points and the average value has been reported. The electrical conductivity of the PTCNT-COOH 300, MWCNT, MWCNT-COOH Ag

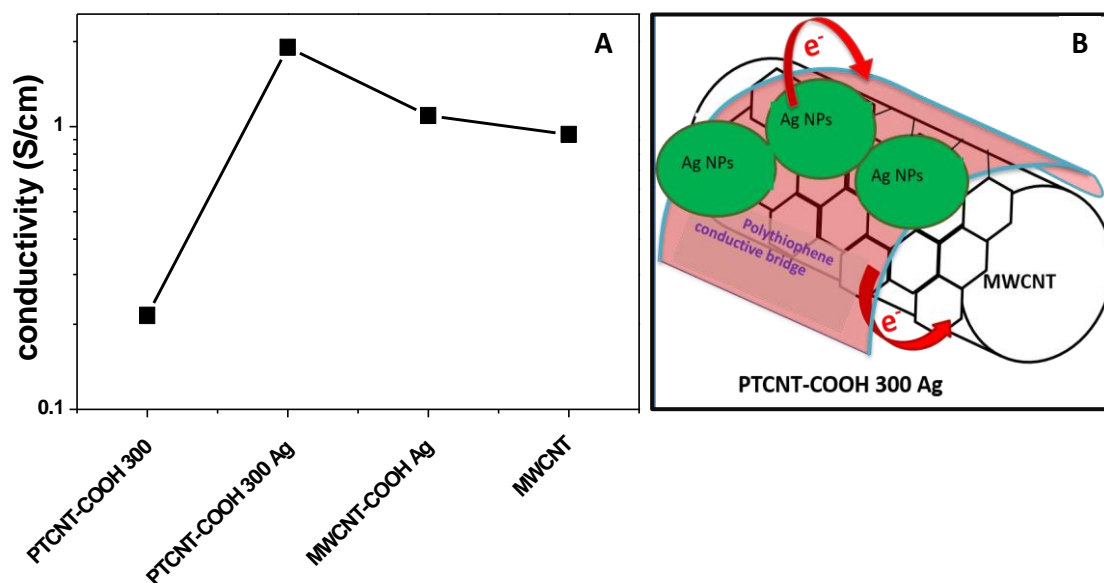


Figure 4.12. Four probe electrical conductivity measurements of PTCNT- COOH 300, PTCNT-COOH 300 Ag and MWCNT-COOH Ag and pristine MWCNT (A). The schematic illustration of polythiophene as a connecting bridge between MWCNT-COOH and silver nanoparticles (B).

and PTCNT-COOH 300 Ag were 1.64, 8.66, 12.40 and 80.76 S/cm, respectively (see **Figure 4.12. (a)**). The electrical conductivity of polythiophene was less than pristine multiwalled carbon nanotube and polythiophene-functionalized multiwalled carbon nanotube binary nanocomposites. Effective charge transfer of the charge carriers in binary and ternary nanocomposites resulted in higher electrical conductivity. The silver nanoparticles loaded polythiophene-functionalized MWCNT nanocomposites were an interesting case of ternary conducting polymer nanocomposite due to conducting polythiophene layer. The conducting polythiophene layer acts as a conductive bridge that transfers electrical charges between more conducting silver and multiwalled carbon nanotube via a hopping mechanism. Therefore the overall electrical conductivity of the system increases (see **Figure 4.12 (b)**).

Thermal stability of PTCNT-COOH 300, MWCNT-COOH Ag and PTCNT-COOH 300 Ag have been carried out using thermogravimetric analysis at a heating rate of 20°C per minute under an inert nitrogen atmosphere (see **Figure 4.13.**). The thermal stability of PTCNT-COOH 300 Ag was found to be higher than PTCNT-COOH 300. Sample PTCNT-COOH 300 Ag has shown 10 % weight loss at 620°C.⁴³

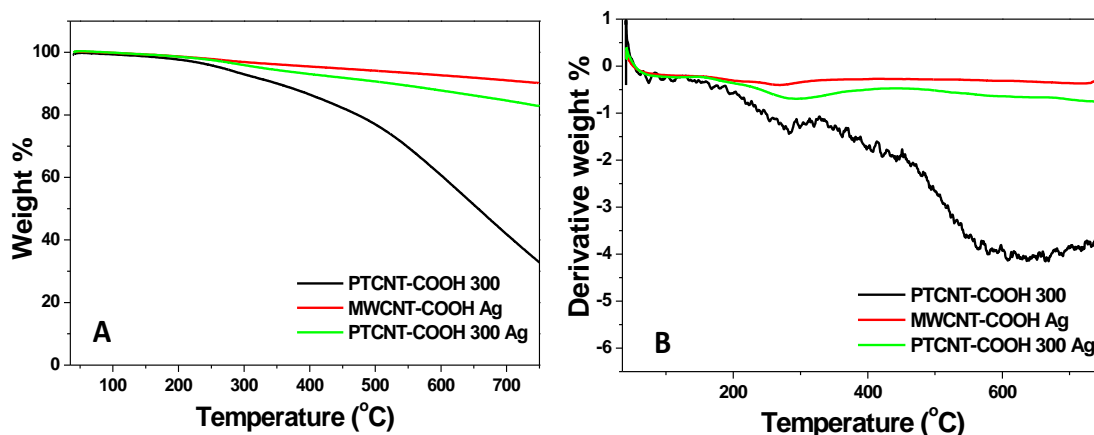


Figure 4.13. Thermograms (A) and differential thermograms (B) of PTCNT-COOH 300, MWCNT-COOH Ag and PTCNT-COOH 300 Ag

Accommodation of silver nanoparticles in ternary composite PTCNT-COOH 300 Ag enhances the thermal conductivity of the system.⁴⁴ The high thermal conductivity of multiwalled carbon nanotube and silver nanoparticles might have played a crucial role in enhancing thermal stability by building a perfect heat transfer network in ternary nanocomposites even though it contains a high percentage of thermally less stable polythiophene.⁴⁵ The highest thermal stability obtained for MWCNT-COOH Ag for 10% weight loss was 750 °C, which was devoid of the polymer sample. Therefore, the thermal stability and thermal conductivity of PTCNT-COOH 300 (binary composite) and functionalized MWCNT-COOH could be increased significantly by making entangled silver nanoparticle ternary nanocomposites.⁴⁶ Differential thermal analysis exhibited that decomposition of functionalized MWCNT-COOH was observed from 510° C. Whereas decomposition rate of PTCNT-COOHs was observed in two stages, one stage from 260 to 340°C due to degradation of polythiophene and the other one starting from 470°C due to the CNT structural decomposition (see **Figure 4.13. (b)**). Good thermal stability of MWCNT-COOH Ag and PTCNT-COOH 300 Ag was observed with a much lower rate of decomposition, so they can perform as suitable materials in high temperature applications.

The pH sensitivity of the ternary nanocomposite system has been checked by the leaching tendency of embedded silver in ternary nanocomposite in acidic, basic and neutral media (see **Figure 4.14.**). The stability of the ternary nanocomposites at

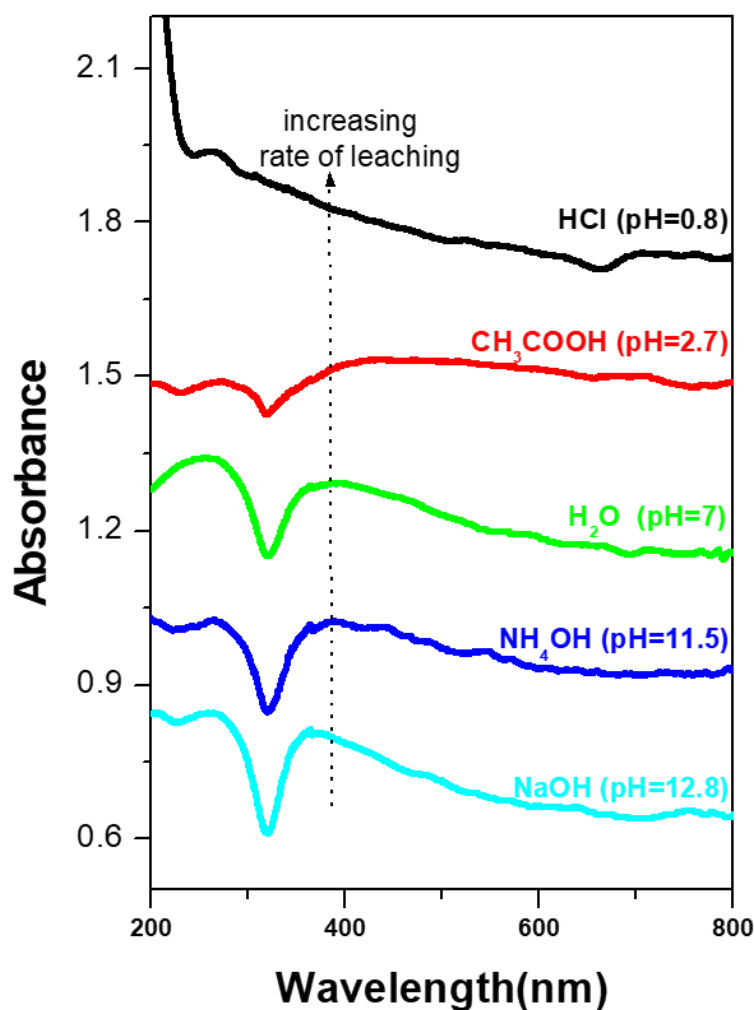


Figure 4.14. UV-vis spectra of PTCNT-COOH 300 Ag after 3 h of stirring and washing with different media of different pH.

different pH has been checked via UV-vis absorption spectroscopy by noting the changes in the surface plasmon peak (> 360 nm). The study revealed that silver nanoparticles have good stability against leaching in basic medium (high pH). Compared to NaOH medium, leached silver nanoparticles percentage in other media such as NH_4OH , H_2O and CH_3COOH are 11.79%, 29.23% and 60% respectively. Badawy et al. reported that electrostatically stabilized silver nanoparticles exhibit high degree of aggregation at low pH (acidic conditions). The surface charge densities will be less negative at low pH of the medium and resulted higher particle-particle interaction. As pH of the medium decreases the silver nanoparticles get aggregated easily and into larger particles. The larger particles get leached out easily from the surface of composite.⁴⁷ Ternary nanocomposites can be effectively utilized for catalytic applications in a basic medium and therefore, they can be a durable catalyst with

Preparation of Silver Nanoparticles Entangled Ternary Nanocomposites

Table 4.2. Comparison study of our work with similar systems reported in the literature.

	components	Synthetic method of nanoparticles	Solvent/solvents used for synthesis of nanoparticles	Reducing agent/reagent for nanoparticle synthesis	Size of nanoparticles	Functionalizations carried out for MWCNT	Suggesting dispersion medium for further processing	Conductivity S/cm	Thermal stability	Extended study based on application	Reference number
Our work	Polythiophene, acid functionalized MWCNT, silver nanoparticles	Chemical	H ₂ O	Vitamin-C-reductant	25±8 nm	Carboxylic acid functionalization	H ₂ O, ethanol	80.76 S/cm	10% weight loss at ~620°	Leaching study of silver nanoparticles in different pH	-
Same system in literature	PEDOT/polystyrene sulfonate, MWCNT, silver nanoparticles	Chemical	DCM	NaBH ₄ -reductant	~128± 28 nm	Ethylene diamine functionalization	DCM	-	-	Improving electrical conductivity of polycarbonate matrix	15
Similar Systems in literature	Poly(2-thiophene methylamine), MWCNT, CdS nanoparticles	Chemical	DMF and water	Na ₂ S-reagent	Average size=3.1 nm	-	-	-	10% weight loss at ~320°	Optical limiting enhancement	48
	Polythiophene, MWCNT, gold nanoparticles	Chemical	H ₂ O	Thiophene-reductant	average size=4.3 nm	-	-	-	-	-	41
	Polythiophene, MWCNT, gold nanoparticles	Chemical	Hexane and H ₂ O	Thiophene-reductant	~5 nm and ~15 nm	-	-	-	-	Electrochemical sensing of dopamine	50
	Polythiophene, MWCNT, platinum nanoparticles	Electrochemical	-	-	Nanocluster formation	Oxidation by acid treatment	-	-	-	Electrochemical sensor for Bisphenol A	51
	Polyaniline, MWCNT, silver nanoparticles	Chemical	H ₂ O	Aniline	Single nanoparticles - 5-30 nm Agglomerated nanoparticles - 50-95 nm	Carboxylic acid functionalization	-	4.24 S/cm	10% weight loss at ~320°	High performance supercapacitor or electrode	2
	Polypyrrolone, MWCNT, silver nanoparticles	Chemical	H ₂ O	Trisodium citrate dihydrate	30 nm	Carboxylic acid functionalization	-	4.01 S/cm	-	Electromagnetic shielding	49
		UV-reduction	H ₂ O	UV	30-35 nm	Carboxylic acid functionalization	-	5.12 S/cm	-		

multiple uses.^{48,49} Present work has significant advantages over other systems, especially in cost, efficiency and many other improved properties related to conductivity and thermal stability in nanocomposites. Synthesis of tangled silver nanoparticles embedded on polythiophene-functionalized multiwalled carbon nanotubes have been adopted in the cheapest and greener medium. Comparison of ternary and binary silver nanocomposites with other literatures are given in **Table 4.2**. The binary and ternary nanocomposites have been prepared efficiently on a laboratory scale with reproducibility and with improved processability. Therefore, the ternary nanocomposites prepared will open a doorway to different applications such as high-performance electrochemical electrodes, polymer supercapacitors, sensors, SERS tags, thermoelectric materials, catalytic applications and so on.⁴⁹⁻⁵³

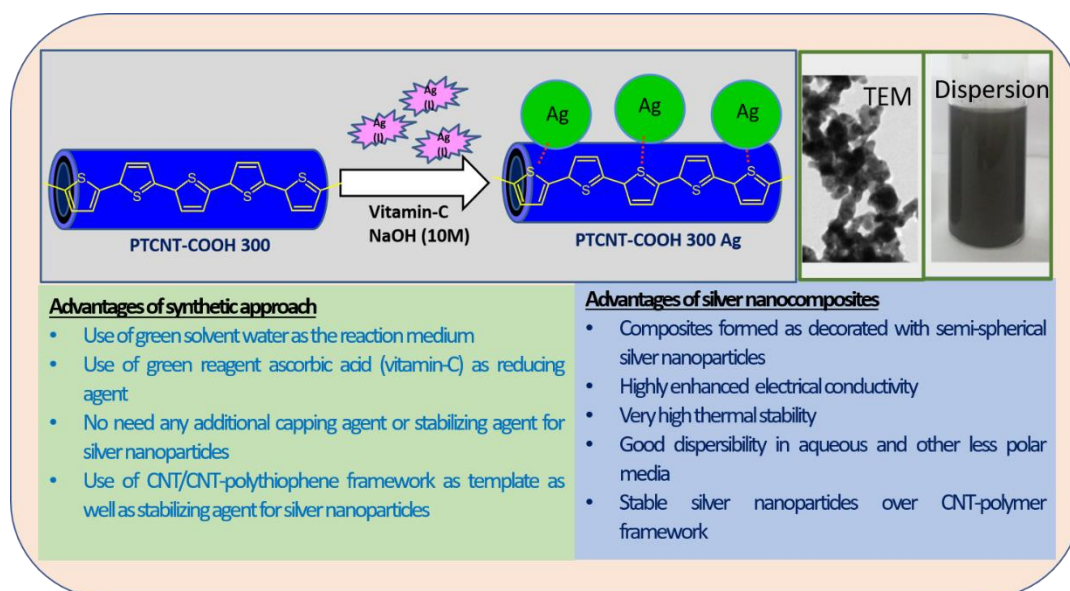


Figure 4.15. Illustration of the formation of water-dispersible ternary nanocomposite and its advantageous outcomes.

4.4. Conclusion

In summary, the present work demonstrated a facile and green synthetic approach to prepare water-dispersible, highly conductive and thermally stable ternary silver nanoparticles embedded polythiophene-functionalized multiwalled carbon nanotube nanocomposite (PTCNT-COOH 300 Ag) by efficiently utilizing the aqueous dispersion of binary polythiophene-functionalized multiwalled carbon nanotube nanocomposites (PTCNT-COOH 300) as a nanofibrous platform as well as the co-component matrix in its ternary composite. Here, we could effectively establish a facile synthesis of PTCNT-COOH 300 Ag from the dispersed state of PTCNT-COOH 300

binary composite by reduction of silver nitrate using ascorbic acid in green solvent water. A binary multiwalled carbon nanotube-silver nanocomposites (MWCNT-COOH Ag) were also synthesised using a similar in-situ reduction strategy. Formation of PTCNT-COOH 300 Ag and MWCNT-COOH Ag were primarily characterized by FT-IR spectroscopy, FT-Raman spectroscopy, XPS analysis and X-ray diffraction pattern analysis. The formation of crystalline silver nanoparticles in PTCNT-COOH 300 Ag was confirmed by WXRd analysis by noting the sharp crystalline peaks at 38.15° , 44.33° , 64.52° and 77.46° indicated by Bragg's reflections from (111), (200), (220) and (311) planes. Scanning and transmission electron microscopic analysis gave information about the formation of embedded silver nanoparticles on PTCNT-COOH 300 with an average size of 25 ± 8 nm in PTCNT-COOH 300 Ag. UV-vis spectra of PTCNT-COOH 300 Ag and MWCNT-COOH Ag have shown surface plasmon resonance of silver nanoparticles as a shoulder up to 550 nm. Tangled silver nanoparticles formed in the ternary nanocomposites were embedded over polythiophene-functionalized multiwalled carbon nanotube by the complex formation of sulfur atoms of thiophene moiety with silver. PTCNT-COOH 300 Ag exhibited higher electrical conductivity and thermal stability (two times higher) than PTCNT-COOH 300 for 10% weight loss due to the presence of embedded silver nanoparticles. The important and promising outcomes of the present investigations were summarized in **Figure 4.15**. The silver nanocomposites could effectively utilize catalytical, antibacterial, electrical and thermal applications based on their dispersibility, reusability, enhanced electrical conductivity and thermal stability.

References

1. Watt, J.; Collins, A. M.; Vreeland, E. C.; Montano, G. A.; Huber, D. L. Magnetic Nanocomposites and Their Incorporation into Higher Order Biosynthetic Functional Architectures. *ACS Omega* **2018**, *3* (1), 503–508. <https://doi.org/10.1021/acsomega.7b02031>.
2. Dhibar, S.; Das, C. K. Silver Nanoparticles Decorated Polyaniline/Multiwalled Carbon Nanotubes Nanocomposite for High-Performance Supercapacitor Electrode. *Ind. Eng. Chem. Res.* **2014**, *53* (9), 3495–3508. <https://doi.org/10.1021/ie402161e>.
3. Feng, M.; Sun, R.; Zhan, H.; Chen, Y. Decoration of Carbon Nanotubes with CdS Nanoparticles by Polythiophene Interlinking for Optical Limiting Enhancement. *Carbon N. Y.* **2010**, *48* (4), 1177–1185. <https://doi.org/10.1016/j.carbon.2009.11.041>.
4. Ohlan, A.; Singh, K.; Chandra, A.; Dhawan, S. K. Microwave Absorption Behavior of Core-Shell Structured Poly (3,4-Ethylenedioxy Thiophene)/Barium Ferrite Nanocomposites. *ACS Appl. Mater. Interfaces* **2010**, *2* (3), 927–933. <https://doi.org/10.1021/am900893d>.

5. Chakraborty, I.; Chakrabarty, N.; Senapati, A.; Chakraborty, A. K. CuO@NiO/Polyaniline/MWCNT Nanocomposite as High-Performance Electrode for Supercapacitor. *J. Phys. Chem. C* **2018**, *122* (48), 27180–27190. <https://doi.org/10.1021/acs.jpcc.8b08091>.
6. Malekkiani, M.; Heshmati Jannat Magham, A.; Ravari, F.; Dadmehr, M. Facile Fabrication of Ternary MWCNTs/ZnO/Chitosan Nanocomposite for Enhanced Photocatalytic Degradation of Methylene Blue and Antibacterial Activity. *Sci. Rep.* **2022**, *12* (1). <https://doi.org/10.1038/s41598-022-09571-5>.
7. Hou, Y.; Cheng, Y.; Hobson, T.; Liu, J. Design and Synthesis of Hierarchical MnO₂ Nanospheres/Carbon Nanotubes/Conducting Polymer Ternary Composite for High Performance Electrochemical Electrodes. *Nano Lett.* **2010**, *10* (7), 2727–2733. <https://doi.org/10.1021/nl101723g>.
8. Tang, L.; Duan, F.; Chen, M. Silver Nanoparticle Decorated Polyaniline/Multiwalled Super-Short Carbon Nanotube Nanocomposites for Supercapacitor Applications. *RSC Adv.* **2016**, *6* (69), 65012–65019. <https://doi.org/10.1039/c6ra12442a>.
9. Patole, A.; Ventura, I. A.; Lubineau, G. Thermal Conductivity and Stability of a Three-Phase Blend of Carbon Nanotubes, Conductive Polymer, and Silver Nanoparticles Incorporated into Polycarbonate Nanocomposites. *J. Appl. Polym. Sci.* **2015**, *132* (30). <https://doi.org/10.1002/app.42281>.
10. Drury, A.; Chaure, S.; Kröll, M.; Nicolosi, V.; Chaure, N.; Blau, W. J. Fabrication and Characterization of Silver/Polyaniline Composite Nanowires in Porous Anodic Alumina. *Chem. Mater.* **2007**, *19* (17), 4252–4258. <https://doi.org/10.1021/cm071102s>.
11. Abou El-Nour, K. M. M.; Eftaiha, A.; Al-Warthan, A.; Ammar, R. A. A. Synthesis and Applications of Silver Nanoparticles. *Arab. J. Chem.* **2010**, *3* (3), 135–140. <https://doi.org/10.1016/j.arabjc.2010.04.008>.
12. Dhibar, S.; Das, C. K. Silver Nanoparticles Decorated Polyaniline/Multiwalled Carbon Nanotubes Nanocomposite for High-Performance Supercapacitor Electrode. *Ind. Eng. Chem. Res.* **2014**, *53* (9), 3495–3508. <https://doi.org/10.1021/ie402161e>.
13. Tang, L.; Duan, F.; Chen, M. Silver Nanoparticle Decorated Polyaniline/Multiwalled Super-Short Carbon Nanotube Nanocomposites for Supercapacitor Applications. *RSC Adv.* **2016**, *6* (69), 65012–65019. <https://doi.org/10.1039/c6ra12442a>.
14. Sarkar, A. K.; Sanna, A.; Banerjee, C.; Mandre, N. R.; Panda, A. B.; Pal, S. Crosslinked Biopolymer Stabilized Exfoliated Titanate Nano Sheet Supported AgNPs: A Green Sustainable Ternary Nanocomposite Hydrogel for Catalytic and Antimicrobial Activity, Sustainable Chem. Eng. **2017**, *5* (2), 1881–1891. <https://doi.org/10.1021/acssuschemeng.6b02594>.
15. Patole, A.; Lubineau, G. Carbon Nanotubes with Silver Nanoparticle Decoration and Conductive Polymer Coating for Improving the Electrical Conductivity of Polycarbonate Composites. *Carbon N. Y.* **2015**, *81* (1), 720–730. <https://doi.org/10.1016/j.carbon.2014.10.014>.
16. Reddy, K. R.; Sin, B. C.; Ryu, K. S.; Kim, J. C.; Chung, H.; Lee, Y. Conducting Polymer Functionalized Multi-Walled Carbon Nanotubes with Noble Metal Nanoparticles: Synthesis, Morphological Characteristics and Electrical Properties. *Synth. Met.* **2009**, *159* (7–8), 595–603. <https://doi.org/10.1016/j.synthmet.2008.11.030>.
17. Elhalawany, N.; Awad, M. A.; Zahran, M. K. Synthesis, Characterization, Optical and Electrical Properties of Novel Highly Dendritic Polythiophene Nanocomposites with Silver and/or Gold. *J. Mater. Sci. Mater. Electron.* **2018**, *29* (11), 8970–8977. <https://doi.org/10.1007/s10854-018-8921-7>.
18. Lee, C. J.; Karim, M. R.; Lee, M. S. Synthesis and Characterization of Silver/Thiophene Nanocomposites by UV-Irradiation Method. *Mater. Lett.* **2007**, *61* (13), 2675–2678. <https://doi.org/10.1016/j.matlet.2006.10.021>.
19. Ates, M.; Caliskan, S.; Ozten, E. A Ternary Nanocomposite of Reduced Graphene Oxide, Ag Nanoparticle and Polythiophene Used for Supercapacitors. *Fullerenes Nanotub. Carbon Nanostructures* **2018**, *26* (6), 360–369. <https://doi.org/10.1080/1536383X.2018.1438414>.

20. Tessonnier, J. P.; Ersen, O.; Weinberg, G.; Pham-Huu, C.; Su, D. S.; Schlögl, R. Selective Deposition of Metal Nanoparticles inside or Outside Multiwalled Carbon Nanotubes. *ACS Nano* **2009**, *3* (8), 2081–2089. <https://doi.org/10.1021/nn900647q>.
21. Shaham, G.; Veisi, H.; Hekmati, M. Silver Nanoparticle-Decorated Multiwalled Carbon Nanotube/Pramipexole Nanocomposite: Synthesis, Characterization and Application as an Antibacterial Agent. *Appl. Organomet. Chem.* **2017**, *31* (10). <https://doi.org/10.1002/aoc.3737>.
22. Tran Hoang, P.; Salazar, N.; Porkka, T. N.; Joshi, K.; Liu, T.; Dickens, T. J.; Yu, Z. Engineering Crack Formation in Carbon Nanotube-Silver Nanoparticle Composite Films for Sensitive and Durable Piezoresistive Sensors. *Nanoscale Res. Lett.* **2016**, *11* (1). <https://doi.org/10.1186/s11671-016-1626-z>.
23. Lee, J. W.; Cho, J. Y.; Kim, M. J.; Kim, J. H.; Park, J. H.; Jeong, S. Y.; Seo, S. H.; Lee, G. W.; Jeong, H. J.; Han, J. T. Synthesis of Silver Nanoparticles Embedded with Single-Walled Carbon Nanotubes for Printable Elastic Electrodes and Sensors with High Stability. *Sci. Rep.* **2021**, *11* (1). <https://doi.org/10.1038/s41598-021-84386-4>.
24. Castle, A. B.; Gracia-Espino, E.; Nieto-Delgado, C.; Terrones, H.; Terrones, M.; Hussain, S. Hydroxyl-Functionalized and N-Doped Multiwalled Carbon Nanotubes Decorated with Silver Nanoparticles Preserve Cellular Function. *ACS Nano* **2011**, *5* (4), 2458–2466. <https://doi.org/10.1021/nn200178c>.
25. Olivares, F.; Peón, F.; Henríquez, R.; del Río, R. S. Strategies for Area-Selective Deposition of Metal Nanoparticles on Carbon Nanotubes and Their Applications: A Review. *J. Mater. Sci.* **2022**, *57* (4), 2362–2387. <https://doi.org/10.1007/s10853-021-06710-7>.
26. Zhang, S.; Lu, Q.; Zhang, C.; Zhou, Y.; Liu, M.; Zhang, Y.; Deng, L. Green Synthesis of Silver-Carbon Nanocomposites with Extraordinary Stability and Robust Antibacterial Activity against Bacterial Diseases in Fish. *ACS Appl. Bio Mater.* **2022**, *5* (3), 1064–1072. <https://doi.org/10.1021/acsabm.1c01116>.
27. Kumari, S.; Sharma, P.; Yadav, S.; Kumar, J.; Vij, A.; Rawat, P.; Kumar, S.; Sinha, C.; Bhattacharya, J.; Srivastava, C. M.; Majumder, S. A Novel Synthesis of the Graphene Oxide-Silver (GO-Ag) Nanocomposite for Unique Physiochemical Applications. *ACS Omega* **2020**, *5* (10), 5041–5047. <https://doi.org/10.1021/acsomega.9b03976>.
28. AL-Refai, H. H.; Ganash, A. A.; Hussein, M. A. Polythiophene and Its Derivatives –Based Nanocomposites in Electrochemical Sensing: A Mini Review. *Mater. Today Commun.* **2021**, *26*. <https://doi.org/10.1016/j.mtcomm.2020.101935>.
29. Tang, L.; Duan, F.; Chen, M. Silver Nanoparticle Decorated Polyaniline/Multiwalled Super-Short Carbon Nanotube Nanocomposites for Supercapacitor Applications. *RSC Adv.* **2016**, *6* (69), 65012–65019. <https://doi.org/10.1039/c6ra12442a>.
30. Wilson, J.; Radhakrishnan, S.; Sumathi, C.; Dharuman, V. Polypyrrole-Polyaniline-Au (PPy-PANi-Au) Nano Composite Films for Label-Free Electrochemical DNA Sensing. *Sensors Actuators, B Chem.* **2012**, *171–172*, 216–222. <https://doi.org/10.1016/j.snb.2012.03.019>.
31. Miller, A. J.; Hatton, R. A.; Silva, S. R. P. Water-Soluble Multiwall-Carbon-Nanotube-Polythiophene Composite for Bilayer Photovoltaics. *Appl. Phys. Lett.* **2006**, *89* (12). <https://doi.org/10.1063/1.2356115>.
32. Bazzouai, E. A.; Lévi, G.; Aeiyaich, S.; Aubard, J.; Marsault, J. P.; Lacaze, P. C. SERS Spectra of Polythiophene in Doped and Undoped States. *J. Phys. Chem.* **1995**, *99* (17), 6628–6634. <https://doi.org/10.1021/j100017a052>.
33. Shi, G.; Xu, J.; Fu, M. Raman Spectroscopic and Electrochemical Studies on the Doping Level Changes of Polythiophene Films during Their Electrochemical Growth Processes. *J. Phys. Chem. B* **2002**, *106* (2), 288–292. <https://doi.org/10.1021/jp013023o>.
34. Zhang, N.; Yu, X.; Hu, J.; Xue, F.; Ding, E. Synthesis of Silver Nanoparticle-Coated Poly(Styrene-Co-Sulfonic Acid) Hybrid Materials and Their Application in Surface-

- Enhanced Raman Scattering (SERS) Tags. *RSC Adv.* **2013**, *3* (33), 13740–13747. <https://doi.org/10.1039/c3ra40888d>.
35. Jiang, H.; Moon, K. S.; Li, Y.; Wong, C. P. Surface Functionalized Silver Nanoparticles for Ultrahigh Conductive Polymer Composites. *Chem. Mater.* **2006**, *18* (13), 2969–2973. <https://doi.org/10.1021/cm0527773>.36.
 36. Li, H.; Zhou, B.; Lin, Y.; Gu, L.; Wang, W.; Fernando, K. A. S.; Kumar, S.; Allard, L. F.; Sun, Y. P. Selective Interactions of Porphyrins with Semiconducting Single-Walled Carbon Nanotubes. *J. Am. Chem. Soc.* **2004**, *126* (4), 1014–1015. <https://doi.org/10.1021/ja037142o>.
 37. Ranjan, P.; Shankar, S.; Popovitz-Biro, R.; Cohen, S. R.; Kaplan-Ashiri, I.; Dadosh, T.; Shimon, L. J. W.; Višić, B.; Tenne, R.; Lahav, M.; Van Der Boom, M. E. Decoration of Inorganic Nanostructures by Metallic Nanoparticles to Induce Fluorescence, Enhance Solubility, and Tune Band Gap. *J. Phys. Chem. C* **2018**, *122* (12), 6748–6759. <https://doi.org/10.1021/acs.jpcc.8b00510>.
 38. Lee, C. J.; Karim, M. R.; Lee, M. S. Synthesis and Characterization of Silver/Thiophene Nanocomposites by UV-Irradiation Method. *Mater. Lett.* **2007**, *61* (13), 2675–2678. <https://doi.org/10.1016/j.matlet.2006.10.021>.
 39. Dhibar, S.; Das, C. K. Electrochemical Performances of Silver Nanoparticles Decorated Polyaniline/Graphene Nanocomposite in Different Electrolytes. *J. Alloys Compd.* **2015**, *653*, 486–497. <https://doi.org/10.1016/j.jallcom.2015.08.158>.
 40. Malassis, L.; Dreyfus, R.; Murphy, R. J.; Hough, L. A.; Donnio, B.; Murray, C. B. One-Step Green Synthesis of Gold and Silver Nanoparticles with Ascorbic Acid and Their Versatile Surface Post-Functionalization. *RSC Adv.* **2016**, *6* (39), 33092–33100. <https://doi.org/10.1039/c6ra00194g>.
 41. Oliveira, M. M.; Zarbin, A. J. G. Carbon Nanotubes Decorated with Both Gold Nanoparticles and Polythiophene. *J. Phys. Chem. C* **2008**, *112* (48), 18783–18786. <https://doi.org/10.1021/jp8052482>.
 42. Lee, C. J.; Karim, M. R.; Lee, M. S. Synthesis and Characterization of Silver/Thiophene Nanocomposites by UV-Irradiation Method. *Mater. Lett.* **2007**, *61* (13), 2675–2678. <https://doi.org/10.1016/j.matlet.2006.10.021>.
 43. Kuila, B. K.; Park, K.; Dai, L. Soluble P3HT-Grafted Carbon Nanotubes: Synthesis and Photovoltaic Application. *Macromolecules* **2010**, *43* (16), 6699–6705. <https://doi.org/10.1021/ma100917p>.
 44. Tamboli, M. S.; Kulkarni, M. V.; Patil, R. H.; Gade, W. N.; Navale, S. C.; Kale, B. B. Nanowires of Silver-Polyaniline Nanocomposite Synthesized via in Situ Polymerization and Its Novel Functionality as an Antibacterial Agent. *Colloids Surfaces B Biointerfaces* **2012**, *92*, 35–41. <https://doi.org/10.1016/j.colsurfb.2011.11.006>.
 45. Zhan, Y.; Ren, Y.; Wan, X.; Zhang, J.; Zhang, S. Dielectric Thermally Conductive and Stable Poly(Arylene Ether Nitrile) Composites Filled with Silver Nanoparticles Decorated Hexagonal Boron Nitride. *Ceram. Int.* **2018**, *44* (2), 2021–2029. <https://doi.org/10.1016/j.ceramint.2017.10.147.46>.
 46. M.T. Ramesan, V. Santhi, In situ synthesis, characterization, conductivity studies of polypyrrole/silver doped zinc oxide nanocomposites and their application for ammonia gas sensing, *J. Mater. Sci. Mater. Electron.* *28* (2017) 18804–18814. doi:10.1007/s10854-017-7830-5.
 47. M.T. Ramesan, V. Santhi, In situ synthesis, characterization, conductivity studies of polypyrrole/silver doped zinc oxide nanocomposites and their application for ammonia gas sensing, *J. Mater. Sci. Mater. Electron.* *28* (2017) 18804–18814. doi:10.1007/s10854-017-7830-5.
 48. El Badawy AM, Luxton TP, Silva RG, Scheckel KG, Suidan MT, Tolaymat TM. Impact of environmental conditions (pH, ionic strength, and electrolyte type) on the surface charge and aggregation of silver nanoparticles suspensions. *Environ Sci Technol.* *2010*;44(4):1260–6.
 49. Hedberg, J.; Skoglund, S.; Karlsson, M. E.; Wold, S.; Odnevall Wallinder, I.; Hedberg, Y. Sequential Studies of Silver Released from Silver Nanoparticles in Aqueous Media

Preparation of Silver Nanoparticles Entangled Ternary Nanocomposites

- Simulating Sweat, Laundry Detergent Solutions and Surface Water. *Environ. Sci. Technol.* **2014**, *48* (13), 7314–7322. <https://doi.org/10.1021/es500234y>.
50. No Title. <https://doi.org/10.1021/es9035557.49>. M. Feng, R. Sun, H. Zhan, Y. Chen, Decoration of carbon nanotubes with CdS nanoparticles by polythiophene interlinking for optical limiting enhancement, *Carbon* **N. Y.** *48* (2010) 1177–1185. doi:10.1016/j.carbon.2009.11.041.
51. I.Ebrahimi, M.P. Gashti, Polypyrrole-MWCNT-Ag composites for electromagnetic shielding: Comparison between chemical deposition and UV-reduction approaches, *J. Phys. Chem. Solids.* **118** (2018) 80–87. doi:10.1016/j.jpcs.2018.03.008.
52. Inagaki, C. S.; Oliveira, M. M.; Bergamini, M. F.; Marcolino-Junior, L. H.; Zarbin, A. J. G. Facile Synthesis and Dopamine Sensing Application of Three Component Nanocomposite Thin Films Based on Polythiophene, Gold Nanoparticles and Carbon Nanotubes. *J. Electroanal. Chem.* **2019**, *840*, 208–217. <https://doi.org/10.1016/j.jelechem.2019.03.066>.
53. Wan, J.; Si, Y.; Li, C.; Zhang, K. Bisphenol a Electrochemical Sensor Based on Multi-Walled Carbon Nanotubes/Polythiophene/Pt Nanocomposites Modified Electrode. *Anal. Methods* **2016**, *8* (16), 3333–3338. <https://doi.org/10.1039/c6ay00850j>.
54. Ebrahimi, I.; Gashti, M. P. Polypyrrole-MWCNT-Ag Composites for Electromagnetic Shielding: Comparison between Chemical Deposition and UV-Reduction Approaches. *J. Phys. Chem. Solids* **2018**, *118*, 80–87. <https://doi.org/10.1016/j.jpcs.2018.03.008>.

Chapter 5

Active Solvent Hydrogen Enhanced Catalytic Reduction of p-Nitrophenol using Binary and Ternary Silver Nanocomposites and its Antibacterial Action

5.1. Introduction

Heterogeneous catalysis has tremendous applications in many organic transformations, as seen in many industrial and academic research.¹⁻⁷ Heterogeneous transition metal nanocatalysts have attracted significant attention because of their mild reaction conditions, recyclability, enhanced catalytic performance, and simple separation strategies.⁸⁻²¹ Among different transition metal nanocatalysts, silver nanoparticles, in particular, possess special features such as easiness of synthesis, good catalytic activity, remarkable electrical and optical properties, less toxicity and cost effectiveness.²²⁻²⁴ Silver nanoparticles could function as stable nanocatalysts for desired applications via stabilizing them with capping molecules, surfactants, and polymer matrices.^{22,25,26} Heterogeneous catalysts have good prospects in recovery and reusability than homogeneous catalysts. However, the former inherently exhibits poor solubility/dispersibility.^{27, 28} Bare colloidal nanoparticles have an aggregation effect with time which reduces catalytic activity with storage.^{8,9} Besides that, colloidal nanoparticles require a tedious process to purify from the mother liquid. In contrast, heterogeneous catalysts can be purified by simple washing and filtration. Moreover, the irreversible nature of homogeneous silver colloidal systems restricts them to single catalytic use. Therefore, facile, green, and cost-effective metal nanoparticle-supported heterogeneous nanocomposites with good dispersibility in water or other solvents deserve immense attention in recent times. Lee and co-workers studied silver

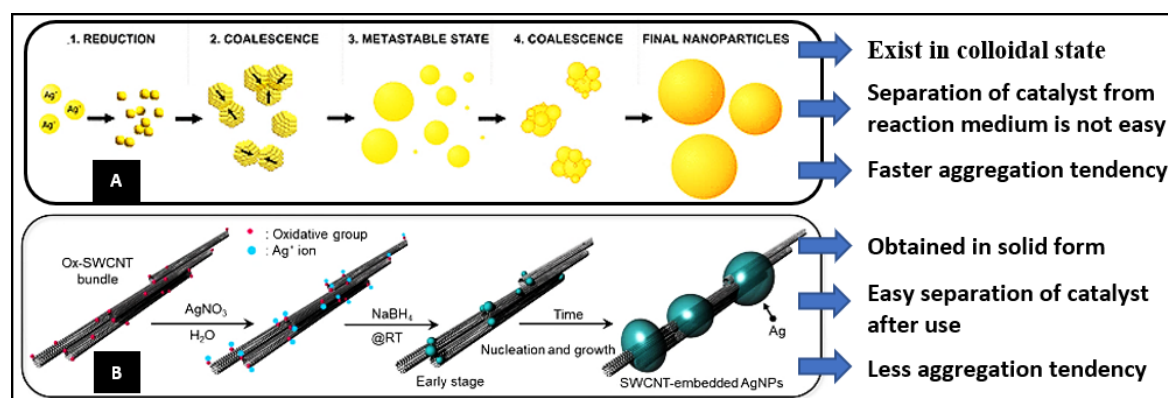


Figure 5.1. Illustration of formation of colloidal silver nanoparticles without having host material (A) and formation of CNT-hosted silver nanoparticles (B) (Adapted from Lee et al. 2021).

nanoparticles embedded in single-walled carbon nanotube nanocomposites for wearable electronics and sensor applications in which carbon nanotubes function as hosts for silver nanoparticles against agglomeration (see **Figure 5.1**).²⁹ Polymer/carbon nanomaterial

hosted metal nanocatalysts have been recognized as green catalysts because of the energy benefits in catalytic use and catalytic recyclability without significant loss of nanoparticles.³⁰ The polyelectrolyte-carbon nanotube host system nanocomposites could provide good dispersibility, charged cationic or anionic side chains, and mechanical stability.³⁰ Conducting polymers were recently used for the preparation of conducting polymer-multiwalled carbon nanotube nanocomposites by in situ polymerization. Conducting polythiophene-MWCNT nanocomposites have high electrical conductivity, good optical properties, biocompatibility, environmental/thermal stability, and better host interactions with metal nanoparticles.³¹ The stability of metal nanoparticles against oxidation, agglomeration and leaching from the supporting framework remained as the critical issues to be addressed for the performance of heterogeneous polymer/carbon nanomaterial supported metal nanocatalysts.²⁸⁻³⁵

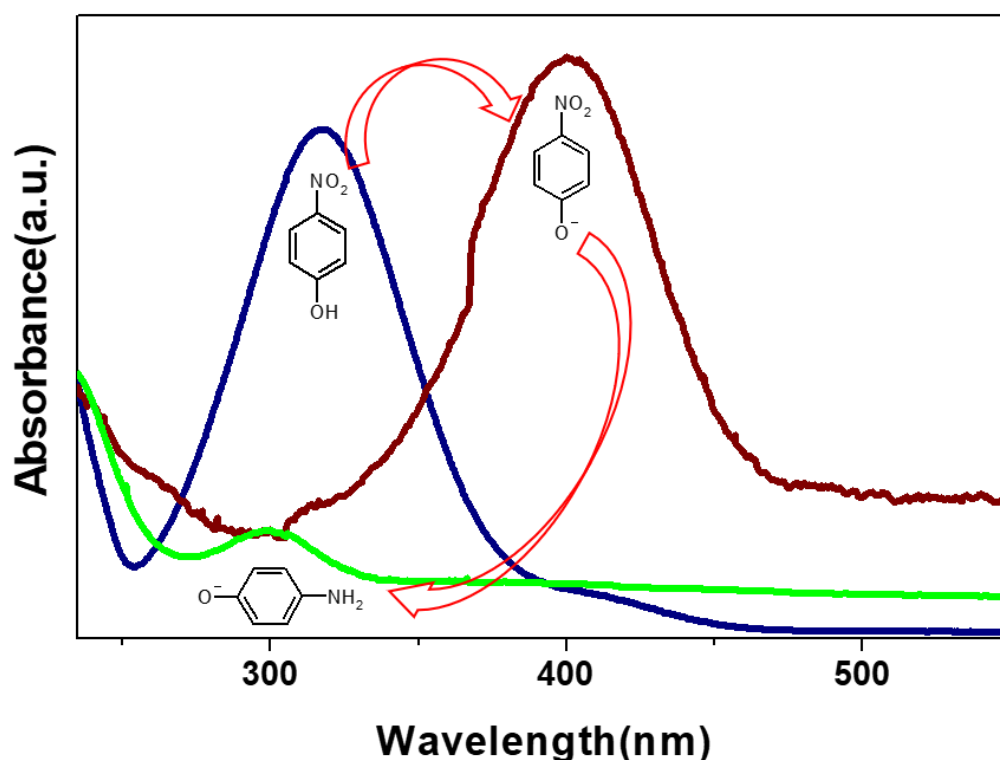


Figure 5.2. UV-Vis spectra of *p*-nitrophenol, *p*-nitrophenolate ion and reduced product *p*-amino phenolate ion by adding a reducing agent and a suitable catalyst.

Catalytic reduction of *p*-nitrophenol using sodium borohydride as a hydride source in the presence of different nanocatalysts is considered as a typical model reaction due to mild reaction conditions, moderate reaction kinetics, and simple experimental setup.³⁶⁻³⁸ The changes that occurred in UV-vis spectra in different stages during the catalytic

reduction of *p*-nitrophenol is shown in **Figure 5.2**. The high reaction rate was not achieved until we used an excessive sodium borohydride to exhibit pseudo-first-order and more than the minimum quantity as a catalyst. Therefore, catalytic reduction of *p*-nitrophenol requires some reaction conditions improvements to obtain enhanced catalytic conversion with minimum reagents and catalyst (see **Figure 5.3**). Acceleration of the reaction kinetics with some metal salts or other reagents has been conducted previously in the literature.³⁹⁻⁴² The mechanism of the catalytic reduction of *p*-nitrophenol for substantiating the source of hydrogens remains ambiguous.^{39,43-47} Recently, Zhao et al. investigated the catalytic reduction of *p*-nitrophenol with sodium borohydride using a deuterium isotope experiment. Their work substantiated the requirement of polar protic solvents, and it acts as the source of hydrogen rather than a hydride reducer.⁴³ Fountoulaki et al. studied kinetic isotope effects on catalytic reduction of *p*-nitrophenol using NaBH₄ and NaBD₄, which has given evidence for B-H bond cleavage at rate-determining step and in-situ formation of Au-H.⁴⁴ More validating evidence is required to understand the role of water and other protic solvents for the hydrogenation of *p*-nitrophenol.

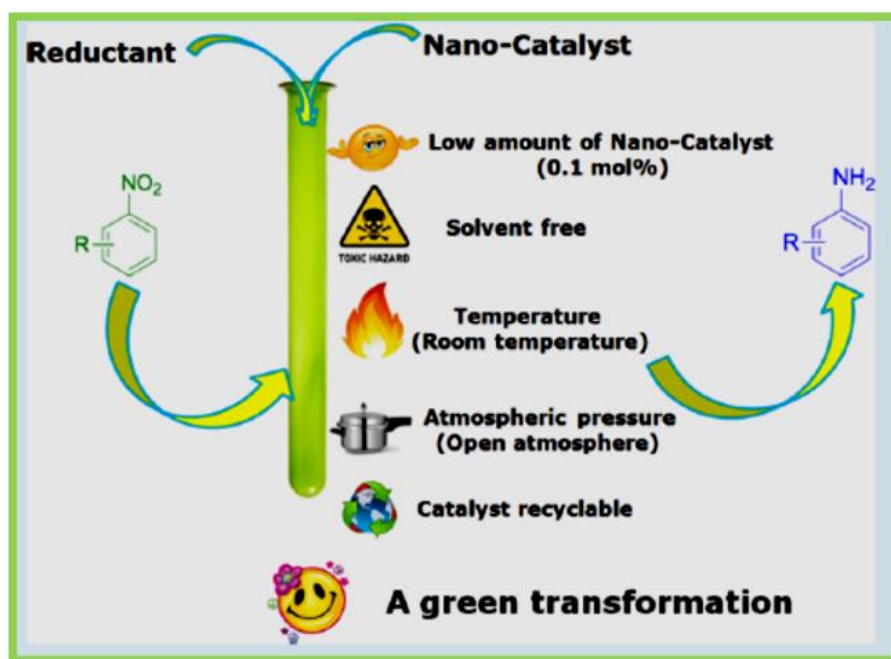


Figure 5.3. Accounting the benefits of nanocatalysts in model nitrophenol reduction reaction (adapted from Bhairi et al. 2018)

The present chapter focuses on the reduction reaction of *p*-nitrophenol to *p*-aminophenol in the presence of ternary (TNC) and binary nanocatalysts (BNC); both

Chapter 5

contain silver nanoparticles embedded on different hosts, polythiophene-functionalized multiwalled carbon nanotubes nanocomposite, and functionalized multiwalled carbon nanotubes, respectively. The kinetics of binary silver nanocatalyst ($k = 0.0364 \text{ s}^{-1}$) were two to three times faster than ternary nanocatalyst ($k = 0.0134 \text{ s}^{-1}$). The optimum nanocatalyst concentration for reducing p-nitrophenol at concentration $1 \times 10^{-4} \text{ M}$ was determined to be 0.06 mg/mL . We have carried out the reaction kinetics of nitrophenol in polar protic and aprotic solvents miscible with water. The glycerol-water mixture (5%-30%) acts as energizing solvent for nitrophenol reduction with NaBH_4 . By employing a green solvent combination of 10% glycerol, the catalytic activity factor enhanced to $936.50 \text{ s}^{-1}\text{g}^{-1}$ (3 times higher activity than in water as solvent); therefore, we could reduce catalyst concentration and sodium borohydride concentration approximately to one-sixth. A plausible mechanism demonstrated for the nitrophenol reduction using sodium borohydride and active hydrogens in the solvent. Ternary silver nanocatalyst has shown better dispersion than binary nanocatalyst, which lead us to study the antimicrobial properties. The ternary nanocomposites with a lower atomic percentage of silver nanoparticles was attached to the less cytotoxic polythiophene layer act as an efficient antibacterial agent against *Escherichia coli* bacteria.⁴⁸⁻⁵⁰ In summary, binary silver nanocatalyst (BNC) functioned as an efficient catalyst for reducing p-nitrophenol, whereas ternary nanocatalyst (TNC) acts as excellent antibacterial material against *Escherichia coli* bacteria in solution.⁵¹⁻⁵⁶

5.2. Experimental

5.2.1. Materials and reagents: Sodium borohydride was purchased from Sigma Aldrich. Para-nitrophenol was purchased from LOBA chemicals. Para-aminophenol was purchased from NICE chemicals. Acetone, glycerol (anhydrous), ethylene glycol, and 1,4-dioxane were purchased from Merck chemicals, India. Deionized water was used as a solvent in catalysis and for nutrient broth preparation (a mixture of peptone, NaCl , and yeast extract from NICE chemicals and beef extract from Merck chemicals, India).

5.2.2. Measurements and Instruments: UV-vis absorption spectra of the samples were recorded by Shimadzu UV-VIS spectrophotometer, UV 1800 series in the range 250-500 nm with deionized water. The powder wide-angle X-ray diffraction of the samples was measured using PANALYTICAL, Aeris research X-ray diffractometer with 2θ values ranging from 10 to 80° . Field emission scanning electron microscopy (FE-SEM) and EDX

element mapping images were recorded using ZEISS SIGMA™. XPS analysis was conducted using PHI 5000 Versa Probe II, ULVAC-PHI Inc, USA X-ray photoelectron spectrometer. Optical densities of *E. coli* inoculated samples were recorded in an antibacterial assay using AU2701 UV-VIS double beam spectrophotometer, systronics.

5.2.3. Reaction kinetics using different nanocatalyst concentrations: Different concentrations of ternary silver nanocatalysts (TNCs) were prepared by dispersing 0.5 mg, 1.0 mg, 1.5 mg and 2.5 mg of TNCs in p-nitrophenol solution (25 mL, 1.0×10^{-4} M) via sonication to obtain 0.02 mg/mL, 0.04 mg/mL, 0.06 mg/mL and 0.10 mg/mL respectively. The respective concentrations abbreviated as TNC-0.02, TNC-0.04, TNC-0.06, and TNC-0.10, where the figures show the concentrations in mg/mL. Similarly, binary nanocatalysts (BNCs) designated as BNC-0.02, BNC-0.04, BNC-0.06, and BNC-0.10 for same concentrations.

A typical procedure is showed below to determine the reaction kinetics using nanocatalyst concentration TNC-0.06. Ternary nanocatalyst TNC (1.5 mg) was dispersed in p-nitrophenol (25 mL, 1.0×10^{-4} M) by sonication for 15 min. Freshly prepared NaBH₄ solution (2 mL, 1.0×10^{-1} M) was added to 2 mL of a sonicated mixture of p-nitrophenol and TNC (0.06 mg/mL) taken in a vial, after that shaken for 10 s. We have mixed p-nitrophenol-nanocatalyst reaction mixture and sodium borohydride solution in equal volume for all catalytical studies, therefore the final concentrations of p-nitrophenol, sodium borohydride, and nanocatalyst reduced to half (**Table 5.1**). UV-vis absorption spectra were recorded automatically in regular intervals of time by the preset program. UV-vis absorption spectra of p-nitrophenol reduction using different nanocatalyst concentrations TNC-0.02, BNC-0.02, TNC-0.04, BNC-0.04, BNC-0.06, TNC-0.10, and BNC-0.10 were recorded using the same reaction conditions. The rate constants were calculated from the linear fit plots of UV-vis absorbance of the final mixture.

5.2.4. Recycling studies using nanocatalysts: TNC (7 mg) was dispersed in p-nitrophenol solution (5 mL, 2.33×10^{-3} M) by sonication for 15 min. Freshly prepared NaBH₄ solution (5 mL, 2.33 M) was added to the above mixture. The reaction mixture was shaken well for one minute, then kept undisturbed for 10 min, and centrifuged. After centrifugation for three min, filtrate decanted, and then UV-vis absorption spectra were recorded. The residue (nanocatalyst) was washed with deionized water, and catalytical activities continued for four more consecutive cycles using the same method. A similar

procedure was repeated using BNC nanocatalyst (7 mg) instead of TNC for six catalytic cycles.

5.2.5. Recycling effects of nanocatalysts on morphology and composition: The nanocatalyst TNC (25 mg) was dispersed in p-nitrophenol solution (25 mL, 1.66×10^{-3} M) by sonication for 15 min. Freshly prepared NaBH_4 solution (25 mL, 1.66 M) was added and shaken well for one minute to the above mixture. It was kept undisturbed for 10 min to complete the reaction and then filtered. The nanocatalyst residue obtained was again dispersed in p-nitrophenol solution (25 mL, 1.66×10^{-3} M) and repeated the process up to the 9th cycle in the same manner. After the third, sixth, and ninth catalytic cycles, a portion (one-third of the initial amount of catalyst) of the residue was separated and centrifuged to recover the catalyst. The residue was washed with water and acetone, then dried in a vacuum oven at 60°C for 1 hour. The morphology and composition of nanocatalysts recorded using powder X-ray diffraction, X-ray photoelectron spectroscopy, and scanning electron microscopy. The same procedure was repeated using BNC nanocatalyst to find any difference in morphology and composition.

5.2.6. TNC catalyzed reduction in different volume percentages of glycerol-water mixtures: TNC (1.5 mg) was dispersed in p-nitrophenol solution (25 mL, 1.0×10^{-4} M) by sonication for 15 min. NaBH_4 solution (5 mL) prepared in different volume percentages of the glycerol-water mixture was added to the P-NP-TNC mixture (5 mL) taken in different vials. The final percentage volumes of glycerol in water were 5% v/v, 10% v/v, 20% v/v, 30% v/v, 40% v/v and 50% v/v. The time for reaction completion was obtained from the change in colour of the reaction mixture from greenish-yellow to colourless. The same procedure was repeated for BNC catalyzed reduction of p-nitrophenol in different volume percentages of solvent mixtures. The other solvent mixtures such as ethylene glycol in water, ethanol in water, and 1, 4-dioxane in water were similarly used as solvent media for catalytic reduction of P-NP using nanocatalysts.

5.2.7. Calibration curve of 4-aminophenolate to find the relative yield of product: Different concentrations of p-aminophenol (5×10^{-4} M, 1×10^{-4} M, 5×10^{-5} M, 1×10^{-5} M, 5×10^{-6} M, 1×10^{-6} M, 5×10^{-7} M, 1×10^{-7} M) were taken in 10 mL deionized water. Freshly prepared NaBH_4 solution (10 mL, 1×10^{-1} M) is added to each concentration of p-aminophenol. UV-vis spectra of all above concentrations were recorded to get a calibration

curve and it can be used to quantify the concentration of p-aminophenol formed in unknown samples.

5.2.8. Large scale reduction of p-nitrophenol: Binary nanocatalyst BNC (1.8 mg) was dispersed in 10 mL p-nitrophenol solution (0.15 g, 0.108 M, 15 g/L) and sonicated for 15 min. To this NaBH₄ solution (10 mL, 2.695 M, P-NP: NaBH₄ molar ratio is 1:25) freshly prepared in 10% glycerol-water mixture was added and magnetically stirred for one hour. The completion of the reaction was observed from the colour change of greenish yellow colour of p-nitrophenol to the colourless p-aminophenolate product in one hour. Completion of the reaction was also monitored by recording UV-vis spectra of colourless p-aminophenolate product formed after one hour.

5.2.9. Antibacterial study using ternary nanocatalyst TNC: The nutrient broth was prepared by dissolving NaCl (0.5 %), peptone (0.5 %), beef extract (0.3 %) and yeast extract (0.3 %) in double-distilled water. The pH was adjusted to 7.4 and sterilized by autoclaving at 15 lbs pressure (121°C) for 15 min. The stock solution of dispersed TNC (200 µg/mL) was prepared in 50 mL nutrient broth by sonication for 30 min. Different concentrations of TNC nanocatalyst such as 1×10^{-1} µg/mL, 5×10^{-1} µg/mL, 1 µg/mL, 5 µg/mL, 10 µg/mL, 20 µg/mL, 30 µg/mL, 40 µg/mL, 80 µg/mL, 120 µg/mL, 160 µg/mL were prepared by adding 5 µL, 25 µL, 50 µL, 250 µL, 500 µL, 1000 µL, 1500 µL, 2000 µL, 4000 µL, 6000 µL and 8000 µL of stock solution (200 µg/mL) to nutrient broth to obtain 10 mL of total volume. The stock solution also took for antibacterial activity.

Samples containing broth mixtures were sonicated for 10 min. All tubes were inoculated with 50 µL of actively growing *E. coli* culture and incubated overnight in a thermal shaker at 37 °C. After incubation, microbial growth in each tube was studied using a UV-vis double beam spectrophotometer by measuring optical density at 660 nm. Positive and negative controls were used to validate the results.

The same experiment was repeated using lactose broth instead of nutrient broth. The preparation of lactose broth is as follows: lactose (0.5 %), peptone (0.5 %) and beef extract (0.3 %) were dissolved in 1 L of double distilled water. The pH was adjusted to 6.9 and sterilized by autoclaving at 15 lbs pressure (121 °C) for 15 min.

5.3. Results and Discussion

5.3.1. Comparison of TNC and BNC nanocatalysts

Silver nanoparticles embedded ternary nanocatalyst (TNC) and binary nanocatalyst (BNC) were obtained by reducing silver nitrate solution using ascorbic acid as a reducing agent. Polythiophene-functionalized MWCNT nanocomposites and functionalized multiwalled carbon nanotubes were used as host materials for silver nanoparticles in TNC and BNC. Functionalization of multiwalled carbon nanotube was achieved by refluxing MWCNT (0.40 g) with nitric acid (5 M, 50 mL) at 100°C. Functionalization of multiwalled carbon nanotubes reduces the aggregation tendency of MWCNT in nanocomposites and significantly improves processability. Polythiophene-functionalized multiwalled carbon nanotube (PTCNT-COOH) binary nanocomposites were used to prepare ternary silver nanocatalyst (TNC) which contains conducting polythiophene layer. The forces of attraction between functionalized multiwalled carbon nanotube and polythiophene were predominantly non-covalent attractive forces such as π -interaction, hydrogen bonding and van der Waals forces. Silver nanoparticles were directly attached to the functionalized multiwalled carbon nanotubes (MWCNT-COOH) in binary silver nanocatalysts (BNC). The preparation, properties, and characterization of PTCNT-COOH 300 Ag (TNC) and MWCNT-COOH Ag (BNC) have been discussed in chapter 4.⁵⁷

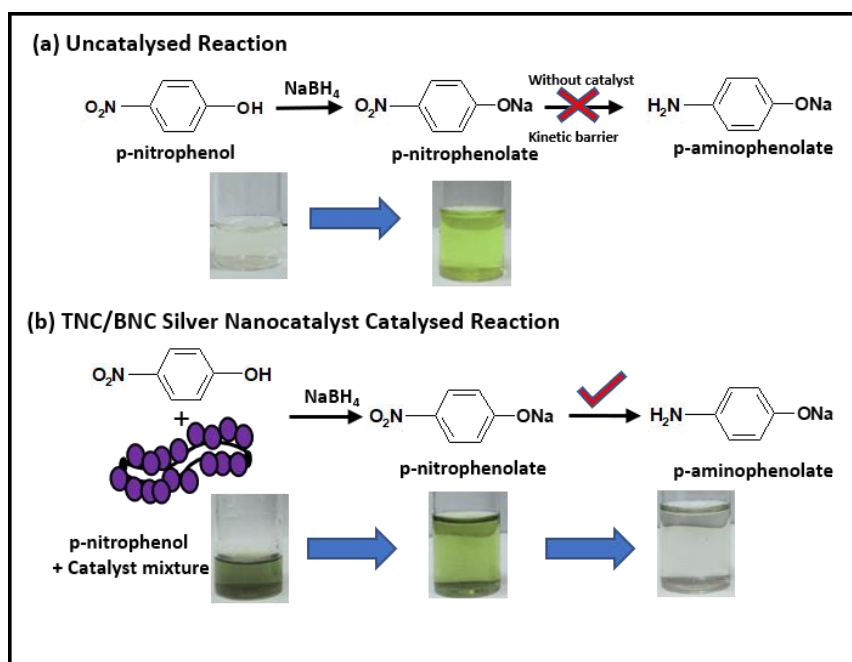


Figure 5.4. Schematic representation of (a) reactions of p-nitrophenol with NaBH₄ and (b) silver nanocatalysts (BNC/TNC) catalyzed reaction of p-nitrophenol using NaBH₄.

Table 5.1. Name of nanocatalyst, initial concentrations of P-NP, NaBH₄, nanocatalyst, final concentrations of P-NP, NaBH₄, nanocatalysts, solvents, rate constant (k), and the activity factor.

Sl. No.	Catalyst ^a	Initial concentrations of reaction mixtures			Final concentration of reaction mixture			Solvent	k ^b (s ⁻¹)	Acti vity fact or ^c (s ⁻¹ g ⁻¹)
		P-NP in 2 mL (mM)	NaBH ₄ in 2 mL (M)	TNC/ BNC (mg/m L)	P-NP in 4 mL (mM)	NaBH ₄ in 4 mL (M)	BNC/ TNC (mg/ mL)			
1	TNC-0.02	0.01	0.10	0.02	0.005	0.05	0.01	water	1.40x10 ⁻³	35.00
2	TNC-0.03	0.01	0.10	0.03	0.005	0.05	0.015	10% glycerol + water	-	-
3	TNC-0.04	0.01	0.10	0.04	0.005	0.05	0.02	water	4.90x10 ⁻³	61.25
4	TNC-0.06	0.01	0.10	0.06	0.005	0.05	0.03	water	1.34x10 ⁻³	113.34
5	TNC-0.10	0.01	0.10	0.10	0.005	0.05	0.05	water	3.99x10 ⁻²	199.50
6	BNC-0.01	0.01	0.10	0.01	0.005	0.05	0.005	10% glycerol +water	1.87x10 ⁻²	936.50
7	BNC-0.02	0.01	0.10	0.02	0.005	0.05	0.01	water	1.10x10 ⁻³	27.50
8	BNC-0.03	0.01	0.10	0.03	0.005	0.05	0.015	10% glycerol+ water	-	-
9	BNC-0.04	0.01	0.10	0.04	0.005	0.05	0.02	water	1.59x10 ⁻²	198.75
10	BNC-0.06	0.01	0.10	0.06	0.005	0.05	0.03	water	3.64x10 ⁻²	303.34
11	BNC-0.10	0.01	0.10	0.10	0.005	0.05	0.05	water	5.40x10 ⁻²	270.00

^a Ternary nanocatalyst (TNC) or binary nanocatalyst (BNC) taken in different concentrations. ^b The rate constant obtained from the time dependent UV-vis studies. ^c The ratio rate constant divided by the weight of the catalyst used.

Heterogeneous ternary and binary nanocatalysts were utilized to convert p-nitrophenol to p-aminophenol in an aqueous medium. Due to the kinetic energy barrier, the reduction of nitrophenols to aminophenols did not proceed without a catalyst. Therefore, adding sodium borohydride to p-nitrophenol produces a greenish-yellow solution of p-nitrophenolate ion (see Figure 5.4.).⁵⁸ On the other hand, in the presence of ternary or binary nanocatalysts, colourless p-aminophenolate ions were formed from the greenish-yellow coloured p-nitrophenolate ion. The sonication process helps to adsorb the p-nitrophenol to the active sites of nanocatalysts.⁵⁹

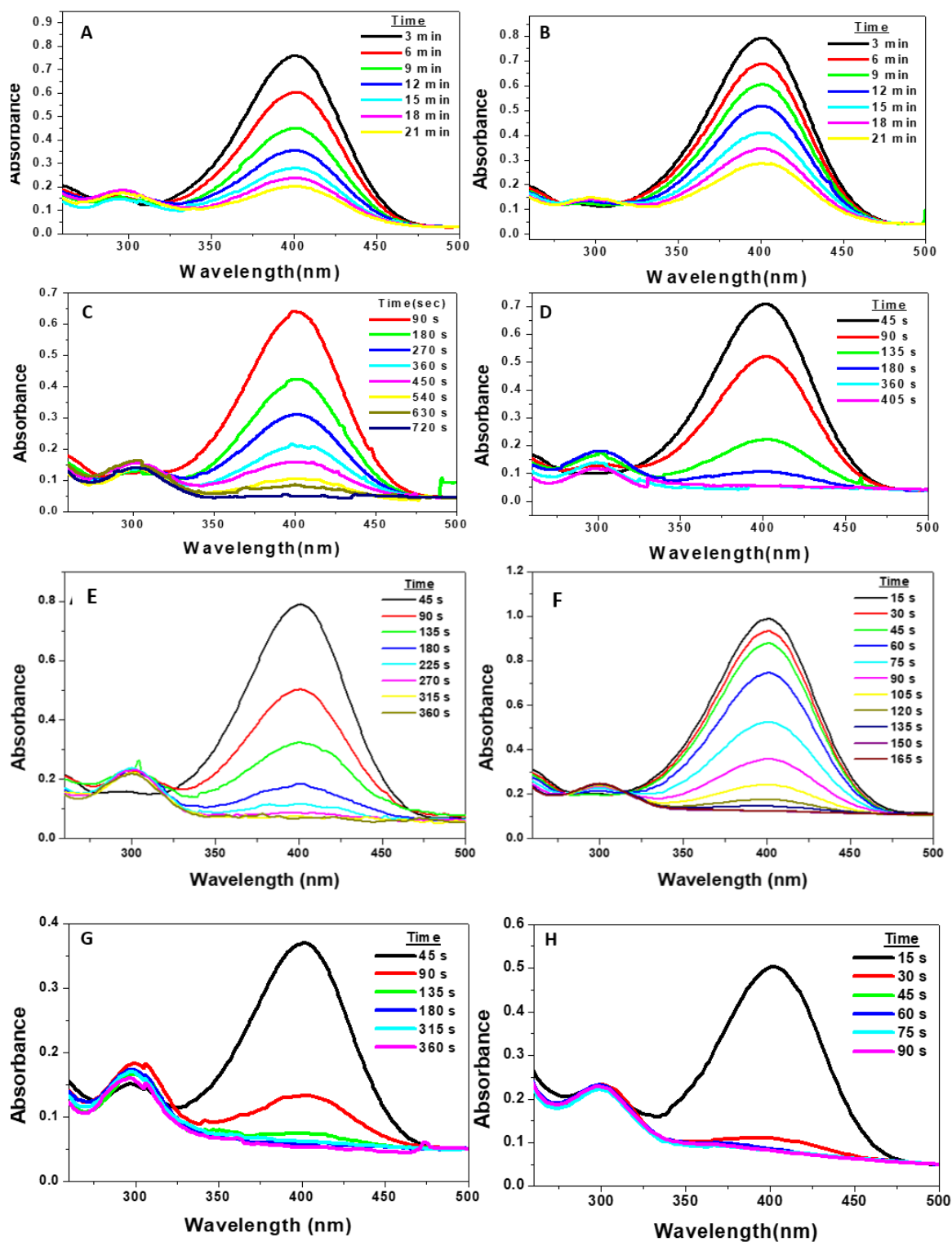


Figure 5.5. UV-vis absorption spectra for reduction of *p*-nitrophenol using catalyst TNC-0.02 (A), BNC-0.02 (B), TNC-0.04 (C), BNC-0.04 (D) TNC-0.06 (E), BNC-0.06 (F), TNC-0.10 (G) and BNC-0.10 (H) in consecutive time intervals.

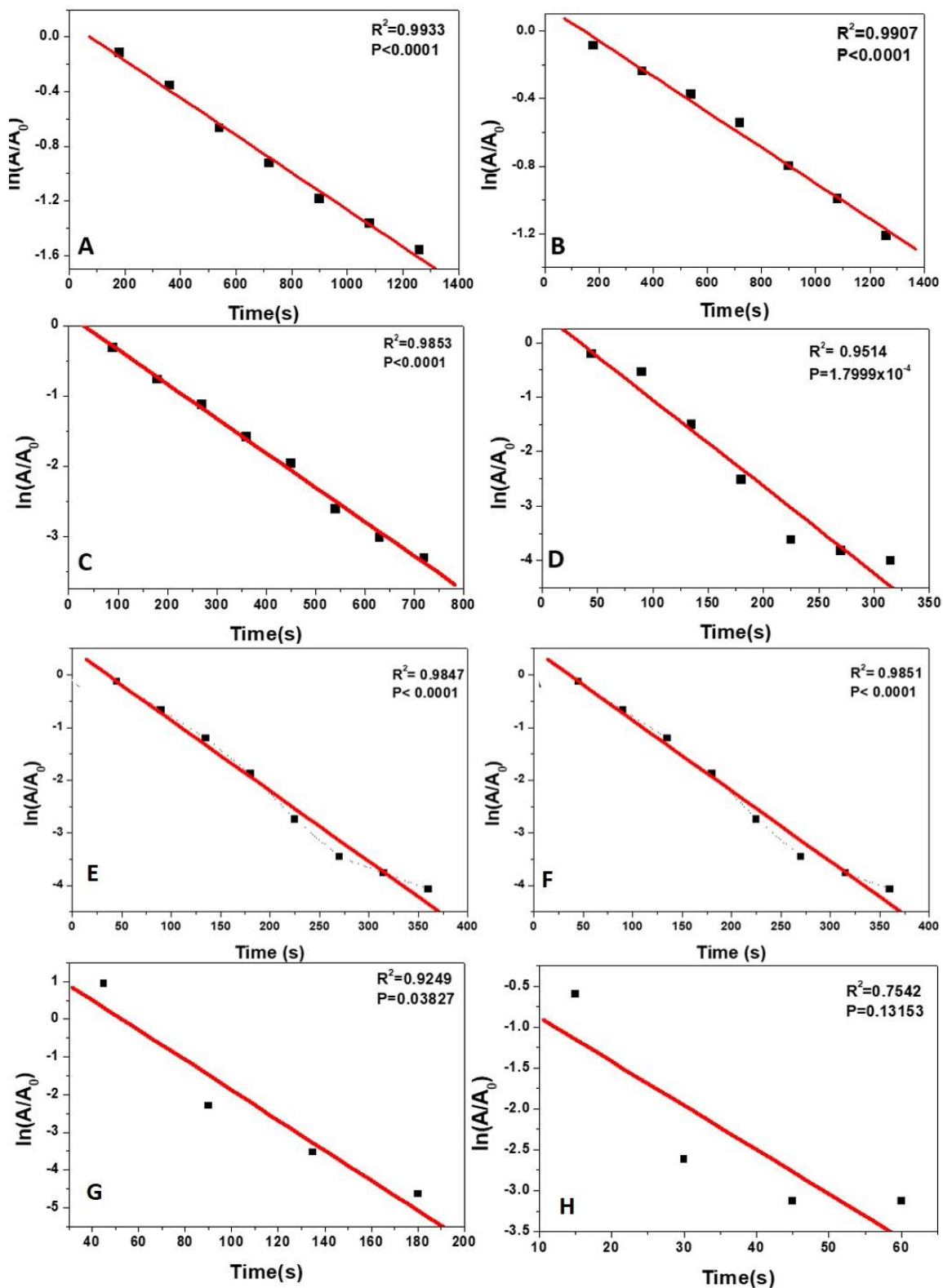


Figure 5.6. Linear relationship plot of $\ln(A/A_0)$ against time for *p*-nitrophenol reduction using TNC-0.02 (A), BNC-0.02 (B), TNC-0.04 (C), BNC-0.04 (D) TNC-0.06 (E), BNC-0.06 (F), TNC-0.10 (G) and BNC-0.10 (H)

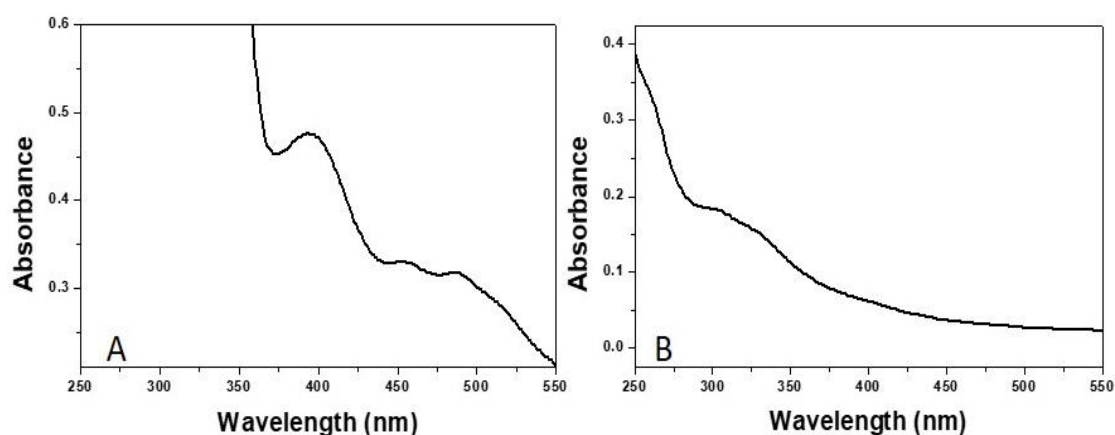


Figure 5.7. UV-vis absorption spectra of silver nano colloids after one day of synthesis(A) and silver nano colloids after 7 days of synthesis(B).

The catalytic conversion of p-nitrophenol to p-aminophenol was monitored by UV-vis absorbance spectroscopy by noting the decrease in p-nitrophenolate ion peak at 400 nm in successive time intervals after the start of the reaction. Silver nanocatalysts were named TNC-0.02, BNC-0.02, TNC-0.04, BNC-0.04, TNC-0.06, BNC-0.06, TNC-0.10, and BNC-0.10, in which digits represent the concentration of ternary or binary nanocatalysts in mg/mL initially taken in aqueous P-NP solution for catalytic studies (see **Table 5.1.**). The p-nitrophenolate ion peak at 400 nm was produced immediately by adding sodium borohydride solution. As time progresses, the p-nitrophenolate ion peak intensity decreases with a concomitant increase of the new peak at 298 nm, corresponding to the p-aminophenolate ion (see **Figure 5.2.**).⁵⁸ The complete suppression of the peak at 400 nm indicated the reaction completion. Time-dependent UV-vis absorption spectra of nanocatalyst concentration TNC-0.02, BNC-0.02, TNC-0.04, BNC-0.04, TNC-0.06, BNC-0.06, TNC-0.10, and BNC-0.10 were recorded (see **Figure 5.5.**). The rate constants for this catalytically driven reaction were obtained by plotting $\ln(A/A_0)$ against time (see **Figure 5.6.**). The reaction follows pseudo-first-order kinetics; therefore, the rate constant can be obtained from the line's slope from linear regression fit.^{60,61} The resultant rate constants were 0.0014 s^{-1} , 0.0011 s^{-1} , 0.0049 s^{-1} , 0.0159 s^{-1} , 0.0134 s^{-1} , 0.0364 s^{-1} , 0.0399 s^{-1} and 0.0540 s^{-1} respectively for the catalytic concentrations TNC-0.02, BNC-0.02, TNC-0.04, BNC-0.04, TNC-0.06, BNC-0.06, TNC-0.10 and BNC-0.10. Activity factor (the ratio of rate constant to the weight of catalyst used) were also calculated as $35.00\text{ s}^{-1}\text{ g}^{-1}$, $27.50\text{ s}^{-1}\text{ g}^{-1}$, $61.25\text{ s}^{-1}\text{ g}^{-1}$, $198.75\text{ s}^{-1}\text{ g}^{-1}$, $113.34\text{ s}^{-1}\text{ g}^{-1}$, $303.34\text{ s}^{-1}\text{ g}^{-1}$, $199.50\text{ s}^{-1}\text{ g}^{-1}$ and $270.00\text{ s}^{-1}\text{ g}^{-1}$.

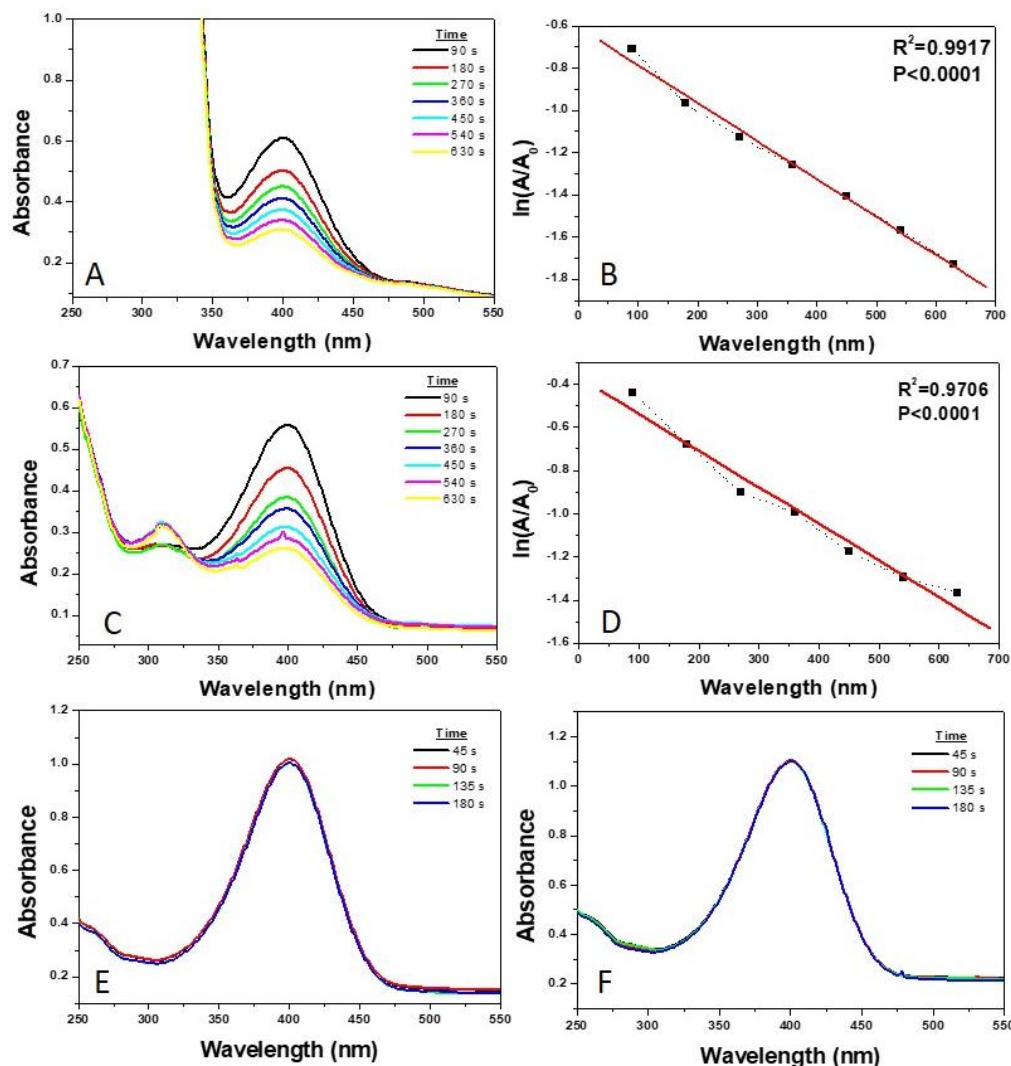


Figure 5.8. UV-vis absorption spectra of reduction of *p*-nitrophenol using NaBH_4 using homogeneous colloidal silver nanoparticles as catalyst (A) and its linear relationship plot of $\ln(A/A_0)$ against time on first day after the synthesis of silver nano colloid (B). UV-vis absorption spectra of reduction of *p*-nitrophenol using NaBH_4 using homogeneous colloidal silver nanoparticles catalyst (C) and its linear relationship plot of $\ln(A/A_0)$ (D) against time on seventh day after the synthesis of silver nanocolloid. UV-vis absorption spectra of reduction of *p*-nitrophenol using NaBH_4 using PTCNT-COOH 300 as catalyst (E) and reduction of *p*-nitrophenol using NaBH_4 using MWCNT-COOH as catalyst (F).

g^{-1} for TNC-0.02, BNC-0.02, TNC-0.04, BNC-0.04, TNC-0.06, BNC-0.06, TNC-0.10 and BNC-0.10 respectively (see **Table 5.1.**). Rate constants of TNC-0.02 and BNC-0.02 are almost equal, but as nanocatalysts' concentration increases, approximately 2 to 3 times greater catalytic activity was obtained for BNC rather than TNC. Silver nanoparticles

decorated TNC, and BNC nanocatalysts rely on electrons flow from NaBH_4 to *p*-nitrophenol (P-NP) through silver nanoparticles for catalytic reduction. The slow kinetics of TNC compared with BNC could be attributed to the electrical movement of electrons into conducting polythiophene layer.^{57,62} Control experiments conducted using silver nanoparticles (Ag NPs) have shown characteristic surface plasmon resonance peaks at 400 nm in freshly prepared conditions (see **Figure 5.7. A**). The rate constant for *p*-nitrophenol reduction using Ag NPs (~ 0.03 mg/mL final concentration) was found ($k = 1.82 \times 10^{-3} \text{ s}^{-1}$) to be approximately in the same range that obtained for TNC-0.02 and BNC-0.02 (see **Figure 5.8. A and B**). In colloidal silver nanoparticles, the surface plasmon resonance peak was overlapped with the nitrophenolate ion peak, making it difficult to note the reaction completion (see **Figure 5.8. A**). The reduction reaction carried out after the ageing of Ag NPs solution for seven days has shown a slight decrease in the rate constant and settling of nano colloidal silver nanoparticles (see **Figure 5.8. C**). Besides, the UV-vis absorption spectra of colloidal silver nanoparticles taken after seven days do not possess surface plasmon resonance peaks (see **Figure 5.7. B**). Although colloidal silver nanoparticles in freshly prepared conditions act as good catalysts, their aggregation tendency, stability, and recyclability were major issues. Control experiments conducted using MWCNT-COOH and PTCNT-COOH 300 without silver nanoparticles have not shown catalytic activity (see **Figure 5.8 E and F**). Functionalized multiwalled carbon nanotubes/polymer play a vital role as a heterogeneous framework to accommodate silver nanoparticles to prevent agglomeration, rapid oxidation, and leaching.

5.3.2. Optimization of nanocatalyst amount.

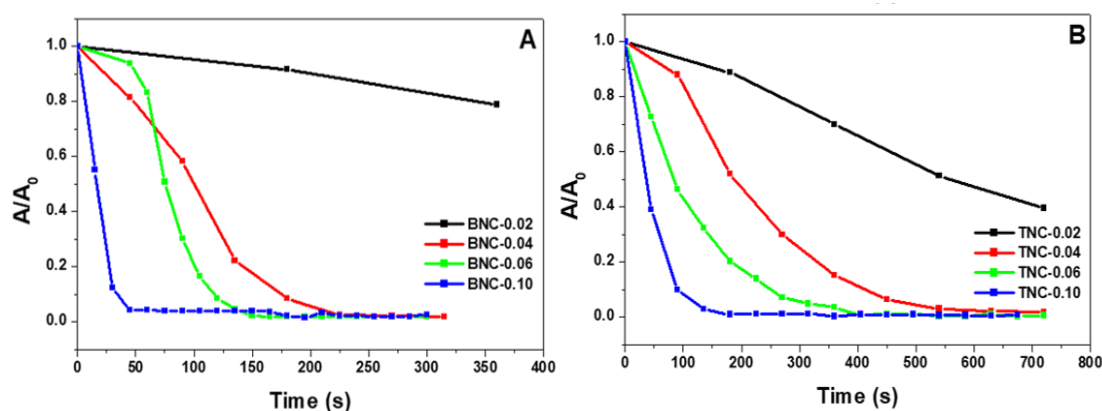


Figure 5.9. Plot of (A/A_0) against time for TNC catalysed reactions (A) and BNC catalysed reactions (B) for different concentrations of catalyst 0.02 mg/mL, 0.04 mg/mL, 0.06 mg/mL, and 0.10 mg/mL taken in *p*-nitrophenol solution.

Table 5.2. Comparing catalysts, concentrations of reagents, rate constants, and activity factors obtained in the present study with recent other literature reports.

Sl. No.	Catalyst	Catalyst Amount	p-aminophenol		NaBH ₄		Rate constant (k)		Activity factor		Ref.
			Conc.	Vol. (mL)	Conc.	Vol. (mL)	s ⁻¹	min ⁻¹	s ⁻¹ g ⁻¹	min ⁻¹ g ⁻¹	
1	Ag NPs-PANI/MWCNT	1.00 mg	0.10 mM	0.2 mL	0.1 M	2 mL	0.0054	-	5.40	-	(1)
2	Ag@MW CNTs-polymer	10 mg	0.10 mM	15 mL	5 mM	15 mL	0.0079	-	11.64	-	(2)
3	NiS-NiCo ₂ O ₄ @C	0.017 mg/mL	0.1 mM	3 mL	0.08 M	-	-	1.78	-	-	(3)
4	Ag CD-MA@Fe MNps (AgNC)	5 mg	0.12 mM	1.5 mL	12 mM	1.5 mL	-	0.674	-	-	(4)
5	Pd@PUN	30 mg	0.10 mM	20 mL	40 mM	10 mL	-	4.96	-	-	(5)
6	Ag@PD A@poly(M-POSS)	0.005 mg/mL	20 mM	50 μL	0.2 M	20 mL	-	0.837	-	1.67 × 10 ⁵	(6)
7	PSMAA/Ag	2 mg	0.1 mM	2 mL	60 mM	0.5 mL	0.0082	-	-	-	(7)
8	Fe ₃ O ₄ -CS-Ag NPs	2 mg/mL	0.125 mM	2 mL	0.5 M	0.1 mL	-	0.56	-	-	(8)
9	TNC-0.06	0.06 mg/mL	0.01 mM	2 mL	0.1 M	2 mL	0.0134	0.804	113.34	6.8 × 10 ³	Present work
10	BNC-0.06	0.06 mg/mL	0.01 mM	2 mL	0.1 M	2 mL	0.0364	2.184	303.34	1.8 × 10 ⁴	

The optimum nanocatalyst concentrations of TNC and BNC for reducing *p*-nitrophenol (1.0×10^{-4} M) were selected by plotting A/A_0 against time for different catalyst concentrations (see **Figure 5.9**). The optimum nanocatalyst concentration has been selected based on the minimum quantity of a nanocatalyst needed to catalyze reaction at a measurable speed. In general, for all catalyst concentrations, as the time increases, the A/A_0 value decreases and reaches a steady minimum in the curve, corresponding to the completion of the reaction. The time required to reach a steady minimum for TNC-0.04, TNC-0.06, and TNC-0.10 were 550 s, 315 s, and 150 s, and that for BNC-0.04, BNC-0.06 and BNC-0.10 were 225 s, 150 s, and 50 s respectively. Therefore, even though TNC-0.10 and BNC-0.10 have given faster reaction kinetics than TNC-0.06 and BNC-0.06, the latter was selected as optimum catalyst concentration due to lower catalyst concentration and

measurable speed. By considering other literature works reported recently on p-nitrophenol reduction using different metal incorporated nanocomposites, one of the leading catalytic activities observed in both BNC and TNC catalyzed reduction (see **Table 5.2.** for comparison with other reports).

5.3.3. Recycling studies.

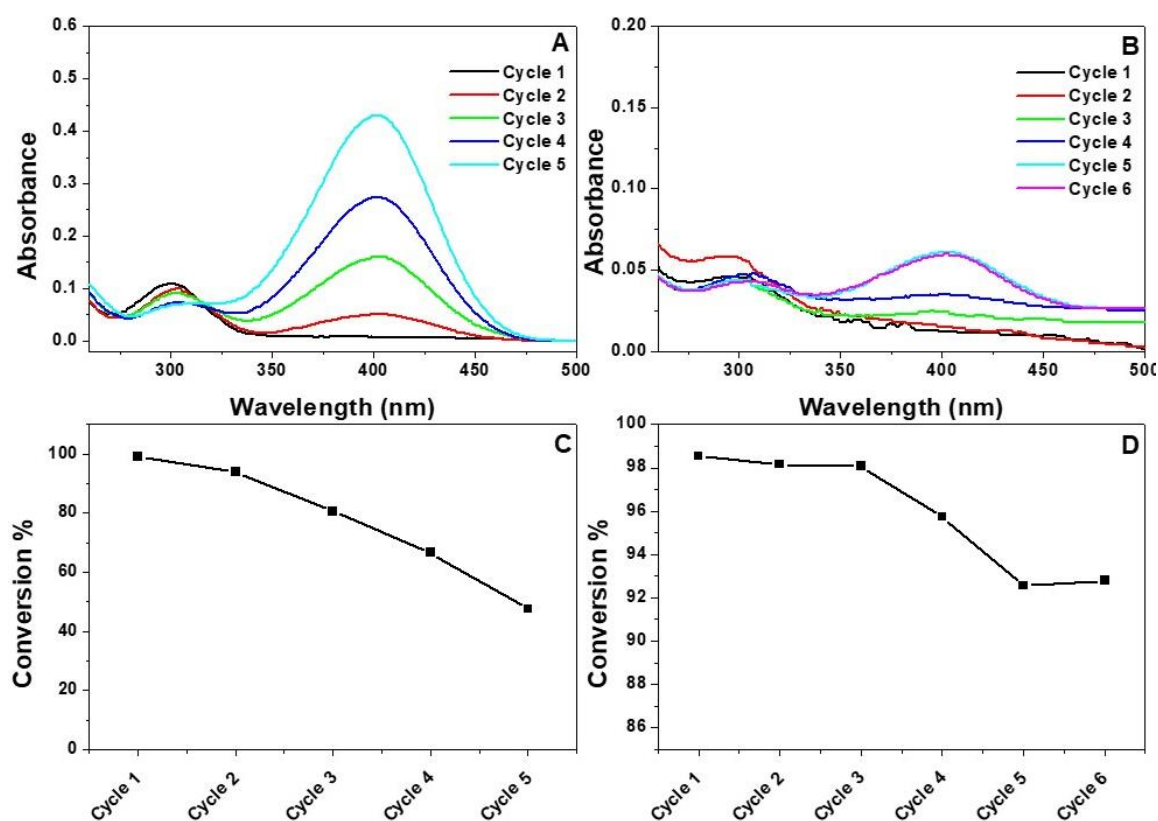


Figure 5.10. UV-vis absorption spectra of TNC 0.06 catalyzed (A) and BNC-0.06 catalyzed reaction (B) for successive catalytic cycles. Catalytic conversion percentage of TNC-0.06 (C) and BNC-0.06 (D) in successive catalytic cycles.

The recycling studies of the nanocatalysts TNC and BNC were carried out, and catalytic efficiency in the recycling process was recorded via UV-vis absorption spectra (see **Figure 5.10.**). TNC was recycled and analyzed for five consecutive cycles and BNC for six consecutive cycles by fixing the reaction time as 10 min for each cycle. Here catalyst was recovered by centrifugation and reused for the next catalytic cycle after washing with water. The catalytic conversion (%) of p-nitrophenol to p-aminophenol has been determined using the equation,

$$\text{Conversion (\%)} = \left(1 - \frac{A}{A_0}\right) \times 100$$

Where A_0 and A are the absorption maxima of the *p*-nitrophenolate ion at the initial time (t_0) and monitoring time (t), respectively. Catalytic conversion (%) for successive cycles indicated better BNC efficiency than TNC for six catalytic cycles (see **Figure 5.10. C** and **D**). TNC has shown catalytic conversion of 47.56 % in the 5th catalytic cycle, whereas BNC has shown 92.80 % conversion in the 6th cycle in identical conditions. The conversion (%) obtained from the UV-vis absorbance spectroscopy have revealed that nanocatalyst BNC activates the reaction more than TNC in multiple cycles. Nanocatalysts recovered from the reaction mixture via centrifugation and washing before subsequent uses. TNC being better dispersive than BNC via sonication, have more leaching effect of silver than the latter case.

5.3.4. Elemental composition and morphology of recycled nanocatalysts.

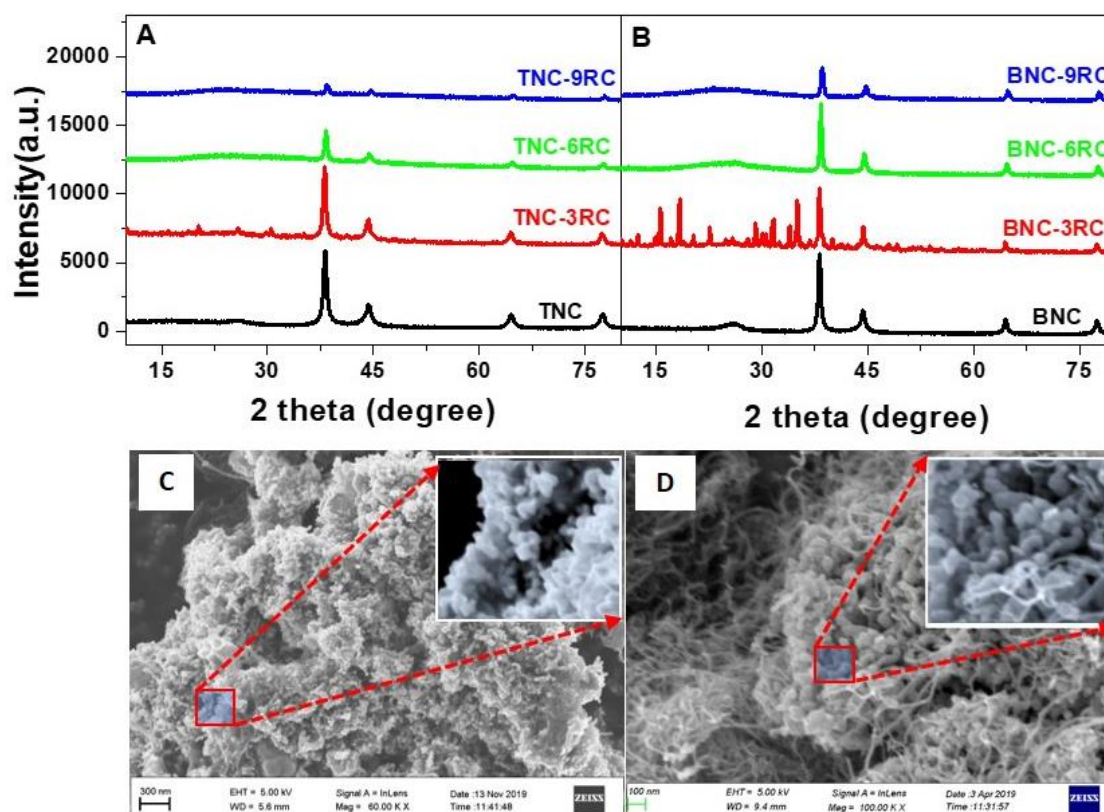


Figure 5.11. X-ray diffraction patterns of TNC and recycled TNCs (A), BNC and recycled BNCs (B) after 3rd, 6th and 9th catalytic cycles. FE-SEM images of TNC (C) and BNC (D) as pristine nanocatalyst (enlarged portion is shown in inset).

We have subjected the recycled catalysts to powder X-ray diffraction studies to trace changes during the recycling (see **Figure 5.11. A** and **5.11. B**). TNC and BNC obtained after the third, sixth, and ninth cycles were named TNC-3RC, TNC-6RC, TNC-

9RC, BNC-3RC, BNC-6RC, BNC-9RC; the figure represents the recycle number. Comparison of powder X-ray diffraction patterns of pristine catalysts with recycled catalysts revealed that intensity of crystalline diffraction peaks corresponding to silver nanoparticles at 2θ values 38.15° , 44.33° , 64.52° and 77.46° were decreased considerably after the 6th catalytic cycle (see **Figure 5.11. A** and **5.11. B**).⁴⁵ A substantial decrease in intensity of diffraction peaks of silver nanoparticles was noticeable on the 9th catalytic cycle of TNC than BNC. The more decrease in TNC nanocatalyst intensity than the BNC nanocatalyst in higher catalytic cycles was due to the loss of a higher amount of silver nanoparticles during separation, washing, and sonication. The diffraction pattern of BNC-3RC has given crystalline peaks other than silver nanoparticles matching with the crystalline form of sodium metaborate formed as a by-product from sodium borohydride (see **Figure 5.12**).^{24,63-65} The inner core structure of the recycled nanocatalysts TNC-3RC and BNC-3RC were determined using X-ray photoelectron spectroscopy (see **Table 5.12**). Functionalized multiwalled carbon nanotubes contain 94.42 atomic percent of C 1s and 5.58 atomic percent of O 2s.⁵⁷ Recycled binary nanocatalyst BNC-3RC have shown characteristic peaks of C 1s (284.77 eV), O 1s (532.47 eV), Na 1s (1072.27 eV), Ag 3d (374.44 eV) and B 1s (192.77 eV) with atomic percentage of 91.0%, 6.6 %, 1.3 %, 0.8 % and 0.2% respectively. On the other hand, TNC-3RC have shown characteristic peaks of C

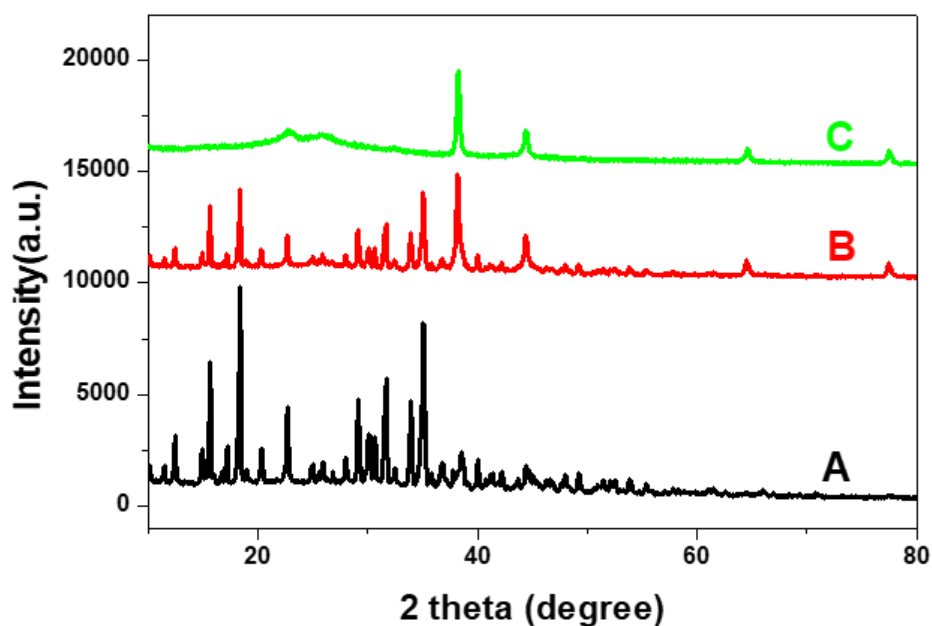


Figure 5.12. WXR D patterns of (A) byproduct separated from the reaction residue, (B) BNC-3RC and (C) BNC-3RC after repeated centrifugation and washing.

1s (284.78 eV), O 1s (532.18 eV), Na 1s (1074.08 eV), Ag 4s (102.11 eV), B 1s (192.77 eV) and S 2p (166.47 eV) with atomic percentage 76.9 %, 21.9 %, 0.3 %, 0.5 %, 0.2 % and 0.1 % respectively. The higher atomic percentage of C1s in BNC-3RC (91.0 %) than TNC-3RC (76.9 %) was mainly due to the binary components, which consists of functionalized multiwalled carbon nanotubes and silver nanoparticles only. The presence of sodium metaborate hydrates as a by-product, intermediate layer of conducting polythiophene, and dopants influence the total atomic percent of TNC (see **Figure 5.13.**). The atomic composition of silver atoms of BNC-3RC was higher than TNC-3RC, which matches with powder x-ray diffraction data. The decrease in the atomic percentage of silver could be due to the separation of silver nanoparticles in the recycling process.

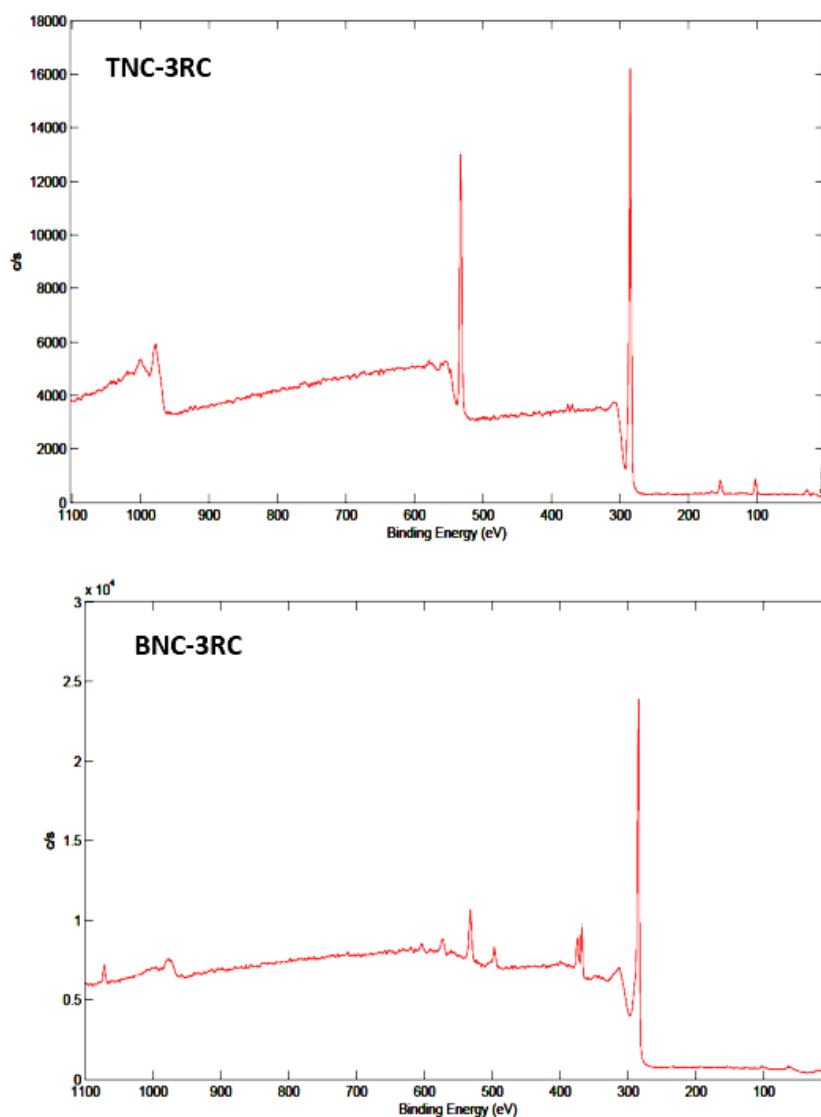


Figure 5.13. XPS spectra of TNC-3RC and BNC-3RC.

Chapter 5

Silver nanoparticles embedded pristine TNC and BNC nanocatalysts were subjected to field emission scanning electron microscopy. TNC contains silver nanoparticles with an average size of 25 ± 5 nm, which exists in a tangled manner on the PTCNT-COOH 300 framework, whereas BNC contains nanoparticles with an average size of 45 ± 5 nm supported on MWCNT-COOH (see **Figure 5.11. C** and **D** for FESEM images of TNC and BNC before catalytic use). The surface morphology and elemental distribution of the recycled catalyst surface have been traced by scanning electron microscopy and energy dispersive X-ray (EDX) analysis (see **Figure 5.14. C, D, E** and **F**). FE-SEM images of recycled nanocatalysts TNC-3RC and BNC-3RC have shown hexagonal crystalline faces over the nanocatalysts (**Figure 5.14. A** and **5.14. B**). The EDX elemental dot mapping showed a sodium atom percentage of 11.84 % on the TNC surface and 14.18 % on the BNC surface. The presence of sodium atoms and higher oxygen mass percentage from dot mapping images indicated the formation of sodium metaborate hydrates deposited in the hexagonal phase over the nanocatalyst surface. The recycled nanocatalyst TNC-3RC and BNC-3RC contain 1.61 and 1.00 atomic percent of silver atoms within the EDX analysis limitations (see **Table 5.3**). A mechanistic view of recycled nanocatalyst (TNC or BNC) represented after catalytic hydrogenation of p-nitrophenol using sodium borohydride (shown in **Figure 5.14. G**). TNC and BNC could be reused for many cycles; however, the metaborates trapped in nanocatalysts could mask the catalytic activity.

Table 5.3. The atomic percentage of C, O, Na, B, Ag, and S in TNC-3RC and BNC-3RC.

Element	From XPS analysis ^a	
	TNC-3RC (atom %)	BNC-3RC (atom %)
C	76.9	91.0
O	21.9	6.6
Na	0.3	1.3
B	0.2	0.2
Ag	0.5	0.8
S	0.1	-

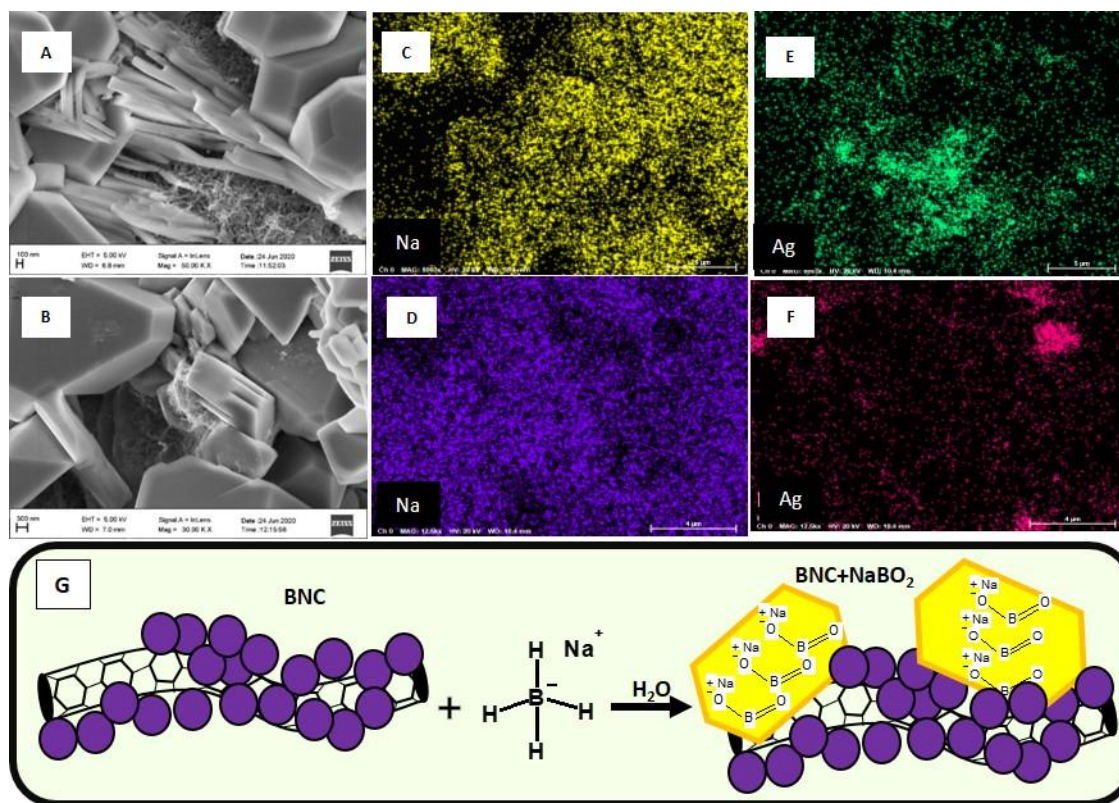


Figure 5.14. FE-SEM images of TNC-3RC (A) and BNC-3RC (B), EDX colour mapping of sodium in TNC-3RC (C), sodium in BNC-3RC (D), silver in TNC-3RC (E) and silver in BNC-3RC (F). Schematic representation of the existence of metaborate by-product over a recycled catalyst (G).

5.3.5. Optimization of solvent-water mixture for reduction.

The kinetic and mechanistic aspects of BNC and TNC catalyzed *p*-nitrophenol reduction were systematically studied using different solvent-water mixtures like glycerol-water, ethylene glycol-water, ethanol-water, and 1,4-dioxane-water. The different catalyst concentrations like TNC-0.03, BNC-0.03, TNC-0.06, and BNC-0.06 were used to reduce *p*-nitrophenol (1.0×10^{-4} M, 5 mL) by the addition of NaBH₄ (1.0×10^{-1} M, 5 mL) in the presence of different volume % of solvent-water mixtures. The time of decolourization was noted as the time to complete the reaction. The reaction completion time versus different volume percentages of solvent-water mixtures (5 % v/v, 10 % v/v, 20 % v/v, 30 % v/v, 40 % v/v and 50 % v/v) were plotted (see **Figure 5.15.**). The reduction reaction has shown a faster reaction in glycerol-water, and ethylene glycol-water mixture, especially in the 5% - 30% percent volume, and after that, the reaction slows down as the medium's viscosity increases. In the ethanol-water mixture, the reaction rate was slower than in the above two mixtures and decolourization time increased as the volume percentage of ethanol increased.

The least reactivity was observed in 1,4-dioxane-water mixture, which could be easily understood from the non-availability of the active hydrogen in it. Therefore, the order of catalytic reactivity obtained in different solvent-water mixtures was glycerol-water > ethylene glycol-water > ethanol-water > 1,4-dioxane-water.

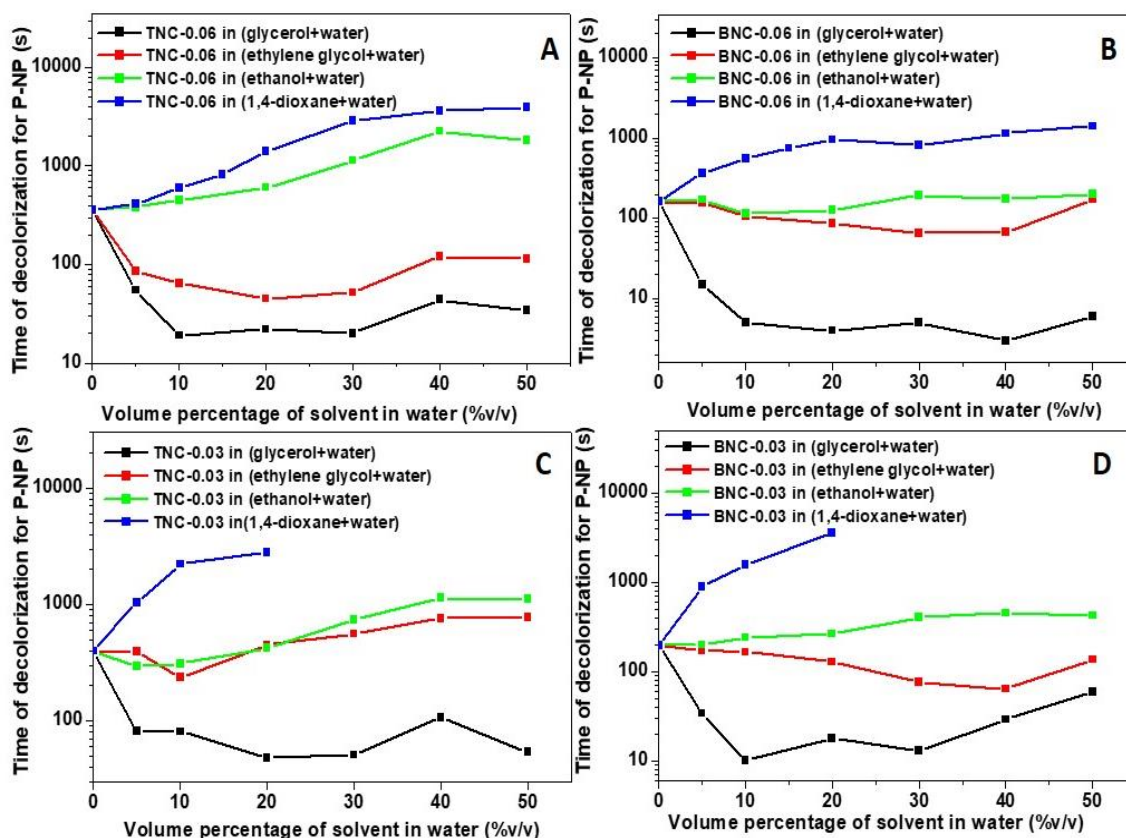


Figure 5.15. Time of decolourization plotted against different volume percentage of solvent-water mixture using P-NP: NaBH_4 molar ratio 1:1000 with TNC-0.06, BNC-0.06, TNC-0.03 and BNC-0.03 catalysts.

5.3.6. Optimization of [P-NP]: $[\text{NaBH}_4]$ molar ratio.

Catalytic hydrogenation of p-nitrophenol was conducted by varying the molar ratio of [P-NP]: $[\text{NaBH}_4]$ using TNC-0.06 and BNC-0.06 in a 10% v/v glycerol-water mixture. The [P-NP] to $[\text{NaBH}_4]$ molar ratio has varied from 1:50, 1:100, 1:150, 1:250, 1:500 to 1:1000 in water and 10% glycerol-water mixture by fixing the concentration of P-NP solution as 1×10^{-4} M. The decolorization time in catalytic reduction versus NaBH_4 to P-NP molar ratio was plotted (see **Figure 5.16. A**). The decolorization studies have revealed that reaction follows pseudo-first-order kinetics approximately at a mole ratio 500 in water, which was reduced to 250 in the glycerol-water mixture.⁶¹ A major disadvantage of

reducing

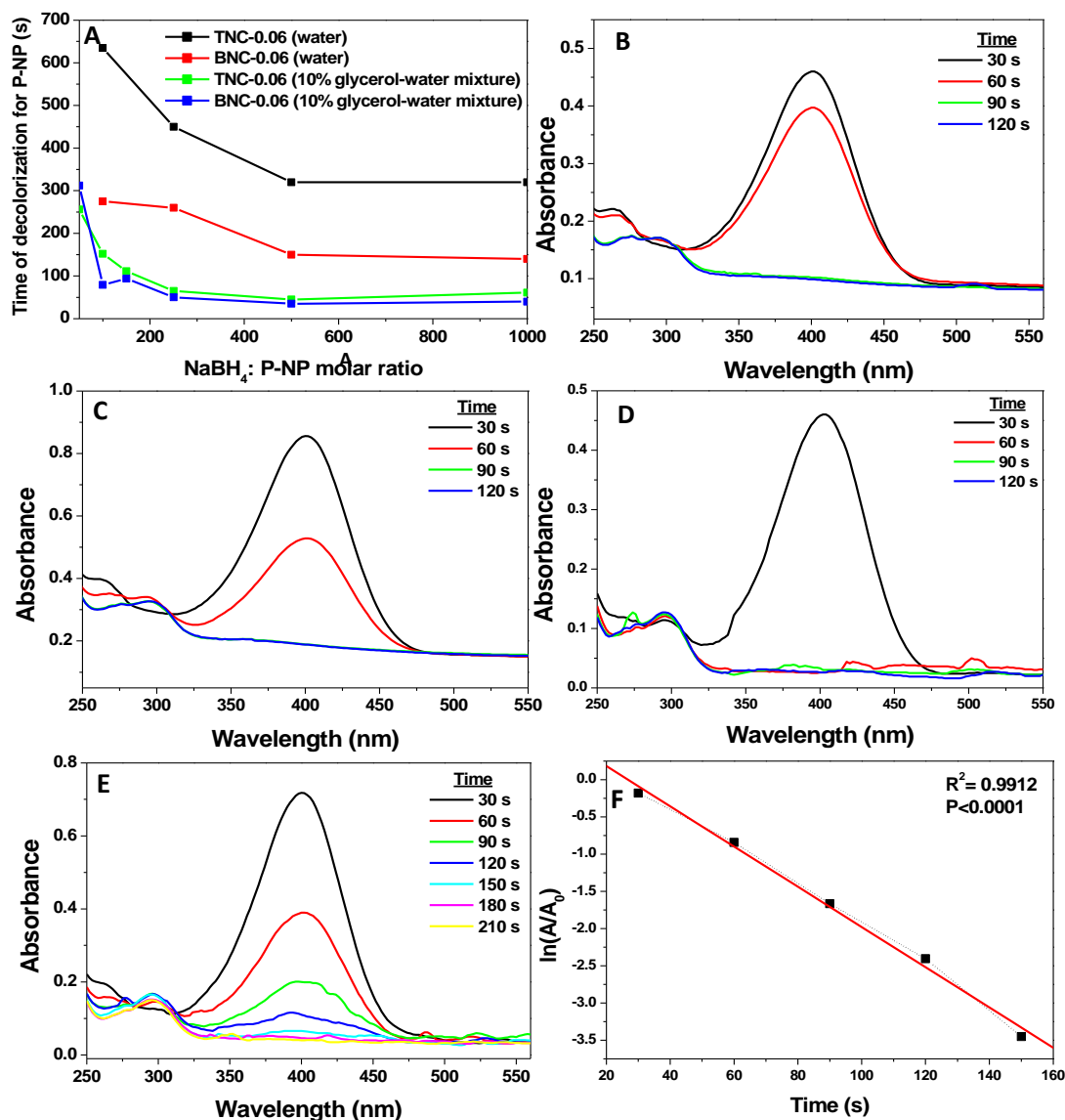


Figure 5.16. Time of decolourization plotted against different NaBH_4 concentrations in water and 10% glycerol-water mixture using TNC-0.06 and BNC-0.06 catalysts (A). UV-vis absorption spectra of reduction of *p*-nitrophenol using catalyst TNC-0.06 [PNP: NaBH_4 molar ratio 1:100](B) using BNC-0.06 [PNP: NaBH_4 molar ratio 1:100] (C) and BNC-0.03 [PNP: NaBH_4 molar ratio 1:200] [D] in 10% glycerol-water solvent mixture. UV-vis absorption spectra of reduction of *p*-nitrophenol using catalyst BNC-0.01 [PNP: NaBH_4 molar ratio 1:200 (E) and linear relationship plot of $\ln(A/A_0)$ against time for BNC-0.01 for PNP: NaBH_4 molar ratio 1:200 (F) in 10% glycerol-water solvent mixture.

nitrophenols with sodium borohydride in water was the excess utilization of NaBH_4 to obtain a reasonable reaction rate. Therefore, minimizing the NaBH_4 for *p*-nitrophenol

reduction can ensure more economic gain to the synthetic strategy and reduced toxicity effects. The UV-vis absorption spectra were recorded to show the minimum utilization of catalyst with P-NP to NaBH_4 molar ratio 1:100 in 10% glycerol- water mixture TNC-0.06, BNC-0.06, BNC-0.03 catalyst concentrations were shown in Figure 5.16. B, C and D. In the presence of a 10% glycerol-water mixture, BNC-0.03 exhibited the same kinetics as BNC-0.06 in water with P-NP to NaBH_4 molar ratio 1:1000. More interestingly, the catalytic reduction of p-nitrophenol executed with a minimal concentration of BNC-0.01 catalyst and P-NP to NaBH_4 molar ratio of 1: 200, excellent activity factor of $936.5 \text{ s}^{-1}\text{g}^{-1}$ was obtained in a 10% glycerol-water solvent mixture (see **Figure 5.16. E and F**).

5.3.7. The proposed mechanism for catalytic reduction.

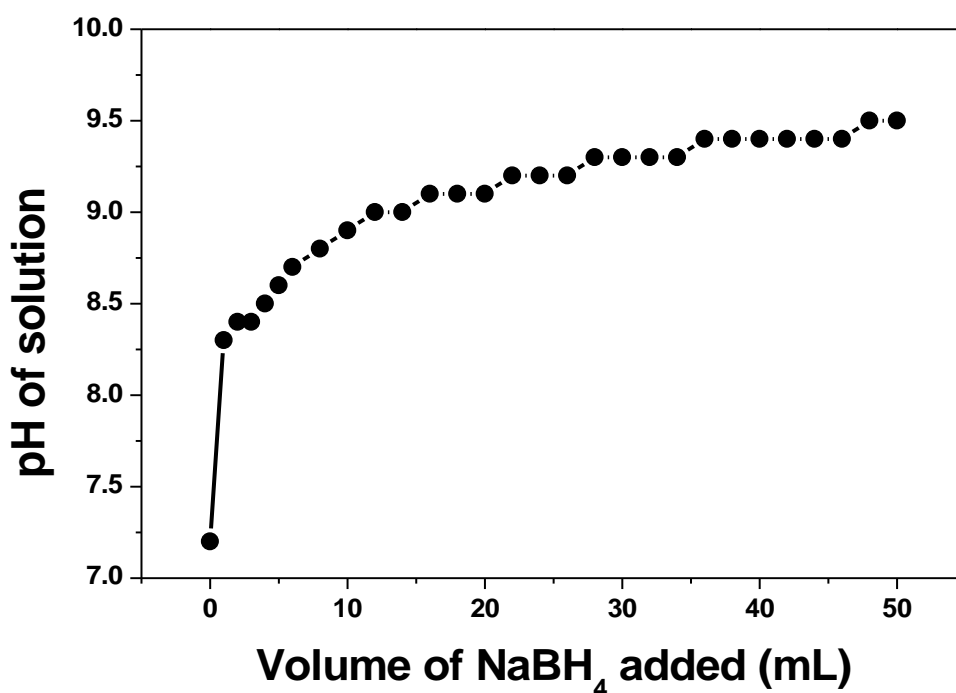


Figure 5.17. Change in pH of glycerol-water mixture (20%) by the addition of NaBH_4 .

The catalytic reduction of p-nitrophenol using NaBH_4 as the reductant remains controversial. TNC and BNC catalytic performance in different solvent mixtures led us to gain some mechanistic evidence about the hydrogen source used to reduce p-nitrophenol. Many possible ways of reduction mechanisms were discussed in the literature.^{39,43-48} It was already reported in the literature that the reduction of p-nitrophenol did not occur in nonpolar solvents.^{39,43,44} But the involvement of protic solvents using NaBH_4 as a reducing agent for p-nitrophenol reduction is still inexplicit in its research. In the present experiment, it was noticeable that solvent mixtures like glycerol- water and ethylene glycol-water have

shown higher activity than water. Other solvent mixtures such as ethanol-water and 1,4-dioxane-water mixture have shown a slower reduction rate than water, giving prime evidence of active solvent hydrogen involvement in the nitro group's hydrogenation reaction. Sodium borohydride undergoes hydrolysis with water or solvolysis with other solvents containing active hydrogens and produces hydrogen gas.⁶⁶ Rate of hydrogen molecule production due to solvolysis in the investigated solvent-mixtures at 5% v/v - 30% v/v follow the order glycerol-water > ethylene glycol-water > water > ethanol-water > 1,4-dioxane-water. Three active hydrogens per molecule present in glycerol could be the reason for production of three hydrogen molecules by combining with hydride ions from sodium borohydride. Ethylene glycol has two active hydrogens; water and ethanol have one active hydrogen each, from which a corresponding number of hydrogen molecules could be produced by solvolysis. The ethanol-water mixture has comparably less capacity to form hydrogen molecules than water since NaBH₄ exhibited low solubility in ethanol than water. The 1,4-dioxane with hydrogens in closed chains was not active as other solvents. The 1,4-dioxane-water mixture, therefore, has minimal hydrogen production capacity. A direct influence was visible towards active hydrogens' contribution from different solvent molecules to reduce the nitro group. Neither the sodium borohydride nor the active hydrogen-bearing solvent molecules alone could directly ensure the nitrophenol hydrogenation completely. The active hydrogens in solvent molecules combine with the hydride ion from sodium borohydride to produce hydrogen molecules, making reduction reaction feasible. The pH of NaBH₄, glycerol, and glycerol-NaBH₄ mixture in water was checked using a pH meter. The pH of 20% glycerol was 7.2, and that of NaBH₄ solution (1x10⁻¹ M) was 10.3. The NaBH₄ solution (1x10⁻¹ M) was added to the glycerol (25 mL, 20%) solution, the pH of the corresponding solution mixtures was checked with the addition of 2 mL each. A graph was plotted with the volume of NaBH₄ solution added against the pH of the reaction mixture (see **Figure 5.17.**). The reaction mixture's pH increased by NaBH₄ addition and reached a pH of 9.5 by adding 50 mL 1 × 10⁻¹ M NaBH₄ solution. The reduction mainly happened in alkaline conditions; therefore, the production of hydrogen molecules by the reaction of NaBH₄ with active solvent hydrogen was the major factor rather than the change in pH. The dielectric constant of solvent mixtures on the reduction rate was studied.⁶⁷⁻⁶⁹ Solvent mixtures used in the present study have lower dielectric constants than water; however, reaction rates in the glycerol-water mixture and ethylene glycol-water mixture exhibited a higher reaction rate than in water. A plausible

mechanism has been shown in **Figure 5.18**. Two probable reasons could be attributed here for catalytic hydrogenation of nitro group by the silver nanocatalyst. Active hydrogen species could be produced via solvolysis of the glycerol-water mixture with sodium borohydride has the primary role in enhancing the catalytic reduction rate.^{21,70,71} This reactive hydrogen species gets adsorbed on the catalyst's surface to convert p-nitrophenol to p-aminophenol.^{21,72} Second possibility was the conventional way of catalytic hydrogenation by the hydrogen molecules produced in the solvolysis.^{40,47} Faster kinetics of the p-nitrophenol reduction in glycerol-water mixture using NaBH₄ as reductant indicates that the major path could be highly energetically reactive hydrogen species involved in reduction.

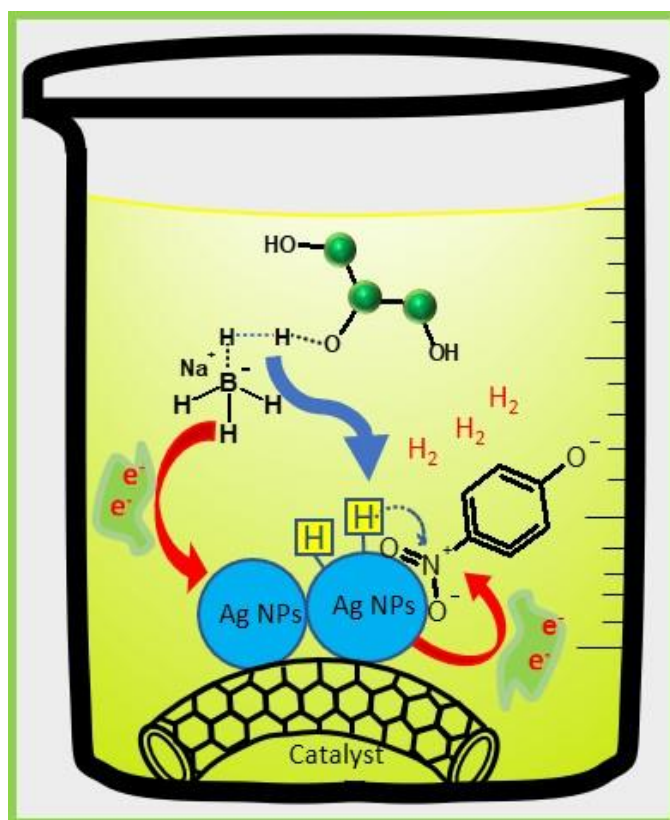


Figure 5.18. Mechanism of active solvent enhanced green catalytic reduction of p-nitrophenol using NaBH₄ in 10% glycerol-water mixture.

5.3.8. Relative yield and industrial-scale reduction of p-nitrophenol.

The relative yield of the p-aminophenolate ion was obtained from the calibration curve of known concentrations of p-aminophenolate (see **Figure 5.18**). Different p-aminophenol solution concentrations were prepared from 5.0×10^{-4} M to 1.0×10^{-7} M. For

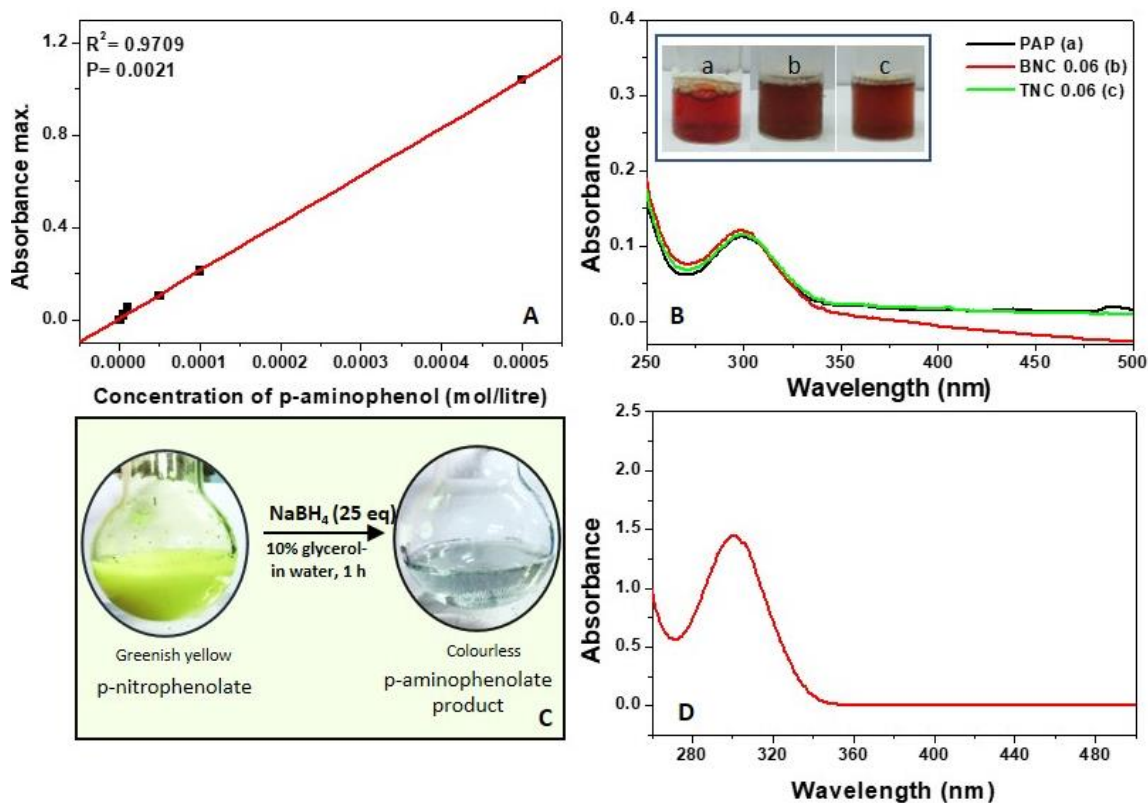


Figure 5.19. Calibration plot of *p*-aminophenol in different concentrations (1×10^{-7} M to 5×10^{-4} M) (A), UV-vis absorption spectra of the standard solution of *p*-aminophenolate ion, *p*-aminophenolate obtained from catalytic reduction using TNC-0.06 and BNC-0.06 (in 1×10^{-4} M) (B), reduction of *p*-nitrophenol in concentrated solution (10 mL, 15 g/L) using P-NP: NaBH₄ molar ratio 1:25 and BNC-0.18 (0.18 mg/mL) in 10% glycerol-water mixture (C), and UV-vis spectrum *p*-aminophenolate produced by bulk concentration scale reduction (D).

measuring the absorbance of the *p*-aminophenolate ion, a freshly prepared NaBH₄ solution (10 mL, 1.0×10^{-1} M) was added to each known concentration of *p*-aminophenol. The absorbance of *p*-aminophenolate ion obtained from nano catalytic reduction of *p*-nitrophenol (1.0×10^{-4} M) almost matched the known concentration of aminophenol, indicating complete conversion (see **Figure 5.19. B**). The synthetic utility of amino phenolate product has been substantiated by diazotization reaction (inset of **Figure 5.19. B**). Catalytical conversion of *p*-nitrophenol to *p*-aminophenol in 10% glycerol-water mixture using minimum P-NP to NaBH₄ molar ratio (1:25), by taking nanocatalyst concentration BNC-0.18 could be extended to high concentration scale up for industrial catalysis (near to the saturation limit of *p*-nitrophenol in water). The reaction completion was observed in green reaction conditions within one hour (see **Figure 5.19. C** for

photographs). The reaction mixture's UV-vis absorption spectra taken after one-hour reaction time have shown a peak at 298 nm corresponding to p-aminophenolate ion (see **Figure 5.19. D**). The absence of the p-nitrophenolate ion peak at 400 nm and the appearance of a single peak at 298 nm validated the complete reduction of p-nitrophenol to p-aminophenolate. Aminophenol's widespread applications in commercial and industrial fields demand bulk-scale hydrogenation of nitrophenol, which can be successfully prepared using heterogeneous silver nanocatalysts and by the utilization of a less volume percentage of glycerol.^{73,74}

5.3.9. Antibacterial activity:

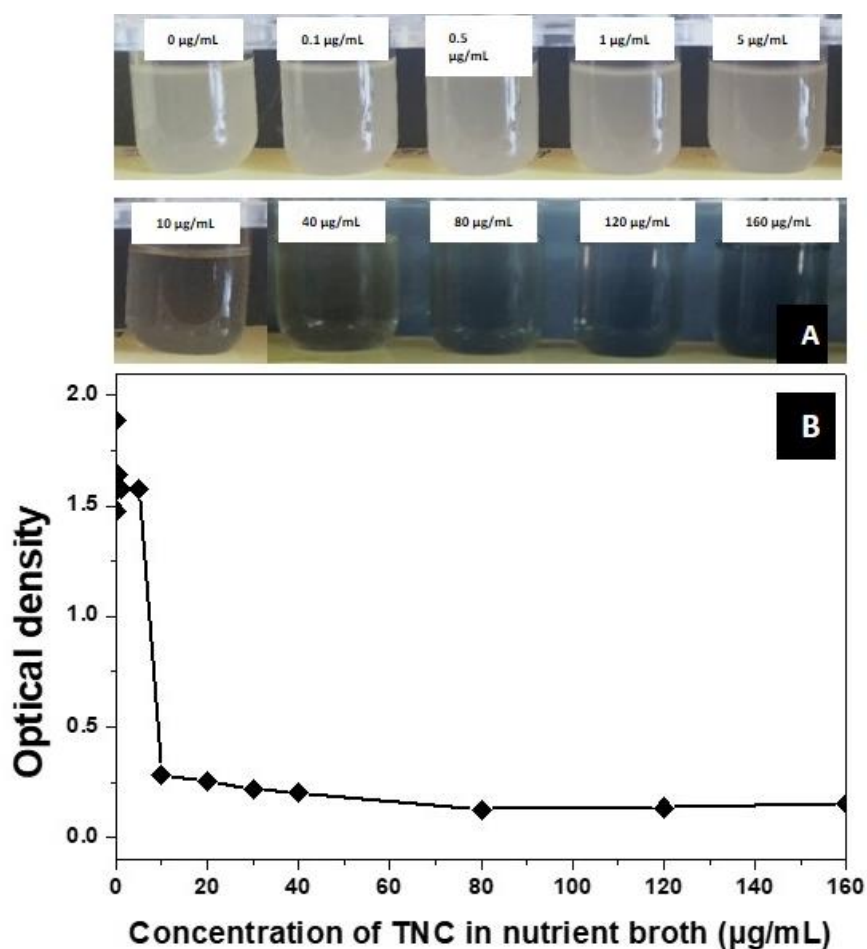


Figure 5.20. Photographs of mixtures of *E. coli* bacteria culture with different concentrations of TNC taken after overnight incubation (A). The plot of optical density versus the concentration of TNC for the antibacterial study at 660 nm (B).

Antibacterial activity studies of the nanocomposite TNC have been carried out on *Escherichia coli*, a frequently used model organism in life science research.^{75,76} Silver nanoparticles act as good antibacterial agents depending on particle size and shape.^{25,26} Ternary silver nanocatalysts (TNC) have been taken for antibacterial study in different doses due to their ability to maintain appreciable dispersion for longer. Antibacterial activity and minimum inhibitory concentration (MIC) of nanocomposite have been studied by the tube dilution method. Different concentrations of TNC such as $1 \times 10^{-1} \mu\text{g/mL}$, $5 \times 10^{-1} \mu\text{g/mL}$, $1 \mu\text{g/mL}$, $5 \mu\text{g/mL}$, $10 \mu\text{g/mL}$, $20 \mu\text{g/mL}$, $30 \mu\text{g/mL}$, $40 \mu\text{g/mL}$, $80 \mu\text{g/mL}$, $120 \mu\text{g/mL}$ and $160 \mu\text{g/mL}$ were prepared. The mixtures were dispersed in a boiling tube for 10 min, and 50 μL actively growing *E. coli* culture was used as the inoculum for all tubes. It was incubated in a thermal shaker overnight at 37 °C. Microbial growth in liquid medium was characterized by increased turbidity, for that incubation tubes were examined under bright light. The white turbidity resulting from *E. Coli* bacterial growth was almost absent in the medium above $10 \mu\text{g/mL}$ concentration of TNC (**Figure 5.20. A**). The result indicates that TNC exhibits good antibacterial activity against gram-negative *E. Coli* bacteria. Quantitative antibacterial activity was assessed by measuring optical density at 660 nm using a UV-vis double beam spectrophotometer. A graph was plotted by taking optical density versus the concentration of TNC used for antibacterial studies (see **Figure 5.20. B**). The nutrient broth-TNC mixture has high optical density for concentrations between $5 \times 10^{-1} \mu\text{g/mL}$ - $10 \mu\text{g/mL}$ due to the bacterial growth; however, at $10 \mu\text{g/mL}$ of the nanocatalyst, the optical density considerably suppressed due to the inhibition to the growth of the bacterial culture. MIC of TNC was estimated as $10 \mu\text{g/mL}$, comparable with the reference range of commercial antimicrobial agents.⁷⁷⁻⁷⁹ TNC with one-dimensional nanostructure in which silver nanoparticles are attached to MWCNT via less cytotoxic polythiophene layer.^{49,57,62a} Silver nanoparticles attached to the nanocomposite can be biocidal by physicochemical interaction with bacterial cells.²⁶ Comparison study of antibacterial activity of MWCNT-COOH, PTCNT-COOH-300 Ag nanoparticles solution (Ag NPs), BNC, and TNC against *E. coli* bacteria was carried out in lactose broth [lactose broth was selected here to repeat antibacterial activity in another medium] (see **Figure 5.21**). TNC has shown higher antibacterial activity against *E. Coli* bacteria in the dosage of $10 \mu\text{g/mL}$ and above. Silver nanoparticles in the dosage of $10 \mu\text{g/mL}$ have lower antibacterial activity than TNC, which may be due to the aggregation effect of some of the

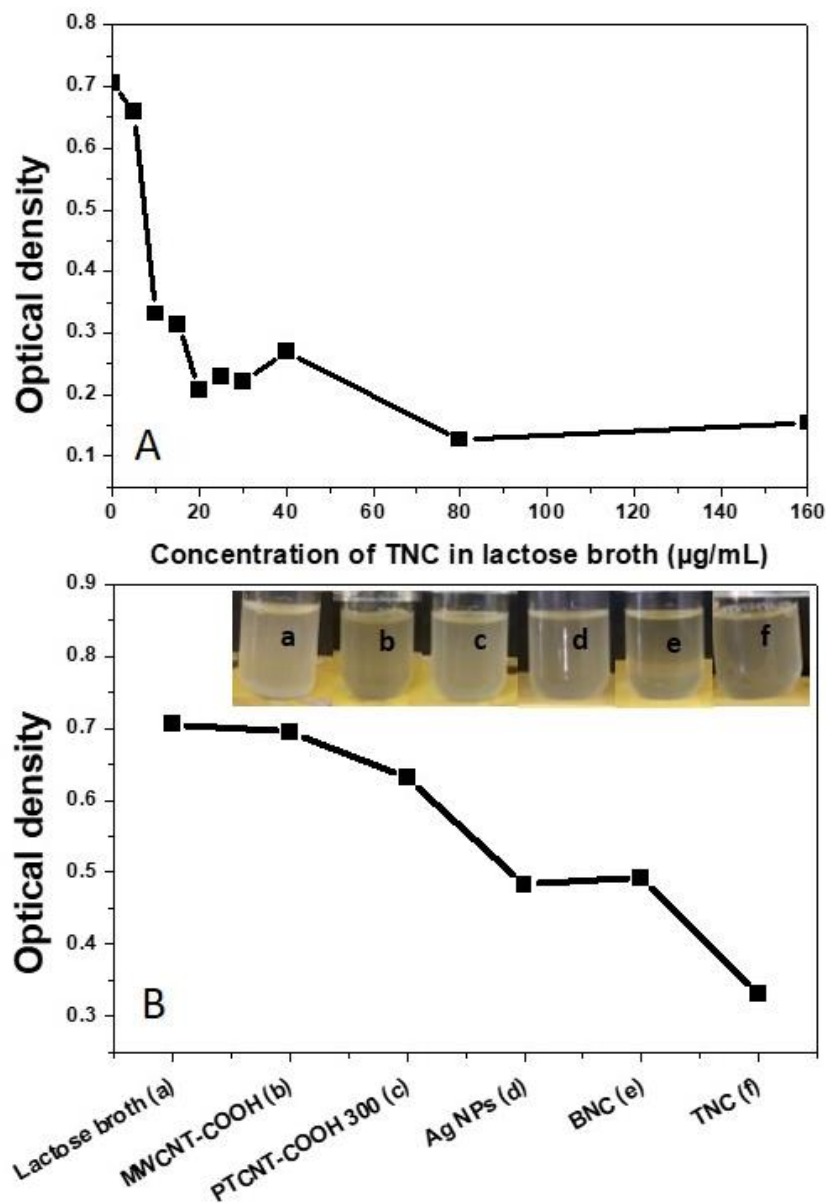


Figure 5.21. The plot of optical density against the concentration of TNC in lactose broth used in the antibacterial study (A) and plot and photographs of comparison of antibacterial activity of MWCNT-COOH, PTCNT-COOH 300, Ag NPs, BNC and TNC (B).

Ag NPs during the incubation period. BNC exhibited lower antibacterial activity than that of TNC due to the incapability to maintain stable dispersion for the overnight incubation period. MWCNT-COOH and PTCNT-COOH 300 have no observable antibacterial activity in these 10 µg/mL - 30 µg/mL concentrations. The well-dispersed state of TNC made them highly competent for bacterial inactivation, good dispersion provides more nano-surface active sites for interacting with bacteria.⁴⁸ The properties of excellent water dispersibility and recovering nature could be combined with the high antibacterial activity of TNC;

thereby, it could find unique applications in different applications such as water disinfection, medical fields, and textile industries.^{48,49} In this chapter ternary and binary nanocomposites demonstrated with their efficient catalytic activity and antibacterial efficiency. We could also illustrate involvement of active hydrogens in catalytic hydrogenation of *p*-nitrophenol (see **Figure 5.22.**).

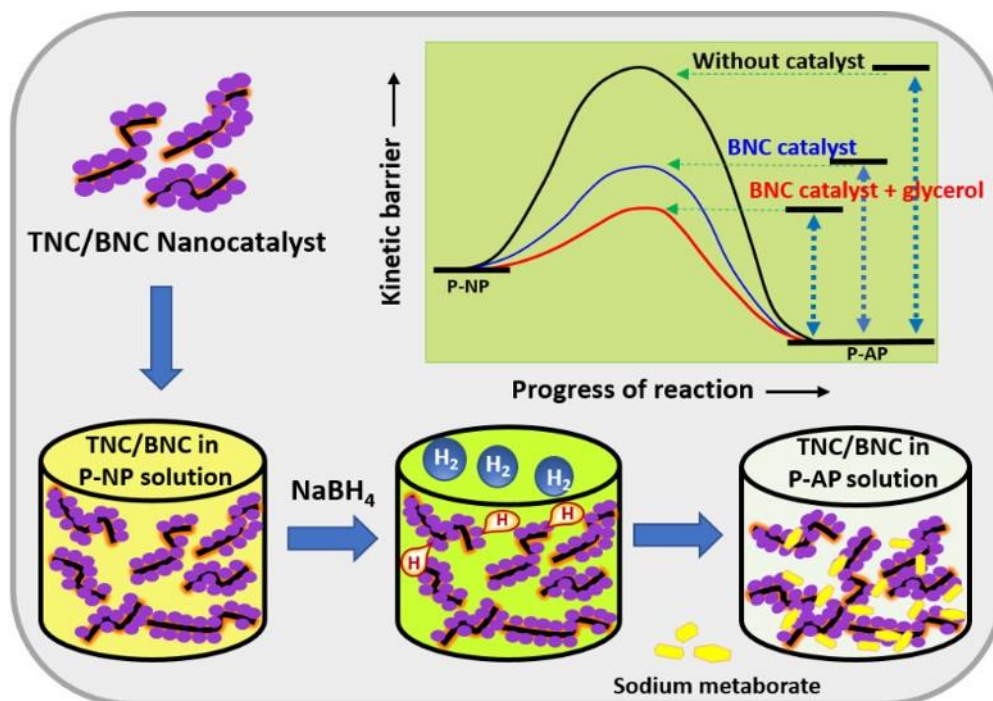


Figure 5.22. Illustration of involvement of active hydrogens in catalytic hydrogenation of p-nitrophenol

5.4. Conclusion

We have studied the active solvent hydrogens enhanced catalytic hydrogenation of *p*-nitrophenol using NaBH₄ using two types of heterogeneous silver nanocatalysts. Polymer-supported silver nanoparticles embedded functionalized MWCNT ternary nanocomposites (TNC) and silver nanoparticles directly embedded functionalized MWCNT nanocomposites (BNC). The nanocatalyst BNC was found to exhibit higher catalytic performance than TNC in conversion percentage and recyclable efficiency. Separate control experiments using Ag NPs solution, MWCNT-COOH, and PTCNT-COOH revealed Ag NPs act as a catalyst for the reduction and functionalized multiwalled carbon nanotube (MWCNT-COOH) acts as a supporting framework for stabilizing silver nanoparticles and polythiophene layer to improve the dispersing nature of the

Chapter 5

nanocomposites. Comparative study of the kinetics of p-nitrophenol reduction in water and different solvent-water mixtures such as 1,4-dioxane-water, ethanol-water, ethylene glycol-water, and glycerol-water have been demonstrated. The 10 % glycerol-water mixture was an efficient green solvent mixture for the enhanced reduction rate. By utilizing the minimum amount of catalyst (0.005 mg/mL) and P-NP: NaBH₄ molar ratio 1:200 in a glycerol-water mixture, a fast reduction of p-nitrophenol was obtained with an activity factor of 936.50 s⁻¹ g⁻¹. A plausible mechanism of hydrogen source for converting nitro group to amino group by the solvolysis of NaBH₄ in a protic solvent has been proposed. Active hydrogens present in the solvent molecules were showing a direct impact on accelerating P-NP reduction using NaBH₄. High concentration scale preparation of p-aminophenol by a simple green organic reaction set up with a modest reaction time of one hour has been achieved by reducing p-nitrophenol (1.08 × 10⁻¹ M) using catalyst concentration BNC-0.18 and NaBH₄ (2.69 M). The ternary nanocatalyst TNC could also act as an efficient antibacterial agent against the widely used model organism *Escherichia coli* with a minimum concentration of 10 µg/mL.

References

1. Heveling, J. Heterogeneous Catalytic Chemistry by Example of Industrial Applications. *J. Chem. Educ.* **2012**, *89* (12), 1530–1536. <https://doi.org/10.1021/ed200816g>.
2. Liu, L.; Corma, A. Metal Catalysts for Heterogeneous Catalysis: From Single Atoms to Nanoclusters and Nanoparticles. *Chem. Rev.* **2018**, *118* (10), 4981–5079. <https://doi.org/10.1021/acs.chemrev.7b00776>.
3. Mizuno, N.; Misono, M. Heterogeneous Catalysis. *Chem. Rev.* **1998**, *98* (1), 199–217. <https://doi.org/10.1021/cr960401q>.
4. Chandrasekhar, V.; Athimoolam, A. New Hybrid Inorganic-Organic Polymers as Supports for Heterogeneous Catalysis: A Novel Pd(O) Metalated Cyclophosphazene-Containing Polymer as an Efficient Heterogeneous Catalyst for the Heck Reaction. *Org. Lett.* **2002**, *4* (12), 2113–2116. <https://doi.org/10.1021/ol026098z>.
5. Friend, C. M.; Xu, B. Heterogeneous Catalysis: A Central Science for a Sustainable Future. *Acc. Chem. Res.* **2017**, *50* (3), 517–521. <https://doi.org/10.1021/acs.accounts.6b00510>.
6. Zhou, Y.; Huang, R.; Ding, F.; Brittain, A. D.; Liu, J.; Zhang, M.; Xiao, M.; Meng, Y.; Sun, L. Sulfonic Acid-Functionalized α-Zirconium Phosphate Single-Layer Nanosheets as a Strong Solid Acid for Heterogeneous Catalysis Applications. *ACS Appl. Mater. Interfaces* **2014**, *6* (10), 7417–7425. <https://doi.org/10.1021/am5008408>.
7. Shi, J. On the Synergetic Catalytic Effect in Heterogeneous Nanocomposite Catalysts. *Chem. Rev.* **2013**, *113* (3), 2139–2181. <https://doi.org/10.1021/cr3002752>.
8. Liu, X.; Wen, X.; Hoffmann, R. Surface Activation of Transition Metal Nanoparticles for Heterogeneous Catalysis: What We Can Learn from Molecular Dynamics. *ACS Catal.* **2018**, *8* (4), 3365–3375. <https://doi.org/10.1021/acscatal.7b04468>.
9. Zhao, P.; Feng, X.; Huang, D.; Yang, G.; Astruc, D. Basic Concepts and Recent Advances in Nitrophenol Reduction by Gold- and Other Transition Metal Nanoparticles. *Coord. Chem. Rev.* **2015**, *287*, 114–136. <https://doi.org/10.1016/j.ccr.2015.01.002>.

10. Campelo, J. M.; Luna, D.; Luque, R.; Marinas, J. M.; Romero, A. A. Sustainable Preparation of Supported Metal Nanoparticles and Their Applications in Catalysis. *ChemSusChem* **2009**, *2* (1), 18–45. <https://doi.org/10.1002/cssc.200800227>.
11. Astruc, D. Introduction: Nanoparticles in Catalysis. *Chem. Rev.* **2020**, *120* (2), 461–463. <https://doi.org/10.1021/acs.chemrev.8b00696>.
12. Deshmukh, S. P.; Dhodamani, A. G.; Patil, S. M.; Mullani, S. B.; More, K. V.; Delekar, S. D. Interfacially Interactive Ternary Silver-Supported Polyaniline/Multiwalled Carbon Nanotube Nanocomposites for Catalytic and Antibacterial Activity. *ACS Omega* **2020**, *5* (1), 219–227. <https://doi.org/10.1021/acsomega.9b02526>.
13. Alshehri, S. M.; Almuqati, T.; Almuqati, N.; Al-Farraj, E.; Alhokbany, N.; Ahamad, T. Chitosan Based Polymer Matrix with Silver Nanoparticles Decorated Multiwalled Carbon Nanotubes for Catalytic Reduction of 4-Nitrophenol. *Carbohydr. Polym.* **2016**, *151*, 135–143. <https://doi.org/10.1016/j.carbpol.2016.05.018>.
14. Ahmad, S.; Yang, C.; Xie, W.; Deng, Z.; Zhang, H.; Zhao, Y.; Su, X. Molten Salt-Templated Synthesis of Ternary NiS–NiCo₂O₄@C Composites as High Performance Catalysts for 4-Nitro Phenol Reduction and Supercapacitor. *Carbon N. Y.* **2020**, *158*, 912–921. <https://doi.org/10.1016/j.carbon.2019.11.081>.
15. Nariya, P.; Das, M.; Shukla, F.; Thakore, S. Synthesis of Magnetic Silver Cyclodextrin Nanocomposite as Catalyst for Reduction of Nitro Aromatics and Organic Dyes. *J. Mol. Liq.* **2020**, *300*. <https://doi.org/10.1016/j.molliq.2019.112279>.
16. Yang, X.; Jiang, X.; Bashir, M. S.; Kong, X. Z. Preparation of Highly Uniform Polyurethane Microspheres by Precipitation Polymerization and Pd Immobilization on Their Surface and Their Catalytic Activity in 4-Nitrophenol Reduction and Dye Degradation. *Ind. Eng. Chem. Res.* **2020**, *59* (7), 2998–3007. <https://doi.org/10.1021/acs.iecr.9b06367>.
17. Kibar, G.; Dinç, D. Ş. Ö. In-Situ Growth of Ag on Mussel-Inspired Polydopamine@poly(M-POSS) Hybrid Nanoparticles and Their Catalytic Activity. *J. Environ. Chem. Eng.* **2019**, *7* (5). <https://doi.org/10.1016/j.jece.2019.103435>.
18. Liao, G.; Zhao, W.; Li, Q.; Pang, Q.; Xu, Z. Novel Poly (Acrylic Acid)-Modified Tourmaline/Silver Composites for Adsorption Removal of Cu(II) Ions and Catalytic Reduction of Methylene Blue in Water. *Chem. Lett.* **2017**, *46* (11), 1631–1634. <https://doi.org/10.1246/cl.170785>.
19. Liao, G.; Fang, J.; Li, Q.; Li, S.; Xu, Z.; Fang, B. Ag-Based Nanocomposites: Synthesis and Applications in Catalysis. *Nanoscale* **2019**, *11* (15), 7062–7096. <https://doi.org/10.1039/c9nr01408j>.
20. Liao, G.; Li, Q.; Zhao, W.; Pang, Q.; Gao, H.; Xu, Z. In-Situ Construction of Novel Silver Nanoparticle Decorated Polymeric Spheres as Highly Active and Stable Catalysts for Reduction of Methylene Blue Dye. *Appl. Catal. A Gen.* **2018**, *549*, 102–111. <https://doi.org/10.1016/j.apcata.2017.09.034>.
21. Liao, G.; Gong, Y.; Zhong, L.; Fang, J.; Zhang, L.; Xu, Z.; Gao, H.; Fang, B. Unlocking the Door to Highly Efficient Ag-Based Nanoparticles Catalysts for NaBH₄-Assisted Nitrophenol Reduction. *Nano Res.* **2019**, *12* (10), 2407–2436. <https://doi.org/10.1007/s12274-019-2441-5>.
22. Sarkar, A. K.; Saha, A.; Midya, L.; Banerjee, C.; Mandre, N.; Panda, A. B.; Pal, S. Cross-Linked Biopolymer Stabilized Exfoliated Titanate Nanosheet-Supported AgNPs: A Green Sustainable Ternary Nanocomposite Hydrogel for Catalytic and Antimicrobial Activity. *ACS Sustain. Chem. Eng.* **2017**, *5* (2), 1881–1891. <https://doi.org/10.1021/acssuschemeng.6b02594>.
23. Liu, R.; Hou, Y.; Jiang, S.; Nie, B. Ag(I)-Hived Fullerene Microcube as an Enhanced Catalytic Substrate for the Reduction of 4-Nitrophenol and the Photodegradation of Orange G Dye. *Langmuir* **2020**, *36* (19), 5236–5242. <https://doi.org/10.1021/acs.langmuir.0c00580>.

24. Kolya, H.; Kuila, T.; Kim, N. H.; Lee, J. H. Bioinspired Silver Nanoparticles/Reduced Graphene Oxide Nanocomposites for Catalytic Reduction of 4-Nitrophenol, Organic Dyes and Act as Energy Storage Electrode Material. *Compos. Part B Eng.* **2019**, *173*. <https://doi.org/10.1016/j.compositesb.2019.106924>.
25. González, A. L.; Noguez, C.; Beránek, J.; Barnard, A. S. Size, Shape, Stability, and Color of Plasmonic Silver Nanoparticles. *J. Phys. Chem. C* **2014**, *118* (17), 9128–9136. <https://doi.org/10.1021/jp5018168>.
26. Tejamaya, M.; Römer, I.; Merrifield, R. C.; Lead, J. R. Stability of Citrate, PVP, and PEG Coated Silver Nanoparticles in Ecotoxicology Media. *Environ. Sci. Technol.* **2012**, *46* (13), 7011–7017. <https://doi.org/10.1021/es2038596>.
27. Astruc, D., Lu, F., & Aranzaes, J. R. (2005). Nanoparticles as recyclable catalysts: The frontier between homogeneous and heterogeneous catalysis. *Angewandte Chemie - International Edition*, *44*(48), 7852–7872. <https://doi.org/10.1002/anie.200500766>
28. Yu, B.; Han, B.; Jiang, X.; Zhou, C.; Xia, K.; Gao, Q.; Wu, J. Toward High Activity and Durability: An Oxygen-Rich Boron Nitride-Supported Au Nanoparticles for 4-Nitrophenol Hydrogenation. *J. Phys. Chem. C* **2019**, *123* (16), 10389–10397. <https://doi.org/10.1021/acs.jpcc.9b00600>.
29. Lee, J. W.; Cho, J. Y.; Kim, M. J.; Kim, J. H.; Park, J. H.; Jeong, S. Y.; Seo, S. H.; Lee, G. W.; Jeong, H. J.; Han, J. T. Synthesis of Silver Nanoparticles Embedded with Single-Walled Carbon Nanotubes for Printable Elastic Electrodes and Sensors with High Stability. *Sci. Rep.* **2021**, *11* (1). <https://doi.org/10.1038/s41598-021-84386-4>.
30. (a) Shifrina, Z. B.; Matveeva, V. G.; Bronstein, L. M. Role of Polymer Structures in Catalysis by Transition Metal and Metal Oxide Nanoparticle Composites. *Chem. Rev.* **2020**, *120* (2), 1350–1396. <https://doi.org/10.1021/acs.chemrev.9b00137>. (b) Bilalis, P.; Katsigiannopoulos, D.; Avgeropoulos, A.; Sakellariou, G. Non-Covalent Functionalization of Carbon Nanotubes with Polymers. *RSC Adv.* **2014**, *4* (6), 2911–2934. <https://doi.org/10.1039/c3ra44906h>.
31. Zahed, B.; Hosseini-Monfared, H. A Comparative Study of Silver-Graphene Oxide Nanocomposites as a Recyclable Catalyst for the Aerobic Oxidation of Benzyl Alcohol: Support Effect. *Appl. Surf. Sci.* **2015**, *328*, 536–547. <https://doi.org/10.1016/j.apsusc.2014.12.078>.
32. Baruah, B.; Gabriel, G. J.; Akbashev, M. J.; Booher, M. E. Facile Synthesis of Silver Nanoparticles Stabilized by Cationic Polynorbornenes and Their Catalytic Activity in 4-Nitrophenol Reduction. *Langmuir* **2013**, *29* (13), 4225–4234. <https://doi.org/10.1021/la305068p>.
33. Gangu, K. K.; Maddila, S.; Jonnalagadda, S. B. A Review on Novel Composites of MWCNTs Mediated Semiconducting Materials as Photocatalysts in Water Treatment. *Sci. Total Environ.* **2019**, *646*, 1398–1412. <https://doi.org/10.1016/j.scitotenv.2018.07.375>.
34. Liao, G.; Gong, Y.; Zhang, L.; Gao, H.; Yang, G. J.; Fang, B. Semiconductor Polymeric Graphitic Carbon Nitride Photocatalysts: The “Holy Grail” for the Photocatalytic Hydrogen Evolution Reaction under Visible Light. *Energy Environ. Sci.* **2019**, *12* (7), 2080–2147. <https://doi.org/10.1039/c9ee00717b>.
35. Ali, G. A. M.; Megiel, E.; Cieciorński, P.; Thalji, M. R.; Romański, J.; Algarni, H.; Chong, K. F. Ferrocene Functionalized Multi-Walled Carbon Nanotubes as Supercapacitor Electrodes. *J. Mol. Liq.* **2020**, *318*. <https://doi.org/10.1016/j.molliq.2020.114064>.
36. Zhan, W.; Yu, S.; Gao, L.; Wang, F.; Fu, X.; Sui, G.; Yang, X. Bioinspired Assembly of Carbon Nanotube into Graphene Aerogel with “Cabbagelike” Hierarchical Porous Structure for Highly Efficient Organic Pollutants Cleanup. *ACS Appl. Mater. Interfaces* **2018**, *10* (1), 1093–1103. <https://doi.org/10.1021/acsami.7b15322>.
37. Liu, T.; Sun, Y.; Jiang, B.; Guo, W.; Qin, W.; Xie, Y.; Zhao, B.; Zhao, L.; Liang, Z.; Jiang, L. Pd Nanoparticle-Decorated 3D-Printed Hierarchically Porous TiO₂Scaffolds for the Efficient Reduction of a Highly Concentrated 4-Nitrophenol Solution. *ACS Appl. Mater. Interfaces* **2020**, *12* (25), 28100–28109. <https://doi.org/10.1021/acsami.0c03959>.

38. Kästner, C.; Thünemann, A. F. Catalytic Reduction of 4-Nitrophenol Using Silver Nanoparticles with Adjustable Activity. *Langmuir* **2016**, *32* (29), 7383–7391. <https://doi.org/10.1021/acs.langmuir.6b01477>.
39. Li, Z.; He, M.; Wen, Y.; Zhang, X.; Hu, M.; Li, R.; Liu, J.; Chu, J.; Ma, Z.; Xing, X.; Yu, C.; Wei, Z.; Li, Y. Highly Monodisperse Cu-Sn Alloy Nanoplates for Efficient Nitrophenol Reduction Reaction via Promotion Effect of Tin. *Inorg. Chem.* **2020**, *59* (2), 1522–1531. <https://doi.org/10.1021/acs.inorgchem.9b03370>.
40. Scholten, J. D.; Leal, B. C.; Dupont, J. Transition Metal Nanoparticle Catalysis in Ionic Liquids. *ACS Catal.* **2012**, *2* (1), 184–200. <https://doi.org/10.1021/cs200525e>.
41. Shirin, S.; Roy, S.; Rao, A.; Pillai, P. P. Accelerated Reduction of 4-Nitrophenol: Bridging Interaction Outplays Reducing Power in the Model Nanoparticle-Catalyzed Reaction. *J. Phys. Chem. C* **2020**, *124* (35), 19157–19165. <https://doi.org/10.1021/acs.jpcc.0c06237>.
42. Neal, R. D.; Hughes, R. A.; Sapkota, P.; Ptasinska, S.; Neretina, S. Effect of Nanoparticle Ligands on 4-Nitrophenol Reduction: Reaction Rate, Induction Time, and Ligand Desorption. *ACS Catal.* **2020**, *10* (17), 10040–10050. <https://doi.org/10.1021/acscatal.0c02759>.
43. Zhao, Y.; Li, R.; Jiang, P.; Zhang, K.; Dong, Y.; Xie, W. Mechanistic Study of Catalytic Hydride Reduction of -NO₂ to -NH₂ Using Isotopic Solvent and Reducer: The Real Hydrogen Source. *J. Phys. Chem. C* **2019**, *123* (25), 15582–15588. <https://doi.org/10.1021/acs.jpcc.9b02684>.
44. Fountoulaki, S.; Daikopoulou, V.; Gkizis, P. L.; Tamiolakis, I.; Armatas, G. S.; Lykakis, I. N. Mechanistic Studies of the Reduction of Nitroarenes by NaBH₄ or Hydrosilanes Catalyzed by Supported Gold Nanoparticles. *ACS Catal.* **2014**, *4* (10), 3504–3511. <https://doi.org/10.1021/cs500379u>.
45. Das, R.; Sypu, V. S.; Paumo, H. K.; Bhaumik, M.; Maharaj, V.; Maity, A. Silver Decorated Magnetic Nanocomposite (Fe₃O₄@PPy-MAA/Ag) as Highly Active Catalyst towards Reduction of 4-Nitrophenol and Toxic Organic Dyes. *Appl. Catal. B Environ.* **2019**, *244*, 546–558. <https://doi.org/10.1016/j.apcatb.2018.11.073>.
46. Narayanan, R. K.; Devaki, S. J. Brawny Silver-Hydrogel Based Nanocatalyst for Reduction of Nitrophenols: Studies on Kinetics and Mechanism. *Ind. Eng. Chem. Res.* **2015**, *54* (4), 1197–1203. <https://doi.org/10.1021/ie5038352>.
47. Mogudi, B. M.; Ncube, P.; Meijboom, R. Catalytic Activity of Mesoporous Cobalt Oxides with Controlled Porosity and Crystallite Sizes: Evaluation Using the Reduction of 4-Nitrophenol. *Appl. Catal. B Environ.* **2016**, *198*, 74–82. <https://doi.org/10.1016/j.apcatb.2016.05.051>.
48. Krystosiak, P.; Tomaszewski, W.; Megiel, E. High-Density Polystyrene-Grafted Silver Nanoparticles and Their Use in the Preparation of Nanocomposites with Antibacterial Properties. *J. Colloid Interface Sci.* **2017**, *498*, 9–21. <https://doi.org/10.1016/j.jcis.2017.03.041>.
49. Zako, T.; Sakono, M.; Kobayashi, T.; Sörgjerd, K.; Nilsson, K. P. R.; Hammarström, P.; Lindgren, M.; Maeda, M. Cell Interaction Study of Amyloid by Using Luminescent Conjugated Polythiophene: Implication That Amyloid Cytotoxicity Is Correlated with Prolonged Cellular Binding. *ChemBioChem* **2012**, *13* (3), 358–363. <https://doi.org/10.1002/cbic.201100467>.
50. Moreira, T.; Laia, C. A. T.; Zangoli, M.; Antunes, M.; Di Maria, F.; De Monte, S.; Liscio, F.; Parola, A. J.; Barbarella, G. Semicrystalline Polythiophene-Based Nanoparticles Deposited from Water on Flexible PET/ITO Substrates as a Sustainable Approach toward Long-Lasting Solid-State Electrochromic Devices. *ACS Appl. Polym. Mater.* **2020**, *2* (8), 3301–3309. <https://doi.org/10.1021/acsapm.0c00440>.
51. Moghayed, M.; Goharshadi, E. K.; Ghazvini, K.; Ahmadzadeh, H.; Ranjbaran, L.; Masoudi, R.; Ludwig, R. Kinetics and Mechanism of Antibacterial Activity and Cytotoxicity of Ag-RGO Nanocomposite. *Colloids Surfaces B Biointerfaces* **2017**, *159*, 366–374. <https://doi.org/10.1016/j.colsurfb.2017.08.001>.

52. Murugan, E.; Vimala, G. Effective Functionalization of Multiwalled Carbon Nanotube with Amphiphilic Poly(Propyleneimine) Dendrimer Carrying Silver Nanoparticles for Better Dispersability and Antimicrobial Activity. *J. Colloid Interface Sci.* **2011**, *357* (2), 354–365. <https://doi.org/10.1016/j.jcis.2011.02.009>.
53. Liao, G.; He, F.; Li, Q.; Zhong, L.; Zhao, R.; Che, H.; Gao, H.; Fang, B. Emerging Graphitic Carbon Nitride-Based Materials for Biomedical Applications. *Prog. Mater. Sci.* **2020**, *112*. <https://doi.org/10.1016/j.pmatsci.2020.100666>.
54. Liao, G.; Gong, Y.; Yi, C.; Xu, Z. Soluble, Antibacterial, and Anticorrosion Studies of Sulfonated Polystyrene/Polyaniline/Silver Nanocomposites Prepared with the Sulfonated Polystyrene Template. *Chinese J. Chem.* **2017**, *35* (7), 1157–1164. <https://doi.org/10.1002/cjoc.201600816>.
55. Marambio-Jones, C.; Hoek, E. M. V. A Review of the Antibacterial Effects of Silver Nanomaterials and Potential Implications for Human Health and the Environment. *J. Nanoparticle Res.* **2010**, *12* (5), 1531–1551. <https://doi.org/10.1007/s11051-010-9900-y>.
56. Gozdziowska, M.; Cichowicz, G.; Markowska, K.; Zawada, K.; Megiel, E. Nitroxide-Coated Silver Nanoparticles: Synthesis, Surface Physicochemistry and Antibacterial Activity. *RSC Adv.* **2015**, *5* (72), 58403–58415. <https://doi.org/10.1039/c5ra09366j>.
57. Swathy, T. S.; Jinish Antony, M. Tangled Silver Nanoparticles Embedded Polythiophene-Functionalized Multiwalled Carbon Nanotube Nanocomposites with Remarkable Electrical and Thermal Properties. *Polymer (Guildf)*. **2020**, *189*. <https://doi.org/10.1016/j.polymer.2020.122171>.
58. Wang, Z.; Xu, C.; Gao, G.; Li, X. Facile Synthesis of Well-Dispersed Pd-Graphene Nanohybrids and Their Catalytic Properties in 4-Nitrophenol Reduction. *RSC Adv.* **2014**, *4* (26), 13644–13651. <https://doi.org/10.1039/c3ra47721e>.
59. Feng, Y.; Yin, J.; Liu, S.; Wang, Y.; Li, B.; Jiao, T. Facile Synthesis of Ag/Pd Nanoparticle - Loaded Poly(Ethylene Imine) Composite Hydrogels with Highly Efficient Catalytic Reduction of 4-Nitrophenol. *ACS Omega* **2020**, *5* (7), 3725–3733. <https://doi.org/10.1021/acsomega.9b04408>.
60. Liao, G.; Chen, J.; Zeng, W.; Yu, C.; Yi, C.; Xu, Z. Facile Preparation of Uniform Nanocomposite Spheres with Loading Silver Nanoparticles on Polystyrene-Methyl Acrylic Acid Spheres for Catalytic Reduction of 4-Nitrophenol. *J. Phys. Chem. C* **2016**, *120* (45), 25935–25944. <https://doi.org/10.1021/acs.jpcc.6b09356>.
61. Gu, S.; Wunder, S.; Lu, Y.; Ballauff, M.; Fenger, R.; Rademann, K.; Jaquet, B.; Zaccone, A. Kinetic Analysis of the Catalytic Reduction of 4-Nitrophenol by Metallic Nanoparticles. *J. Phys. Chem. C* **2014**, *118* (32), 18618–18625. <https://doi.org/10.1021/jp5060606>.
62. (a) Kaloni, T. P.; Giesbrecht, P. K.; Schreckenbach, G.; Freund, M. S. Polythiophene: From Fundamental Perspectives to Applications. *Chem. Mater.* **2017**, *29* (24), 10248–10283. <https://doi.org/10.1021/acs.chemmater.7b03035>. (b) Swathy, T. S.; Jose, M. A.; Antony, M. J. AOT Assisted Preparation of Ordered, Conducting and Dispersible Core-Shell Nanostructured Polythiophene – MWCNT Nanocomposites. *Polymer (Guildf)*. **2016**, *103*, 206–213. <https://doi.org/10.1016/j.polymer.2016.09.047>. (c) Jose, M. A., Varghese, S., Antony, M. J., (2016). In situ chemical oxidative polymerisation for ordered conducting polythiophene nanostructures in presence of dioctyl sodium sulfosuccinate. *Indian Journal of Chemistry*, *55A*. 292-297
63. Pozun, Z. D.; Rodenbusch, S. E.; Keller, E.; Tran, K.; Tang, W.; Stevenson, K. J.; Henkelman, G. A Systematic Investigation of p -Nitrophenol Reduction by Bimetallic Dendrimer Encapsulated Nanoparticles. *J. Phys. Chem. C* **2013**, *117* (15), 7598–7604. <https://doi.org/10.1021/jp312588u>.
64. Ortiz-Quinonez, J. L.; Pal, U. Borohydride-Assisted Surface Activation of Co₃O₄/CoFe₂O₄ Composite and Its Catalytic Activity for 4-Nitrophenol Reduction. *ACS Omega* **2019**, *4* (6), 10129–10139. <https://doi.org/10.1021/acsomega.9b00118>.
65. Chen, W.; Ouyang, L. Z.; Liu, J. W.; Yao, X. D.; Wang, H.; Liu, Z. W.; Zhu, M. Hydrolysis and Regeneration of Sodium Borohydride (NaBH₄) – A Combination of Hydrogen

- Production and Storage. *J. Power Sources* **2017**, *359*, 400–407. <https://doi.org/10.1016/j.jpowsour.2017.05.075>.
66. (a) Schlesinger, H. I.; Brown, H. C.; Finholt, A. E.; Gilbreath, J. R.; Hoekstra, H. R.; Hyde, E. K. Sodium Borohydride, Its Hydrolysis and Its Use as a Reducing Agent and in the Generation of Hydrogen. *J. Am. Chem. Soc.* **1953**, *75* (1), 215–219. <https://doi.org/10.1021/ja01097a057>. (b) Alhokbany, N.; Ahama, T.; Ruksana; Naushad, M.; Alshehri, S. M. AgNPs Embedded N- Doped Highly Porous Carbon Derived from Chitosan Based Hydrogel as Catalysts for the Reduction of 4-Nitrophenol. *Compos. Part B Eng.* **2019**, *173*. <https://doi.org/10.1016/j.compositesb.2019.106950>.
67. Åkerlöf, G. Dielectric Constants of Some Organic Solvent-Water Mixtures at Various Temperatures. *J. Am. Chem. Soc.* **1932**, *54* (11), 4125–4139. <https://doi.org/10.1021/ja01350a001>.
68. Mohsen-Nia, M.; Amiri, H.; Jazi, B. Dielectric Constants of Water, Methanol, Ethanol, Butanol and Acetone: Measurement and Computational Study. *J. Solution Chem.* **2010**, *39* (5), 701–708. <https://doi.org/10.1007/s10953-010-9538-5>.
69. Jouyban, A.; Soltanpour, S. Prediction of Dielectric Constants of Binary Solvents at Various Temperatures. *J. Chem. Eng. Data* **2010**, *55* (9), 2951–2963. <https://doi.org/10.1021/je1000632>.
70. Brown, H. C.; Mead, E. J.; Rao, B. C. S. A Study of Solvents for Sodium Borohydride and the Effect of Solvent and the Metal Ion on Borohydride Reductions. *J. Am. Chem. Soc.* **1955**, *77* (23), 6209–6213. <https://doi.org/10.1021/ja01628a044>.
71. Wang, W.; Niu, J.; Yang, Z. An Efficient Reduction of Unsaturated Bonds and Halogen-Containing Groups by Nascent Hydrogen over Raney Ni Catalyst. *J. Hazard. Mater.* **2020**, *389*. <https://doi.org/10.1016/j.jhazmat.2019.121912>.
72. Song, J.; Huang, Z. F.; Pan, L.; Li, K.; Zhang, X.; Wang, L.; Zou, J. J. Review on Selective Hydrogenation of Nitroarene by Catalytic, Photocatalytic and Electrocatalytic Reactions. *Appl. Catal. B Environ.* **2018**, *227*, 386–408. <https://doi.org/10.1016/j.apcatb.2018.01.052>.
73. Clarke, C. J.; Tu, W. C.; Levers, O.; Bröhl, A.; Hallett, J. P. Green and Sustainable Solvents in Chemical Processes. *Chem. Rev.* **2018**, *118* (2), 747–800. <https://doi.org/10.1021/acs.chemrev.7b00571>.
74. Kitanosono, T.; Masuda, K.; Xu, P.; Kobayashi, S. Catalytic Organic Reactions in Water toward Sustainable Society. *Chem. Rev.* **2018**, *118* (2), 679–746. <https://doi.org/10.1021/acs.chemrev.7b00417>.
75. Xiu, Z. M.; Zhang, Q. B.; Puppala, H. L.; Colvin, V. L.; Alvarez, P. J. J. Negligible Particle-Specific Antibacterial Activity of Silver Nanoparticles. *Nano Lett.* **2012**, *12* (8), 4271–4275. <https://doi.org/10.1021/nl301934w>.
76. Andrews, J. M. Determination of Minimum Inhibitory Concentrations. *J. Antimicrob. Chemother.* **2001**, *48* (SUPPL. 1), 5–16. https://doi.org/10.1093/jac/48.suppl_1.5.
77. Ramalingam, B.; Parandhaman, T.; Das, S. K. Antibacterial Effects of Biosynthesized Silver Nanoparticles on Surface Ultrastructure and Nanomechanical Properties of Gram-Negative Bacteria Viz. Escherichia Coli and Pseudomonas Aeruginosa. *ACS Appl. Mater. Interfaces* **2016**, *8* (7), 4963–4976. <https://doi.org/10.1021/acsami.6b00161>.
78. Antony, R.; Marimuthu, R.; Murugavel, R. Bimetallic Nanoparticles Anchored on Core-Shell Support as an Easily Recoverable and Reusable Catalytic System for Efficient Nitroarene Reduction. *ACS Omega* **2019**, *4* (5), 9241–9250. <https://doi.org/10.1021/acsomega.9b01023>.
79. Deshmukh, S. P.; Patil, S. M.; Mullani, S. B.; Delekar, S. D. Silver Nanoparticles as an Effective Disinfectant: A Review. *Mater. Sci. Eng. C* **2019**, *97*, 954–965. <https://doi.org/10.1016/j.msec.2018.12.102>.

Chapter 6

Ternary and Binary Silver Nanocatalysts for Reduction of Water Soluble and Insoluble Azodyes and Azobenzene

6.1. Introduction

Azo dyes are the major synthetic colourants used in many industries like textile, printing, cosmetics, leather, paint, and fiber due to their good tinctorial properties and attractive colours imparted with most types of stuff.¹⁻⁴ They are generally considered mutagenic and carcinogenic due to benzidine, naphthalene or similar aromatic systems in their structure.^{5,6} It adversely affects the life cycle of aquatic and human life. Moreover, synthetic organic azo dyes like methyl orange, congo red, etc. are non-biodegradable in normal conditions, creating harmful effects on their discharge to the environment.⁷ Various methods classified into physical, chemical and biological processes could be used to treat the dye effluents such as adsorption, solvent extraction, photochemical, electrochemical, chemical reactions, bacterial reactions, etc.⁷⁻¹³ Azo dyes exhibit prolonged photo and thermal stability. Therefore their treatment creates some obstacles in the degradation methods used.¹⁴ Implementation of some traditional treatment techniques might also lead to drawbacks like low product yield (s), high cost, formation of hazardous by-products or sludge, wastage of reagents and incomplete purification. On the other hand, chemical and photochemical degradation of dyes can efficiently achieve good degradation yields with the help of suitable catalysts.^{15,16} The use of heterogeneous nanocatalysts would be worthwhile due to their advantages such as large area of active sites, recycling ability and cost effectiveness.¹⁷⁻²⁰ Heterogeneous catalytic reduction would be effective for the treatment of industrial dye effluents in high concentration for waste-water management.

Azobenzene is the core moiety of azodyes for which chemoselective reduction to hydrazobenzene or reductive cleavage to aniline or both reduction products are obtained (see **Figure 6.1**).²¹⁻³⁴ Selective hydrazoarenes synthesis is important for preparing polymers, pharmaceuticals, food additives, and dyes. Hydrazobenzene can easily undergo rearrangement in strongly acidic conditions to obtain benzidine, an important intermediate in synthetic organic chemistry.^{25,29} Hydrazobenzene is an important precursor to produce 4,4'-diaminobiaryls, azoarenes and azodyes.²⁷ Traditionally, hydrazobenzene can be achieved from nitrobenzene by reducing it with Zn in methanol medium. However, more facile methods are later frequently reported for nitrobenzene to hydrazobenzene conversion.

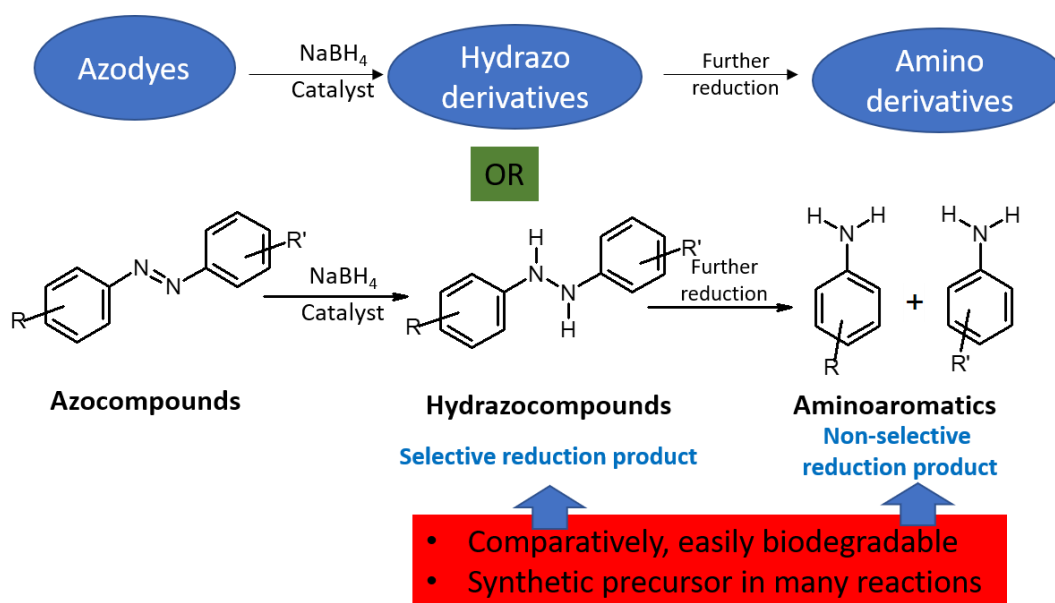


Figure 6.1. Consecutive reduction in azo compounds to form chemo-selective product hydrazo compounds and followed by non-selective amino aromatics products.

Hydrazobenzene was also prepared from another synthetic precursor azobenzene by selective hydrogenation utilizing expensive methods such as industrial photocatalytic reduction, electrochemical reduction using lead-containing electrodes and reduction using hydrazines in the presence of noble transition metals, use of substantial amounts of metal reductants such as Na, Mg, Zn etc., and rare earth metal compounds incorporated methods.²³⁻³¹ More facile methods of azocompounds to hydrazocompounds conversion are being in progress. Shiraishi and co-workers demonstrated photocatalytic hydrogenation of azobenzene to hydrazobenzene using ethanol on cadmium sulfide as a green synthesis. As a result of this hydrogenation, Cd^0 is formed. They found that the saturated N-N bond in hydrazobenzene does not interact with Cd^0 (see **Figure 6.2. (A)**).²⁹ Pei et. al reported conversion of azobenzene to hydrazobenzene using NaNbO_3 as a green strategy for the semi-hydrogenation. The interaction between NaNbO_3 and hydrazobenzene is the root cause of this partial hydrogenation and inability to produce aniline (see **Figure 6.2. (B)**).³⁰ Use of heterogeneous nanocatalysts for chemical reduction for azo- to hydrazo conversion is very rarely reported. Recently Hong and co-workers carried out a subsidiary study of azo benzene to hydrazo benzene conversion using NaBH_4 in ethanol medium with polystyrene supported Au nanoparticles as heterogeneous nanocatalyst along with the

main work of hydrazoarene formation from nitroarene (see **Figure 6.3.**).³¹ Some other important reports of azo to hydrazo compounds conversion in literature are tabulated in **Table 6.1.**^{21,23,25,32,33}

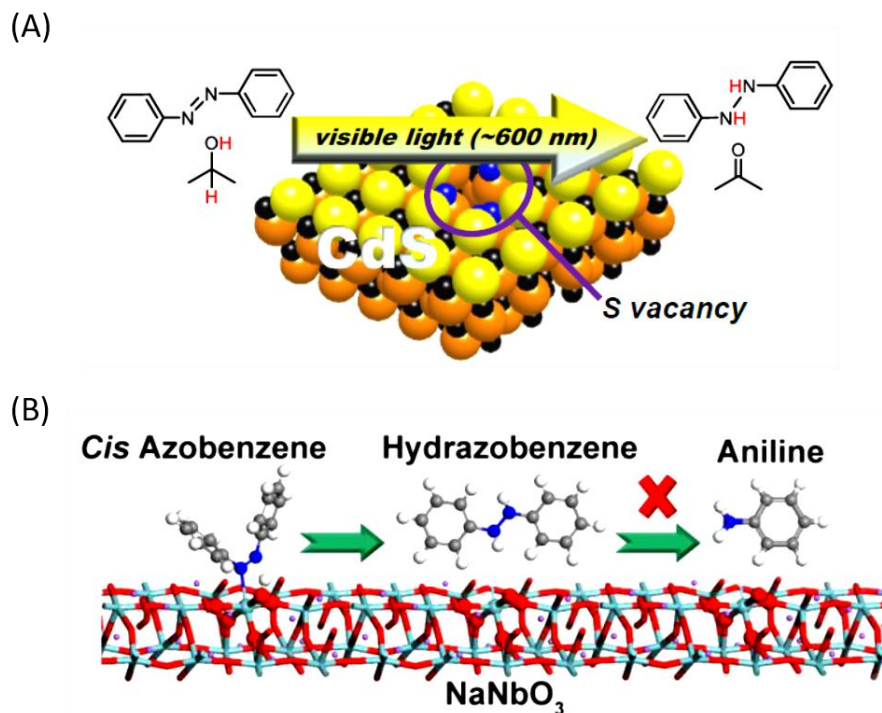


Figure 6.2. Illustration of photocatalytic transfer hydrogenation of azobenzene to hydrazobenzene (A) with alcohol on cadmium sulfide (adapted from Shiraishi et al. 2012 and (B) using NaNbO_3 catalyst (adapted from Pei et al. 2020)

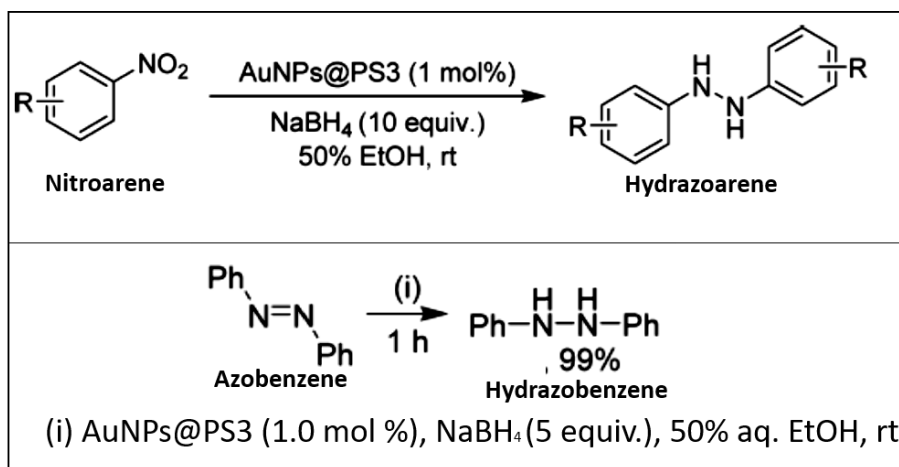
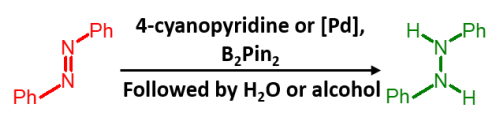
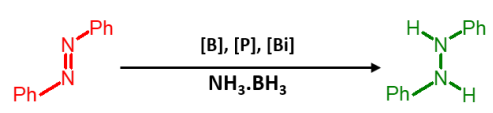
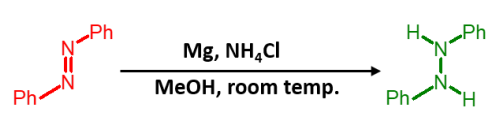
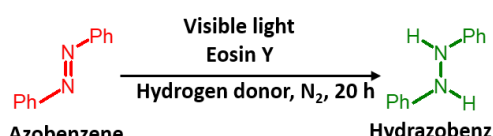
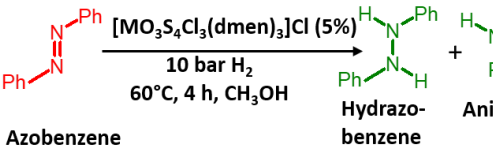


Figure 6.3. Synthesis of Hydrazoarenes formation from nitroarenes and azobenzene (Adapted from Hong et al. 2021)

Table 6.1. Literature reports of hydrogenation of azobenzene to hydrazobenzene

Sl. No.	Conversion with reagents	Type of reduction	Ref.
(1)	 4-cyanopyridine or [Pd], B_2Pin_2 Followed by H_2O or alcohol	Chemical reduction	21
(2)	 [B], [P], [Bi] $NH_3.BH_3$	Chemical reduction	32
(3)	 Mg, NH_4Cl MeOH, room temp.	Chemical reduction	25
(4)	 Visible light Eosin Y Hydrogen donor, N_2 , 20 h Azobenzene → Hydrazobenzene	Photochemical reduction	33
(5)	 $[MO_3S_4Cl_3(dmen)_3]Cl$ (5%) 10 bar H_2 60°C, 4 h, CH_3OH Azobenzene → Hydrazobenzene + Aniline	Chemical reduction	23

In this chapter, catalytic decolourisations of different azodyes (methyl orange, congo red, methyl red and sudan III) were carried out in water or ethanol- water mixture by chemical reduction with sodium borohydride in the presence of ternary silver nanocatalyst (PTCNT-COOH 300 Ag, abbreviated as TNC) or binary silver nanocatalyst (MWCNT-COOH Ag₂, abbreviated as BNC). Hydrophilic or hydrophobic based azodyes were selected based on the structure and functional groups present in their structure. An aqueous medium was used to treat hydrophilic azo dyes like methyl orange and congo red. Hydrophobic azo dyes are difficult to handle in an aqueous medium due to poor solubility in water. Herein, the ethanol-water mixture in suitable proportions was effectively used as the media for the degradation treatment of hydrophobic azo dyes (methyl red and Sudan III). A mechanistic study of the product on decolourisation process was carried out as a control on azobenzene by investigating its isolated product. The selection of mild and green methodologies for the dye treatments and hydrogenation of azobenzene attracts great research interest and in the present study binary and ternary silver nano composites, BNC and TNC acted as a sustainable heterogeneous catalysts for it.

6.2. Experimental

6.2.1. Materials and reagents: Methyl orange, congo red, methyl red and sudan III were purchased from Nice chemicals, NaBH₄ was purchased from Sigma Aldrich. Distilled water and distilled ethanol were used for all decolourisation studies.

6.2.2. Measurements and Instruments: UV-visible spectra of the samples were recorded by Shimadzu UV-Visible spectrophotometer, UV 1800 series in the range 200-800 nm with distilled ethanol and deionized water. High-Resolution Mass Spectrometry (HR-MS) of the product was carried out using Thermo Fisher Scientific Exactive mass spectrometer with Accella 600 HPLC system and PDA detector. ¹H NMR spectra of the samples were taken with Bruker Avance 400 MHz FT-NMR spectrometer.

6.2.3. Catalytic decolourisation study of methyl orange and congo red using BNC-0.04 catalyst: Nanocatalyst BNC (1.00 mg, 0.04 mg/mL) was added to the aqueous solution of methyl orange (1.0×10^{-4} M, 25 mL) taken in a standard flask and, sonicated for 15 min to obtain well-dispersed state of reactant catalyst mixture. The BNC catalyst with a concentration 0.04 mg/mL is represented as BNC-0.04. Freshly prepared NaBH₄ solution (1.0×10^{-1} M, 5 mL) was added to 5 mL of methyl orange-BNC mixture taken in a 30 mL vial and shaken for 10 s. We have mixed methyl orange-catalyst reaction mixture and NaBH₄ solution in equal volume for all catalytical studies, therefore the final concentration of methyl orange, NaBH₄ and catalyst reduced to half. Time for complete decolourisation of the reaction mixture was noted. Catalytic decolourisation with catalytic concentration of BNC in methyl orange solution such as BNC-0.06 and BNC-0.08 were carried out similarly.

The same procedure was also repeated for the dye congo red instead of methyl orange with the concentration of BNC as 0.04 mg/mL, 0.06 mg/mL, 0.08 mg/mL and 0.10 mg/mL in the congo red solution.

6.2.4. UV-vis absorption study of reductive decolourisation of methyl orange and congo red: BNC (1.00 mg, 0.04 mg/mL) was added to a solution of methyl orange (1.0×10^{-4} M, 25 mL) taken in a standard flask. Sonicated for 15 min to obtain a well dispersed reactant catalyst mixture with a catalyst concentration of 0.04 mg/mL. Freshly prepared NaBH₄ solution (1.0×10^{-1} M, 2 mL) was added to 2 mL of methyl

Chapter 6

orange-BNC mixture taken in a vial and shaken for 10 seconds. UV-vis absorption spectra were recorded in regular time intervals by a preset program.

The same procedure was repeated for reductive decolourisation of congo red dye using BNC-0.04 nanocatalyst in an aqueous medium. The UV-vis absorption study was also conducted for the reductive decolourisation of methyl orange and congo red in an aqueous medium using TNC-0.04 catalyst with the same procedure. The TNC catalyst concentration 0.04 mg/mL was represented as TNC-0.04.

6.2.5. Catalytic decolourisation study of methyl red and sudan III using BNC-0.04 catalyst: Nanocatalyst BNC (1.00 mg, 0.04 mg/mL) was added to the solution of methyl red (1.0×10^{-4} M, 25 mL) in 33% ethanol-water mixture, taken in a standard flask. Sonicated for 15 min to obtain a well dispersed state of reactant-catalyst mixture with a catalyst concentration of 0.04 mg/mL. Freshly prepared NaBH_4 solution (1.0×10^{-1} M, 5 mL) prepared in 33 % ethanol-water mixture was added to 5 mL of methyl red-BNC mixture taken in a vial and shaken for 10 s. Time for complete decolourisation of the reaction mixture was also noted. Catalytic decolourisation of methyl red with the catalytic concentration of BNC-0.02, BNC-0.06 and BNC-0.08 were repeated in a similar manner.

The same procedure was used with the dye sudan III instead of methyl red for the other catalyst concentrations of BNC such as BNC-0.02, BNC-0.04, BNC-0.06 and BNC-0.08 in the sudan III solution prepared in 66% ethanol-water mixture.

6.2.6. UV-vis absorption study of reductive decolourisation of methyl red and sudan III: Methyl red solution (1.0×10^{-4} M, 25 mL) was prepared in a 33 % ethanol-water mixture. TNC (1.00 mg, 0.04 mg/mL) was added and dispersed for 15 min to get a catalyst concentration of 0.04 mg/mL. Freshly prepared NaBH_4 solution (1.0×10^{-1} M, 2 mL) in 33 % ethanol-water mixture was added to 2 mL of methyl orange-TNC mixture taken in a vial and shaken for 10 s. UV-vis absorption spectra were recorded in a preset program in regular time intervals.

UV-vis absorption spectra was used to monitor reductive decolourisation for Sudan III (in 66 % ethanol-water mixture) and azobenzene (in 33 % ethanol-water mixture) using BNC-0.04 catalyst with the same procedure.

6.2.7. Large scale reduction of azobenzene: Azobenzene solution (0.10 g, 0.027 M, 25 mL) was prepared in 50% ethanol-water mixture. To this solution binary nanocatalyst BNC (0.18 mg/mL) was added and sonicated for 15 min. Freshly prepared NaBH₄ solution (1.917 g, AB: NaBH₄ molar ratio=1:100, 25 mL) was added to the obtained azobenzene-catalyst dispersion mixture. It was then magnetically stirred for 15 min. The reaction mixture turned colourless. The product formed was isolated with ether separation in a separating funnel and dried. A colourless solid was formed which gradually turned yellow, as an isolated product. Yield: 0.064 g. ¹H NMR, (400 MHz, CHCl₃, δ ppm): 5.57 (s,2H), 6.85 (d, 6H) and 7.2 (t, 4H).

6.2.8. Recycling studies using nanocatalysts: TNC (7 mg) was dispersed in azobenzene solution (5 mL, 2.33 × 10⁻³ M) in 50% ethanol -water mixture by sonication. Freshly prepared NaBH₄ solution (5 mL, 2.33 M) was added to the above mixture. The reaction mixture was shaken well for one minute, then kept undisturbed for 10 min, and centrifuged. After centrifugation for three min, filtrate was decanted, and then UV-vis absorption spectra were recorded. The residue (nanocatalyst) was washed with deionized water, and catalytical activities continued for five more consecutive cycles using the same method. A similar procedure was repeated using BNC nanocatalyst (7 mg) instead of TNC for five catalytic cycles.

6.3. Results and discussion

6.3.1. Ternary and binary silver nanocomposites (TNC and BNC) as nanocatalyst for reductive decolourisation of azo dyes

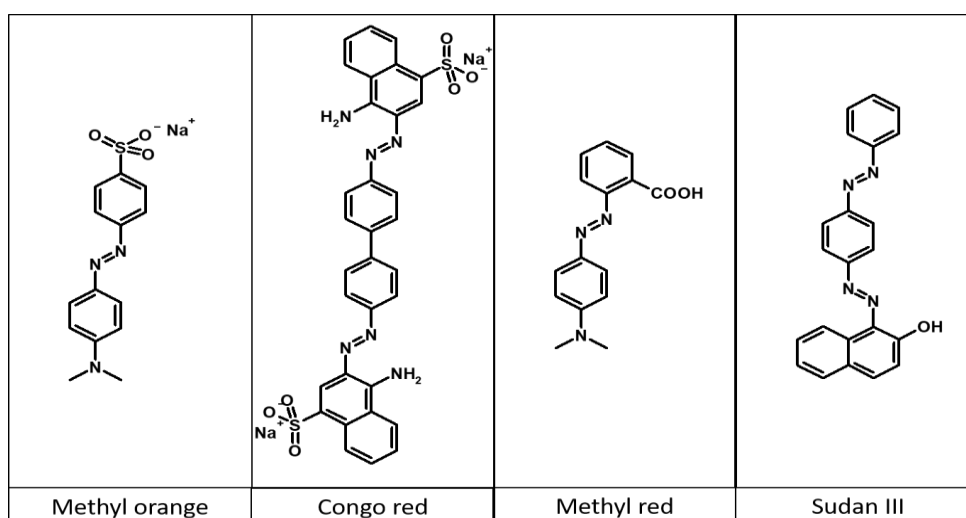


Figure 6.4. Chemical structure of different azo dyes

Chapter 6

Table 6.2. Name of azo compounds, concentration and volume of azo compounds used, amount of NaBH₄ used, name of catalyst and concentration of catalyst with respective rate constant and activity factor in the catalytic reduction/decolourisation.

Azo compounds	Amount of azo compounds used		Amount of NaBH ₄ used		Catalyst and conc. (mg/mL)	Reaction medium	Rate constant (s ⁻¹)	Activity factor (s ⁻¹ g ⁻¹)
	Conc. (M)	V (mL)	Conc. (M)	V (mL)				
Methyl orange	1x10 ⁻⁴	2	1x10 ⁻¹	2	BNC, 0.04	Water	1.03x10 ⁻²	129.13
	1x10 ⁻⁴	2	1x10 ⁻¹	2	TNC, 0.04	Water	1.00x10 ⁻¹	1255.00
Congo red	1x10 ⁻⁴	2	1x10 ⁻¹	2	BNC, 0.04	Water	5.46x10 ⁻³	68.25
	1x10 ⁻⁴	2	1x10 ⁻¹	2	TNC, 0.04	Water	1.02x10 ⁻²	128.00
Methyl red	1x10 ⁻⁴	2	1x10 ⁻¹	2	BNC, 0.04	33% ethanol	9.23 x10 ⁻³	115.38
	1x10 ⁻⁴	2	1x10 ⁻¹	2	TNC, 0.04	33% ethanol	2.50 x10 ⁻⁴	3.13
Sudan III	1x10 ⁻⁴	2	1x10 ⁻¹	2	BNC, 0.04	66% ethanol	5.47x10 ⁻³	68.37
	1x10 ⁻⁴	2	1x10 ⁻¹	2	TNC, 0.04	66% ethanol	8.39 x10 ⁻³	104.88
Azobenzene	1x10 ⁻⁴	2	1x10 ⁻¹	2	BNC, 0.04	33% ethanol	1.03 x10 ⁻²	128.13
Azobenzene	1x10 ⁻⁴	2	1x10 ⁻¹	2	TNC, 0.04	33% ethanol	2.59 x10 ⁻¹	3232.50

Ternary nanocomposite (PTCNT-COOH 300 Ag or TNC) consists of silver nanoparticles embedded polythiophene-functionalized multiwalled carbon nanotube and binary nanocomposite (MWCNT-COOH Ag or BNC) consists of functionalized multiwalled carbon nanotube-silver nanoparticles, they were effectively used as a catalyst for the reductive decolourisation of water soluble azo dyes such as methyl orange, congo red and insoluble organic azo dyes such as methyl red and Sudan III. TNC and BNC were prepared by in-situ reduction of silver ions in the presence of dispersed state of PTCNT-COOH 300 and MWCNT-COOH nanocomposites, respectively. Synthesis and characterizations of TNC and BNC were previously reported in chapter 4 with the names PTCNT-COOH 300 Ag and MWCNT-COOH Ag respectively. FE-SEM images of PTCNT-COOH 300 Ag and MWCNT-COOH Ag were obtained as nearly spherical silver nanoparticles entangled with PTCNT-COOH or MWCNT-COOH nanotubular structures. The average size of silver nanoparticles in TNC and BNC was measured as 25 ± 8 nm and 45 ± 5 nm, respectively (see **Figure 4.10. in chapter 4**). The reduction of organic azo dyes was carried out using NaBH₄ as

a reducing agent and TNC or BNC as the nanocatalyst. Treatment of azodyes (1×10^{-4} M, 2 mL) with NaBH_4 solution (1×10^{-1} M, 2 mL) in a dispersed state of TNC or BNC catalysts led to decolourisation of the dye stuff. The colour of the dye faded gradually with the progress of the reaction and finally became colourless. The chemical structure of different azo dyes used to conduct the degradation study is given in **Figure 6.4**. Synthetic conditions and corresponding amounts of reactant, reagent and catalyst used in catalytic reduction and outcomes are given in **Table 6.2**.

6.3.2. Optimization of the amount of catalyst for reduction of water-soluble azo dyes

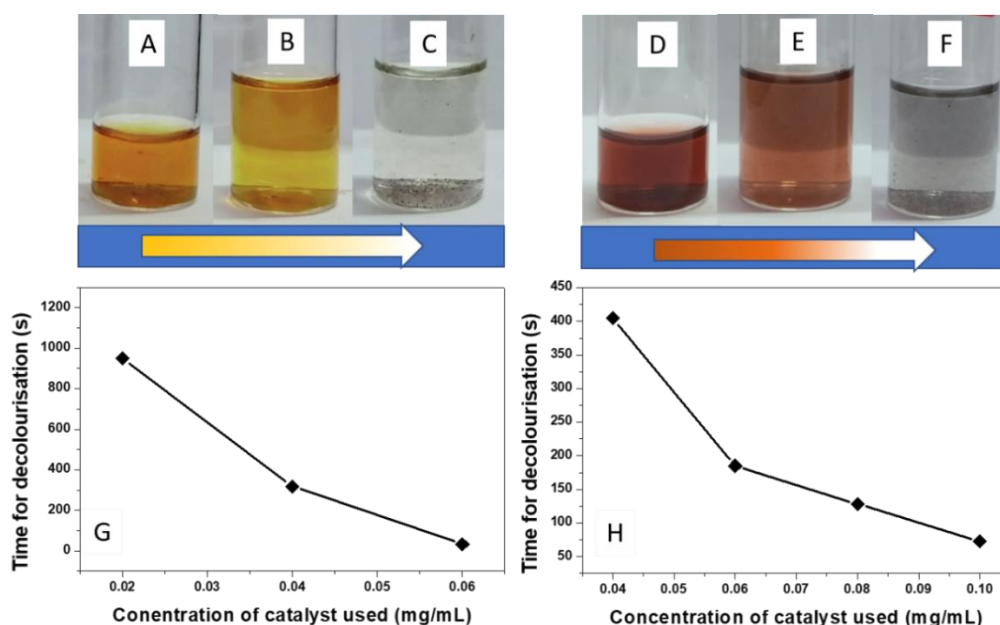


Figure 6.5. Photographs of reductive decolourisation of water-soluble azo dyes methyl orange (initial stage (A), middle stage (B) and final stage (C), and congo red (initial stage (D), middle stage (E) and final stage (F). Plots of decolourisation time against catalyst concentration used for methyl orange (G) and Congo red (H).

Accomplishing partial or complete reduction of azo-bond(s) in azo dyes is indicated by decolouration of the reaction mixture. Here, the time for decolourisation of different organic azo dyes was noticed during reduction treatment conducted in different concentrations of BNC catalyst (as shown in **Figure 6.5**). The concentrations of BNC catalyst was as varied as 0.02 mg/mL, 0.04 mg/mL and 0.06 mg/mL for methyl orange and 0.04 mg/mL, 0.06 mg/mL, 0.08 mg/mL and 0.10 mg/mL for congo red for

obtaining its optimum catalyst concentrations. A graph has been plotted for the time for decolourisation against the catalyst concentration (see **Figure 6.5. G and H**). The optimum catalyst concentration was selected as 0.04 mg/mL for methyl orange and congo red. The optimum catalyst concentration was selected as the minimum amount of catalyst, which exhibited moderate reaction kinetics. BNC-0.04 also provide good comparison of kinetics of catalytic decolourisation of both water soluble azo dyes methyl orange and congo red.

6.3.3. Kinetics of reductive decolourisation of water soluble organic azo dyes

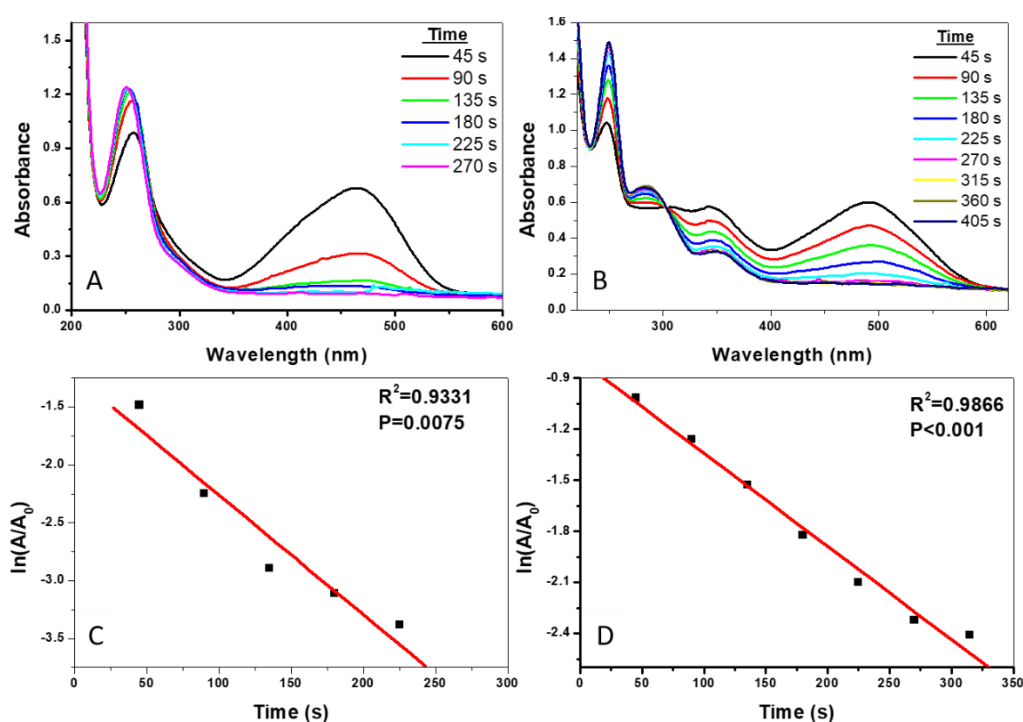


Figure 6.6. UV-vis absorption spectra of catalytic reduction of methyl orange (A) and congo red (B) using BNC-0.04 catalyst in different time intervals. Linear relationship plot of $\ln(A/A_0)$ against time for reduction of methyl orange (C) and congo red (D) using catalyst BNC-0.04.

Reductive decolourisation of water soluble organic azo dyes (1×10^{-4} M, 2 mL) was carried out in the presence of BNC or TNC nanocatalyst (0.04 mg/mL) using NaBH_4 (1×10^{-1} M, 2 mL) as a reductant in the aqueous medium. The reaction kinetics was monitored using UV-vis absorption spectroscopy in consecutive time intervals by means of a preset time program (see **Figure 6.6. A, B and 6.7 A, B**). For the catalytic reduction of methyl orange, the intensity of the peak with an absorption maximum at

470 nm corresponds to azo group, gradually diminished with time, and then disappeared (see **Figure 6.6. A** and **Figure 6.7. A**). The time for the disappearance of the peak at 470 nm was selected as the time for the completion of the reaction. The bright orange colour of the reaction medium faded and finally decolourised on completion of the reaction. The highly intense orange colour of azo dyes like methyl orange was observed due to extended conjugation with chromophore groups in the molecule.^{34,35} The peak with an absorption maximum at 258 nm underwent a blue shift with time with increased intensity up to 251 nm as a result of structural changes. Catalytic reduction of another azo dye congo red was also carried out with sodium borohydride as reductant and BNC or TNC as a catalyst in an aqueous medium. The completion of the reaction has been monitored by recording the absorption spectra of the reaction mixture in consecutive time intervals (see **Figure 6.6. B** and **6.7. B**). The progress of the reduction reaction was observed as a continuous decrease in the intensity of the major absorption peak at an absorption maximum of 498 nm. The completion of the reaction was identified as the time at which the peak at 498 nm vanished. The brownish red colour of the mixture of congo red with the catalyst also faded and turned colourless on completion of the reaction. Methyl orange and congo red was decolourised in the presence of BNC nanocatalyst in the reaction mixture in about 315 s and 270 s, respectively (see **Figure 6.6. A and B**). Likewise, TNC catalysed decolourisation of methyl orange and congo red was carried out and completion of the reaction was attained at 135 s and 215 s, respectively (see **Figure 6.7. A and B**).

The rate constants for reductive decolourisation of methyl orange and congo red was obtained from linear regression fit of the graph plotted for $\ln(A/A_0)$ against the time of the reaction progress (see **Figure 6.6. C, D** and **Figure 6.7 C, D**). The rate constant for reductive decolourisation of methyl orange and congo red using catalysts BNC was found to be $1.03 \times 10^{-2} \text{ s}^{-1}$ and $5.46 \times 10^{-3} \text{ s}^{-1}$, respectively (see **Figure 6.6. C and D**). The corresponding activity factor for BNC catalysed decolourisation of methyl orange and congo red were $129.13 \text{ s}^{-1} \text{ g}^{-1}$ and $68.25 \text{ s}^{-1} \text{ g}^{-1}$ respectively. The mono azo dye methyl orange and bis-azo dye congo red exhibited rate constant for decolourisation using TNC catalysts as $1.00 \times 10^{-1} \text{ s}^{-1}$ and $1.02 \times 10^{-2} \text{ s}^{-1}$ respectively (see **Figure 6.7. C and D**). The activity factors exhibited by TNC catalysed decolourisation of methyl orange and congo red were $1255.00 \text{ s}^{-1} \text{ g}^{-1}$ and $128.00 \text{ s}^{-1} \text{ g}^{-1}$, respectively. Mono azo dye methyl orange, for which decolourisation rate constant is found as higher than that

of congo red, since it was required to reduce two azo groups per molecule in congo red than one azo group in methyl orange using the same amount of reducing agent. TNC exhibited higher rate constant and activity factor than BNC for methyl orange and congo red reductive decolourisation. TNC is a heterogeneous nanocomposite catalyst which was easily dispersed in aqueous medium than BNC. Higher dispersibility of TNC nanocomposites system is due to the conducting polymer incorporated coreshell morphology of the particular nanocomposites framework. The improved aqueous solubility of the TNC catalyst may be responsible for the higher activity factor of ternary nanocatalysts by providing a more active site to the reduction reaction.

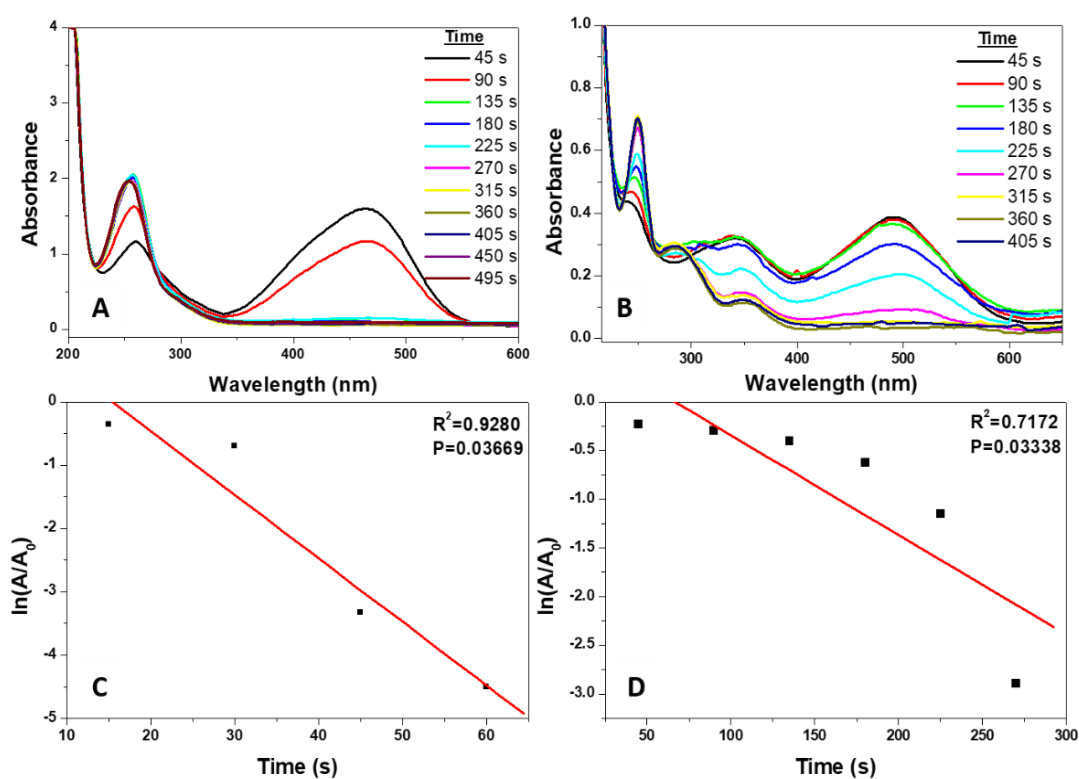


Figure 6.7. UV-vis absorption spectra of catalytic reduction of methyl orange (A) and congo red (B) using TNC-0.04 catalyst in different time intervals. Linear relationship plot of $\ln(A/A_0)$ against time for reduction of methyl orange (C) and congo red (D) using catalyst TNC-0.04.

6.3.4. Optimization of the amount of catalyst for reductive decolourisation of water-insoluble/partially soluble organic azo dyes

Methyl red and Sudan III are two azo dyes exhibiting poor solubility in water.^{34,35} Thus the decolourisation study of the respective azodyes were carried out in

suitable proportion of the ethanol-water mixture. The composition of ethanol in the reaction medium was obtained by checking the minimum volume of ethanol added with water giving maximum solubility to the azo dye. Methyl red is a mono azo dye and sudan III is a bis azo dye. Optimization of nanocatalyst concentration in the reaction mixture was attained by comparing the time for decolourisation of partially aqueous soluble methyl red and almost water insoluble sudan III in different concentrations of catalyst BNC (see **Figure 6.8.**). Different concentrations of BNC nanocatalyst taken for both the azo dyes were 0.02 mg/mL, 0.04 mg/mL, 0.06 mg/mL, and 0.08 mg/mL. A graph was plotted to represent the time required for decolourisation against different concentrations of catalyst BNC. The optimum catalyst concentration was selected as 0.04 mg/mL for methyl red and sudan III, which is the minimum concentration for exhibiting a moderately good and observable reaction rate.

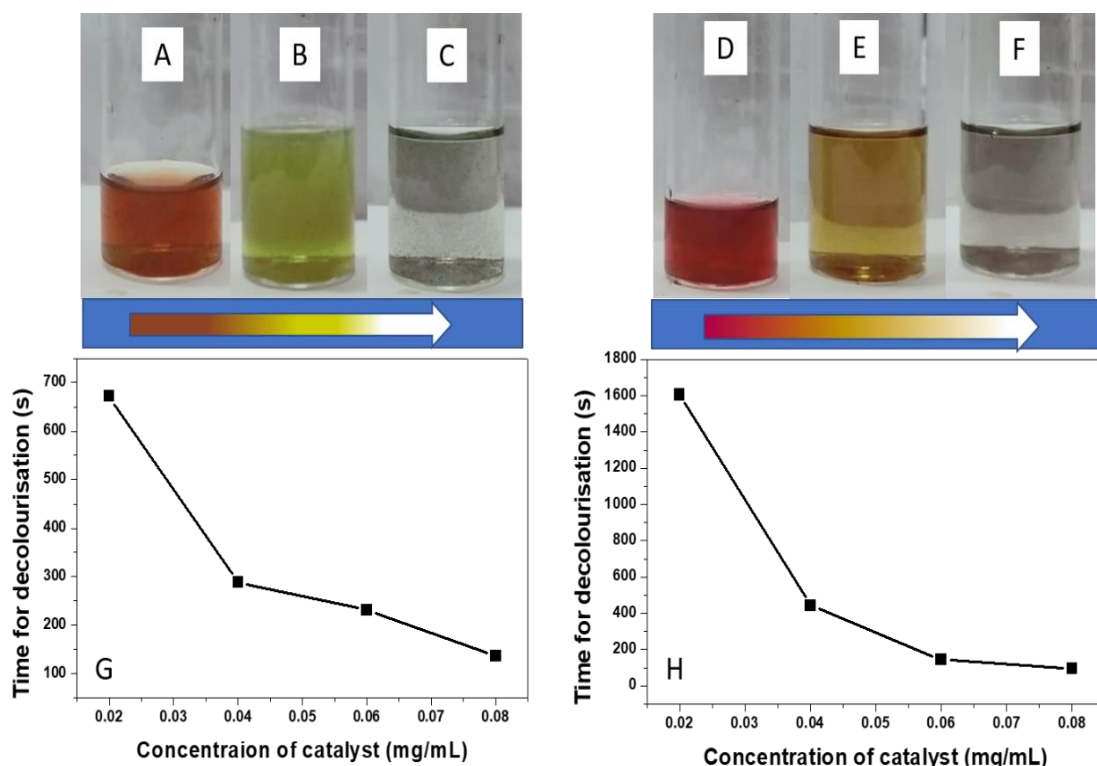


Figure 6.8. Photographs of reductive decolourisation of water-insoluble or partially soluble azo dyes methyl red (initial stage (A), middle stage (B) and final stage (C), and Sudan III (initial stage (D), middle stage (E) and final stage (F). Plots of decolourisation time against the catalyst concentration used for methyl red (G) and sudan III (H).

6.3.5. Kinetics of reductive decolourisation of water-insoluble/partially soluble organic azo dyes

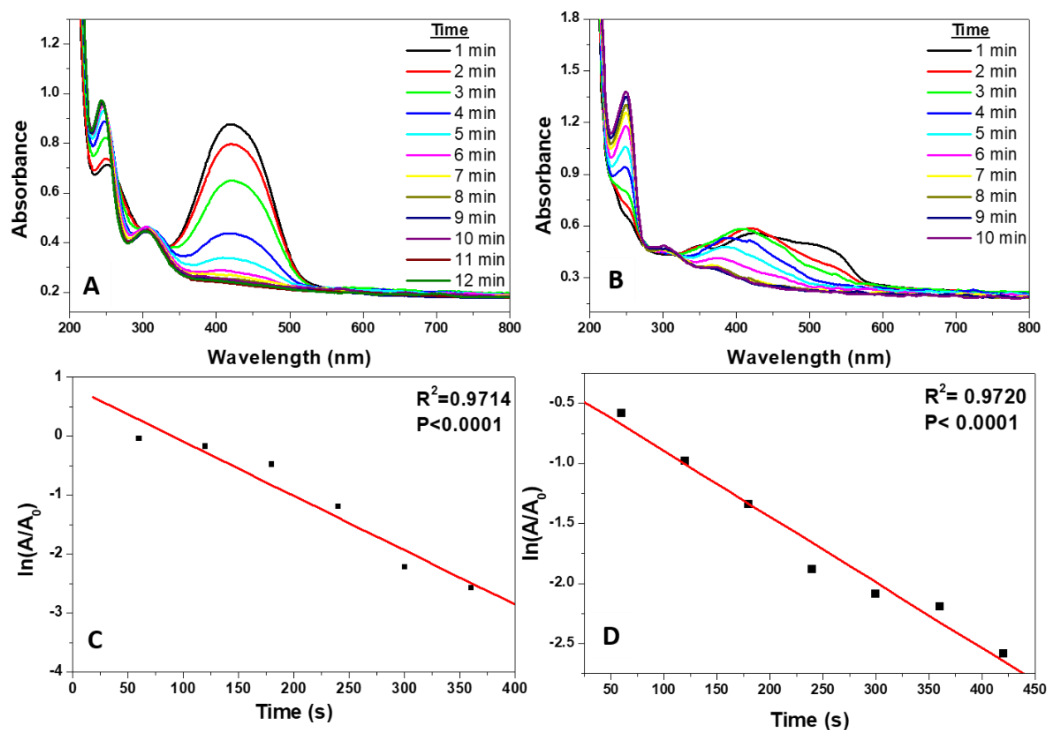


Figure 6.9. UV-vis absorption spectra of catalytic reduction of methyl red (A) and sudan III (B) using BNC-0.04 catalyst in different time intervals. Linear relationship plot of $\ln(A/A_0)$ against time for reduction of methyl red (C) and sudan III (D) using catalyst BNC-0.04.

Catalytic reduction and kinetics of azo dyes such as methyl red (partially soluble in water) and sudan III (almost insoluble in water) were carried out successfully in ethanol-water mixture. Methyl red and Sudan III exhibited good solubility in ethanol. An aqueous mixture of ethanol was selected as the reaction medium instead ethanol alone, as the reductant sodium borohydride exhibited poor solubility in ethanol. The proportion of ethanol and water in the reaction medium was chosen by checking the minimum volume of ethanol to prepare each azo dye solution in the ethanol-water mixture. Solution of methyl red and Sudan III has been respectively prepared using 33% ethanol and 77% ethanol in water. Reductive decolourisation of methyl red and Sudan III was carried out using the same procedure as discussed for water soluble azo

dyes, but in a different reaction medium of ethanol-water mixture. UV-vis absorption spectra of the reaction mixture were recorded after adding sodium borohydride in

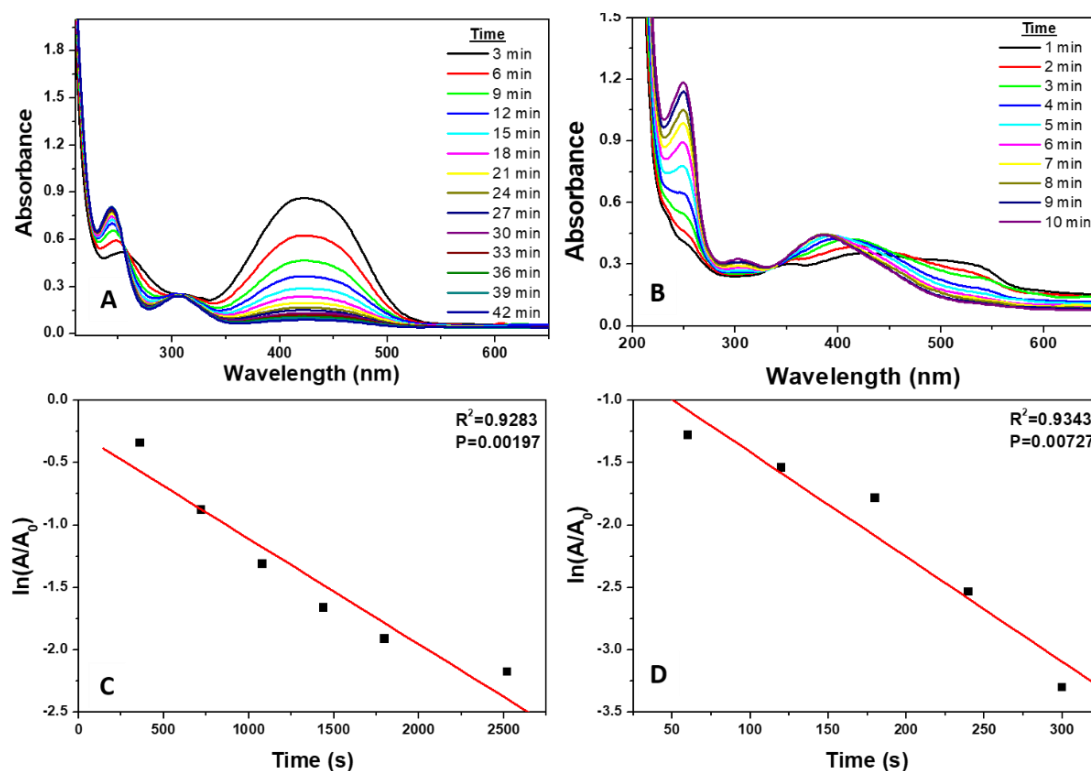


Figure 6.10. UV-vis absorption spectra of catalytic reduction of methyl red (A) and sudan III (B) using TNC-0.04 catalyst in different time intervals. Linear relationship plot of $\ln(A/A_0)$ against time for reduction of methyl red (C) and sudan III (D) using catalyst TNC-0.04.

consecutive time intervals (see **Figure 6.9. A and B**). UV-vis spectra of methyl red exhibited peak corresponding to azo group(s) at absorption maximum 420 nm. The intensity of peak corresponding to azo group decreases with time. As reaction progresses intensity of peak at 244 nm increased in the UV-vis spectra, and intensity became stable after completion of reaction. Time dependent UV-vis spectra of sudan III exhibited gradual disappearance of a broad peak from 511 nm with a successive blue shift to the absorption maximum in each interval. The completion of reaction for methyl red and sudan III using BNC catalyst was observed at 8 min (480 s) and 7 min (420 s), respectively (see **Figure 6.9. A and B**). The corresponding rate constants for BNC catalysed reduction of methyl red and Sudan III were $9.23 \times 10^{-3} \text{ s}^{-1}$ and $5.47 \times 10^{-3} \text{ s}^{-1}$ respectively (see **Figure 6.9. C and D**). The activity factor obtained for BNC-0.04 for catalytic reduction for methyl red was $115.38 \text{ s}^{-1} \text{ g}^{-1}$ and that of Sudan III was 68.37 s^{-1}

Chapter 6

g^{-1} . TNC catalyst was also used for the reductive decolourisation of methyl red and sudan III azo dyes in ethanol-water mixture, repeated using the same procedure conducted for BNC catalysed reduction of corresponding dyes. The completion of the reaction was observed for methyl red reduction was 36 min (2160 s) and that for sudan III reduction was 7 min (420 s) (see **Figure 6.10. A and B**). Corresponding rate constants obtained for reductive decolourisation of methyl red and sudan III were $2.50 \times 10^{-4} \text{ s}^{-1}$ and $8.39 \times 10^{-3} \text{ s}^{-1}$ respectively (see **Figure 6.10. C and D**). Activity factors were also calculated for TNC catalyst as $3.13 \text{ s}^{-1} \text{ g}^{-1}$ and $104.88 \text{ s}^{-1} \text{ g}^{-1}$ respectively for methyl red and sudan III reduction.

Table 6.3. Comparison of present study with literature reported for catalytic decolourisation methyl orange, congo red, methyl red and Sudan III using NaBH_4 as reducing agent, in terms of the amount of azo dye used, amount of NaBH_4 used, the concentration of catalyst, type of catalyst (homogeneous or heterogeneous) and obtained rate constant.

Sl. no.	Dye system	Dye		NaBH_4		Concentration of catalyst used	Catalyst	Rate constant	Ref.
		Concentration	volume	concentration	volume				
1	Methyl orange	1×10^{-5} mg/L	1 mL	1×10^{-2} M	1 mL	9 mg	-	0.1326 min^{-1}	39
2	Methyl orange	1×10^{-4} M	2 mL	1×10^{-1} M	50 μL	0.14 mg/mL	Au@NiAg	0.0266 s^{-1}	2
3	Methyl orange	2×10^{-4} M	500 μL	5×10^{-2} M		0.14 mg/mL (100 μL)	MPCTP-Ag	0.5787 min^{-1}	40
4	Methyl orange	161 μM		68.20 mM		0.60 μM	Ag- γ - Fe_2O_3 -CS	$2.7 \times 10^4 \text{ dm}^3 \text{ mol}^{-1} \text{ s}^{-1}$	41
5	Methyl orange, Congo red	20 μL	0.01 M	250 μL	0.1 M	5 mg/mL (10 μL)	Cu-NMOF/Ce-doped-Mg-Al-LDH	$3.1 \times 10^{-2} \text{ s}^{-1}$	42
6	Methyl orange, Congo red	0.04 mM	3 mL	0.5 mL	0.5 M	10 mg	Ni/TP	$43 \times 10^{-1} \text{ s}^{-1}$	43
7	Congo red	50 mg/L	500 mL	50 mL	0.1 M	250 mg/L	SMt/g-C3N4/Au NPs	5.91 min^{-1}	18
8	Congo red	10 mg/L	5 mL	0.1 mol/L	4 mL	5×10^{-3} mol/L (1 mL)	Ag NPs	-	3
9	Congo red			100 μL	100mM	20 μL	Si@p-RuNP	-	1
10	Methyl red	50 mM	10 mL	1 mM	3 mL	0.31 mg	Ag NPs	$9.68 \times 10^{-3} \text{ s}^{-1}$	44
11	Methyl red, Congo red	1 mM	3 mL	0.5 M	0.5 mM	10 mg	Ag/Gp catalyst	Congo red: $1.84 \times 10^{-3} \text{ s}^{-1}$	45

Catalytic Reduction of Azo dyes and Azobenzene

Sl. no.	Dye system	Dye		NaBH ₄		Concentration of catalyst used	Catalyst	Rate constant	Ref.
		concentration	volume	concentration	volume	concentration			
12	Methyl red	1 mM	2 mL	10 Mm	1 mL	8 mg	Ag NPs doped carbon dots	0.0233 s ⁻¹	46
13	Methyl red, Congo red, Methyl orange	1x10 ⁻⁴ M	1 mL	3 mg		4 mg	Pd NPs@chitosan-MWCNT	-	19
14	Methyl orange	1x10 ⁻⁵ M	1 mL	5x10 ⁻² M	0.1 mL	5 mg	Pd-CS-g-C ₃ N ₄	0.03 s ⁻¹	20
15	Methyl orange	1x10 ⁻⁴ M	2 mL	1x10 ⁻¹ M	2 mL	0.04 mg/mL	BNC-0.04	1.03x10 ⁻² s ⁻¹	Present study
							TNC-0.04	1.00x10 ⁻¹ s ⁻¹	
	Congo red	1x10 ⁻⁴ M	2 mL	1x10 ⁻¹ M	2 mL	0.04 mg/mL	BNC-0.04	5.46x10 ⁻³ s ⁻¹	
							TNC-0.04	1.02x10 ⁻² s ⁻¹	
	Methyl red	1x10 ⁻⁴ M	2 mL	1x10 ⁻¹ M	2 mL	0.04 mg/mL	BNC-0.04	9.23 x10 ⁻³ s ⁻¹	
							TNC-0.04	2.50 x10 ⁻⁴ s ⁻¹	
	Sudan III	1x10 ⁻⁴ M	2 mL	1x10 ⁻¹ M	2 mL	0.04 mg/mL	BNC-0.04	5.47x10 ⁻³ s ⁻¹	
							TNC-0.04	8.39 x10 ⁻³ s ⁻¹	

Comparing the rate constants and activity factor of BNC and TNC catalysed decolourisation reduction reactions of water-soluble azo dyes (methyl orange and congo red) with less soluble azo dyes (methyl red and Sudan III) revealed that water soluble azo dyes exhibited a higher rate of reaction. Relative reductive decolourisation of water-soluble azo dyes indicated that bis-azo dye congo red exhibited a rate constant almost half of methyl orange decolourisation since it was required to reduce two azo groups per molecule in congo red using the same amount of reducing agent. On the contrary, less aqueous soluble bis azo dyes Sudan III exhibited a higher rate of reductive decolourisation reaction than mono azo dye methyl red. Methyl red consists of intramolecular hydrogen bonding between the azo group's nitrogen and carboxylic acid group present in its ortho position. Therefore, a decrease in rate of reaction for methyl red reduction may be due to the intramolecular hydrogen bond, which could restrain the reactive site of the azo bond from participating in the reaction.^{36,37} Comparison study was conducted for reductive decolourisation of azo dyes such as methyl orange, congo red, methyl red and Sudan III with previous literature reports on catalytic reduction/decolourisation of corresponding dyes using NaBH₄ reductant (see **Table 6.3**).³⁸⁻⁴⁵ Comparing concentration and volume of azo dyes and reductant used, with other works in literature, the present study was noted to utilize a very minimum amount

of catalyst concentration (0.04 mg/mL in 2 mL initial azo dye solution taken). The rate constants and activity factor measured on the reduction of each azo dye were found as very competent with other literature reports. Among the rate constants obtained in the present study, the reduction of water-soluble mono azo dye methyl orange using TNC catalyst was found to have the highest value. The aqueous insoluble azo dyes were reduced in the ethanol-water mixture, which is also a remarkable green solvent mixture for the sodium borohydride reduction.

6.3.6. Kinetics of catalytic reduction of azobenzene, recyclability studies and mechanism

Catalytic reduction of azobenzene was conducted using nanocatalysts concentration BNC-0.04 and TNC-0.04 with the reducing agent NaBH_4 in ethanol-water mixture. The visible colour change was not observable for azobenzene reduction in the low concentration (1×10^{-4} M) under study. UV-vis absorption spectroscopy was used to analyse the rate of reduction of azobenzene using the BNC and TNC catalyst system (see **Figure 6.11. A and C**). Azobenzene solution (1×10^{-4} M, 50 mL) was prepared in 33% ethanol solution in water. The reduction reaction was completed in ~ 240 s and ~ 120 s using BNC-0.04 catalyst and TNC-0.04 catalyst, respectively, by treating with the same volume of 1×10^{-1} M NaBH_4 . Kinetic analysis was further carried out using linear regression fit of the graph plotted for $\ln(A/A_0)$ against the progress of the reaction (see **Figure 6.11 B and D**). The reaction rate constant and corresponding activity factor using BNC-0.04 nanocatalyst was $1.025 \times 10^{-2} \text{ s}^{-1}$ and $128.13 \text{ s}^{-1} \text{ g}^{-1}$, and for TNC-0.04 nanocatalyst, it was $2.586 \times 10^{-1} \text{ s}^{-1}$ and $3232.50 \text{ s}^{-1} \text{ g}^{-1}$, respectively. Therefore, the ternary nanocomposite exhibited a higher rate constant than the binary nanocatalyst for azobenzene reduction. Large-scale reduction of azobenzene was achieved as a model reaction to azo compounds, by taking azobenzene (0.10 g, 0.027 M, 25 mL) and on treatment with NaBH_4 solution (2.027 M, 25 mL) in the presence of BNC-0.18 (see **Figure 6.11. C**). The progress of the reaction was monitored as a gradual change of the reddish orange colour of azobenzene solution to the colourless product. The completion of the reaction was monitored as the time at which reaction mixture get decolourised. The completion of the reaction for the large-scale reduction was accomplished within a short reaction time of 15 minutes, which promises the future utilisation of a catalyst for industrial-scale running of reductive decolourisation of azo compounds.

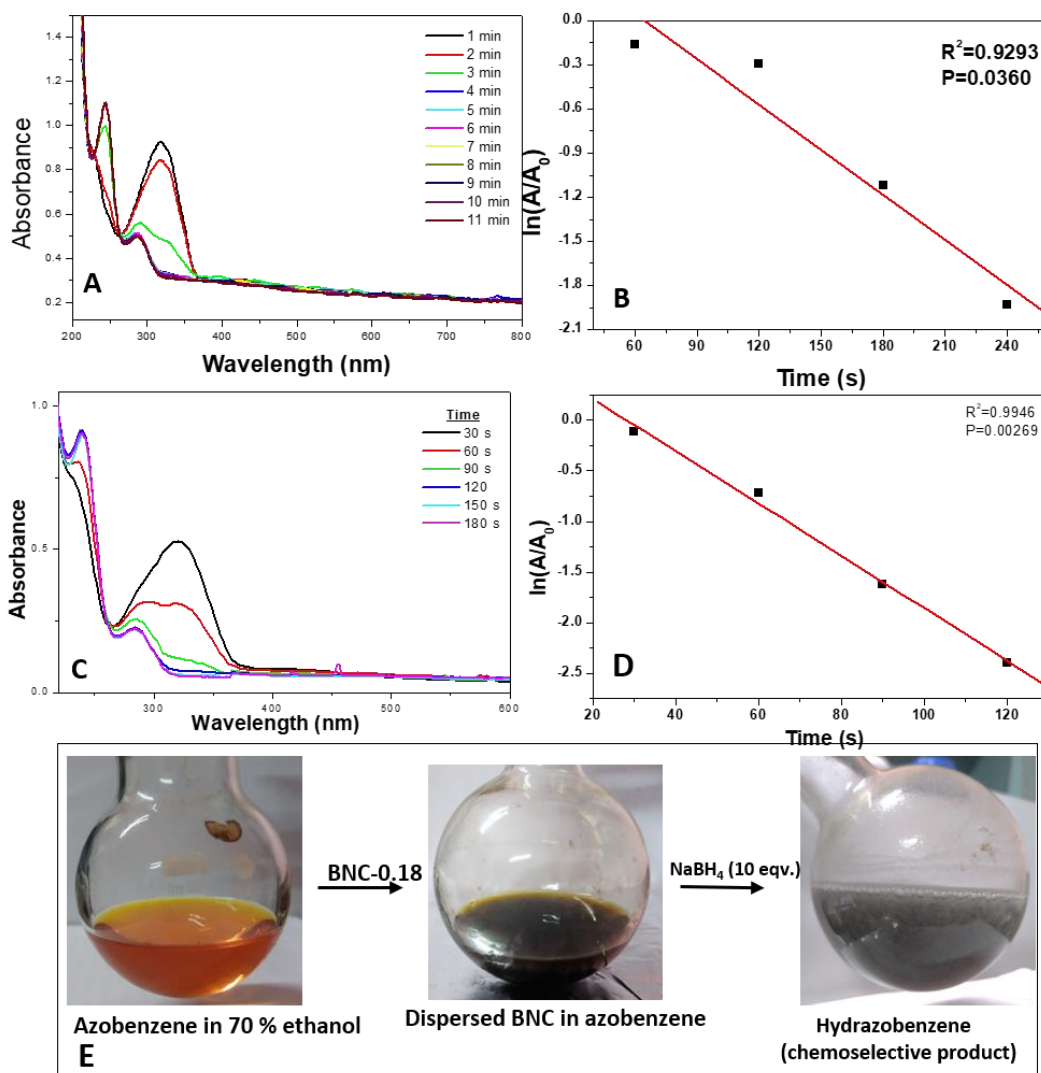


Figure 6.11. UV-vis absorption spectra of catalytic reduction of azobenzene using BNC-0.04 (A) catalyst and TNC-0.04 (C) in different time intervals. Linear relationship plot of $\ln(A/A_0)$ against time for reduction of azobenzene using catalyst BNC-0.04 (B) catalyst and TNC-0.04 (D). Large scale reduction of azobenzene (E)

The recycling studies of the nanocatalysts TNC and BNC were carried out, and catalytic efficiency in the recycling process was recorded via UV-vis absorption spectra (see **Figure 6.12.**). Conversion percentage of azobenzene reduction product was calculated using UV-vis spectra. BNC was recycled and analysed for five consecutive cycles and TNC for six consecutive cycles by fixing the reaction time as 10 min for each cycle. Here catalyst was recovered by centrifugation and reused for the next catalytic cycle after washing with water. BNC has shown catalytic conversion of 70.78 % in the 5th catalytic cycle, whereas TNC has shown 83.63 % conversion in the 6th cycle

Chapter 6

in identical conditions. Catalytic conversion (%) for successive cycles indicated better TNC efficiency than BNC for higher catalytic cycles. The conversion (%) obtained from the UV-vis absorbance spectroscopy have revealed that nanocatalyst TNC activates the reaction comparably greater than BNC in multiple cycles. Nanocatalysts were recovered from the reaction mixture via centrifugation and washing before subsequent uses.

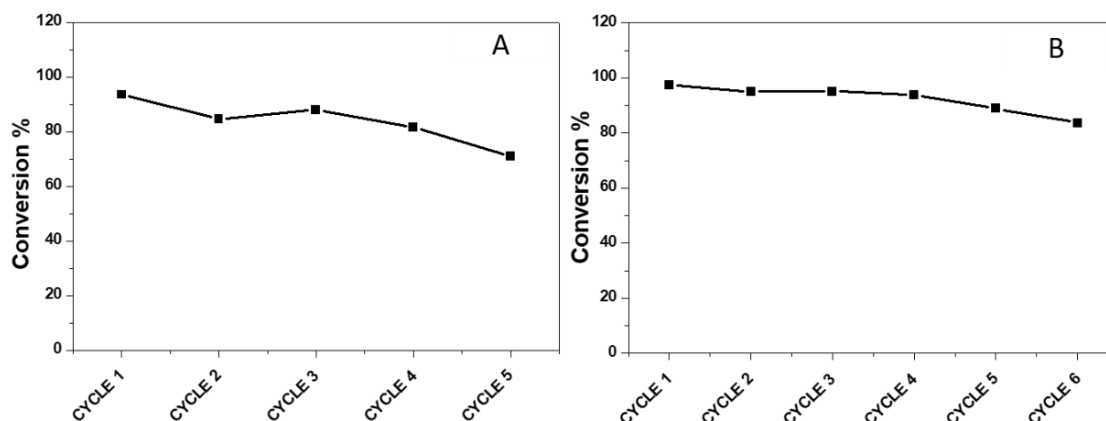


Figure 6.12. Catalytic conversion percentage of BNC-0.04 (A) and TNC-0.04 (B) in successive catalytic cycles of azobenzene reduction.

The reaction product(s) obtained after large-scale catalytic reduction of azobenzene was isolated by ether extraction. The product obtained was a colourless solid that turned pale yellow with time. Mechanistic investigation of isolated product was carried out using ^1H NMR spectroscopy and high-resolution mass spectroscopy. Expected products of azobenzene reduction are hydrazobenzene, aniline, or both. Hydrazobenzene is formed due to the chemoselective hydrogenation of azobenzene, whereas aniline is the product of uncontrollable hydrogenation of azobenzene. Both these products individually contribute to different applications having synthetic importance in organic chemistry. The preparation of selectively formed hydrazobenzene is synthetically more prominent because of one step economically viable preparation strategy. The purity of the product and the obtained yield are also important for consideration. While analysing the isolated product of catalytic reduction

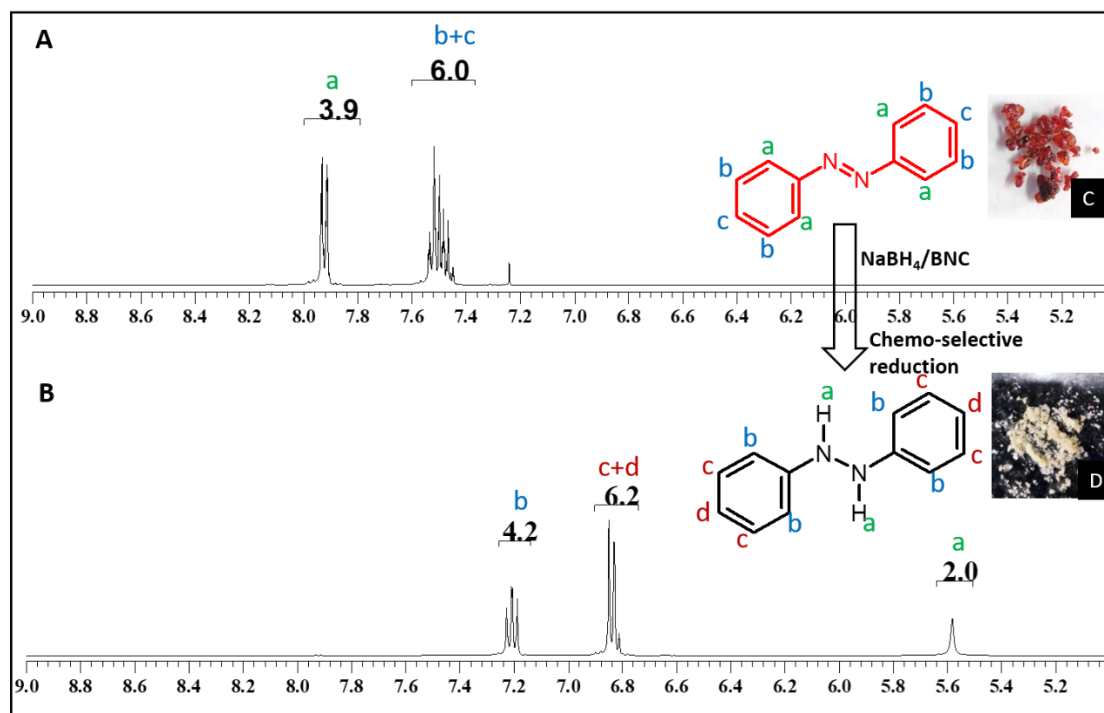


Figure 6.13. NMR spectra of azobenzene (A) and catalytic reduction product of azobenzene (B). Photographs of purchased azobenzene (C) and isolated product of azobenzene after catalytic reduction with BNC-0.18 (D)

of azobenzene, the melting point of the isolated product was determined as 125°C (the solid started to melt at 122°C and melted completely at 125°C), which is comparable to the melting point of hydrazobenzene. Product determination was carried out with ^1H NMR spectroscopy in deuteriated chloroform. ^1H NMR spectra of azobenzene (AB) and reduction product (AB-P) were recorded separately (see **Figure 6.13**). ^1H NMR spectra (400 MHz, CHCl_3 , δ ppm) of AB was 7.5 (m, 6H) and 7.95 (d, 4H). ^1H NMR spectra (400 MHz, CHCl_3 , δ ppm) of AB-P were 5.57 (s, 2H), 6.85 (d, 6H) and 7.2 (t, 4H). The peak shifts in ^1H NMR spectra and the corresponding number of hydrogens for peak intensities of azobenzene reduction product AB-P was observed as that of hydrazobenzene.⁴⁶ High-resolution mass spectra of AB-P were recorded to confirm the formation of hydrazobenzene product.^{47,48} AB-P exhibited mass spectra peaks having m/z values 168.06 (highest abundant peak), 185.11 (second highest abundance) and 108.07. The peak at 185.11 can be attributed to protonated hydrazobenzene and further degradations occur to obtain other peaks at lower m/z values 168.06 and 108.07. Positions of HR-MS peaks are the same in position as observed for hydrazobenzene in literature, and this confirmed the formation of 100 % of hydrazobenzene product as a

result of catalytic reduction of azobenzene. Solvents active hydrogen combined with sodium borohydride liberate hydrogen molecules and reduce the azobenzene reactant with the help of relay of electrons from NaBH_4 to reactant moiety through conducting nanocatalyst. The plausible mechanism of azobenzene reduction using NaBH_4 as a reducing agent with TNC or BNC as a catalyst, is illustrated in **Figure 6.14**. (with reference to the mechanism proposed for the reduction of nitrophenol discussed in chapter 5).

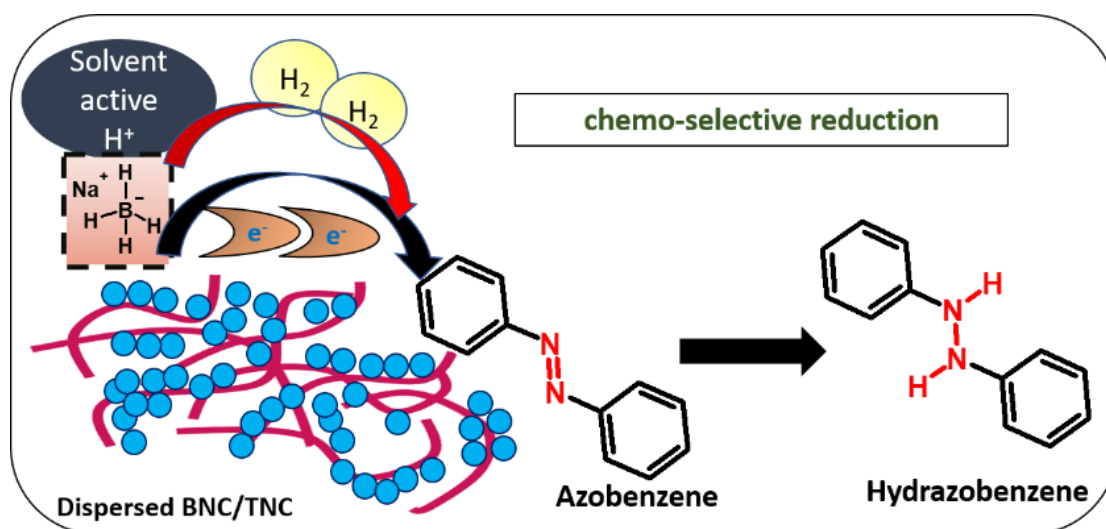


Figure 6.14. Illustration of plausible mechanism for catalytic chemoselective hydrogenation of azobenzene

Large-scale reduction of azobenzene can be taken as a model reaction for azocompounds decolourisation study using sodium borohydride reductant and heterogeneous silver nanocatalysts. Selective hydrogenation of azobenzene to hydrazobenzene by the utilisation of BNC and similar activity using TNC nanocatalysts assures the future industrial-scale treatment. The utilisation of a green solvent ethanol-water mixture to reduce less polar organic azo compounds is attractive factor for reduction. Kinetic analyses revealed that higher performance using ternary nanocatalyst TNC than binary nanocatalyst BNC for reductive treatment of azo dyes such as methyl orange, congo red and the less water-soluble azo dye sudan III. Binary nanocatalyst BNC is more suitable for the reductive treatment of methyl red azo dye (see **Figure 6.15**)

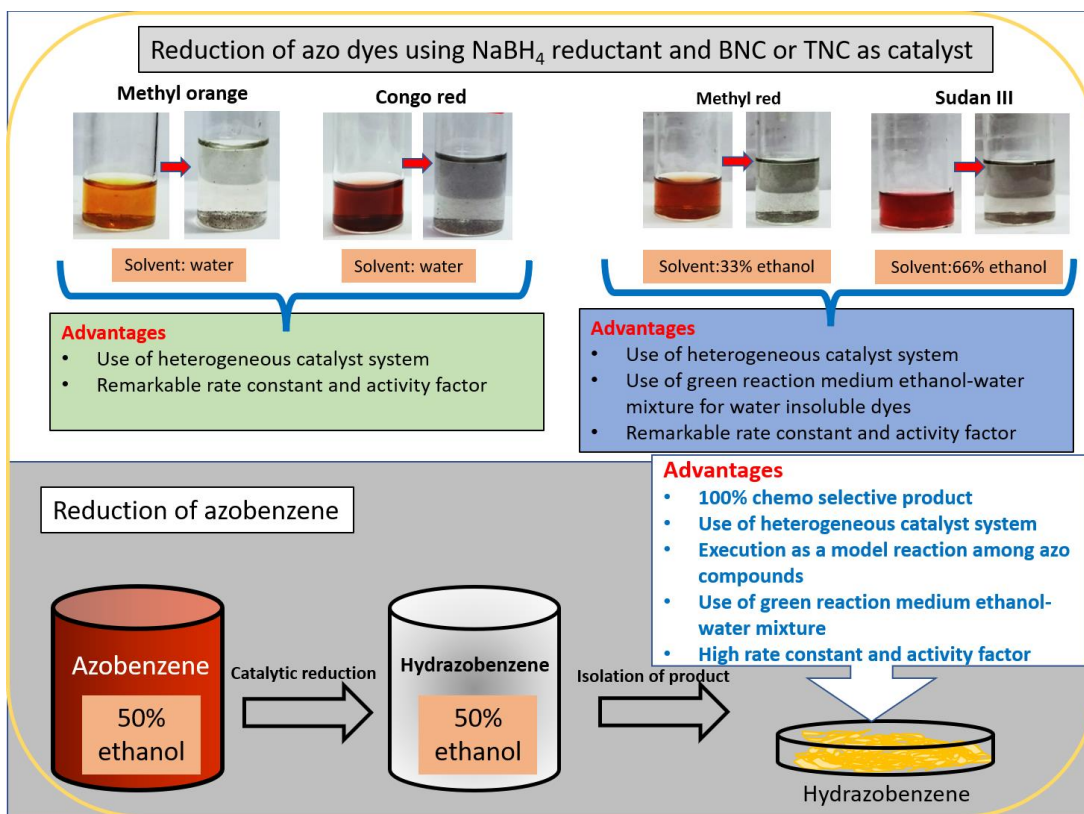


Figure 6.15. Outline of reductive treatment of azo compounds carried out in present study and their advantages.

6.4. Conclusion

Decolourisation of azo dyes by catalytic reduction was carried out with NaBH_4 as a reducing agent and in the presence of a dispersed form of the binary nanocatalyst BNC or the ternary nanocatalyst TNC. Decolourisation of water-soluble azo dyes methyl orange and congo red was conducted in an aqueous medium and that of less water soluble azo dyes methyl red and Sudan III was achieved in a suitable proportion of ethanol-water green solvent mixture. The rate constants of decolourisation was obtained for methyl orange, congo red, methyl red and sudan III were $1.03 \times 10^{-2} \text{ s}^{-1}$, $5.46 \times 10^{-3} \text{ s}^{-1}$, $9.23 \times 10^{-3} \text{ s}^{-1}$ and $5.47 \times 10^{-3} \text{ s}^{-1}$ respectively by using nanocatalyst BNC-0.04. At the same time, the rate of decolourisation using nanocatalyst TNC-0.04 were $1.00 \times 10^{-1} \text{ s}^{-1}$, $1.02 \times 10^{-2} \text{ s}^{-1}$, $2.50 \times 10^{-4} \text{ s}^{-1}$ and $8.39 \times 10^{-3} \text{ s}^{-1}$ for methyl orange, congo red, methyl red and Sudan III respectively. Chemoselective catalytic reduction of azo benzene was conducted in 33% ethanol-water mixture with the reducing agent NaBH_4 and BNC-0.04 as catalyst. The reduction rate was obtained as $1.025 \times 10^{-2} \text{ s}^{-1}$ and the corresponding activity factor as $128.13 \text{ s}^{-1} \text{ g}^{-1}$. The investigation of isolated product was

conducted with ^1H NMR spectroscopy and high-resolution mass spectroscopy which revealed formation of 100% pure and selective product hydrazobenzene. High concentration reduction of azobenzene was also attained in a very short time of 10 minutes. HRMS fragmentation spectrum of AB-P has observed with the molecular ion values 168, 185 and 180 as m/z values confirming the formation of hydrazobenzene as the product in azobenzene reduction.

References

1. Sahoo, A.; Patra, S. A Combined Process for the Degradation of Azo-Dyes and Efficient Removal of Aromatic Amines Using Porous Silicon Supported Porous Ruthenium Nanocatalyst. *ACS Appl. Nano Mater.* **2018**, *1* (9), 5169–5178. <https://doi.org/10.1021/acsanm.8b01152>.
2. Kulkarni, S.; Jadhav, M.; Raikar, P.; Raikar, S.; Raikar, U. Core-Shell Novel Composite Metal Nanoparticles for Hydrogenation and Dye Degradation Applications. *Ind. Eng. Chem. Res.* **2019**, *58* (9), 3630–3639. <https://doi.org/10.1021/acs.iecr.8b06094>.
3. Ghiorghita, C. A.; Dragan, E. S.; Bucatariu, F.; Schwarz, D.; Blegescu, C.; Mihai, M. Green Synthesis of Ag Nanoparticles with Uncommon Behaviour towards NaBH_4 in Presence of Congo Red Using Polyelectrolyte Multilayers Containing Sodium Carboxymethyl Cellulose. *Colloids Surfaces A Physicochem. Eng. Asp.* **2020**, *585*. <https://doi.org/10.1016/j.colsurfa.2019.124157>
4. Vidhu, V. K.; Philip, D. Catalytic Degradation of Organic Dyes Using Biosynthesized Silver Nanoparticles. *Micron* **2014**, *56*, 54–62. <https://doi.org/10.1016/j.micron.2013.10.006>.
5. Pielesz, A.; Baranowska, I.; Rybak, A.; Włochowicz, A. Detection and Determination of Aromatic Amines as Products of Reductive Splitting from Selected Azo Dyes. *Ecotoxicol. Environ. Saf.* **2002**, *53* (1), 42–47. <https://doi.org/10.1006/eesa.2002.2191>.
6. Peng, W.; Ding, F.; Peng, Y. K.; Jiang, Y. T.; Zhang, L. Binding Patterns and Structure-Affinity Relationships of Food Azo Dyes with Lysozyme: A Multitechnique Approach. *J. Agric. Food Chem.* **2013**, *61* (50), 12415–12428. <https://doi.org/10.1021/jf4039327>.
7. Al-Tohamy, R.; Ali, S. S.; Li, F.; Okasha, K. M.; Mahmoud, Y. A. G.; Elsamahy, T.; Jiao, H.; Fu, Y.; Sun, J. A Critical Review on the Treatment of Dye-Containing Wastewater: Ecotoxicological and Health Concerns of Textile Dyes and Possible Remediation Approaches for Environmental Safety. *Ecotoxicol. Environ. Saf.* **2022**, *231*. <https://doi.org/10.1016/j.ecoenv.2021.113160>.
8. Mezohegyi, G.; van der Zee, F. P.; Font, J.; Fortuny, A.; Fabregat, A. Towards Advanced Aqueous Dye Removal Processes: A Short Review on the Versatile Role of Activated Carbon. *J. Environ. Manage.* **2012**, *102*, 148–164. <https://doi.org/10.1016/j.jenvman.2012.02.021>.
9. Stolz, A. Basic and Applied Aspects in the Microbial Degradation of Azo Dyes. *Appl. Microbiol. Biotechnol.* **2001**, *56* (1–2), 69–80. <https://doi.org/10.1007/s002530100686>.
10. Sun, L.; Mo, Y.; Zhang, L. A Mini Review on Bio-Electrochemical Systems for the Treatment of Azo Dye Wastewater: State-of-the-Art and Future Prospects. *Chemosphere* **2022**, *294*. <https://doi.org/10.1016/j.chemosphere.2022.133801>.
11. Hu, C.; Hu, X.; Wang, L.; Qu, J.; Wang, A. Visible-Light-Induced Photocatalytic Degradation of Azodyes in Aqueous AgI/TiO₂ Dispersion. *Environ. Sci. Technol.* **2006**, *40* (24), 7903–7907. <https://doi.org/10.1021/es061599r>.
12. Zhang, W.; Liu, N.; Xu, L.; Qu, R.; Chen, Y.; Zhang, Q.; Liu, Y.; Wei, Y.; Feng, L. Polymer-Decorated Filter Material for Wastewater Treatment: In Situ Ultrafast Oil/Water

- Emulsion Separation and Azo Dye Adsorption. *Langmuir* **2018**, *34* (44), 13192–13202. <https://doi.org/10.1021/acs.langmuir.8b02834>.
13. Vijayaraghavan, R.; Vedaraman, N.; Surianarayanan, M.; MacFarlane, D. R. Extraction and Recovery of Azo Dyes into an Ionic Liquid. *Talanta* **2006**, *69* (5), 1059–1062. <https://doi.org/10.1016/j.talanta.2005.12.042>.
 14. Lučić, M.; Milosavljević, N.; Radetić, M.; Šaponjić, Z.; Radoičić, M.; Krušić, M. K. The Potential Application of TiO₂/Hydrogel Nanocomposite for Removal of Various Textile Azo Dyes. *Sep. Purif. Technol.* **2014**, *122*, 206–216. <https://doi.org/10.1016/j.seppur.2013.11.002>.
 15. Chen, W.; Lu, W.; Yao, Y.; Xu, M. Highly Efficient Decomposition of Organic Dyes by Aqueous-Fiber Phase Transfer and in Situ Catalytic Oxidation Using Fiber-Supported Cobalt Phthalocyanine. *Environ. Sci. Technol.* **2007**, *41* (17), 6240–6245. <https://doi.org/10.1021/es070002k>.
 16. El-Subruiti, G. M.; Eltaweil, A. S.; Sallam, S. A. Synthesis of Active MFe₂O₄/γ-Fe₂O₃ Nanocomposites (Metal = Ni or Co) for Reduction of Nitro-Containing Pollutants and Methyl Orange Degradation. *Nano* **2019**. <https://doi.org/10.1142/S179329201950125X>.
 17. Kurtan, U.; Amir, M.; Yildiz, A.; Baykal, A. Synthesis of Magnetically Recyclable MnFe₂O₄@SiO₂@Ag Nanocatalyst: Its High Catalytic Performances for Azo Dyes and Nitro Compounds Reduction. *Appl. Surf. Sci.* **2016**, *376*, 16–25. <https://doi.org/10.1016/j.apsusc.2016.02.120>.
 18. Zhang, P.; Wang, F.; Qin, Y.; Wang, N. Exfoliated Graphitic Carbon Nitride Nanosheets/Gold Nanoparticles/Spherical Montmorillonite Ternary Porous Heterostructures for the Degradation of Organic Dyes. *ACS Appl. Nano Mater.* **2020**, *3* (8), 7847–7857. <https://doi.org/10.1021/acsanm.0c01355>.
 19. Sargin, I.; Baran, T.; Arslan, G. Environmental Remediation by Chitosan-Carbon Nanotube Supported Palladium Nanoparticles: Conversion of Toxic Nitroarenes into Aromatic Amines, Degradation of Dye Pollutants and Green Synthesis of Biaryls. *Sep. Purif. Technol.* **2020**, *247*. <https://doi.org/10.1016/j.seppur.2020.116987>.
 20. Yılmaz Baran, N.; Baran, T.; Çalışkan, M. Production of Pd Nanoparticles Embedded on Micro-Sized Chitosan/Graphitic Carbon Nitride Hybrid Spheres for Treatment of Environmental Pollutants in Aqueous Medium. *Ceram. Int.* **2021**, *47* (19), 27736–27747. <https://doi.org/10.1016/j.ceramint.2021.06.199>.
 21. Song, M.; Zhou, H.; Wang, G.; Ma, B.; Jiang, Y.; Yang, J.; Huo, C.; Wang, X. C. Visible-Light-Promoted Diboron-Mediated Transfer Hydrogenation of Azobenzenes to Hydrazobenzenes. *J. Org. Chem.* **2021**, *86* (6), 4804–4811. <https://doi.org/10.1021/acs.joc.1c00394>.
 22. Abdullah, H.; Kuo, D. H.; Gultom, N. S. NN Bond Cleavage of Azobenzene: Via Photocatalytic Hydrogenation with Dy-Doped Zn(O,S): The Progress from Hydrogen Evolution to Green Chemical Conversion. *Catal. Sci. Technol.* **2019**, *9* (10), 2651–2663. <https://doi.org/10.1039/c9cy00502a>.
 23. Guillamón, E.; Oliva, M.; Andrés, J.; Llusar, R.; Pedrajas, E.; Safont, V. S.; Algarra, A. G.; Basallote, M. G. Catalytic Hydrogenation of Azobenzene in the Presence of a Cuboidal Mo₃S₄Cluster via an Uncommon Sulfur-Based H₂Activation Mechanism. *ACS Catal.* **2021**, *11* (2), 608–614. <https://doi.org/10.1021/acscatal.0c05299>.
 24. Abdullah, H.; Ko, Y. R.; Kuo, D. H.; Gultom, N. S. Effects of Tin in La-Sn-Codoped Zn(O,S) Photocatalyst to Strongly Cleave the Azo Bond in Azobenzene with in Situ Generated Hydrogen. *ACS Appl. Mater. Interfaces* **2020**, *12* (14), 16186–16199. <https://doi.org/10.1021/acsami.9b19885>.
 25. Sridhara, M. B.; Srinivasa, G. R.; Gowda, D. C. Ammonium Chloride Mediated Reduction of Azo Compounds to Hydrazo Compounds. *ChemInform* **2004**, *35* (34). <https://doi.org/10.1002/chin.200434083>.
 26. Léonard, E.; Mangin, F.; Villette, C.; Billamboz, M.; Len, C. Azobenzenes and Catalysis. *Catal. Sci. Technol.* **2016**, *6* (2), 379–398. <https://doi.org/10.1039/c4cy01597e>.

27. Hu, M.; Liu, Y.; Liang, Y.; Dong, T.; Kong, L.; Bao, M.; Wang, Z. X.; Peng, B. Dearomative Di- and Trifunctionalization of Aryl Sulfoxides via [5,5]-Rearrangement. *Nat. Commun.* **2022**, *13* (1). <https://doi.org/10.1038/s41467-022-32426-6>.
28. Prasad, H. S.; Gowda, S.; Abiraj, K.; Gowda, D. C. Catalytic Transfer Hydrogenation of Azo Compounds to Hydrazo Compounds Using Inexpensive Commercial Zinc Dust and Hydrazinium Monoformate. *Synth. React. Inorg. Met. Chem.* **2003**, *33* (4), 717–724. <https://doi.org/10.1081/SIM-120020334>.
29. Serhan, M.; Sprowls, M.; Jackemeyer, D.; Long, M.; Perez, I. D.; Maret, W.; Tao, N.; Forzani, E. Total Iron Measurement in Human Serum with a Smartphone. *AIChE Annu. Meet. Conf. Proc.* **2019**, 2019-November. <https://doi.org/10.1039/x0xx00000x>.
30. Pei, L.; Wang, J.; Fan, C.; Ge, H.; Waclawik, E. R.; Tan, H.; Liu, M.; Gu, X.; Zheng, Z. The Key Role of Photoisomerisation for the Highly Selective Photocatalytic Hydrogenation of Azobenzene to Hydrazobenzene over NaNbO₃ Fibre Photocatalyst. *J. Photochem. Photobiol. A Chem.* **2020**, *400*. <https://doi.org/10.1016/j.jphotochem.2020.112655>.
31. Hong, J. E.; Jung, Y.; Park, Y.; Park, Y. Highly Selective Synthesis of Hydrazoarenes from Nitroarenes via Polystyrene-Supported Au-Nanoparticle-Catalyzed Reduction: Application to Azoarenes, Aminoarenes, and 4,4'-Diaminobiaryls. *ACS Omega* **2020**, *5* (13), 7576–7583. <https://doi.org/10.1021/acsomega.0c00402>.
32. (a) Ding, F.; Zhang, Y.; Zhao, R.; Jiang, Y.; Bao, R. L. Y.; Lin, K.; Shi, L. B(C₆F₅)₃-Promoted Hydrogenations of N-Heterocycles with Ammonia Borane. *Chem. Commun.* **2017**, *53* (66), 9262–9264. <https://doi.org/10.1039/c7cc04709f>. (b) Chacón-Terán, M. A.; Rodríguez-Lugo, R. E.; Wolf, R.; Landaeta, V. R. Transfer Hydrogenation of Azo Compounds with Ammonia Borane Using a Simple Acyclic Phosphite Precatalyst. *Eur. J. Inorg. Chem.* **2019**, 2019 (39–40), 4336–4344. <https://doi.org/10.1002/ejic.201900572>. (c) Wang, F.; Planas, O.; Cornella, J. Bi(I)-Catalyzed Transfer-Hydrogenation with Ammonia-Borane. *J. Am. Chem. Soc.* **2019**, *141* (10), 4235–4240. <https://doi.org/10.1021/jacs.9b00594>.
33. Hartwig, J. F. Regioselectivity of the Borylation of Alkanes and Arenes. *Chem. Soc. Rev.* **2011**, *40* (4), 1992–2002. <https://doi.org/10.1039/c0cs00156b>.
34. Grebenkin, S. Y.; Syutkin, V. M.; Baranov, D. S. Mutual Orientation of the N→π* and π → Π* Transition Dipole Moments in Azo Compounds: Determination by Light-Induced Optical Anisotropy. *J. Photochem. Photobiol. A Chem.* **2017**, *344*, 1–7. <https://doi.org/10.1016/j.jphotochem.2017.04.031>.
35. Prasad, H. S.; Gowda, S.; Abiraj, K.; Gowda, D. C. Catalytic Transfer Hydrogenation of Azo Compounds to Hydrazo Compounds Using Inexpensive Commercial Zinc Dust and Hydrazinium Monoformate. *Synth. React. Inorg. Met. Chem.* **2003**, *33* (4), 717–724. <https://doi.org/10.1081/SIM-120020334>.
36. Ros, A.; Fernández, R.; Lassaletta, J. M. Functional Group Directed C-H Borylation. *Chem. Soc. Rev.* **2014**, *43* (10), 3229–3243. <https://doi.org/10.1039/c3cs60418g>.
37. Neeve, E. C.; Geier, S. J.; Mkhallid, I. A. I.; Westcott, S. A.; Marder, T. B. Diboron(4) Compounds: From Structural Curiosity to Synthetic Workhorse. *Chem. Rev.* **2016**, *116* (16), 9091–9161. <https://doi.org/10.1021/acs.chemrev.6b00193>.
38. Sahin, M.; Gubbuk, I. H. Green Synthesis of Palladium Nanoparticles and Investigation of Their Catalytic Activity for Methylene Blue, Methyl Orange and Rhodamine B Degradation by Sodium Borohydride. *React. Kinet. Mech. Catal.* **2022**, *135* (2), 999–1010. <https://doi.org/10.1007/s11144-022-02185-y>.
39. Shi, X.; Huang, C.; Zheng, Z.; Zhong, B.; Ding, G.; Li, J.; You, L.; Wang, S. Preparation of Magnetically Recoverable MPCTP-Ag Composite Nanoparticles and Their Application as High-Performance Catalysts. *Langmuir* **2021**, *37* (34), 10249–10258. <https://doi.org/10.1021/acs.langmuir.1c00944>.
40. Kaloti, M.; Kumar, A. Sustainable Catalytic Activity of Ag-Coated Chitosan-Capped γ-Fe₂O₃ Superparamagnetic Binary Nanohybrids (Ag-γ-Fe₂O₃@CS) for the Reduction of Environmentally Hazardous Dyes - A Kinetic Study of the Operating Mechanism

- Analyzing Methyl Orange Reduction. *ACS Omega* **2018**, *3* (2), 1529–1545. <https://doi.org/10.1021/acsomega.7b01498>.
41. Iqbal, K.; Iqbal, A.; Kirillov, A. M.; Liu, W.; Tang, Y. Hybrid Metal-Organic-Framework/Inorganic Nanocatalyst toward Highly Efficient Discoloration of Organic Dyes in Aqueous Medium. *Inorg. Chem.* **2018**, *57* (21), 13270–13278. <https://doi.org/10.1021/acs.inorgchem.8b01826>.
 42. Ismail, M.; Khan, M. I.; Khan, S. B.; Akhtar, K.; Khan, M. A.; Asiri, A. M. Catalytic Reduction of Picric Acid, Nitrophenols and Organic Azo Dyes via Green Synthesized Plant Supported Ag Nanoparticles. *J. Mol. Liq.* **2018**, *268*, 87–101. <https://doi.org/10.1016/j.molliq.2018.07.030>.
 43. Barman, K.; Chowdhury, D.; Baruah, P. K. Bio-Synthesized Silver Nanoparticles Using Zingiber Officinale Rhizome Extract as Efficient Catalyst for the Degradation of Environmental Pollutants. *Inorg. Nano-Metal Chem.* **2020**, *50* (2), 57–65. <https://doi.org/10.1080/24701556.2019.1661468>.
 44. Ismail, M.; Khan, M. I.; Khan, M. A.; Akhtar, K.; Asiri, A. M.; Khan, S. B. Plant-Supported Silver Nanoparticles: Efficient, Economically Viable and Easily Recoverable Catalyst for the Reduction of Organic Pollutants. *Appl. Organomet. Chem.* **2019**, *33* (8). <https://doi.org/10.1002/aoc.4971>.
 45. Bhagavanth, R. R.; Dadigala, R.; Bandi, R.; Seku, K.; Koteswararao, D.; Mangatayaru K, G.; Shalan, A. E. Microwave-Assisted Preparation of a Silver Nanoparticles/N-Doped Carbon Dots Nanocomposite and Its Application for Catalytic Reduction of Rhodamine B, Methyl Red and 4-Nitrophenol Dyes. *RSC Adv.* **2021**, *11* (9), 5139–5148. <https://doi.org/10.1039/d0ra10679h>.
 46. Zhou, H.; Fan, R.; Yang, J.; Sun, X.; Liu, X.; Wang, X. C. N, N-Diisopropylethylamine-Mediated Electrochemical Reduction of Azobenzenes in Dichloromethane. *J. Org. Chem.* **2022**. <https://doi.org/10.1021/acs.joc.2c01949>.
 47. Shine, H. J.; Zmuda, H.; Park, K. H.; Kwart, H.; Horgan, A. G.; Brechbiel, M. Benzidine Rearrangements. 16. The Use of Heavy-Atom Kinetic Isotope Effects in Solving the Mechanism of the Acid-Catalyzed Rearrangement of Hydrazobenzene. The Concerted Pathway to Benzidine and the Nonconcerted Pathway to Diphenylene. *J. Am. Chem. Soc.* **1982**, *104* (9), 2501–2509. <https://doi.org/10.1021/ja00373a028>.
 48. Yu, K.; Zhang, H.; He, J.; Zare, R. N.; Wang, Y.; Li, L.; Li, N.; Zhang, D.; Jiang, J. In Situ Mass Spectrometric Screening and Studying of the Fleeting Chain Propagation of Aniline. *Anal. Chem.* **2018**, *90* (12), 7154–7157. <https://doi.org/10.1021/acs.analchem.8b02498>.

Chapter 7

CTAB Complexed Poly(3-thiophene ethanol) - Functionalized MWCNT Nanocomposites for Supercapacitor Application

7.1 Introduction

Establishing new supercapacitor electrode materials is an active area of research for developing energy storage devices.¹⁻⁴ Unlike conventional dielectric capacitors, supercapacitors exhibit sound energy density output, a better life cycle, and good energy storage capability. Supercapacitors have widespread applications in electric vehicles, pulse power systems, portable power systems and in renewable energy devices.^{5,6} Therefore, developing efficient supercapacitor materials would provide a sustainable storage platform for clean energy production, energy storage, and energy backup systems. High power density, environmental stability, simple operational mechanism, and recyclability are the significant demands for suitable electrode materials in supercapacitor devices.⁵⁻⁸

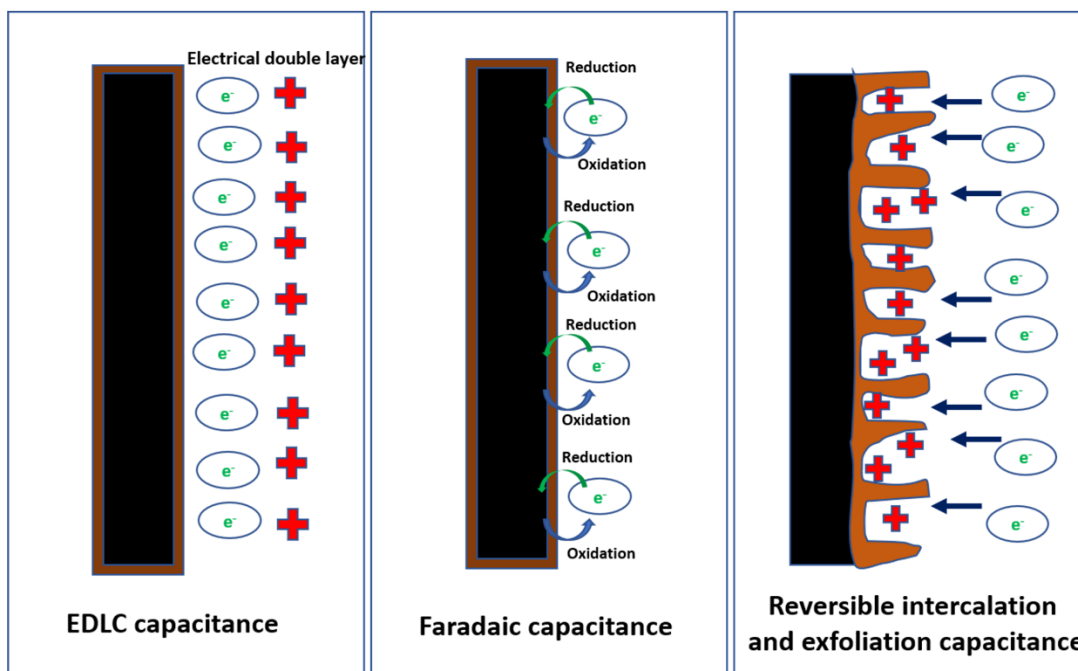


Figure 7.1. Schematic representations of three types of capacitance based on energy storage mechanism: electrical double layer capacitance (a), reversible faradaic capacitance (b), and reversible intercalation and exfoliation capacitance (c).

Based on the energy storage mechanism, generally, super capacitance can be classified into three types; electrical double-layer capacitance (EDLC), faradaic capacitance, and intercalation and exfoliation capacitance (see **Figure 7.1.**)⁹⁻¹⁰ Selection of supercapacitor electrode material is an important criterion for generating robust, sustainable, and durable devices. Carbonaceous materials such as carbon

nanotubes, graphene, graphite, activated carbon, etc. can act as energy storage materials with an electric double-layer mechanism. Carbon nanotubes are distinguishable with their nano or sub-nanometer pores on their one-dimensional nanotubular surface, which is reasonable for accumulating charges as an electrochemical double-layer assortment.¹⁰⁻¹³ Metal oxides, metal hydroxides, and conducting polymers exhibit pseudocapacitive (sequence of faradaic, intercalation, and electrosorption processes) behaviour when used as electrode materials in capacitor applications.^{10,12,14-16} Among these pseudocapacitive materials, conducting polymers are attractive for fabricating lightweight, flexible, less toxic, metal-free power storage and delivery systems.^{12,14}

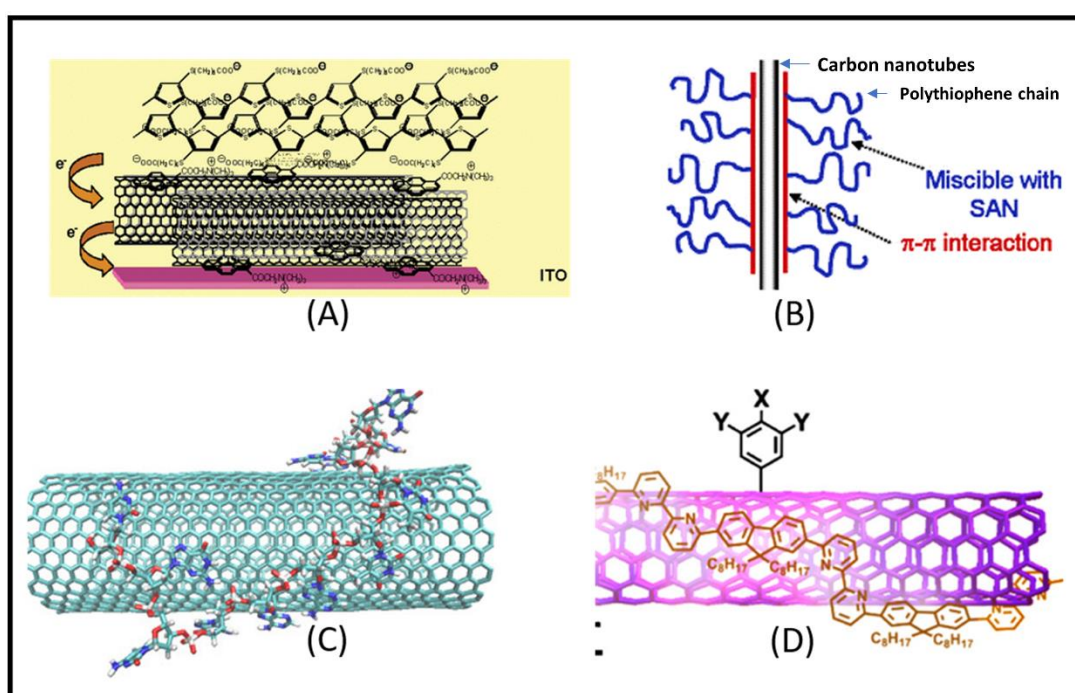


Figure 7.2. Literature reports of functionalized conducting polymer-carbon nanotube nanocomposites: (A) SWCNT-Pyrene⁺-polythiophene nanocomposite (adapted from Rahman et al. 2005), (B) polythiophene-graft-poly(methyl methacrylate) (PMMA) as compatibilizer, for poly(styrene-co-acrylonitrile)/MWCNT nanocomposites (adapted from Kim et al. 2005) (C) Single-Stranded DNA-Single-Walled Carbon Nanotube Hybrid (adapted from Ghosh et al. 2005) and (D) conducting polyfluorene copolymer-Wrapped Carbon Nanotubes (adapted from Berger et al. 2005).

Polythiophene is an efficient conducting polymer, which is highly desirable for capacitor functions due to its good energy storage capability, electrochemical and environmental stability.¹⁷⁻¹⁹ Enhancement in charge capacity was observed for ultrathin

polythiophenes films as it conserves the large surface area and pore space.²⁰ Combining electric double-layer capacitive materials with pseudocapacitive polythiophene would be advantageous for high power density and processability.^{6,21} Systematic studies on enhancement in capacitive behavior have not much been explored in literature with solid evidence. Supercapacitor electrodes incorporated with conducting polymer may have some obstacles due to poor solubility, lack of surface wettability with electrolyte, and also insufficient conformal coating on other materials.^{19,22} Polythiophene derivatives would be more advantageous than unsubstituted polythiophene chains, for attaining solubility in common solvents and to enhance processability. The drawback of substituted polythiophenes instead of unsubstituted polythiophene was that their electrical conductivity and thermal stability might decrease on derivatization. The loss of conductivity and thermal stability can be maintained or enhanced by merging the conducting polymer with other suitable matrices to obtain heterostructural materials such as blends, nanocomposites, nanohybrids, etc.^{16,18,23,24} Some of the literature reports of functionalized conducting polymer-carbon nanotube nanocomposites that exhibited superior behaviour than individual components in terms of structure as well as properties is shown in **Figure 7.2**.²⁵⁻²⁸

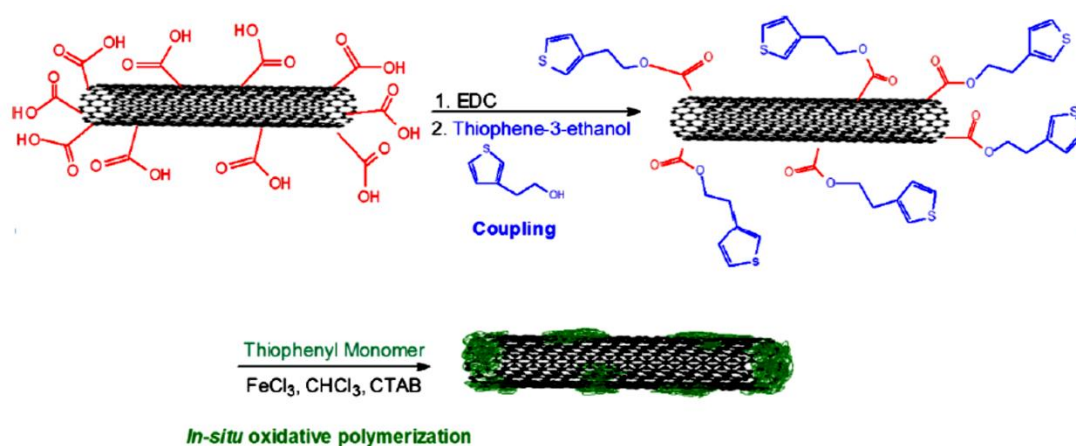


Figure 7.3. EDC-coupled 3-thiophene ethanol monomer to functionalized MWCNT and subsequent in-situ polymerization to prepare nanocomposites (adapted from Harel et al. 2013).

The formation of conducting polythiophene nanocomposites with carbon nanotube would be highly promising as supercapacitor electrode materials as it merges electrical double-layer capacitance characteristics of carbon nanotubes with the

pseudocapacitive behavior of polythiophene.^{29,30} Generally, the preparation of conducting polymer carbon nanotubes nanocomposites can be carried out by three methods; (i) in-situ polymerization of thiophene/functionalized thiophene monomer in the presence of CNT matrix, (ii) solution blending (*ex-situ* route) and (iii) melt mixing (*ex-situ* route).³¹⁻³⁶ In-situ polymerization is more suitable for incorporating insoluble conducting polymers into nanocomposites.³³ On the other hand, solution blending is the strategy for handling soluble forms of conducting polymers toward nanocomposite formation. Soluble forms of conducting polymers attract excellent research interest in nanocomposites formation as the solution blending strategy helps to adopt scalable synthetic procedures with conformally aligned polymer-CNT matrix in nanocomposites.^{19,35} Soluble forms of polythiophenes are usually produced by choosing functionalized monomer of thiophene and modifying it into appropriate derivatives.³⁷ The functionalized monomer 3-thiophene ethanol is a desirable thiophene monomer as the ethanolic group could easily accomplish further reactions with reagents or modify to non-covalent forces.³⁸⁻⁴⁰ There are many reports on the covalent modification of 3-thiophene ethanol for solubility enhancement.^{38,39} Harel et al. reported in-situ polymerization of 3-thiophene ethanol monomer to prepare nanocomposite with carboxylic acid functionalized carbon nanotube by directly coupling monomer on CNT surface, without adopting any further modification to the monomer (see **Figure 7.3**).⁴¹

In this chapter, we have put forward a facile, simple, and scalable synthetic procedure for poly(3-thiophene ethanol)- functionalized multiwalled carbon nanotube nanocomposites preparation. Poly(3-thiophene ethanol) was initially formed by polymerization of 3-thiophene ethanol monomer using ferric chloride as the oxidant in the presence of AOT surfactant in a chloroform medium. The obtained polymer was then transferred to poly(3-thiophene ethanol)-CTAB complex, which was a soluble complex. Poly(3-thiophene ethanol)-multiwalled carbon nanotubes nanocomposites were prepared by solution blending method of the polymer-CTAB complex with dispersed state of MWCNT-COOH. Polymerization was characterized by FT-IR and MALDI-TOF analysis. Poly(3-thiophene ethanol)-CTAB complex formation was studied with fourier transform infrared spectroscopy and matrix-assisted laser desorption/ionization. Other instrumental analyses such as UV-vis spectroscopy, powder X-ray diffraction, surface morphology, electrical conductivity, and thermal

stability have also been carried out for polymer and polymer-MWCNT-COOH nanocomposites. Capacitance studies of nanocomposites were conducted using cyclic voltammetry and galvanostatic charge-discharge analyses.

7.2. Experimental

7.2.1. Materials and reagents used: 3-Thiophene ethanol, multiwalled carbon nanotubes (MWCNT), AOT, and ferric chloride were purchased from Sigma Aldrich. Cetyl trimethyl ammonium bromide, sodium hydroxide, nitric acid, chloroform, diethyl ether, acetone and deionized water were purchased from Merck chemicals.

7.2.2. Measurements and instruments: Fourier transform-infrared spectra of the samples were recorded by Shimadzu IR Affinity 1 spectrometer using the KBr pellet method. UV-vis spectra of the samples were recorded by Shimadzu UV-Visible spectrophotometer, UV 1800 series, in the range 200-800 nm with HPLC grade chloroform and ethanol. The powder wide-angle X-ray diffraction of the samples was measured using PANALYTICAL, Aeris research with 2θ values ranging from 10 to 80°. FE-SEM images were recorded by ZEISS SIGMATM field emission scanning electron microscope (FE-SEM). MALDI-TOF analysis was conducted with Bruker Autoflex max LRF MALDI-TOF mass spectrometer. Thermogravimetric analysis (TGA) of the samples was measured using Perkin Elmer, Diamond TG/DTA in an inert atmosphere of nitrogen at a heating rate of 20°C/min. The four probe electrical conductivity of the samples was measured using DFP-RM-200 with constant current source Model CCS-01 and DC microvoltmeter. Electrochemical studies were carried out with BioLogic VSP electrochemical workstation unit.

7.2.3 Synthesis of PTE: Monomer (3-thiophene ethanol) (0.5 mL, 4.68 mmol) and surfactant AOT (0.22 g, 0.19 mmol) was dissolved in chloroform (10 mL) and sonicated for 5 min. A dispersed form of FeCl₃ (1.06 g, 6.55 mmol) in 5 mL chloroform was added drop by drop to the AOT-thiophene micellar complex mixture and sonicated for 15 min. Subsequently, the reaction mixture was magnetically stirred for 3 h. The polymer thus obtained was filtered and washed using water and acetone. The polymer was then dried in a vacuum oven at 60°C for 3h. Yield: 0.110 g.

7.2.4 Preparation of PTE-CTAB complex: PTE (10 mg) was added into 10 mL dimethyl sulfoxide (DMSO) and taken in a 50 mL RB flask. The mixture was sonicated

for 5 min. Sodium hydroxide (0.0032 g, 0.0792 mmol) was added and magnetically stirred for 5 min. CTAB (0.0289 g, 0.0792 mmol) was then added to the mixture and magnetically stirred for 5 days.

7.2.5 Preparation of PTECNT COOH-10: MWCNT-COOH (0.010 g) dispersed in DMSO (5 mL) was added to the prepared PTE-CTAB complex mixture and sonicated for 15 min. This was then magnetically stirred for 1 h. Double distilled water (100 mL) was then added to it and the resultant product was allowed to precipitate. The powder obtained was then filtered and washed with water. This was then dried in vacuum oven at 80°C for 3 h. Yield: 0.016 g.

PTECNT-COOH 15 and PTECNT-COOH 20 were prepared by changing the amount of MWCNT-COOH added as 15 mg and 20 mg respectively using same procedure (see **Table 7.1.**).

7.2.6. Electrochemical characterization: Electrochemical measurements were carried out via PTE, MWCNT-COOH and PTECNT-COOH nanocomposites coated on glassy carbon electrode as working electrode, platinum electrode as counter electrode and Ag/AgCl electrode as reference electrode, respectively. Samples were dispersed in ethanol solvent and drop cast into the working electrode without adding any additives or binders. The drop casted samples were dried with air blower. The film coating thus formed was subjected to electrochemical analyses such as cyclic voltammetry and galvanostatic charge-discharge analysis. Cyclic voltammograms were recorded in different scan rates (10 mV/s, 20 mV/s, 50 mV/s, 100 mV/s and 200 mV/s) and using different electrolytes (1M HCl, 1M H₂SO₄, 1M KOH and 1M Na₂SO₄). Galvanostatic charge-discharge studies of PTECNT-COOH 20 with different current densities (0.3 mA/g, 0.6 mA/g and 1.0 mA/g) were carried out in 1M H₂SO₄ electrolyte. The cycling stability of cyclic voltammogram of PTECNT-COOH 20 was also determined for 1000 cycles.

7.3. Results and discussion

7.3.1. Preparation of poly(3-thiophene ethanol) (PTE) and PTECNT-COOH nanocomposites

Synthesis of poly(3-thiophene ethanol) was carried out via oxidative chemical polymerization of 3-thiophene ethanol (TE) monomer using ferric chloride as

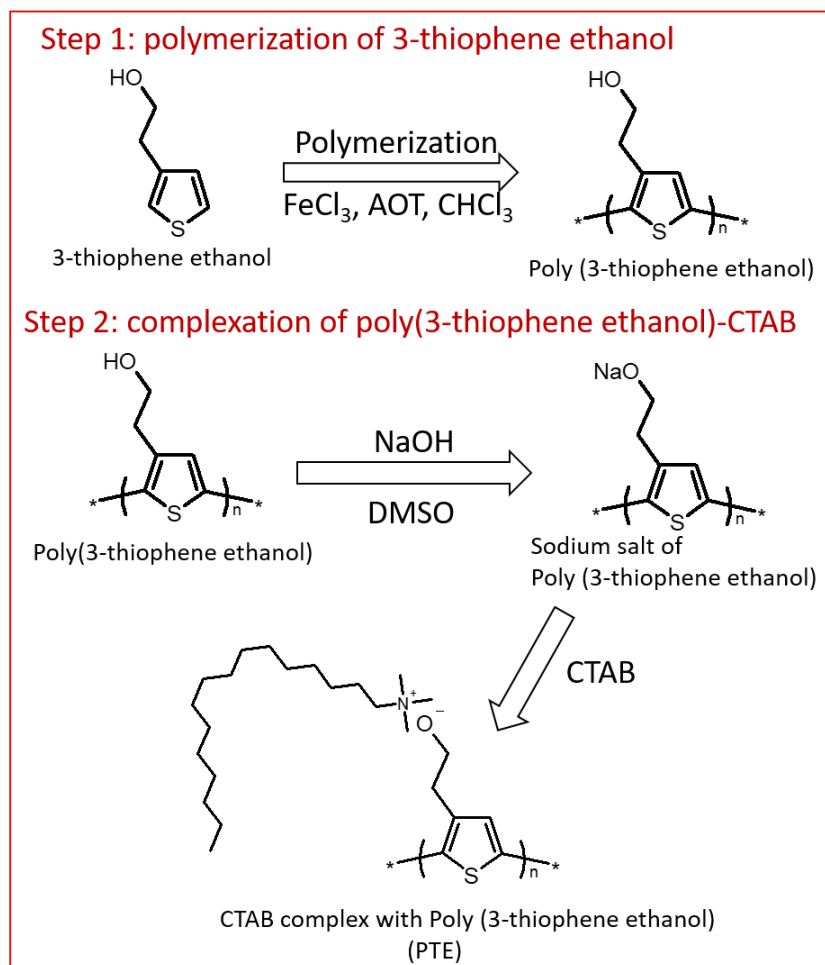


Figure 7.4. Schematic representation of synthesis of PTE-CTAB complex.

the oxidant in the presence of surfactant sodium bis (2-ethyl hexyl) sulfosuccinate (AOT) in chloroform medium (see **Figure 7.4.**). The obtained polymer was then sonicated with NaOH in DMSO solvent, resulting in corresponding sodium salt formation. Afterward, the cationic surfactant cetyl trimethyl ammonium bromide (CTAB) was added, sonicated for 15 min, and magnetically stirred for five days. A bright orange-coloured soluble polymer-CTAB complex was thus obtained. A dispersed form of functionalized MWCNT-COOH in DMSO was added slowly to the polymer-CTAB complex. It was then sonicated for 15 min and magnetically stirred for one hour, which resulted in nanocomposite formation (see **Figure 7.5.** and **Table 7.1.**). In the formation of the polymer-CTAB complex, the first stage was the generation of the sodium salt of the ethoxide side chain of thiophene units on the addition of NaOH. The salt form of the polymer then slowly underwent complexation with the cationic

surfactant CTAB on physical agitation. The complex formation of PTE with surfactant occurred due to non-covalent modification on ethoxide side chains of thiophene subunits in the polymerized form. In this work, soluble polyelectrolyte PTE was prepared using the above mentioned approach which was a less explored way of non-covalent modification.

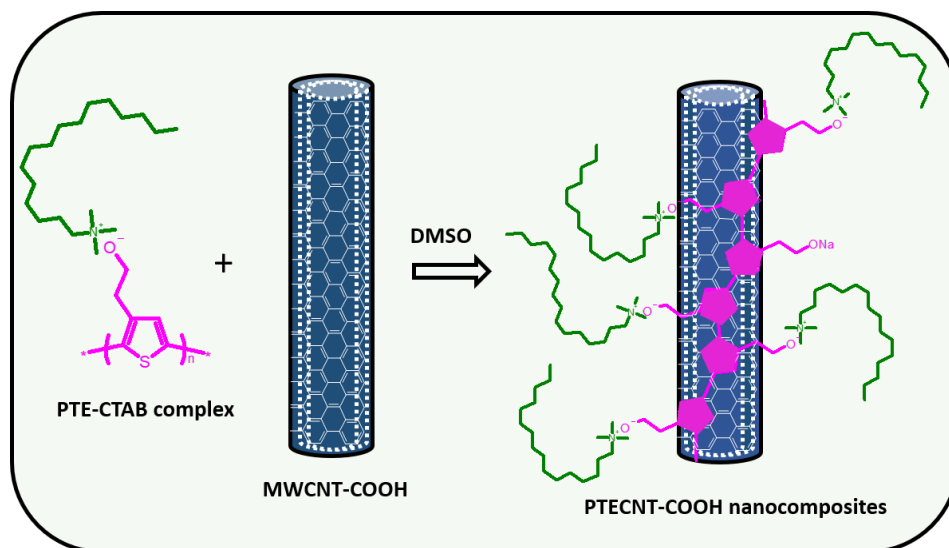


Figure 7.5. Synthesis of PTECNT-COOH nanocomposites by solution blending method.

Table 7.1. PTECNT-COOH samples with the amount of poly(3-thiophene ethanol), CTAB surfactant, MWCNT-COOH used and yield obtained in preparation

Sample	PTE (mg)	CTAB (mmol)	MWCNT-COOH (mg)	Yield (mg)
PTECNT-COOH 10	10	0.0792	10	16
PTECNT-COOH 15	10	0.0792	15	28
PTECNT-COOH 20	10	0.0792	20	36

7.3.2. Characterization of PTE and PTECNT-COOH nanocomposites

The formation of polymer (PTE), PTE-CTAB complex and nanocomposites (PTECNT-COOH 10, PTECNT-COOH 15 and PTECNT-COOH 20) were characterized using fourier transform infrared spectra (see **Figure 7.6.**). PTE shown characteristic peaks at 813 cm^{-1} , 1022 cm^{-1} , 1722 cm^{-1} , 2852 cm^{-1} and $3000\text{-}3700\text{ cm}^{-1}$ indicating C-S stretching vibration, C-O stretching vibration of the ethanolic side chains, stretching vibration of thiophene ring, C-H stretching vibration, and O-H stretching broad vibrational peak respectively.^{42,43} Complexation of PTE with CTAB

surfactant was evident from by FTIR analysis. PTE-CTAB complex exhibited peaks at 826 cm^{-1} , 1035 cm^{-1} , 1624 cm^{-1} , 2865 cm^{-1} and $3150\text{-}3450\text{ cm}^{-1}$. For the complex, the peak at 1035 cm^{-1} was found to get intensified compared to PTE. This might be due to the involvement of C-N stretching vibrations present in the CTAB surfactant. A visible shift was observed for IR frequency peak at 1722 cm^{-1} (in PTE) to 1624 cm^{-1} (in PTE-CTAB complex) due to the free stretching vibration of thiophene rings on complexation.⁴²⁻⁴⁵ PTE-CTAB complex exhibited O-H stretching vibration peak arising from the remaining alcoholic groups, which did not participate in complexation. PTECNT-COOH nanocomposites exhibited major peaks at 1035 cm^{-1} , 1524 cm^{-1} , 1624 cm^{-1} , 2852 cm^{-1} and $3000\text{-}3650\text{ cm}^{-1}$ attributing to C-O stretching vibration from the side chain, aromatic stretching from carbon nanotubes, thiophene ring stretching vibrations, C-H stretching vibration from 3-thiophene ethanol moiety and O-H stretching vibration from polymer side chain respectively.^{42,44,46} Involvement of peaks from the PTE-CTAB complex and MWCNT-COOH in the FT-IR spectra of PTECNT-COOH composites pointed out the effective formation of composites.

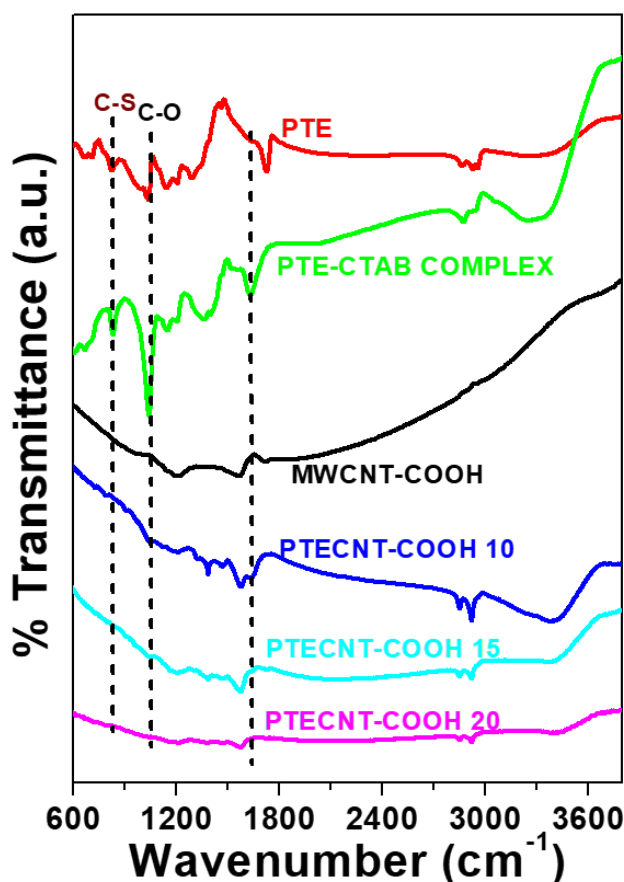


Figure 7.6. FT-IR spectra of PTE, PTE-CTAB complex, MWCNT-COOH, PTECNT-COOH 10, PTECNT-COOH 15 and PTECNT-COOH 20.

Solid-state ordering of polymer nanocomposites were analyzed using powder X-ray diffraction. X-ray diffractograms of PTE, PTE-CTAB complex, PTECNT-COOH 10, and PTECNT-COOH 15 were recorded (see **Figure 7.7.**). PTE exhibited a broad, amorphous peak ranging from 2θ value $10-32^\circ$.⁴⁷ PTE-CTAB complex in which the amorphous peak was changed to partially crystalline with many smaller sharp peaks in it, indicates the formation of short-range ordering in the complexed form of PTE with CTAB. PTECNT-COOH 10 and PTECNT-COOH 15 in which the peak corresponding to (002) plane of multiwalled carbon nanotubes at ($2\theta=26^\circ$) was partially merged with the semi-crystalline peak of PTE-CTAB complex (see **Figure 7.7. inset** also).⁴⁸ Presence of diffraction patterns of individual components (PTE and MWCNT-COOH) in X-ray diffractograms of PTECNT-COOH composites confirmed the effective formation of nanocomposites.

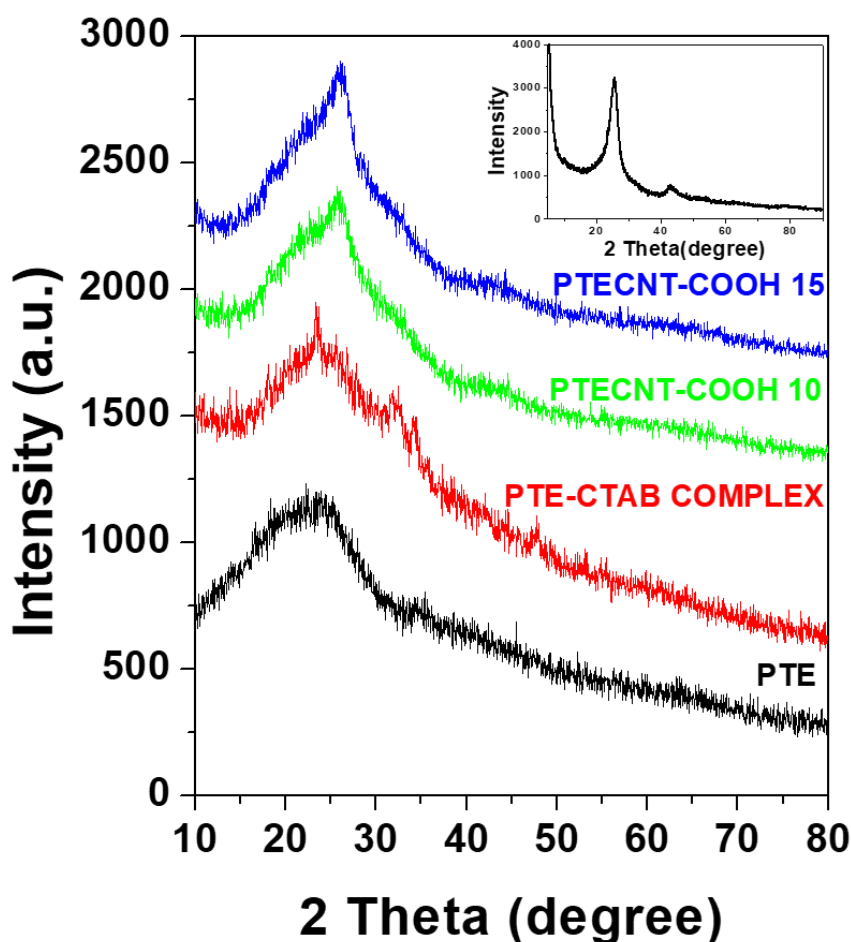


Figure 7.7. Wide angle X-ray diffractograms of PTE, PTE-CTAB complex, PTECNT-COOH 10, PTECNT-COOH 15 and MWCNT-COOH (inset).

7.3.3. Morphological and dispersion studies of polymer and PTECNT-COOH nanocomposites

Surface morphologies of PTE, MWCNT-COOH, and PTECNT-COOH nanocomposites were carried out using field emission scanning electron microscopy (see **Figure 7.8.**). Scanning electron microscopic images of PTE appeared as a continuous bulk mass of polymer with some microcavity structures observed in certain areas. Image of one such microcavity is magnified in **Figure 7.8. (inset)** and some other microcavities are marked using yellow dotted circles in **Figure 7.8.** The cavities are shaped nearly as flower bud and these voids might be formed as the effect of AOT surfactant self-assembly during the polymerization. FE-SEM image of MWCNT-COOH has nanotubular morphology with an outer diameter of $\sim 9 \pm 3$ nm. The morphology of nanocomposites was also found in one-dimensional nanotubes. It was clear from FE-SEM images of composites that no bulk polymer mass was found in the phase-separated form in between the nanotube framework. The outer diameter of nanocomposites with nanotubular structure was observed as $\sim 25 \pm 5$ nm, which is larger than that of functionalized MWCNT-COOH, indicating the effective wrapping of poly(3-thiophene ethanol)-CTAB complex on the outer surface of carbon nanotubes.

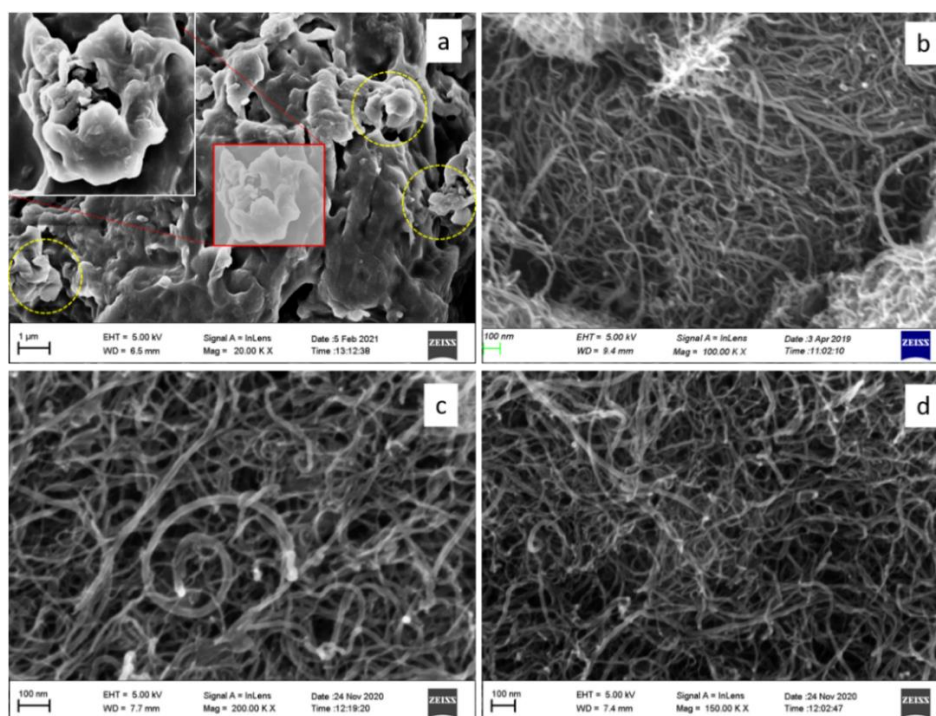


Figure 7.8. Field emission scanning electron microscopic images of (a) PTE, (b) MWCNT-COOH, (c) PTECNT-COOH 10 and (d) PTECNT-COOH 15.

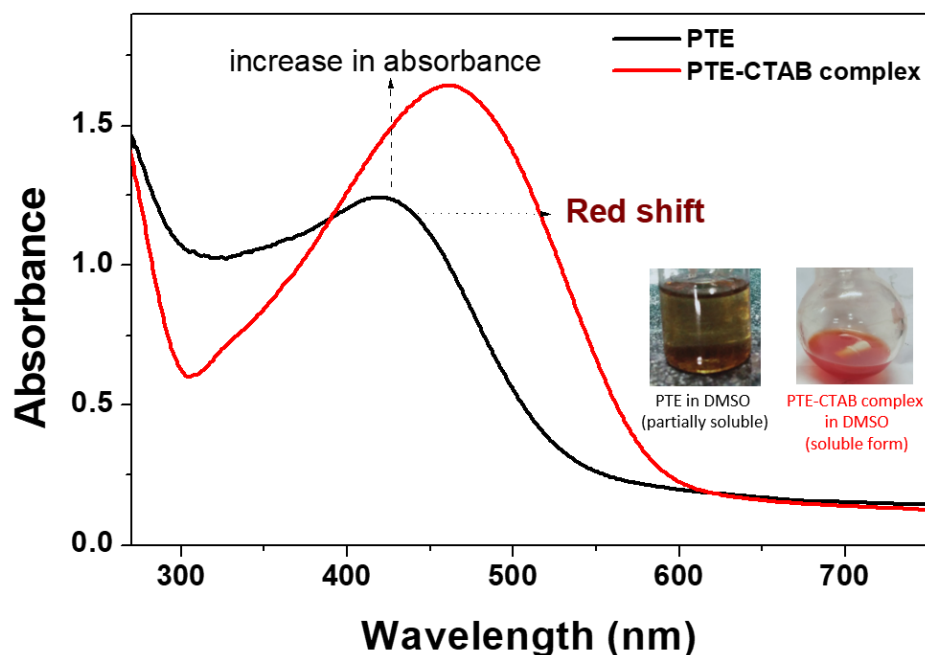


Figure 7.9. UV-vis absorption spectra of PTE and PTE-CTAB complex.

The polymer (PTE) exhibited partial solubility in weakly polar organic solvents such as DMSO and NMP (see the photographs in **Figure 7.9**). Sonication of polymer with NaOH followed by magnetic stirring with cationic surfactant CTAB resulted in the formation of bright orange-coloured complex (PTE-CTAB complex). Absorption studies of polymer PTE and PTE-CTAB complex were carried out with UV-vis spectra (see **Figure 7.9**). PTE exhibited a peak with an absorption maximum at 420 nm corresponding to polaron- π^* transition in polythiophene conjugated chain. For PTE-CTAB complex showed a red shift with broader peak with λ_{max} of 461 nm. The intensity was increased due to the better solubility of the polymer complex in DMSO. The red shift was observed because of the increased extended conjugation of the polythiophene backbone. Complexation of poly(3-thiophene ethanol) with cationic quaternary ammonium surfactant CTAB plausibly released the coiled nature of polymeric chains into a partial rod-like form. This moderate straightening effect might decrease the rotational defects present in PTE chain previously disordered amorphous coiled structure. Insertion of long CTAB chains on polymer creates a sidewise overlap around the polymer, thus restricting the free rotation of polymeric chains to form a coiled structure but promoting partial planarized conformations. As a result, the perturbation in the effective backbone conjugation of polythiophene chains gets decreased and the torsional angles get lessened with a partial straightening effect.^{44,49-51} The complex was then subjected to nanocomposites formation with acid functionalized multiwalled

carbon nanotubes (MWCNT-COOH). Nanocomposites thus prepared resulted in stable dispersions in partially polar solvents such as ethanol, DMSO, and NMP (see **Figure 7.10. A**). UV-vis absorption spectra of PTECNT-COOH 10, PTECNT-COOH 15, and PTECNT-COOH 20 were recorded in the solvent ethanol (see **Figure 7.10 B**). The absorption peak arising from the aromatic π - π^* transition ($\lambda_{\text{max}} = 280 \text{ nm}$) of MWCNT-COOH is well-resolved in the UV-vis absorption spectra of nanocomposites. The π -polaron absorption of the polythiophene backbone is observed as an unresolved tail in longer wavelengths continuous with the absorption peak of carbon nanotubes.

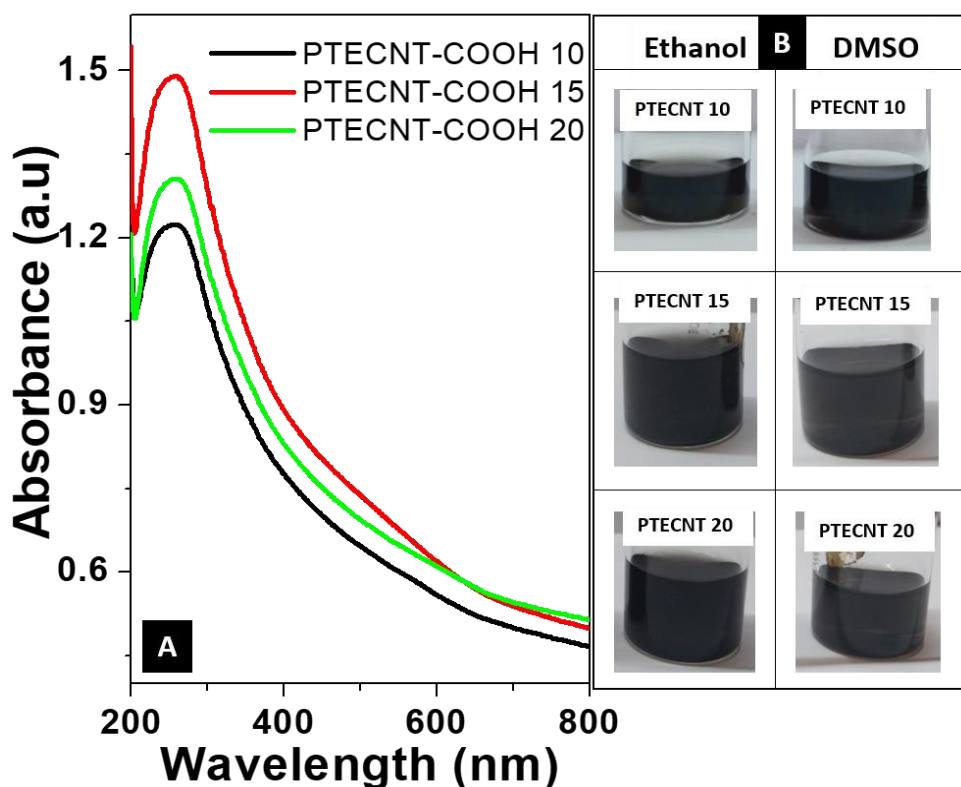


Figure 7.10 UV-visible spectra of PTECNT-COOH 10, PTECNT-COOH 15 and PTECNT-COOH 20 in ethanol and DMSO (A) and Dispersions of PTECNT-10, PTECNT-15 and PTECNT-20 in ethanol (B).

Poly(3-thiophene ethanol) complex, effectively wrapped on MWCNT-COOH producing well-defined nanotubular morphology (clearly evident from FE-SEM images of PTECNT-COOH nanocomposites). The average molecular mass of the PTE-CTAB complex obtained from MALDI TOF analysis was 4312.35 g/mol. Preparation of soluble form of poly(3-thiophene ethanol) complex with CTAB surfactant in DMSO helped to utilise the post polymerization preparation of nanocomposite via simple physical blending approach. Sonicated MWCNT-COOH in DMSO acted as stable

dispersion to accommodate complexed polythiophene chains on it via pi-stacking and wrapping interaction. Partial uncoiling of PTE chains by complexation eases the association with MWCNT-COOH and their stacked arrangement on carbon nanotubes framework. Thereby polymer got effectively wrapped on carbon nanotubes (the outer radius of PTECNT-COOH was measured to be higher than that of MWCNT-COOH). Pristine carbon nanotubes are characterized by their agglomeration tendency due to their inherent bundling nature. The long hydrophobic alkyl chains orienting outside the tubular framework of nanocomposites restrict interchain aggregation (see **Figure 7.11.**). This might create the well-separated tubular morphology of the nanocomposites as seen in FE-SEM images.

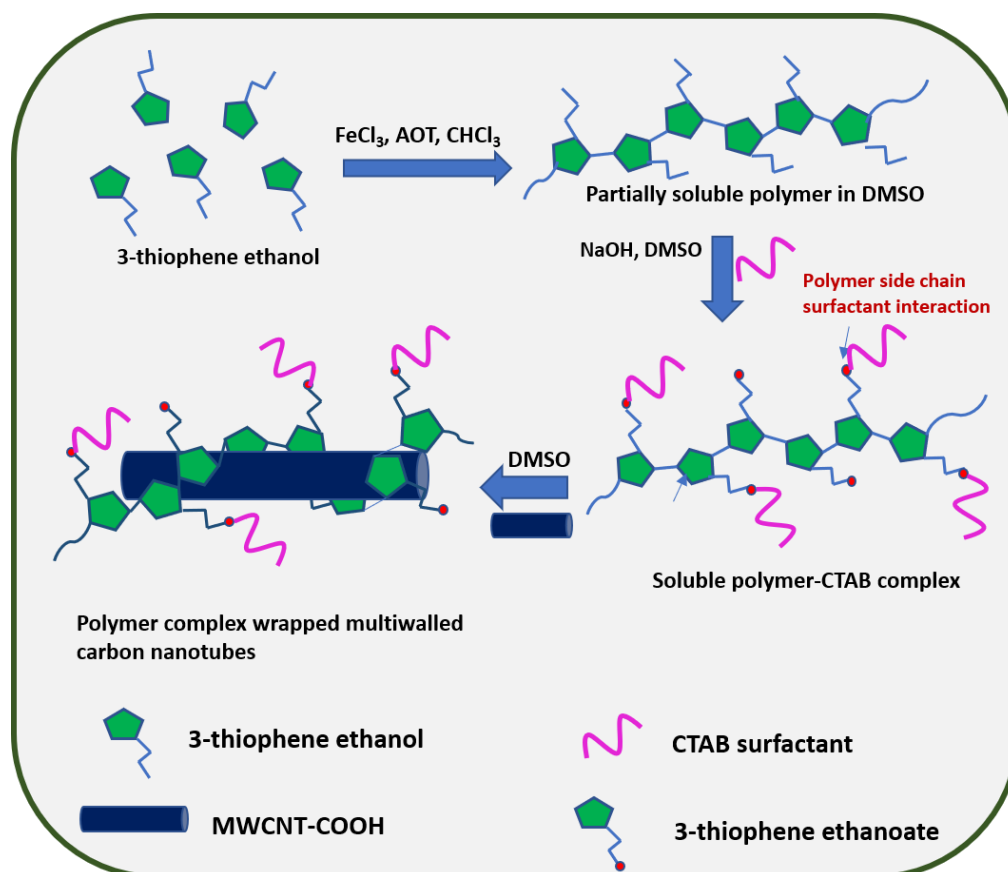


Figure 7.11. Formation mechanism of PTECNT-COOH nanocomposites.

7.3.4. Thermal stability and electrical conductivity of PTECNT-COOH nanocomposites

Thermogravimetric analyses were conducted to compare the thermal stability of PTE and PTECNT-COOH nanocomposites prepared (see **Figure 7.12.**). The thermal profile of PTE exhibited two stages of weight loss; the first stage corresponds to the

decomposition of the side chain and the second stage is attributed to polythiophene backbone cleavage.⁵² PTECNT-COOH nanocomposites exhibited comparably very high thermal stability than the corresponding polymer. In the initial stage of degradation up to 200°C, PTECNT-COOH composites exhibited only 5% weight loss and PTE showed 10 % weight loss. Further polymer undergo 30%, weight loss upto 300°C as observed in the TGA curve . The thermal profile of PTECNT-COOHs was well above that of PTE, indicating less weight loss occurred in the composites particularly up to 300°C, due to the effective interfacial interaction between polymer and carbon nanotubes. PTECNT-COOH nanocomposites exhibited only 25% weight loss at 700° C indicating the high thermal stability.

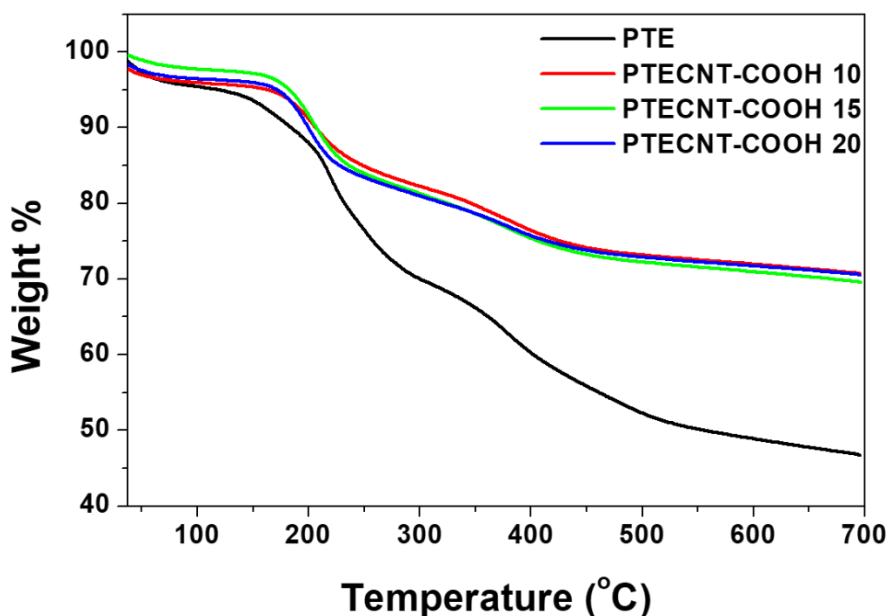


Figure 7.12. Thermal stability of PTE, PTECNT-COOH 10, PTECNT-COOH 15 and PTECNT-COOH 20.

The electrical conductivity of PTE, PTECNT-COOH 15, PTECNT-COOH 20 and MWCNT-COOH was measured using four probe electrical conductivity meter (see **Figure 7.13.**). PTE, PTECNT-COOH 15, PTECNT-COOH 20, and MWCNT-COOH exhibited electrical conductivity of 2.21×10^{-8} , 8.33×10^{-1} , 3.31×10^{-1} , and 2.89 S/cm respectively. Poly(3-thiophene ethanol) exhibited very low conductivity compared to unsubstituted polythiophene PT-25 (reported in chapter 2). Incorporating alkyl functional groups with saturated bonds might decrease the conductivity of substituted conducting polymer poly(3-thiophene ethanol). The electrical conductivity of PTECNT-COOH nanocomposites were observed greater than 10^7 orders than that of

PTE. The less conducting PTE composition in the PTECNT-COOH nanocomposites (ie, between 40 % to 50 %), exhibited a hike in conductivity in the polymer-wrapped state on carbon nanotubes. The hike in conductivity might be due to the strong interfacial interaction between polymer and carbon nanotubes through non-bonded interaction between the partially straightened aromatic conjugated backbones of polymer complex and carbon nanotubes.

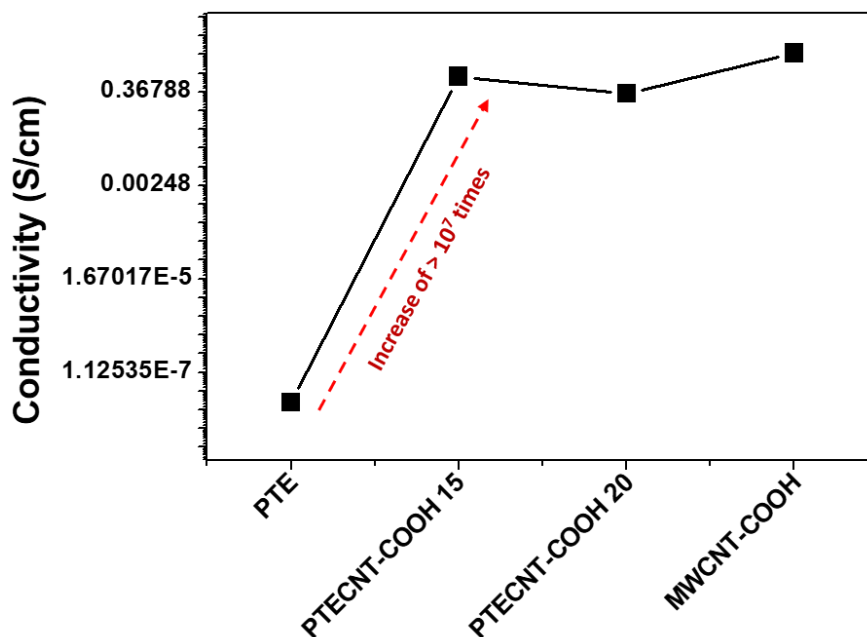


Figure 7.13. Four probe electrical conductivity of PTE, PTECNT-COOH 15, PTECNT-COOH 20 and MWCNT-COOH.

7.3.5. Electrochemical characterisation of PTECNT-COOH nanocomposites

The electrochemical performance of PTE, PTECNT-COOH 10, PTECNT-COOH 15, and PTECNT-COOH 20 were analyzed by cyclic voltammetry and galvanostatic-charge-discharge analysis with a three-electrode configuration (see **Figure 7.14.**). The electrochemical cell consists of a modified glassy carbon electrode as working electrode, a platinum electrode as counter electrode and an Ag/AgCl electrode as the reference electrode. The working electrode was prepared by drop casting ethanol solution of samples on glassy carbon electrode and dried with air blow method. A less resolved peak was observed on the cyclic voltammogram of PTE, indicates that both ionic diffusion and the faradaic process influence the electrochemical performance.^{49,55,56} PTE exhibited nearly willow-shaped CV curves with a faradaic peak. However, a different quasi-rectangular shape of CV curves of the

PTECNT-COOHs indicated the significant contribution from the MWCNT-COOH component to the electrochemical performance of nanocomposites. Carbon nanotubes exhibit electrical double-layer capacitance from the non-faradaic ionic diffusion process, and corresponding CV curves appear nearly rectangular.^{21,53,54} In effect of both faradaic and non-faradaic processes on the PTECNT nanocomposites, the modified glassy carbon electrode was thus found to exhibit pseudocapacitive behaviour.

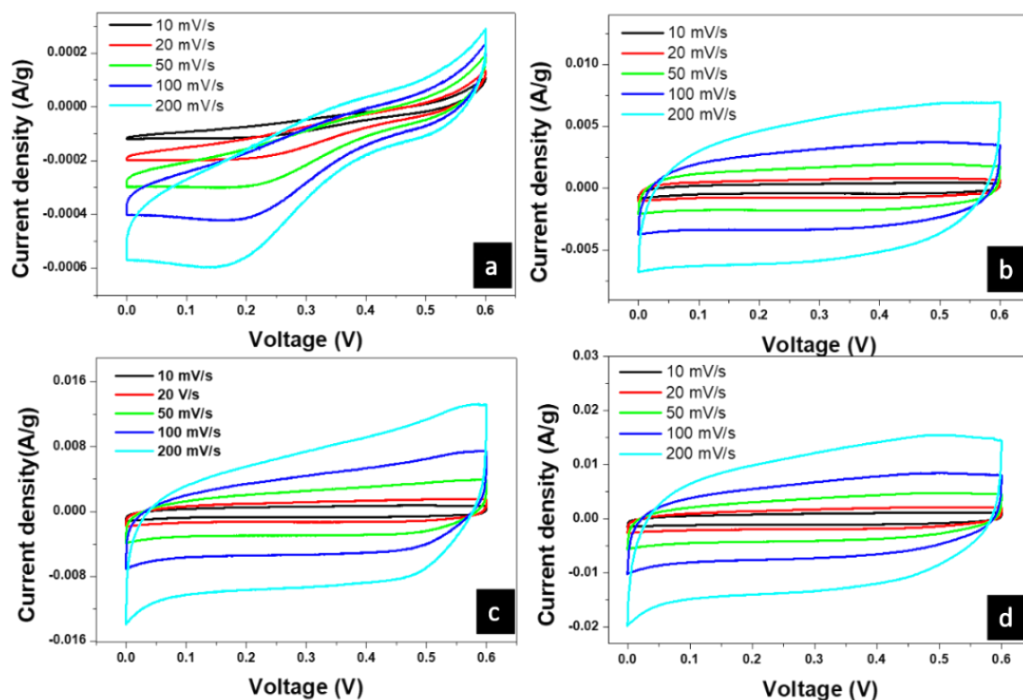


Figure 7.14. Cyclic voltammogram of PTE (a), PTECNT-COOH 10 (b), PTECNT-COOH 15 (c) and PTECNT-COOH 20 (d) in 1M HCl electrolyte.

The cyclic voltammetry investigation of PTE, PTECNT-COOH 10, PTECNT-COOH 15, and PTECNT-COOH 20 were carried out in 1 M HCl electrolyte over the potential range of 0 to 0.6 V. The study was carried out for different scan rates, such as 10 mV/s, 20 mV/s, 50 mV/s, 100 mV/s, and 200 mV/s. By comparing the CV curves of PTECNT nanocomposites, the most effective composition was taken as PTECNT-COOH 20 (nanocomposite obtained by adding 20 mg of MWCNT-COOH) which exhibited largest integral area and the highest specific capacitance. Specific capacitance of samples was quantified using the formula

$$C_{sp} = \frac{\int IdV}{2 * m * SR * V} \dots\dots\dots (1),$$

where 'I' is the current density, 'V' is the potential window, m is the mass of material coated on glassy carbon electrode and 'SR' is the scan rate. $\int IdV$ is obtained as integral area of CV curves.^{23,55} Specific capacitance (C_{sp}) obtained with the samples PTE, PTECNT-COOH 10, PTECNT-COOH 15, and PTECNT-COOH 20 for 10 mV/s were 1.53 F/g, 36.71 F/g, 68.88 F/g, and 90.61 F/g respectively (see **Figure 7.14**). The specific capacitance of samples was observed to increase with an increase in scan rate,

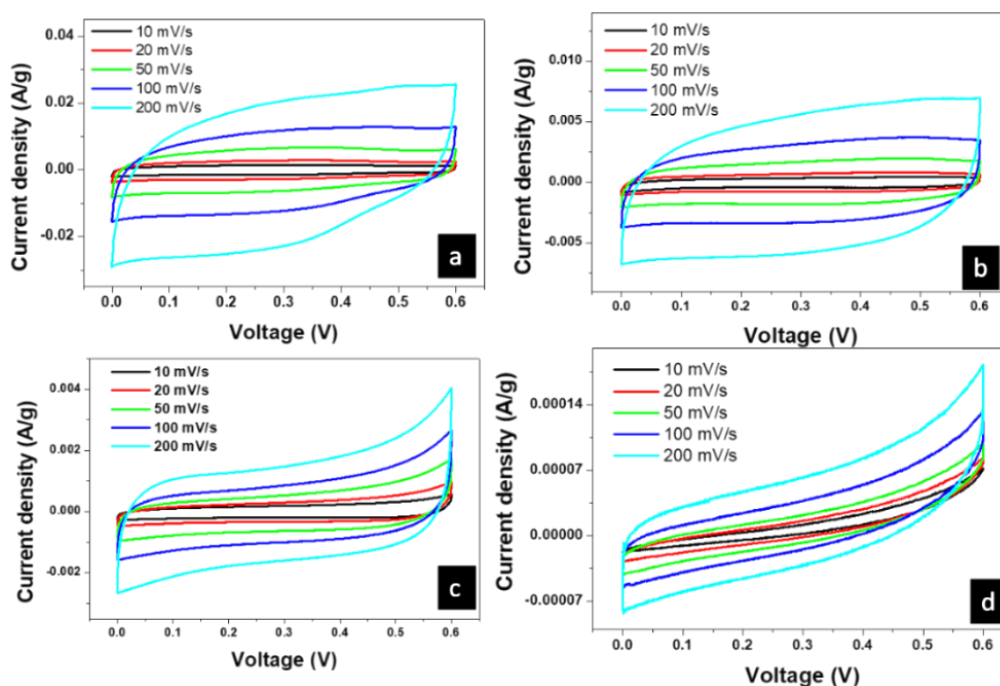


Figure 7.15. Cyclic voltammogram of PTECNT-COOH 20 for different scan rates in the electrolytes 1M HCl (a), 1M H_2SO_4 (b), 1M KOH (c) and 1M Na_2SO_4 (d).

indicating the improvement in ionic diffusion. The diffusion kinetics was observed near the diffusion layer and it become more dynamic, thereby giving higher flux towards electrodes and a higher magnitude of the current. Specific capacitance obtained for PTE was found as comparably very small due to less availability of ion-accessible active sites due to its micro-bulk mass structure. However, the nanotubular network structure of PTECNT nanocomposites could provide a sufficient area of active sites to exhibit good electrochemical performance.

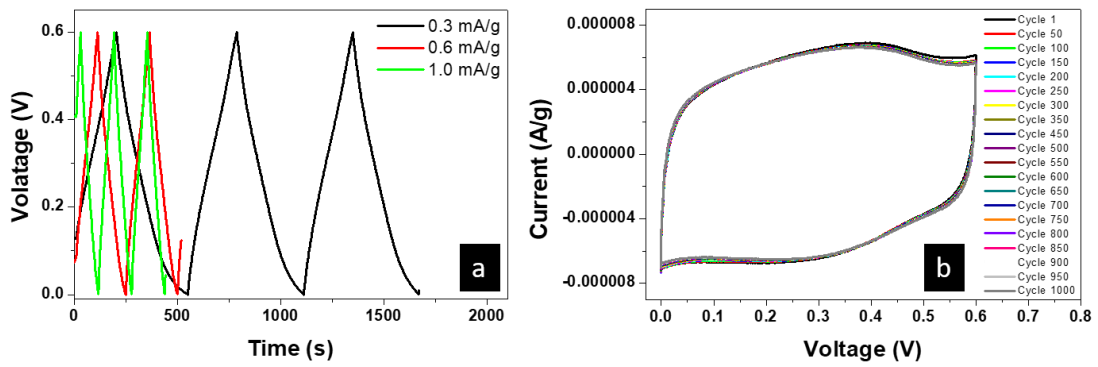


Figure 7.16. Galvanostatic charge-discharge profile of PTECNT-COOH 20 in 1M H₂SO₄ electrolyte (a) and Cycling stability study (cyclic voltammety) of PTECNT-COOH 20 in 1M H₂SO₄ electrolyte up to 1000 cycles (b).

The cyclic voltammograms of PTECNT-COOH 20 were recorded for different electrolyte solutions possessing different combinations of positive and negative ions. The electrolyte concentrations such as 1M HCl, 1M H₂SO₄, 1M KOH, and 1M Na₂SO₄ were used as aqueous solutions (see **Figure 7.15.**). The highest integral area is obtained for the scan rate 10 mV/s in all the samples and corresponding specific capacitance obtained in 1M HCl, 1M H₂SO₄, 1M KOH, and 1M Na₂SO₄ electrolytes are 90.61 F/g, 123.66 F/g, 13.28 F/g, and 38.13 F/g respectively. Among different aqueous electrolytes used, acidic electrolytes (1M H₂SO₄ and 1 M HCl) have given higher values of specific capacitance. Dibasic H₂SO₄ exhibited the highest electrochemical performance having C_{sp} 123.66 F/g. The charging-discharging analysis of PTECNT-COOH 20 nanocomposites was explored with the GCD (Galvanostatic charge-discharge) characteristic profile at different current densities such as 0.3 mA/g, 0.6 mA/g and 1.0 mA/g (see **Figure 7.16. (a)**). Specific capacitance is measured using the formula,

$$C_{sp} = \frac{It}{m\Delta V} \dots\dots\dots (2)$$

Where ‘I’ is the current density, ‘t’ is the discharge time, ‘m’ is the mass of the sample used and ‘ΔV’ is the potential window.^{23,57} The highest C_{sp} obtained was 180 F/g for 10 mA or 0.3 A/g current density. Comparing the involvement of positive and negative ions to vary specific capacitance of PTECNT-COOH 20, the presence of positive hydrogen ions in electrolytes enhanced the specific capacitance to the higher range. In contrast, other cationic species, such as Na⁺ and K⁺ had an insignificant impact on

nanocomposite electrochemical performance, which is significant from the difference obtained for C_{sp} values of PTECNT-COOH 20 in two different but same anion-bearing electrolytes 1M H_2SO_4 and 1M Na_2SO_4 . The GCD profile in which deviation of shape from perfect triangular form indicates appreciable pseudo capacitance functioning from conducting polymer wrapping.⁵⁷ Comparison of charging and discharging in GCD profiles revealed a higher current density of 1.0 mA/g, at which discharging time increases appreciably than charging time. The difference between charging and discharging time is not appreciable at lower current densities. A longer discharging time observed in PTECNT-COOH 20 nanocomposites indicates the more charge storage capability of the PTECNT-COOH-modified glassy carbon electrode.⁷ Other quantitative measurements, such as energy density and power density, were also quantified. Energy density was calculated using the equation,

$$Energy\ density = \frac{CV^2}{8 * 3.6} \dots\dots\dots (2),$$

Where ‘C’ is the specific capacitance in F/g and ‘V’ is the potential window in volts. Then power density was also calculated using the equation,

$$Power\ density = \frac{E}{\Delta t} \dots\dots\dots (3),$$

Where E is the energy density and Δt is the time.⁵⁷ Energy density was obtained as 1.6 Wh/Kg and power density as 19.19 W/Kg. Both energy and power density met moderately good performance for supercapacitors along with its high specific capacitance of 128 F/g. The electrochemical stability of PTECNT-COOH 20 nanocomposite electrode was analyzed with cyclic voltammetry in the scan rate of 200 mV/s for the continuous 1000 cycles (see **Figure 7.16. (b)**). The specific capacitance of 99 % was found to be retained even after 1000 cycles. Supercapacitors with high cycling stability are challenging to generate the long-term output from the electrode materials.^{58,59} Preparation of electrodes by coating as a film without adding additives or binders is another good advantage in a capacitor's economic and efficiency aspects.⁶⁰ In essence, we have put forward a facile physical blending approach for thermally stable and conducting nanocomposites preparation. The composite was effectively demonstrated for applying easily fabricated, moderately good capacitive, energy

efficient, competent power generating and a long-lasting supercapacitor (see **Figure 7.17.**).

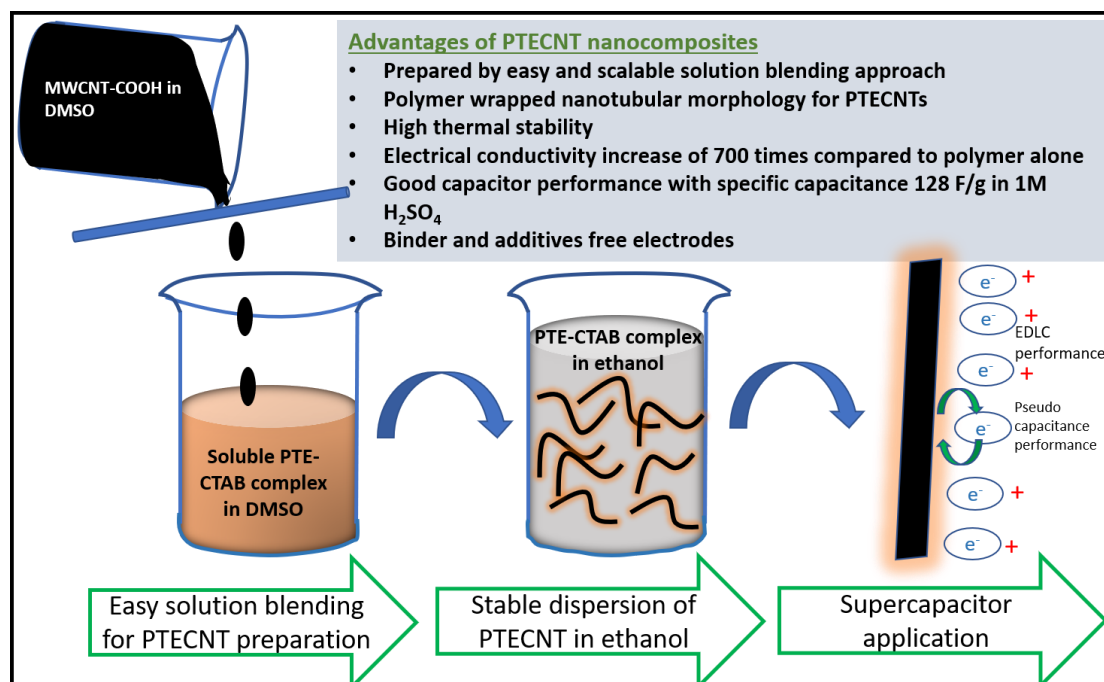


Figure 7.17. Illustration of advantageous outputs of PTECNT-COOH nanocomposites preparation and its supercapacitor application.

7.4. Conclusion

Poly(3-thiophene ethanol)-functionalized multiwalled carbon nanotube nanocomposites (PTECNT-COOH) was prepared by scalable and less complicated physical blending route in DMSO solvent. Poly(3-thiophene ethanol) (PTE) was initially prepared by oxidative chemical polymerisation using ferric chloride as an oxidant in the presence of AOT as surfactant in chloroform medium. PTE is then complexed with cationic surfactant cetyl trimethyl ammonium bromide (CTAB) to obtain the solubilized form of the polymer PTE-CTAB complex. FT-IR analysis and powder X-ray diffraction studies confirms the PTECNT-COOH nanocomposites formation. PTE-CTAB complex exhibited an intensified red shift in absorption spectra, indicating the conformational change of the polymer backbone, resulting in efficient conformationally extended conjugation. PTECNT-COOH composites exhibited stable dispersion in less polar solvents; especially in ethanol, which helped to record UV-vis absorption spectra. Morphological analyses using FE-SEM micrographs gave less agglomerated nanotubular morphology of the nanocomposites. PTECNT-COOH

composites maintained high thermal stability and good electrical conductivity. Additives and binders free preparation of film coating of PTECNT-COOH with green solvent ethanol was achieved for electrochemical characterization. The electrochemical study shows the applicability of PTECNT-COOH nanocomposites as efficient supercapacitor electrode material having a moderately good specific capacitance of 128 F/g with efficient energy density, power output and long-time cycling stability.

References

1. Avasthi, P.; Kumar, A.; Balakrishnan, V. Aligned CNT Forests on Stainless Steel Mesh for Flexible Supercapacitor Electrode with High Capacitance and Power Density. *ACS Appl. Nano Mater.* **2019**, *2* (3), 1484–1495. <https://doi.org/10.1021/acsanm.8b02355>.
2. Kumar, S.; Saeed, G.; Zhu, L.; Hui, K. N.; Kim, N. H.; Lee, J. H. 0D to 3D Carbon-Based Networks Combined with Pseudocapacitive Electrode Material for High Energy Density Supercapacitor: A Review. *Chem. Eng. J.* **2021**, *403*. <https://doi.org/10.1016/j.cej.2020.126352>.
3. Han, J.; Wang, S.; Zhu, S.; Huang, C.; Yue, Y.; Mei, C.; Xu, X.; Xia, C. Electrospun Core-Shell Nanofibrous Membranes with Nanocellulose-Stabilized Carbon Nanotubes for Use as High-Performance Flexible Supercapacitor Electrodes with Enhanced Water Resistance, Thermal Stability, and Mechanical Toughness. *ACS Appl. Mater. Interfaces* **2019**, *11* (47), 44624–44635. <https://doi.org/10.1021/acsami.9b16458>.
4. Yang, Z.; Tian, J.; Yin, Z.; Cui, C.; Qian, W.; Wei, F. Carbon Nanotube- and Graphene-Based Nanomaterials and Applications in High-Voltage Supercapacitor: A Review. *Carbon N. Y.* **2019**, *141*, 467–480. <https://doi.org/10.1016/j.carbon.2018.10.010>.
5. Aydinli, A.; Yuksel, R.; Unalan, H. E. Vertically Aligned Carbon Nanotube – Polyaniline Nanocomposite Supercapacitor Electrodes. *Int. J. Hydrogen Energy* **2018**, *43* (40), 18617–18625. <https://doi.org/10.1016/j.ijhydene.2018.05.126>.
6. Saha, S.; Samanta, P.; Murmu, N. C.; Kuila, T. A Review on the Heterostructure Nanomaterials for Supercapacitor Application. *J. Energy Storage* **2018**, *17*, 181–202. <https://doi.org/10.1016/j.est.2018.03.006>.
7. Dhibar, S.; Bhattacharya, P.; Ghosh, D.; Hatui, G.; Das, C. K. Graphene-Single-Walled Carbon Nanotubes-Poly(3-Methylthiophene) Ternary Nanocomposite for Supercapacitor Electrode Materials. *Ind. Eng. Chem. Res.* **2014**, *53* (33), 13030–13045. <https://doi.org/10.1021/ie501407k>.
8. Li, Y.; Zhou, M.; Wang, Y.; Pan, Q.; Gong, Q.; Xia, Z.; Li, Y. Remarkably Enhanced Performances of Novel Polythiophene-Grafting-Graphene Oxide Composite via Long Alkoxy Linkage for Supercapacitor Application. *Carbon N. Y.* **2019**, *147*, 519–531. <https://doi.org/10.1016/j.carbon.2019.03.030>.
9. Ghosh, A.; Lee, Y. H. Carbon-Based Electrochemical Capacitors. *ChemSusChem* **2012**, *5* (3), 480–499. <https://doi.org/10.1002/cssc.201100645>.
10. Lokhande, P. E.; Chavan, U. S.; Pandey, A. Materials and Fabrication Methods for Electrochemical Supercapacitors: Overview. *Electrochem. Energy Rev.* **2020**, *3* (1), 155–186. <https://doi.org/10.1007/s41918-019-00057-z>.
11. Li, L.; Hu, Z. A.; An, N.; Yang, Y. Y.; Li, Z. M.; Wu, H. Y. Facile Synthesis of MnO₂/CNTs Composite for Supercapacitor Electrodes with Long Cycle Stability. *J. Phys. Chem. C* **2014**, *118* (40), 22865–22872. <https://doi.org/10.1021/jp505744p>.
12. Yu, G.; Hu, L.; Liu, N.; Wang, H.; Vosgueritchian, M.; Yang, Y.; Cui, Y.; Bao, Z. Enhancing the Supercapacitor Performance of Graphene/MnO₂ Nanostructured Electrodes by Conductive Wrapping. *Nano Lett.* **2011**, *11* (10), 4438–4442. <https://doi.org/10.1021/nl2026635>.

13. Huang, Y.; Wang, B.; Liu, F.; Liu, H.; Wang, S.; Li, Q.; Cheng, J.; Zhang, L. Fabrication of Rambutan-like Activated Carbon Sphere/Carbon Nanotubes and Their Application as Supercapacitors. *Energy and Fuels* **2021**, *35* (9), 8313–8320. <https://doi.org/10.1021/acs.energyfuels.1c00189>.
14. Bryan, A. M.; Santino, L. M.; Lu, Y.; Acharya, S.; D'Arcy, J. M. Conducting Polymers for Pseudocapacitive Energy Storage. *Chem. Mater.* **2016**, *28* (17), 5989–5998. <https://doi.org/10.1021/acs.chemmater.6b01762>.
15. Faraji, S.; Ani, F. N. Microwave-Assisted Synthesis of Metal Oxide/Hydroxide Composite Electrodes for High Power Supercapacitors - A Review. *J. Power Sources* **2014**, *263*, 338–360. <https://doi.org/10.1016/j.jpowsour.2014.03.144>.
16. Kumar, K. S.; Choudhary, N.; Jung, Y.; Thomas, J. Recent Advances in Two-Dimensional Nanomaterials for Supercapacitor Electrode Applications. *ACS Energy Lett.* **2018**, *3* (2), 482–495. <https://doi.org/10.1021/acsenergylett.7b01169>.
17. So, R. C.; Carreon-Asok, A. C. Molecular Design, Synthetic Strategies, and Applications of Cationic Polythiophenes. *Chem. Rev.* **2019**, *119* (21), 11442–11509. <https://doi.org/10.1021/acs.chemrev.8b00773>.
18. Kaloni, T. P.; Giesbrecht, P. K.; Schreckenbach, G.; Freund, M. S. Polythiophene: From Fundamental Perspectives to Applications. *Chem. Mater.* **2017**, *29* (24), 10248–10283. <https://doi.org/10.1021/acs.chemmater.7b03035>.
19. Nejati, S.; Minford, T. E.; Smolin, Y. Y.; Lau, K. K. S. Enhanced Charge Storage of Ultrathin Polythiophene Films within Porous Nanostructures. *ACS Nano* **2014**, *8* (6), 5413–5422. <https://doi.org/10.1021/nn500007c>.
20. Wang, X.; Zhu, Y.; Liu, Z.; Yuan, Y.; Qiu, L. Ultrathin Polythiophene Films Prepared by Vertical Phase Separation for Highly Stretchable Organic Field-Effect Transistors. *Adv. Electron. Mater.* **2021**, *7* (11). <https://doi.org/10.1002/aelm.202100591>.
21. Devadas, B.; Imae, T. Effect of Carbon Dots on Conducting Polymers for Energy Storage Applications. *ACS Sustain. Chem. Eng.* **2018**, *6* (1), 127–134. <https://doi.org/10.1021/acssuschemeng.7b01858>.
22. Hashempour, M.; Vincenzo, A.; Bahdanchyk, M.; Bestetti, M. Parameters Influencing the Capacitive Behavior of Carbon Composite Electrodes: Composition, Morphology, Electrical Conductivity, and Surface Chemistry. *J. Solid State Electrochem.* **2018**, *22* (12), 3895–3911. <https://doi.org/10.1007/s10008-018-4095-8>.
23. Alvi, F.; Ram, M. K.; Basnayaka, P. A.; Stefanakos, E.; Goswami, Y.; Kumar, A. Graphene-Polyethylenedioxythiophene Conducting Polymer Nanocomposite Based Supercapacitor. *Electrochim. Acta* **2011**, *56* (25), 9406–9412. <https://doi.org/10.1016/j.electacta.2011.08.024>.
24. Poonam; Sharma, K.; Arora, A.; Tripathi, S. K. Review of Supercapacitors: Materials and Devices. *J. Energy Storage* **2019**, *21*, 801–825. <https://doi.org/10.1016/j.est.2019.01.010>.
25. Rahman, G. M. A.; Guldi, D. M.; Cagnoli, R.; Mucci, A.; Schenetti, L.; Vaccari, L.; Prato, M. Combining Single Wall Carbon Nanotubes and Photoactive Polymers for Photoconversion. *J. Am. Chem. Soc.* **2005**, *127* (28), 10051–10057. <https://doi.org/10.1021/ja050396k>.
26. Kim, K. H.; Jo, W. H. Synthesis of Polythiophene-*graft*-PMMA and Its Role as Compatibilizer for Poly(styrene-*co*-acrylonitrile)/MWCNT Nanocomposites, *Macromolecules*, **2007**, *40* (10), 20189, <https://doi.org/10.1021/ma070127>.
27. Ghosh, S.; Patel, N.; Chakrabarti, R. Probing the Salt Concentration Dependent Nucleobase Distribution in a Single-Stranded DNA-Single-Walled Carbon Nanotube Hybrid with Molecular Dynamics. *J. Phys. Chem. B* **2016**, *120* (3), 455–466. <https://doi.org/10.1021/acs.jpcc.5b12044>.
28. Berger, F. J.; Lüttgens, J.; Nowack, T.; Kutsch, T.; Lindenthal, S.; Kistner, L.; Müller, C. C.; Bongartz, L. M.; Lumsargis, V. A.; Zakharko, Y.; Zaumseil, J. Brightening of Long, Polymer-Wrapped Carbon Nanotubes by Sp³ Functionalization in Organic Solvents. *ACS Nano* **2019**, *13* (8), 9259–9269. <https://doi.org/10.1021/acsnano.9b03792>.

29. Wang, J.; Dai, J.; Yarlagadda, T. Carbon Nanotube-Conducting-Polymer Composite Nanowires. *Langmuir* **2005**, *21* (1), 9–12. <https://doi.org/10.1021/la0475977>.
30. Lota, K.; Khomenko, V.; Frackowiak, E. Capacitance Properties of Poly(3,4-Ethylenedioxythiophene)/Carbon Nanotubes Composites. *J. Phys. Chem. Solids* **2004**, *65* (2–3), 295–301. <https://doi.org/10.1016/j.jpcs.2003.10.051>.
31. Zhan, C.; Yu, G.; Lu, Y.; Wang, L.; Wujcik, E.; Wei, S. Conductive Polymer Nanocomposites: A Critical Review of Modern Advanced Devices. *J. Mater. Chem. C* **2017**, *5* (7), 1569–1585. <https://doi.org/10.1039/c6tc04269d>.
32. Cheung, W.; Chiu, P. L.; Parajuli, R. R.; Ma, Y.; Ali, S. R.; He, H. Fabrication of High Performance Conducting Polymer Nanocomposites for Biosensors and Flexible Electronics: Summary of the Multiple Roles of DNA Dispersed and Functionalized Single Walled Carbon Nanotubes. *J. Mater. Chem.* **2009**, *19* (36), 6465–6480. <https://doi.org/10.1039/b823065j>.
33. Zhou, K.; He, Y.; Xu, Q.; Zhang, Q.; Zhou, A.; Lu, Z.; Yang, L. K.; Jiang, Y.; Ge, D.; Liu, X. Y.; Bai, H. A Hydrogel of Ultrathin Pure Polyaniline Nanofibers: Oxidant-Templating Preparation and Supercapacitor Application. *ACS Nano* **2018**, *12* (6), 5888–5894. <https://doi.org/10.1021/acsnano.8b02055>.
34. Tang, C.; Chen, N.; Hu, X. Conducting Polymer Nanocomposites: Recent Developments and Future Prospects. **2017**, 1–44. https://doi.org/10.1007/978-3-319-46458-9_1.
35. Dunlop, M. J.; Bissessur, R. Nanocomposites Based on Graphene Analogous Materials and Conducting Polymers: A Review. *J. Mater. Sci.* **2020**, *55* (16), 6721–6753. <https://doi.org/10.1007/s10853-020-04479-9>.
36. Yin, S.; Lu, W.; Wu, R.; Fan, W.; Guo, C. Y.; Chen, G. Poly(3,4-Ethylenedioxythiophene)/Te/Single-Walled Carbon Nanotube Composites with High Thermoelectric Performance Promoted by Electropolymerization. *ACS Appl. Mater. Interfaces* **2020**, *12* (3), 3547–3553. <https://doi.org/10.1021/acsmi.9b17947>.
37. Namsheer, K.; Rout, C. S. Conducting Polymers: A Comprehensive Review on Recent Advances in Synthesis, Properties and Applications. *RSC Adv.* **2021**, *11* (10), 5659–5697. <https://doi.org/10.1039/d0ra07800j>.
38. Tran-Van, F.; Carrier, M.; Chevrot, C. Sulfonated Polythiophene and Poly(3,4-Ethylenedioxythiophene) Derivatives with Cations Exchange Properties. *Synth. Met.* **2004**, *142* (1–3), 251–258. <https://doi.org/10.1016/j.synthmet.2003.09.013>.
39. Ghosh, R.; Chatterjee, D. P.; Das, S.; Mukhopadhyay, T. K.; Datta, A.; Nandi, A. K. Influence of Hofmeister I- on Tuning Optoelectronic Properties of Ampholytic Polythiophene by Varying PH and Conjugating with RNA. *Langmuir* **2017**, *33* (44), 12739–12749. <https://doi.org/10.1021/acs.langmuir.7b03147>.
40. Das, S.; Chatterjee, D. P.; Ghosh, R.; Nandi, A. K. Water Soluble Polythiophenes: Preparation and Applications. *RSC Adv.* **2015**, *5* (26), 20160–20177. <https://doi.org/10.1039/c4ra16496b>.
41. Harel, Y.; Azoubel, S.; Magdassi, S.; Lellouche, J. P. A Dispersability Study on Poly(Thiophen-3-Yl-Acetic Acid) and PEDOT Multi-Walled Carbon Nanotube Composites Using an Analytical Centrifuge. *J. Colloid Interface Sci.* **2013**, *390* (1), 62–69. <https://doi.org/10.1016/j.jcis.2012.09.006>.
42. Zhao, Q.; Li, Y.; Hu, K.; Guo, X.; Qu, Y.; Li, Z.; Yang, F.; Liu, H.; Qin, C.; Jing, L. Controlled Synthesis of Nitro-Terminated Poly[2-(3-Thienyl)-Ethanol]/g-C₃N₄Nanosheet Heterojunctions for Efficient Visible-Light Photocatalytic Hydrogen Evolution. *ACS Sustain. Chem. Eng.* **2021**, *9* (21), 7306–7317. <https://doi.org/10.1021/acssuschemeng.1c01308>.
43. Cházaro-Ruiz, L. F.; Kellenberger, A.; Jähne, E.; Adler, H. J.; Khandelwal, T.; Dunsch, L. In Situ ESR-UV-Vis-NIR Spectroelectrochemical Study of the p-Doping of poly [2-(3-Thienyl)Ethyl Acetate] and Its Hydrolyzed Derivatives. *Phys. Chem. Chem. Phys.* **2009**, *11* (30), 6505–6513. <https://doi.org/10.1039/b904529e>.
44. Danesh, C. D.; Starkweather, N. S.; Zhang, S. In Situ Study of Dynamic Conformational Transitions of a Water-Soluble Poly(3-Hexylthiophene) Derivative by Surfactant

- Complexation. *J. Phys. Chem. B* **2012**, *116* (42), 12887–12894. <https://doi.org/10.1021/jp307728r>.
45. Su, G.; Yang, C.; Zhu, J. J. Fabrication of Gold Nanorods with Tunable Longitudinal Surface Plasmon Resonance Peaks by Reductive Dopamine. *Langmuir* **2015**, *31* (2), 817–823. <https://doi.org/10.1021/la504041f>.
 46. Dass, A.; Mulik, S.; Sotiriou-Leventis, C.; Leventis, N. Protection of 2-(3-Thienyl)Ethanol with 3-Thienylacetic Acid and Hard Cross-Linked Conducting Films by Electropolymerization of the Ester. *Synth. Met.* **2006**, *156* (14–15), 966–972. <https://doi.org/10.1016/j.synthmet.2006.06.015>.
 47. Ohlan, A.; Singh, K.; Chandra, A.; Dhawan, S. K. Microwave Absorption Behavior of Core-Shell Structured Poly (3,4-Ethylenedioxy Thiophene)/Barium Ferrite Nanocomposites. *ACS Appl. Mater. Interfaces* **2010**, *2* (3), 927–933. <https://doi.org/10.1021/am900893d>.
 48. Futaba, D. N.; Yamada, T.; Kobashi, K.; Yumura, M.; Hata, K. Macroscopic Wall Number Analysis of Single-Walled, Double-Walled, and Few-Walled Carbon Nanotubes by X-Ray Diffraction. *J. Am. Chem. Soc.* **2011**, *133* (15), 5716–5719. <https://doi.org/10.1021/ja2005994>.
 49. Bilger, D.; Sarkar, A.; Danesh, C.; Gopinadhan, M.; Braggin, G.; Figueroa, J.; Pham, T. V.; Chun, D.; Rao, Y.; Osuji, C. O.; Stefik, M.; Zhang, S. Multi-Scale Assembly of Polythiophene-Surfactant Supramolecular Complexes for Charge Transport Anisotropy. *Macromolecules* **2017**, *50* (3), 1047–1055. <https://doi.org/10.1021/acs.macromol.6b02416>.
 50. Kerfoot, J.; Beton, P. H.; Svatek, S. A.; Korolkov, V. V.; Taniguchi, T.; Watanabe, K.; Antolin, E. Fluorescence and Electroluminescence of J-Aggregated Polythiophene Monolayers on Hexagonal Boron Nitride. *ACS Nano* **2020**, *14* (10), 13886–13893. <https://doi.org/10.1021/acsnano.0c06280>.
 51. Sinsinbar, G.; Palaniappan, A.; Yildiz, U. H.; Liedberg, B. A Perspective on Polythiophenes as Conformation Dependent Optical Reporters for Label-Free Bioanalytics. *ACS Sensors* **2022**, *7* (3), 686–703. <https://doi.org/10.1021/acssensors.1c02476>.
 52. Massoumi, B.; Jaymand, M.; Samadi, R.; Entezami, A. A. In Situ Chemical Oxidative Graft Polymerization of Thiophene Derivatives from Multi-Walled Carbon Nanotubes. *J. Polym. Res.* **2014**, *21* (5). <https://doi.org/10.1007/s10965-014-0442-3>.
 53. Sun, C.; Li, X.; Zhao, J.; Cai, Z.; Ge, F. A Freestanding Polypyrrole Hybrid Electrode Supported by Conducting Silk Fabric Coated with PEDOT:PSS and MWCNTs for High-Performance Supercapacitor. *Electrochim. Acta* **2019**, *317*, 42–51. <https://doi.org/10.1016/j.electacta.2019.05.124>.
 54. Welzel, H. P.; Kossmehl, G.; Schneider, J.; Plieth, W. Reactive Groups on Polymer-Covered Electrodes. 2. Functionalized Thiophene Polymers by Electrochemical Polymerization and Their Application as Polymeric Reagents. *Macromolecules* **1995**, *28* (16), 5575–5580. <https://doi.org/10.1021/ma00120a023>.
 55. Oraon, R.; De Adhikari, A.; Tiwari, S. K.; Nayak, G. C. Enhanced Specific Capacitance of Self-Assembled Three-Dimensional Carbon Nanotube/Layered Silicate/Polyaniline Hybrid Sandwiched Nanocomposite for Supercapacitor Applications. *ACS Sustain. Chem. Eng.* **2016**, *4* (3), 1392–1403. <https://doi.org/acssuschemeng.5b01389>.
 56. Jiang, Y.; Liu, J. Definitions of Pseudocapacitive Materials: A Brief Review. *Energy Environ. Mater.* **2019**, *2* (1), 30–37. <https://doi.org/10.1002/eem2.12028>.
 57. Alabadi, A.; Razzaque, S.; Dong, Z.; Wang, W.; Tan, B. Graphene Oxide-Polythiophene Derivative Hybrid Nanosheet for Enhancing Performance of Supercapacitor. *J. Power Sources* **2016**, *306*, 241–247. <https://doi.org/10.1016/j.jpowsour.2015.12.028>.
 58. Parayangattil Jyothibas, J.; Chen, M. Z.; Lee, R. H. Polypyrrole/Carbon Nanotube Freestanding Electrode with Excellent Electrochemical Properties for High-Performance All-Solid-State Supercapacitors. *ACS Omega* **2020**, *5* (12), 6441–6451. <https://doi.org/10.1021/acsomega.9b04029>.

Chapter 7

59. Parveen, N.; Ansari, M. O.; Cho, M. H. Route to High Surface Area, Mesoporosity of Polyaniline-Titanium Dioxide Nanocomposites via One Pot Synthesis for Energy Storage Applications. *Ind. Eng. Chem. Res.* **2016**, *55* (1), 116–124. <https://doi.org/10.1021/acs.iecr.5b02907>.
60. Zhu, G.; He, Z.; Chen, J.; Zhao, J.; Feng, X.; Ma, Y.; Fan, Q.; Wang, L.; Huang, W. Highly Conductive Three-Dimensional MnO₂-Carbon Nanotube-Graphene-Ni Hybrid Foam as a Binder-Free Supercapacitor Electrode. *Nanoscale* **2014**, *6* (2), 1079–1085. <https://doi.org/10.1039/c3nr04495e>.

Chapter 8

Summary and Conclusions

Polythiophene-multiwalled carbon nanotubes nanocomposites are remarkable in different applications due to their prominent and distinguishable properties. The conducting polythiophene and its derivatives also acquire special attention due to its electrical conductivity, optoelectronic properties, thermal properties, and biocompatibility. Polythiophene-based carbon nanocomposites are one of the most demanding research areas for conducting polymer nanocomposites. Synthetic strategies of polythiophene-carbon nanotube nanocomposites demand facile and productive approaches, which could form well-structured nanocomposites. A structure-property relationship can be fine-tuned in well-structured nanocomposites. Therefore, preparing well-structured nanocomposites to improve physical characteristics is an active area of research. In this work, a study was conducted based on synthetic approaches, characterizations and applications of conducting polythiophene-carbon nanotube nanocomposites. We could also explore and establish new application areas via its properties. **Chapter 1** deals with a literature review of polythiophene-carbon nanotube nanocomposites and also discusses the synthetic methods for polythiophene-carbon nanotube nanocomposites formation, keeping an impact on the general and specific applications based on electrical, thermal, optical, and mechanical properties.

In **Chapter 2**, polythiophene-carbon nanotube nanocomposites (PTCNTs) were prepared by in-situ chemical oxidative polymerization of thiophene with the assistance of sodium bis(2-ethyl hexyl) sulfosuccinate (AOT) surfactant using FeCl_3 as an oxidant in the presence of pristine MWCNT in chloroform. A core-shell nano-structure of the nanocomposites was evidenced in morphological analysis. The influence of surfactant AOT in the formation of core-shell morphology was recognized. Furthermore, the role of AOT as a dopant, surfactant and stabilizing agent was established. The prepared nanocomposites were also characterized by improved electrical conductivity, thermal stability and dispersibility in chloroform. In **Chapter 3**, the functionalization of carbon nanotubes was carried out by treatment with nitric acid. The functionalization of pristine MWCNT resulted in the formation of highly dispersible carbon nanotubes named as MWCNT-COOH. Functionalization of carbon nanotubes increases the processability in synthesizing their nanocomposites with conducting polythiophene, however with minimum carbon nanotube destruction. Polythiophene-functionalized carbon nanotube nanocomposites (PTCNT-COOH) were prepared by in-situ chemical oxidative polymerization of thiophene in the stable dispersion of MWCNT-COOH in

Chapter 8

chloroform using FeCl_3 as oxidant and with the surfactant AOT. The nanocomposites PTCNT-COOHs were characterized by core-shell morphology with a thicker outer shell of polythiophene on carbon nanotube. An enhancement in electrical conductivity and thermal stability was also obtained. The PTCNT-COOH nanocomposites exhibited stable dispersion in polar and less polar media. The dispersion stability of PTCNT-COOH and MWCNT-COOH in water is directed to the preparation of higher-order nanocomposites. In **chapter 4**, a green synthetic approach could establish to produce ternary silver nanoparticles embedded polythiophene-functionalized multiwalled carbon nanotube nanocomposites (PTCNT-COOH 300 Ag) by in-situ chemical reduction with ascorbic acid (vitamin C) in the presence of stable dispersion of binary PTCNT-COOH 300 in water. A binary silver nanocomposite MWCNT-COOH Ag was also prepared using the same synthetic approach. The ternary and binary silver nanocomposites exhibited excellent dispersion stability in various solvents, superior electrical conductivity, and high thermal stability.

In **chapter 5**, the applications of PTCNT-COOH 300 Ag (TNC) and MWCNT-COOH Ag (BNC) were established (i) as heterogeneous catalysts in nitrophenol reduction with the reductant NaBH_4 and (ii) as good antibacterial agents against *E. coli* bacteria. An elaborated study of catalytic nitrophenol reduction in different solvents proved that not only the reductant but also active solvent hydrogens present in solvents also influence the reduction mechanism. An industrial-scale preparation of aminophenol from nitrophenol could be demonstrated in a 10% glycerol-water mixture with a high catalyst activity factor of $936.50 \text{ s}^{-1} \text{ g}^{-1}$. PTCNT-COOH 300 Ag (TNC) exhibited prominent antibacterial activity in a water-based nutrient broth with a low concentration of $10 \text{ }\mu\text{g/mL}$. In **Chapter 6**, the TNC and BNC as heterogeneous catalysts were used for decolourisation of water-soluble and insoluble organic azo dyes. Catalytic decolourisation of water-insoluble azo dyes was effectively carried out in the ethanol-water mixture as the medium and exhibited high rate constants. The product-selective catalytic reduction of azobenzene to hydrazobenzene was also carried out with the BNC nanocatalyst. The large-scale reduction was demonstrated within a short reaction time of 15 min with a minimum nanocatalyst (0.18 mg/mL) and reductant with azobenzene-reductant molar ratio of 1:100.

In **chapter 7**, CTAB complexed poly(3-thiophene ethanol)-functionalized multiwalled carbon nanotube nanocomposites (PTECNT-COOH) were prepared by a simple solution blending approach. The highly stable dispersion of nanocomposites in an ethanol medium has an advantage for solution processability. The PTECNT-COOH nanocomposites have good electrical conductivity and high thermal stability. Furthermore, electrochemical supercapacitor studies of nanocomposites were conducted for which modified glassy carbon electrodes could be prepared without adding additives or binders. The electrochemical performance of nanocomposites revealed the supercapacitor application of PTECNT-20 with a relatively good specific capacitance of 128 F/g. In addition, the composite exhibited excellent electrochemical stability by retaining 99 % capacitance even after 1000 cycles.

Way forward

Facile synthetic strategies would generate promising polythiophene carbon nanotube nanocomposites in various applications. The unique electrical, optical, thermal, and mechanical properties accomplished in such nanocomposites could result in finding suitable nanocomposite applications. We have reported some of these applications of nanocomposites. Furthermore, the prominent characteristic features of these reported nanocomposites may be extended to various other fields of application, including electromagnetic interference shielding, thermoelectric materials, sensor, photovoltaic applications and magnetism.

Publications and Conference Presentations

Journal papers

- [1] T S Swathy, M Jinish Antony* and Naijil George. “Active Solvent Hydrogen Enhanced p-Nitrophenol Reduction Using Heterogeneous Silver Nanocatalysts@Surface Functionalized Multiwalled Carbon Nanotubes”. *Industrial and engineering chemistry research*. Vol: 60, year: 2021, page: 7050-7054. *Publisher: ACS*. DOI: <https://doi.org/10.1021/acs.iecr.1c01371>
- [2] T S Swathy, M Jinish Antony*. “Tangled silver nanoparticles embedded polythiophene functionalized multiwalled carbon nanotube nanocomposites with remarkable electrical and thermal properties”. *Polymer*. Vol: 189, year: 2020, page: 122171. *Publisher: Elsevier*.
DOI: <https://doi.org/10.1016/j.polymer.2020.122171>
- [3] T S Swathy, M Anne Jose, M Jinish Antony*, “AOT assisted preparation of ordered, conducting and dispersible coreshell nanostructured polythiophene MWCNT nanocomposites”. *Polymer*. Vol: 103, year: 2016, page: 206-213. *Publisher: Elsevier*. DOI: <http://dx.doi.org/10.1016/j.polymer.2016.09.047>
- [4] M Jinish Antony*, C Albin Jolly, K Rohini Das, T S Swathy “Normal and reverse AOT micelles assisted interfacial polymerization for polyaniline nanostructures”. *Colloids and Surfaces A*. Vol: 578, Year: 2019, Page: 123627. *Publisher: Elsevier*
DOI: <https://doi.org/10.1016/j.colsurfa.2019.123627>

Conference presentations

- [1] T S Swathy, M Jinish Antony*, “Antibacterial Activity of Water Dispersible Polythiophene-Functionalized Multiwalled Carbon Nanotube-Silver Nanoparticles Ternary Nanocomposite”. *International Conference on Energy and Environment-2019*, Dec 12-14, 2019, TKM College of Arts and Science, Kollam.
- [2] T S Swathy, M Jinish Antony*, “In-situ synthesis and characterization of water dispersible and conducting polythiophene-functionalized multiwalled carbon nanotube nanocomposite”. *International Conference on Supercapacitors, Energy Storage and Applications- 2019*, March 8-10, 2019, C-MET, Thrissur.

- [3] T S Swathy, M Jinish Antony*, “Synthesis and characterization of highly conducting and dispersible nanocomposite of silver nanoparticles decorated on water dispersible polythiophene- multiwalled carbon nanotube nanocomposite” *International Conference on Chemistry and Physics of Materials 2018*, Dec 19-21, 2018. St. Thomas’ College (autonomous) Thrissur.